Title

Mechanistic Studies of Pd-Catalyzed C-N Bond Forming Reactions

Author

Wang, Justin

Publication Date

2020

Peer reviewed|Thesis/dissertation

Mechanistic Studies of Pd-Catalyzed C-N Bond Forming Reactions

By

Justin Wang

A dissertation submitted in partial satisfaction of the
requirements for the degree of
Doctor of Philosophy
in
Chemistry
in the
Graduate Division
of the
University of California, Berkeley

Committee in charge:

Professor John F. Hartwig, Chair
Professor T. Don Tilley
Professor Robert G. Bergman
Professor Jay Keasling

Spring 2020

Abstract

Mechanistic Studies of Pd-Catalyzed C-N Bond Forming Reactions

by

Justin Y. Wang

Doctor of Philosophy in Chemistry

University of California, Berkeley

Professor John F. Hartwig, Chair

This dissertation discusses the development of aminocarbonylation reactions with ammonia and either an aryl or alkyl halide, coupling reactions between hydrazine and aryl halides, and studies of the mechanisms of these two classes of reactions. The synthesis and reactivity of arylnickel(II) amido complexes is also described.

Chapter 1 presents an overview of Pd and Ni-catalyzed C-N coupling reactions. This chapter includes a description of the development of these reactions and a synopsis of the mechanistic studies that have been conducted for each C-N coupling reaction. This chapter also describes the challenges faced when developing systems to catalyze C-N coupling reactions with hydrazine and the mechanistic questions related to that transformation, which have gone unexplored. Pd-catalyzed carbonylative cross-coupling reactions are also discussed, and the mechanism of key elementary steps in these reactions are outlined, which were recently elucidated by work in our group.

Chapter 2 presents a study of the mechanism of a Pd-catalyzed aminocarbonylation reaction between chloroarenes and ammonia. The mechanism of this reaction was proposed based on kinetic, spectroscopic, and computational data. Additionally, ^{13}C KIE measurements and a Hammett analysis were performed to obtain further data on the mechanism of oxidative addition of a chloroarene to a three-coordinate Pd(0) carbonyl complex. A catalyst deactivation pathway, which involved the formation a Pd(I) dimer with bridging carbonyl and hydride ligands, was also elucidated, and the rate-limiting step of the catalytic reaction was shown to be the oxidative addition of chloroarene to Pd(0).

Chapter 3 details efforts to develop and study a Pd-catalyzed aminocarbonylation reaction between aniline and alkyl bromides. Preliminary data obtained for this aminocarbonylation reaction are consistent with oxidative addition of the alkyl halide to a Pd(0) species by a mechanism involving an alkyl radical.

Chapter 4 describes the synthesis and reactivity of a small library of arylnickel(II) amido complexes, which have been crystallographically characterized and are stable at room temperature.

Chapter 5 presents the development and mechanistic study of a Pd-catalyzed C-N coupling reaction between aryl chlorides and hydrazine. Aryl hydrazines can be synthesized in high yield and with catalyst loadings as low as 300 ppm by this protocol. Several examples of aryl hydrazines are provided that are relevant to the synthesis of agrochemicals. The synthesis of an arylpalladium(II) hydrazido species was undertaken and demonstrated to undergo reductive elimination to give aryl hydrazine. Additional mechanistic studies were performed that identified two resting states of the catalyst, an arylpalladium(II) chloride species and an arylpalladium(II)

hydroxo complex. The hydroxo compound reacts with hydrazine to give aryl hydrazine, but this palladium complex was demonstrated to be unselective towards mono- versus diarylation of hydrazine.

Acknowledgements

First and foremost, I have to thank my parents, Chunhong Teng and Zhenggang Wang, and my sister, Joy Wang, for their constant support and encouragement. I could not have done all that I have without your help.

My decision to pursue chemistry was largely due to Professor Masato Koreeda's course in organic chemistry at the University of Michigan, which opened my eyes to the world of synthetic chemistry. My decision to enter graduate school to study chemistry can ultimately be traced back to my fond memories of that class. His dedication for teaching and passion for chemistry is unmatched, and for a long while he was the standard that I judged all chemistry professors against. I also thank my mentors and teachers in chemistry who have helped my development as a researcher. In this respect, I especially have to acknowledge Professors James Jackson and Nathaniel Szymczak for their mentorship and for the opportunity to work in their research labs. I also thank Tyler Carter, Jacob Geri, Souful Bhatia, and many other graduate students that have taken the time out of their own research to mentor me when I was an undergraduate. I still use many of the techniques you have taught me, and I would not be half the researcher that I am without your guidance.

My time in the Hartwig group has been a wild ride, and several of my lab mates and facility operators have helped me navigate my path through graduate school. Peacock, thank you for dealing with all my questions on palladium chemistry, NMR spectroscopy, and kinetics. I would not have made past my first year without all the (unwilling) advice you gave me. Sophie, Haoquan, and York, thank you for being amazing lab mates and for helping me learn the ropes when I first got to Berkeley. I especially have to thank York for his chemistry advice. His suggestion to make Pd(0) ethylene complexes kickstarted my first project. I do not know what would have happened to that project without that compound. Taegyo, thank you for being a capable co-safety officer and an understanding friend. Chris, you were the first person from the Hartwig group that I talked to during my visitation weekend. Thanks for putting up with all my questions, and for warmly welcoming me into the group. My cohort in the Hartwig group is also composed of smart and interesting individuals. Noam, Caleb, Zhennan, and Zach, thank you guys for being a shoulder to lean on during difficult times. I also have to thank Brandon for his irreverent humor and for being a great hiking partner, and Dan for being a good friend and roommate. I still remember your introduction to my GRS presentation. Zhitao, thank you for all your advice related to product isolation. I'll miss your chemistry expertise and seeing you early in the morning. Hasan Celik and Jeff Pelton, I am grateful to you both for your assistance with many difficult NMR spectroscopic experiments. Stephan Zuend, thank you for your guidance and advice during my time developing the C-N coupling reaction with hydrazine. Lastly, John has my gratitude for giving me the opportunity to explore organometallic chemistry and to meet such capable scientists.

TABLE OF CONTENTS

CHAPTER 1

OVERVIEW OF C-N CROSS-COUPLING REACTIONS CATALYZED BY NICKEL AND PALLADIUM AND THEIR MECHANISMS

1.1 Overview of C-N Cross-Coupling Reactions Catalyzed by Nickel and Palladium and their Mechanisms

Palladium and nickel-catalyzed cross-coupling reactions are a powerful means to join fragments by the formation of a carbon-carbon (C-C) or a carbon-heteroatom (C-X) bond. Although C-C bond-forming reactions with Ni or Pd catalysts have been known since the 1900s and 1950s,[1] respectively, only within the last 25 years have methods been developed to reliably and efficiently form C-X bonds.[2] Currently, methods to generate carbon-phosphorus, -sulfur, -oxygen, -nitrogen, and -fluorine bonds have been reported.[3] Out of all of these C-X bond-forming reactions, C-N cross-coupling reactions, which involve the reaction of an aryl halide and an amine to give an aryl amine, has experienced the most development. Its adoption by the pharmaceutical industry to synthesize drug candidates and to prepare active pharmaceutical ingredients and their synthetic intermediates on the kilogram scale is a testament to its synthetic utility.[3a, 4] The generality and reliability of C-N coupling reactions has largely replaced classical methods to generate arylamines, such as the addition of amines to benzyne intermediates, nitration and subsequent reduction, or nucleophilic aromatic substitution.[3a]

Scheme 1.1. Abbreviated Timeline of Developments in Pd-Catalyzed C-N Coupling Reactions.

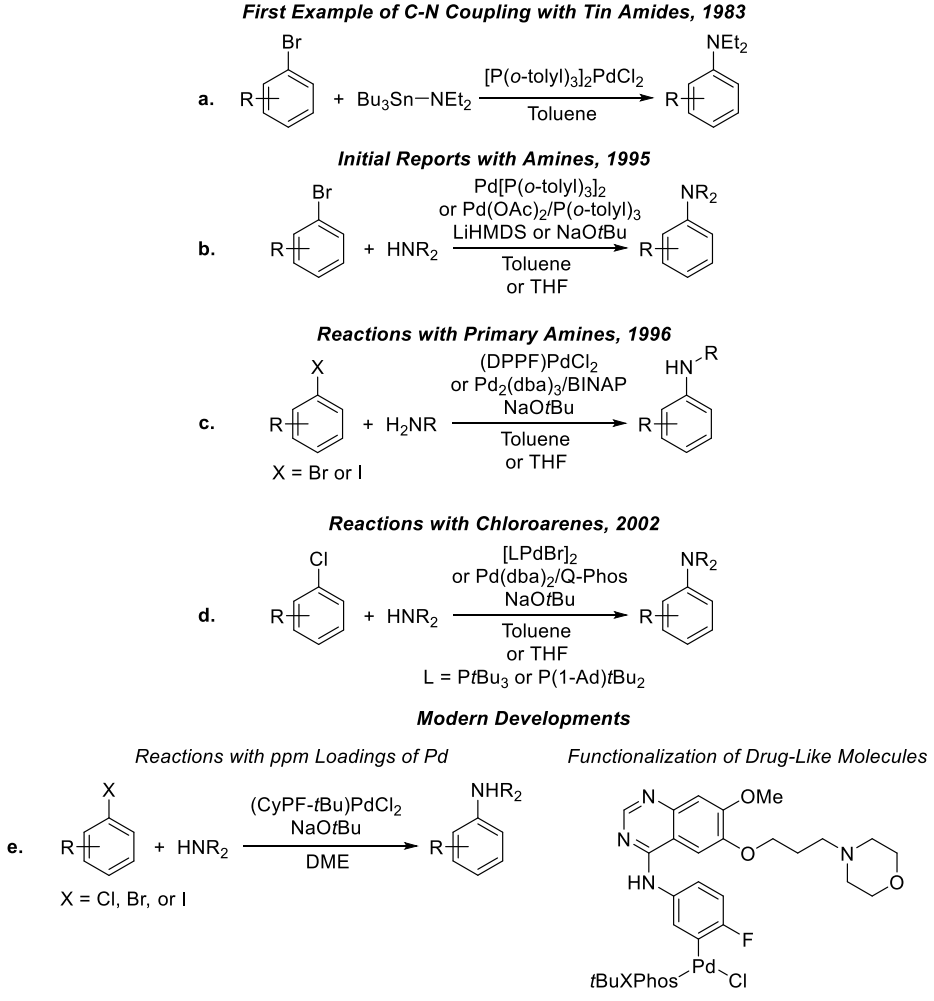

The first report of a C-N bond forming cross-coupling reaction was reported by Kosugi and Migita in 1983 (Scheme 1.1a).[5] This method was capable of coupling electron-rich and electron-poor aryl halides with tin amides to generate arylamines with a palladium catalyst. However, the use of toxic and unstable tin amides discouraged the widespread adoption of this method.[3a, 6] In 1995, more practical methods for C-N cross-coupling reactions were developed separately by Hartwig[7] and Buchwald.[8] In these methods, the combination of amine and base were used in place of the tin amides (Scheme 1.1b). The scope of these initial reactions encompassed the formation of tertiary arylamines from aryl halides and secondary amines with palladium catalysts. However, reactions with primary alkylamines were not tolerated, due to competitive β-hydride elimination to give undesired imine side-products. Subsequent advances in this area utilized bidentate ligands, such as BINAP or DPPF, which inhibited β-hydride elimination by blocking a coordination site on the Pd center that would otherwise be vacant in complexes bearing a monodentate ligand (Scheme 1.1c).[9] These improved protocols enabled the synthesis of secondary amines from primary amines and haloarenes. Later developments enabled the amination of chloroarenes, which are less reactive than iodo- or bromoarenes.[10] This type of reactivity with chloroarenes was first described by Beller in 1997,[11] and expanded by other groups (Scheme 1.1d).[12] More recent developments in Pd catalyzed C-N coupling reactions have centered on enhancing the efficiency of the reaction by identifying means to lower catalyst loadings[13] and on the functionalization of highly decorated and medicinally relevant organic molecules (Scheme 1.1e).[14]

In 1997, Buchwald reported a Ni-catalyzed variant of this C-N cross-coupling reaction.[15] This method enabled the formation of C-N bonds between amines and aryl chlorides with DPPF or phenanthroline-ligated Ni catalysts. Subsequent work by Fort[16] and Knochel[17] with bipy and bromophenanthroline ligands, respectively, expanded the library of viable nickel catalysts for the amination of aryl chlorides. Because nickel is far more earth abundant than palladium, the development of Ni-catalyzed C-N coupling reactions is desirable. The scope of Ni-catalyzed C-N cross coupling reactions has lagged behind that of its palladium analogue, but recent discoveries have begun to close this gap. Prior to Hartwig's report on C-N coupling reactions with primary amines and (BINAP)(Ni)(η^2-NCPh) as catalyst in 2014,[18] C-N coupling reactions with nickel catalysts were largely limited to derivatives of aniline, morpholine, and piperidine nucleophiles.[15-16, 19] Later, Hartwig and Stradiotto concurrently reported the first examples of Ni-catalyzed C-N coupling reactions with ammonia as the nucleophile and Josiphos based structures as ligands.[20] In 2019, Stradiotto expanded the capabilities of Ni-catalyzed C-N coupling reactions to include heteroaryl anilines, sterically hindered, α,α,α-trisubstituted primary alkylamines, and heteroaryl halides with Ni catalysts bearing trioxaphosphaadamantane-containing ligands.[21] Electrochemical Ni-catalyzed C-N coupling reactions have been reported recently by Baran.[22] These methods can be performed at room temperature to generate medicinally relevant heteroarylamines, natural products, and oligopeptides.[22b] Some examples were performed on a 100 g scale to demonstrate the scalability of this electrochemical synthesis. Finally, photochemical Ni-catalyzed C-N coupling methods have been described. An advantage of this method is that this reaction does not require ligand or a photocatalyst with a second metal and can be performed in the presence of air and moisture at room temperature.[23]

Since the initial reports of C-N cross coupling reactions with palladium catalysts, this area of research has undergone tremendous growth. These protocols have evolved from reactions with simple alkyl- and aryl-substituted amines to those occurring with nucleophile sources that include

ammonia, amides, hydrazones, hydrazines, sulfonamides, carbamates, N-heterocycles, and others.[4] The growth of these Pd-catalyzed reactions over their Ni-catalyzed counterparts is in part due to the many mechanistic studies of this reaction with Pd catalysts, which have elucidated pathways for the formation of C-N coupled products.[24] In addition, Pd catalysts are more resistant than Ni catalysts to deactivation that results from reactions with adventitious moisture or oxygen. The mechanism of Pd-catalyzed C-N coupling reactions is broadly outlined in Scheme 1.2. These mechanistic insights arise largely from the ease at which the intermediate Pd species in these reactions are synthesized and the ability to monitor their activity by NMR spectroscopy, due to the diamagnetism of most Pd complexes, which exist as Pd(0) or Pd(II) compounds. In comparison, Ni complexes can exist in a wider range of oxidation states, from Ni(I) to Ni(IV). Due to odd-electron configurations, the favoring of tetrahedral versus a square planar geometry, or small ligand-field splitting energies, Ni complexes can be paramagnetic and thus difficult to characterize by conventional means.[1b] In addition, Pd complexes typically undergo reactions that involve two-electron pathways, such as oxidative addition and reductive elimination. Although Ni complexes can access these two-electron pathways, Ni compounds can also undergo reactions by one-electron pathways to generate radicals or odd-electron metal species.[25]

Scheme 1.2. Generalized Mechanisms of Pd-Catalyzed C-N Coupling Reactions

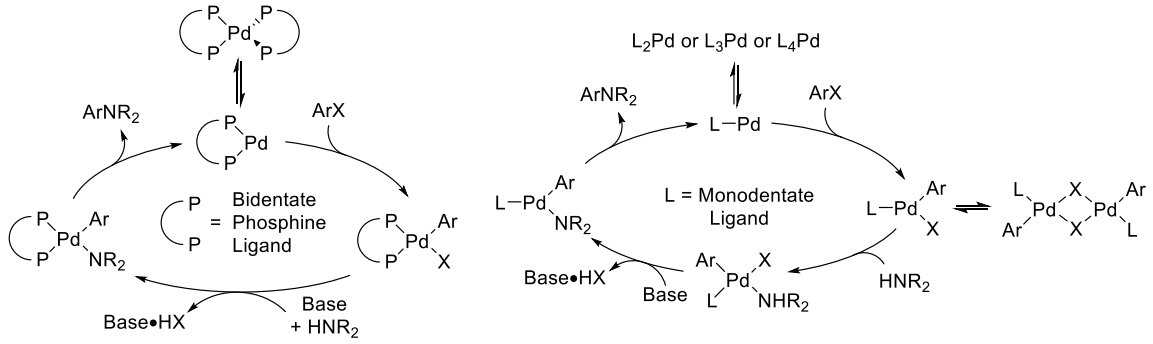

The intermediates of Ni-catalyzed C-N coupling reactions are not as easily synthesized as their palladium analogues. Pd(II) aryl halide complexes have been synthesized by a simple reaction of an aryl halide with a Pd(0) complex.[10a, 26] However, the same reaction with a Ni(0) complex often leads to unwanted comproportionation reactions between Ni(0) and Ni(II) compounds to give paramagnetic Ni(I) species.[27] Moreover, several examples of arylpalladium(II) amido species have been synthesized and demonstrated to be catalytically competent by undergoing reductive elimination to generate the C-N bond in the coupled product and Pd(0).[24b, 24d, 24f, 28] In contrast, no analogous synthesis or reactivity studies of arylnickel amido species have been reported. Together, these factors have made the development and study of Ni-catalyzed cross-coupling reactions to form C-N bonds less straightforward than its Pd-catalyzed counterpart, and mechanistic data on these Ni-catalyzed reactions are less abundant. Despite these challenges, a mechanistic study on Ni-catalyzed C-N coupling reaction involving BINAP ligated Ni catalysts revealed a mechanism involving a Ni(0)/Ni(II) pathway that closely mirrors the analogous Pd-catalyzed pathway.[18] As part of this study, odd-electron pathways involving Ni(I) or Ni(III) species were demonstrated to be non-viable reaction pathways, and the formation of dimeric Ni(I) species proved to be a catalyst

deactivation pathway. Yet, the existence and catalytic competency of a Ni(II) aryl amido species were not demonstrated directly; they were inferred from kinetic data and literature precedence.

Mechanistic studies on a nickel-catalyzed, electrochemical C-N coupling reaction implicated a Ni(I)/Ni(III) catalytic cycle, wherein oxidative addition of the haloarene occurs at a 4,4′-di-*tert*-butyl-2,2′-dipyridyl ligated Ni(I) bromide complex to give a five-coordinate arylnickel(III) dibromide species.[22b] This Ni(III) species then undergoes comproportionation with the Ni(I) species to furnish an arylnickel(II) halide complex. This species then reacts with an amine and base to generate an arylnickel(II) amido species. Instead of undergoing reductive elimination directly, this Ni(II) amido species undergoes oxidization at the anode of the electrochemical cell to produce a five-coordinate arylnickel(III) amido bromide species that undergoes reductive elimination to give the C-N bond in the coupled product. Again, independent synthesis of these arylnickel amido species in the Ni(II) or Ni(III) oxidation state was not performed, and the amido complexes were not observed experimentally. These mechanistic proposals were largely based on computational data. Thus, conflicting reports exist on the catalytic nickel species that are responsible for forming the C-N bond in this reaction, and the synthesis and the reactivity of nickel complexes bearing aryl and amido ligands relevant to C-N coupling reactions is a missing piece of the mechanism of this Ni-catalyzed protocol. Therefore, the study of these compounds and the direct interrogation of their reactivity will reveal details relevant towards the development of improved Ni-catalyzed C-N coupling methods and catalysts. Our efforts to synthesize and study the reactivity of arylnickel(II) amido complexes are described in a following chapter.

1.2 Overview of Pd-Catalyzed C-N Coupling Reactions with Hydrazine

Pd-catalyzed reactions to generate arylamines encompass a wide variety of nitrogen containing nucleophiles, but hydrazine is arguably the most difficult coupling partner to engage in this reaction. Because hydrazine is a potent reductant and can reduce catalytically active Pd(II) to form inactive Pd black,[29] careful selection of a catalyst is required to obtain the arylation of hydrazine and to avoid deactivation of the catalyst. Moreover, the product of this reaction, aryl hydrazine, is expected to be more reactive than hydrazine because aryl hydrazines contains an N-H bond that is more acidic than those in hydrazine, leading to poor selectivity for the monoarylation of hydrazine. Hydrazine also is toxic and explosive under certain conditions.[30] Due to these challenges, only three methods for Pd-catalyzed C-N coupling reactions with hydrazine have been reported thus far.[31] These published examples (Scheme 1.3) require high loadings of Pd catalyst (1-20 mol%) and stoichiometric amounts of an expensive base, NaO*t*Bu.[32] These parameters, together, belie the value of the relatively simple products of these reactions.

Scheme 1.3. Previously Reported Procedures for Pd-Catalyzed C-N Coupling Reactions with Hydrazine

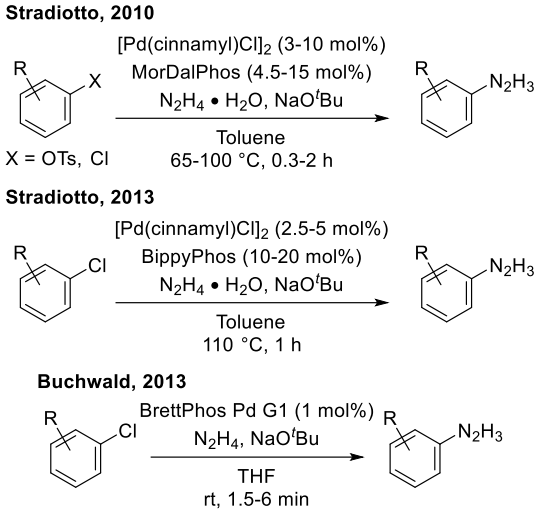

Despite these challenges, aryl hydrazines are important synthetic intermediates in the synthesis of heterocycles, such as indoles,[33] pyrazoles,[34] and triazoles,[35] which are contained in a multitude of biologically active molecules. Pharmaceuticals, such as Celebrex[36] and Rimonabant,[37] and agrochemicals, such as norflurazon[38] and flufenpyr-ethyl,[39] all contain aryl hydrazines in their synthetic routes. Existing methods to synthesize aryl hydrazine involve the diazotization of aniline, followed by reduction.[40] This process not only generates stoichiometric amounts of salt waste, but the aryl diazonium intermediates poses an explosion hazard.[40] Aryl hydrazine can also be synthesized by an S_NAr reaction between hydrazine and an aryl halide, but this reaction is limited to electron-poor arenes and heteroarenes.[41] In contrast to the multiple equivalents of salt generated from the diazotization process, a catalytic C-N coupling reaction generates one equivalent and is more atom economical. The C-N coupling reaction also is expected to be more general than an S_NAr reaction. Although there are many methods to couple aryl halides with protected hydrazines, such as hydrazones and Boc protected hydrazine, these methods require a deprotection step to reveal aryl hydrazine.[4] There are procedures to couple aryl halides with alkyl-substituted hydrazines with Pd catalysts; however, these methods are limited in scope, and the products of these reactions are less synthetically useful than their unsubstituted aryl hydrazine counterpart.[42] Thus, improved methods to produce aryl hydrazines with more economic reagents and efficient catalysts is not only an unmet need but is industrially relevant.

Although numerous mechanistic studies on Pd-catalyzed C-N coupling reactions have been published, no studies of the mechanism of C-N coupling reactions with hydrazine have been reported. The elucidation of the mechanism of C-N coupling reactions with hydrazine can provide an additional means to improve reactivity, such as the identification of deleterious and rate-limiting steps in the catalytic cycle. The reducing properties of hydrazine may lead to deactivation pathways, which may not be observed when an amine is used in place of hydrazine. In addition, the small size of hydrazine may influence the key steps in the catalytic cycle. Mechanistic studies on C-N coupling reactions with ammonia revealed that the rate-limiting step of the catalytic reaction was the reductive elimination of aniline from a Pd(II) aryl amido species.[24d] The slow reductive elimination was proposed to be due to the small size of the amido group and not due to electronic effects that largely govern the rate of reductive elimination of arylamine from

arylpalladium(II) complexes with substituted amido ligands. Due to the similar steric profiles between ammonia and hydrazine, there may be parallels in reactivity between catalysts, and their intermediates, that enable coupling reactions to form C-N bonds with those nucleophiles. Lastly, the origin of the selectivity for mono- versus polyarylation is not clear in these systems. Our efforts in developing an improved method for Pd-catalyzed C-N coupling reactions with hydrazine and the elucidation of its mechanism are described in a later chapter.

1.3 Overview of Pd-Catalyzed Carbonylative Cross-Coupling Reactions and Key Mechanistic Details of these Reactions

Pd-catalyzed carbonylative cross-coupling reactions represent a subset of cross-coupling reactions performed in the presence of carbon monoxide (CO) to furnish carbonyl containing organic molecules. Many carbonylative variants of cross-coupling methods to form C-C and C-X bonds have been disclosed. These reactions form ketones, aldehydes, amides, esters, carboxylic acids, and acid chlorides and have been utilized in industry to synthesize monomers, polymers, and pharmaceuticals.[43] Although the first report of a carbonylative cross-coupling reaction was made by Heck in the 1970s,[44] mechanistic data on these reactions are limited. One important mechanistic aspect that has gone unstudied by experimental means until recently was the oxidative addition of the aryl halide to a Pd(0) complex, which is an elementary step present in all carbonylative cross-coupling reactions with aryl halides. In the presence of CO, Pd(0) complexes form adducts with CO, and the resulting carbonyl compounds have been proposed to be inert towards oxidative addition.[45] Due to the π-acidity of CO, the CO ligands withdraw electron density from the Pd center, which deactivates the Pd(0) carbonyl species towards the oxidative addition of an aryl halide. Because of this bonding interaction between CO and Pd(0), few catalysts for these reactions react with chloroarenes.[45b, 46] In contrast, Pd catalysts that react with aryl chlorides in the absence of CO are more common.[10b] Our group recently revealed that a three-coordinate Pd(0) carbonyl species ligated by a bidentate phosphine underwent oxidative addition of a chloroarene. The identity of the three-coordinate species was revealed by the combination of spectroscopic, kinetic, and computational data and ^{13}C KIE measurements (Scheme 1.4).[47] This oxidative addition pathway is unique in that chloroarenes typically undergo oxidative addition to low-coordinate Pd(0) species, such as one-coordinate Pd(0) complexes of monodentate ligands and two-coordinate Pd(0) complexes of bidentate ligands.[10a, 26d, 26e] Grushin has also studied the oxidative addition of iodoarenes to (Xantphos)$Pd(CO)_2$ complexes by computation and concluded that the iodoarene undergoes oxidative addition to a three-coordinate Pd(0) complex bearing Xantphos and one CO ligand; however, experimental studies on this oxidative addition mechanism were not given.[48]

There are limited examples of Pd-catalyzed carbonylative cross-coupling reactions with ammonia.[43a, 49] The synthesis of primary benzamides by this method are most commonly executed with ammonia surrogates, followed by deprotection.[50] Reactions with ammonia may be difficult to achieve due to the small size of ammonia or the tendency of ammonia to form stable ammine metal complexes.[24d, 51] In one of the few studies on Pd-catalyzed aminocarbonylation, the amide product was proposed to form by C-C bond-forming reductive elimination from an arylpalladium(II) carbamoyl species ligated by triphenylphosphine.[52] However, our group recently demonstrated that benzamide forms during Pd-catalyzed aminocarbonylation with ammonia by C-N bond forming reductive elimination from a phenacylpalladium(II) amido species, which is generated by nucleophilic attack of ammonia at the palladium center of a phenacylpalladium(II) chloride complex and subsequent deprotonation by base (Scheme 1.4).[47] Additional data on the

catalytic reaction revealed that the rate-limiting step was the oxidative addition of chloroarene to a Pd(0) species and catalyst deactivation occurred by protonation of Pd(0) to furnish an inactive Pd(I) dimer containing bridging carbonyl and hydride ligands. (Scheme 1.4).[47] A more detailed examination of this mechanism is given in a subsequent chapter along with our efforts to develop a Pd-catalyzed aminocarbonylation reaction with alkyl bromides.

Scheme 1.4. Proposed Mechanism for Pd-Catalyzed Aminocarbonylation of Chloroarene with Ammonia

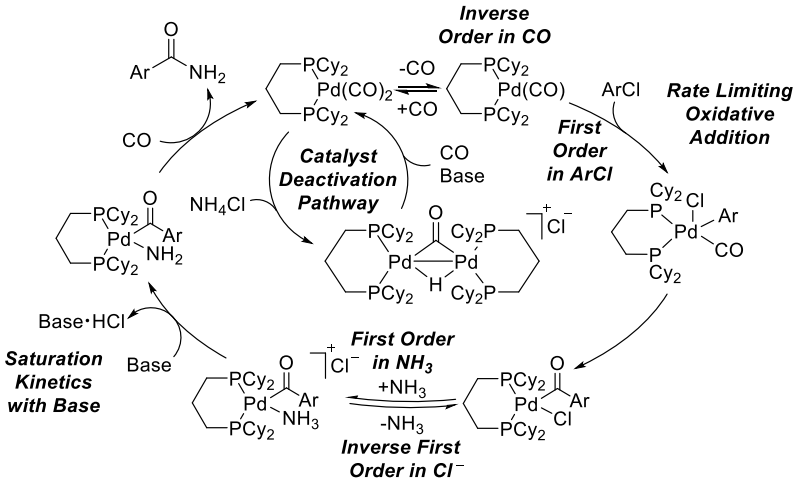

1.4 Summary and Future Directions

Pd and Ni-catalyzed C-N bond forming reactions have become indispensable tools in the synthesis of arylamines. Improvements of these methods have often occurred alongside mechanistic studies that elucidated the workings of these catalytic reactions. Mechanistic data on Pd-catalyzed aminocarbonylation reactions and C-N coupling reactions with hydrazine were limited until our studies on these C-N bond forming reactions. Additionally, we have developed preliminary systems for Pd-catalyzed aminocarbonylation of alkyl halides and methods for the synthesis of arylnickel(II) amido complexes. Future efforts involve improvements in the generality and yield in scope of the Pd-catalyzed aminocarbonylation of alkyl halides and the expansion of the library of arylnickel(II) amido complexes described in this dissertation.

1.5 References

1. (a) Johansson Seechurn, C. C. C.; Kitching, M. O.; Colacot, T. J.; Snieckus, V., Palladium-Catalyzed Cross-Coupling: A Historical Contextual Perspective to the 2010 Nobel Prize. *Angew. Chem. Int. Ed.* **2012,** *51*, 5062-5085; (b) Diccianni, J. B.; Diao, T., Mechanisms of Nickel-Catalyzed Cross-Coupling Reactions. *Trends in Chemistry* **2019,** *1*, 830-844.
2. Dorel, R.; Grugel, C. P.; Haydl, A. M., The Buchwald–Hartwig Amination After 25 Years. *Angew. Chem. Int. Ed.* **2019,** *58*, 17118-17129.
3. (a) Hartwig, J. F., Evolution of a Fourth Generation Catalyst for the Amination and Thioetherification of Aryl Halides. *Acc. Chem. Res.* **2008,** *41*, 1534-1544; (b) Yang, J.; Chen, T.; Han, L.-B., C–P Bond-Forming Reactions via C–O/P–H Cross-Coupling Catalyzed by Nickel. *J. Am. Chem. Soc.* **2015,** *137*, 1782-1785; (c) Wauters, I. D., W.; Stevens, C. V., Preparation of phosphines through C–P bond formation. *Beilstein J. Org.*

Chem. **2014,** *10*, 1064-1096; (d) Sather, A. C.; Buchwald, S. L., The Evolution of Pd0/PdII-Catalyzed Aromatic Fluorination. *Acc. Chem. Res.* **2016,** *49*, 2146-2157.

4. Ruiz-Castillo, P.; Buchwald, S. L., Applications of Palladium-Catalyzed C–N Cross-Coupling Reactions. *Chem. Rev.* **2016,** *116*, 12564-12649.
5. Kosugi, M.; Kameyama, M.; Migita, T., Palladium-Catalyzed Aromatic Amination of Aryl Bromides with N,N-Di-Ethylamino-tributyltin. *Chem. Lett.* **1983,** *12*, 927-928.
6. Hartwig, J. F., Carbon−Heteroatom Bond-Forming Reductive Eliminations of Amines, Ethers, and Sulfides. *Acc. Chem. Res.* **1998,** *31*, 852-860.
7. Louie, J.; Hartwig, J. F., Palladium-catalyzed synthesis of arylamines from aryl halides. Mechanistic studies lead to coupling in the absence of tin reagents. *Tetrahedron Lett.* **1995,** *36*, 3609-3612.
8. Guram, A. S.; Rennels, R. A.; Buchwald, S. L., A Simple Catalytic Method for the Conversion of Aryl Bromides to Arylamines. *Angew. Chem. Int. Ed. Engl.* **1995,** *34*, 1348-1350.
9. (a) Driver, M. S.; Hartwig, J. F., A Second-Generation Catalyst for Aryl Halide Amination: Mixed Secondary Amines from Aryl Halides and Primary Amines Catalyzed by (DPPF)PdCl2. *J. Am. Chem. Soc.* **1996,** *118*, 7217-7218; (b) Wolfe, J. P.; Wagaw, S.; Buchwald, S. L., An Improved Catalyst System for Aromatic Carbon−Nitrogen Bond Formation: The Possible Involvement of Bis(Phosphine) Palladium Complexes as Key Intermediates. *J. Am. Chem. Soc.* **1996,** *118*, 7215-7216.
10. (a) Senn, H. M.; Ziegler, T., Oxidative Addition of Aryl Halides to Palladium(0) Complexes: A Density-Functional Study Including Solvation. *Organometallics* **2004,** *23*, 2980-2988; (b) Littke, A. F.; Fu, G. C., Palladium-Catalyzed Coupling Reactions of Aryl Chlorides. *Angewandte Chemie International Edition* **2002,** *41*, 4176-4211.
11. Beller, M.; Riermeier, T. H.; Reisinger, C.-P.; Herrmann, W. A., First palladium-catalyzed aminations of aryl chlorides. *Tetrahedron Lett.* **1997,** *38*, 2073-2074.
12. (a) Muci, A. R.; Buchwald, S. L., Practical Palladium Catalysts for C-N and C-O Bond Formation. In *Cross-Coupling Reactions: A Practical Guide*, Miyaura, N., Ed. Springer Berlin Heidelberg: Berlin, Heidelberg, 2002; pp 131-209; (b) Stambuli, J. P.; Kuwano, R.; Hartwig, J. F., Unparalleled Rates for the Activation of Aryl Chlorides and Bromides: Coupling with Amines and Boronic Acids in Minutes at Room Temperature. *Angew. Chem. Int. Ed.* **2002,** *41*, 4746-4748; (c) Kataoka, N.; Shelby, Q.; Stambuli, J. P.; Hartwig, J. F., Air Stable, Sterically Hindered Ferrocenyl Dialkylphosphines for Palladium-Catalyzed C−C, C−N, and C−O Bond-Forming Cross-Couplings. *J. Org. Chem.* **2002,** *67*, 5553-5566; (d) Marion, N.; Nolan, S. P., Well-Defined N-Heterocyclic Carbenes−Palladium(II) Precatalysts for Cross-Coupling Reactions. *Acc. Chem. Res.* **2008,** *41*, 1440-1449.
13. (a) Shen, Q.; Ogata, T.; Hartwig, J. F., Highly Reactive, General and Long-Lived Catalysts for Palladium-Catalyzed Amination of Heteroaryl and Aryl Chlorides, Bromides, and Iodides: Scope and Structure–Activity Relationships. *J. Am. Chem. Soc.* **2008,** *130*, 6586-6596; (b) Shen, Q.; Shekhar, S.; Stambuli, J. P.; Hartwig, J. F., Highly Reactive, General, and Long-Lived Catalysts for Coupling Heteroaryl and Aryl Chlorides with Primary Nitrogen Nucleophiles. *Angew. Chem. Int. Ed.* **2005,** *44*, 1371-1375.
14. Uehling, M. R.; King, R. P.; Krska, S. W.; Cernak, T.; Buchwald, S. L., Pharmaceutical diversification via palladium oxidative addition complexes. *Science* **2019,** *363*, 405-408.
15. Wolfe, J. P.; Buchwald, S. L., Nickel-Catalyzed Amination of Aryl Chlorides. *J. Am. Chem. Soc.* **1997,** *119*, 6054-6058.

16. Brenner, E.; Fort, Y., New efficient nickel(0) catalysed amination of aryl chlorides. *Tetrahedron Lett.* **1998,** *39*, 5359-5362.
17. Manolikakes, G.; Gavryushin, A.; Knochel, P., An Efficient Silane-Promoted Nickel-Catalyzed Amination of Aryl and Heteroaryl Chlorides. *J. Org. Chem.* **2008,** *73*, 1429-1434.
18. Ge, S.; Green, R. A.; Hartwig, J. F., Controlling First-Row Catalysts: Amination of Aryl and Heteroaryl Chlorides and Bromides with Primary Aliphatic Amines Catalyzed by a BINAP-Ligated Single-Component Ni(0) Complex. *J. Am. Chem. Soc.* **2014,** *136*, 1617-1627.
19. (a) Chen; Yang, L.-M., Ni(II)−(σ-Aryl) Complex: A Facile, Efficient Catalyst for Nickel-Catalyzed Carbon−Nitrogen Coupling Reactions. *J. Org. Chem.* **2007,** *72*, 6324-6327; (b) Omar-Amrani, R.; Thomas, A.; Brenner, E.; Schneider, R.; Fort, Y., Efficient Nickel-Mediated Intramolecular Amination of Aryl Chlorides. *Org. Lett.* **2003,** *5*, 2311-2314; (c) Desmarets, C.; Schneider, R.; Fort, Y., Nickel-catalysed synthesis of 3-chloroanilines and chloro aminopyridines via cross-coupling reactions of aryl and heteroaryl dichlorides with amines. *Tetrahedron Lett.* **2001,** *42*, 247-250; (d) Park, N. H.; Teverovskiy, G.; Buchwald, S. L., Development of an Air-Stable Nickel Precatalyst for the Amination of Aryl Chlorides, Sulfamates, Mesylates, and Triflates. *Org. Lett.* **2014,** *16*, 220-223.
20. (a) Green, R. A.; Hartwig, J. F., Nickel-Catalyzed Amination of Aryl Chlorides with Ammonia or Ammonium Salts. *Angew. Chem.* **2015,** *127*, 3839-3843; (b) Borzenko, A.; Rotta-Loria, N. L.; MacQueen, P. M.; Lavoie, C. M.; McDonald, R.; Stradiotto, M., Nickel-Catalyzed Monoarylation of Ammonia. *Angew. Chem. Int. Ed.* **2015,** *54*, 3773-3777.
21. (a) Tassone, J. P.; England, E. V.; MacQueen, P. M.; Ferguson, M. J.; Stradiotto, M., PhPAd-DalPhos: Ligand-Enabled, Nickel-Catalyzed Cross-Coupling of (Hetero)aryl Electrophiles with Bulky Primary Alkylamines. *Angew. Chem. Int. Ed.* **2019,** *58*, 2485-2489; (b) Clark, J. S. K.; Ferguson, M. J.; McDonald, R.; Stradiotto, M., PAd2-DalPhos Enables the Nickel-Catalyzed C−N Cross-Coupling of Primary Heteroarylamines and (Hetero)aryl Chlorides. *Angew. Chem. Int. Ed.* **2019,** *58*, 6391-6395.
22. (a) Li, C.; Kawamata, Y.; Nakamura, H.; Vantourout, J. C.; Liu, Z.; Hou, Q.; Bao, D.; Starr, J. T.; Chen, J.; Yan, M.; Baran, P. S., Electrochemically Enabled, Nickel-Catalyzed Amination. *Angew. Chem. Int. Ed.* **2017,** *56*, 13088-13093; (b) Kawamata, Y.; Vantourout, J. C.; Hickey, D. P.; Bai, P.; Chen, L.; Hou, Q.; Qiao, W.; Barman, K.; Edwards, M. A.; Garrido-Castro, A. F.; deGruyter, J. N.; Nakamura, H.; Knouse, K.; Qin, C.; Clay, K. J.; Bao, D.; Li, C.; Starr, J. T.; Garcia-Irizarry, C.; Sach, N.; White, H. S.; Neurock, M.; Minteer, S. D.; Baran, P. S., Electrochemically Driven, Ni-Catalyzed Aryl Amination: Scope, Mechanism, and Applications. *J. Am. Chem. Soc.* **2019,** *141*, 6392-6402.
23. Lim, C.-H.; Kudisch, M.; Liu, B.; Miyake, G. M., C–N Cross-Coupling via Photoexcitation of Nickel–Amine Complexes. *J. Am. Chem. Soc.* **2018,** *140*, 7667-7673.
24. (a) Paul, F.; Patt, J.; Hartwig, J. F., Palladium-catalyzed formation of carbon-nitrogen bonds. Reaction intermediates and catalyst improvements in the hetero cross-coupling of aryl halides and tin amides. *J. Am. Chem. Soc.* **1994,** *116*, 5969-5970; (b) Driver, M. S.; Hartwig, J. F., Energetics and Mechanism of Alkylamine N−H Bond Cleavage by Palladium Hydroxides: N−H Activation by Unusual Acid−Base Chemistry. *Organometallics* **1997,** *16*, 5706-5715; (c) Shekhar, S.; Ryberg, P.; Hartwig, J. F.; Mathew, J. S.; Blackmond, D. G.; Strieter, E. R.; Buchwald, S. L., Reevaluation of the Mechanism of the Amination of Aryl Halides Catalyzed by BINAP-Ligated Palladium Complexes. *J.*

Am. Chem. Soc. **2006,** *128*, 3584-3591; (d) Klinkenberg, J. L.; Hartwig, J. F., Slow Reductive Elimination from Arylpalladium Parent Amido Complexes. *Journal of the American Chemical Society* **2010,** *132*, 11830-11833; (e) Brusoe, A. T.; Hartwig, J. F., Palladium-Catalyzed Arylation of Fluoroalkylamines. *J. Am. Chem. Soc.* **2015,** *137*, 8460-8468; (f) Arrechea, P. L.; Buchwald, S. L., Biaryl Phosphine Based Pd(II) Amido Complexes: The Effect of Ligand Structure on Reductive Elimination. *J. Am. Chem. Soc.* **2016,** *138*, 12486-12493.

25. Diccianni, J. B.; Katigbak, J.; Hu, C.; Diao, T., Mechanistic Characterization of (Xantphos)Ni(I)-Mediated Alkyl Bromide Activation: Oxidative Addition, Electron Transfer, or Halogen-Atom Abstraction. *J. Am. Chem. Soc.* **2019,** *141*, 1788-1796.
26. (a) Roy, A. H.; Hartwig, J. F., Reductive Elimination of Aryl Halides from Palladium(II). *J. Am. Chem. Soc.* **2001,** *123*, 1232-1233; (b) Portnoy, M.; Milstein, D., Mechanism of aryl chloride oxidative addition to chelated palladium(0) complexes. *Organometallics* **1993,** *12*, 1665-1673; (c) Amatore, C.; Pfluger, F., Mechanism of oxidative addition of palladium(0) with aromatic iodides in toluene, monitored at ultramicroelectrodes. *Organometallics* **1990,** *9*, 2276-2282; (d) Barrios-Landeros, F.; Hartwig, J. F., Distinct Mechanisms for the Oxidative Addition of Chloro-, Bromo-, and Iodoarenes to a Bisphosphine Palladium(0) Complex with Hindered Ligands. *J. Am. Chem. Soc.* **2005,** *127*, 6944-6945; (e) Barrios-Landeros, F.; Carrow, B. P.; Hartwig, J. F., Effect of Ligand Steric Properties and Halide Identity on the Mechanism for Oxidative Addition of Haloarenes to Trialkylphosphine Pd(0) Complexes. *Journal of the American Chemical Society* **2009,** *131*, 8141-8154.
27. (a) Tsou, T. T.; Kochi, J. K., Mechanism of oxidative addition. Reaction of nickel(0) complexes with aromatic halides. *J. Am. Chem. Soc.* **1979,** *101*, 6319-6332; (b) Bajo, S.; Laidlaw, G.; Kennedy, A. R.; Sproules, S.; Nelson, D. J., Oxidative Addition of Aryl Electrophiles to a Prototypical Nickel(0) Complex: Mechanism and Structure/Reactivity Relationships. *Organometallics* **2017,** *36*, 1662-1672.
28. Yamashita, M.; Hartwig, J. F., Synthesis, Structure, and Reductive Elimination Chemistry of Three-Coordinate Arylpalladium Amido Complexes. *J. Am. Chem. Soc.* **2004,** *126*, 5344-5345.
29. Wang, Y.; Shi, Y.-F.; Chen, Y.-B.; Wu, L.-M., Hydrazine reduction of metal ions to porous submicro-structures of Ag, Pd, Cu, Ni, and Bi. *J. Solid State Chem.* **2012,** *191*, 19-26.
30. Niemeier, J. K.; Kjell, D. P., Hydrazine and Aqueous Hydrazine Solutions: Evaluating Safety in Chemical Processes. *Org. Process Res. Dev.* **2013,** *17*, 1580-1590.
31. (a) DeAngelis, A.; Wang, D.-H.; Buchwald, S. L., Mild and Rapid Pd-Catalyzed Cross-Coupling with Hydrazine in Continuous Flow: Application to the Synthesis of Functionalized Heterocycles. *Angew. Chem. Int. Ed.* **2013,** *52*, 3434-3437; (b) Lundgren, R. J.; Stradiotto, M., Palladium-Catalyzed Cross-Coupling of Aryl Chlorides and Tosylates with Hydrazine. *Angew. Chem. Int. Ed.* **2010,** *49*, 8686-8690.
32. Schlummer, B.; Scholz, U., Palladium-Catalyzed C–N and C–O Coupling–A Practical Guide from an Industrial Vantage Point. *Adv. Synth. Catal.* **2004,** *346*, 1599-1626.
33. Katrizky, A. R.; Pozharskii, A. F., *Handbook of Heterocyclic Chemistry*. 2nd ed.; Pergamon: Oxford, 2000.
34. Karrouchi, K.; Radi, S.; Ramli, Y.; Taoufik, J.; Mabkhot, Y. N.; Al-aizari, F. A.; Ansar, M. h., Synthesis and Pharmacological Activities of Pyrazole Derivatives: A Review. *Molecules* **2018,** *23*, 134.

35. Potts, K. T., The Chemistry of 1,2,4-Triazoles. *Chem. Rev.* **1961,** *61*, 87-127.
36. Habeeb, A. G.; Praveen Rao, P. N.; Knaus, E. E., Design and Synthesis of Celecoxib and Rofecoxib Analogues as Selective Cyclooxygenase-2 (COX-2) Inhibitors: Replacement of Sulfonamide and Methylsulfonyl Pharmacophores by an Azido Bioisostere. *J. Med. Chem.* **2001,** *44*, 3039-3042.
37. Kotagiri, V. K.; Suthrapu, S.; Mukunda Reddy, J.; Prasad Rao, C.; Bollugoddu, V.; Bhattacharya, A.; Bandichhor, R., An Improved Synthesis of Rimonabant: Anti-Obesity Drug. *Org. Process Res. Dev.* **2007,** *11*, 910-912.
38. Hamprecht, G.; Witschel, M.; Hawkes, T. R.; Edmunds, A. J. F.; Morris, J. A.; van Almsick, A., Herbicides with Bleaching Properties. In *Modern Crop Protection Compounds*, Wiley-VCH Verlag & Co. KGaA: Weinheim, Germany, 2011; pp 197-276.
39. Theodoridis, G.; Liebl, R.; Zagar, C., Protoporphyrinogen IX Oxidase Inhibitors. In *Modern Crop Protection Compounds*, Wiley-VCH Verlag & Co. KGaA: Weinheim, Germany, 2011; pp 163-195.
40. Schirmann, J.-P.; Bourdauducq, P., Hydrazine. In *Ullmann's Encylopedia of Industrial Chemistry*, John Wiley and Sons: New York, 2001.
41. (a) Charier, S.; Ruel, O.; Baudin, J.-B.; Alcor, D.; Allemand, J.-F.; Meglio, A.; Jullien, L., An Efficient Fluorescent Probe for Ratiometric pH Measurements in Aqueous Solutions. *Angew. Chem.* **2004,** *116*, 4889-4892; (b) Sánchez, B.; Calderón, C.; Tapia, R. A.; Contreras, R.; Campodónico, P. R., Activation of Electrophile/Nucleophile Pair by a Nucleophilic and Electrophilic Solvation in a SNAr Reaction. *Front. Chem.* **2018,** *6*; (c) Wilsily, A.; Mennen, S. M.; Cosbie, A.; Milne, J. E., Synthesis of the Hydrazinyl Pyridine Intermediate: Phase-Appropriate Delivery. *Org. Process Res. Dev.* **2017,** *21*, 1286-1293; (d) Cho, H.-J.; Um, I.-H., The α-Effect in SNAr Reaction of 1-Fluoro-2,4-dinitrobenzene with Hydrazine: Ground-State Destabilization versus Transition-State Stabilization. *Bull. Korean Chem. Soc.* **2014,** *35*, 2371-2374; (e) Cho, H.-J.; Kim, M.-Y.; Um, I.-H., The α-Effect in SNAr Reaction of Y-Substituted-Phenoxy-2,4-Dinitrobenzenes with Amines: Reaction Mechanism and Origin of the α-Effect. *Bull. Korean Chem. Soc.* **2014,** *35*, 2448-2452.
42. (a) Siva Kumar, K.; Mahesh Kumar, P.; Sreenivasa Rao, V.; Jafar, A. A.; Meda, C. L. T.; Kapavarapu, R.; Parsa, K. V. L.; Pal, M., A new cascade reaction: concurrent construction of six and five membered rings leading to novel fused quinazolinones. Org. Biomol. Chem. 2012, 10, 3098-3103; (b) Liu, X.; Barry, M.; Tsou, H.-R., Palladium-catalyzed arylation of N,N-dialkylhydrazines and the subsequent conversion to anilines. Tetrahedron Lett. 2007, 48, 8409-8412; (c) Cacchi, S.; Fabrizi, G.; Goggiamani, A.; Sgalla, S., Palladium-Catalyzed N-Arylation of N,N-Dialkylhydrazines with Aryl Chlorides. Adv. Synth. Catal. 2007, 349, 453-458; (d) Cacchi, S.; Fabrizi, G.; Goggiamani, A.; Licandro, E.; Maiorana, S.; Perdicchia, D., Synthesis of N,N-Dialkyl-N'-arylhydrazines via Palladium-Catalyzed N-Arylation by Using N,N-Dialkylhydrazines/2LiCl Adducts. Org. Lett. 2005, 7, 1497-1500.
43. (a) Barnard, C. F. J., Palladium-catalyzed carbonylation - A reaction come of age. *Organometallics* **2008,** *27*, 5402-5422; (b) Magano, J.; Dunetz, J. R., Large-Scale Applications of Transition Metal-Catalyzed Couplings for the Synthesis of Pharmaceuticals. *Chemical Reviews* **2011,** *111*, 2177-2250; (c) Brennführer, A.; Neumann, H.; Beller, M., Palladium-Catalyzed Carbonylation Reactions of Aryl Halides and Related Compounds. *Angewandte Chemie International Edition* **2009,** *48*, 4114-4133; (d) Quesnel,

J. S.; Kayser, L. V.; Fabrikant, A.; Arndtsen, B. A., Acid Chloride Synthesis by the Palladium-Catalyzed Chlorocarbonylation of Aryl Bromides. *Chem. Eur. J.* **2015,** *21*, 9550-9555; (e) Quesnel, J. S.; Arndtsen, B. A., A Palladium-Catalyzed Carbonylation Approach to Acid Chloride Synthesis. *Journal of the American Chemical Society* **2013,** *135*, 16841-16844.

44. Schoenberg, A.; Bartoletti, I.; Heck, R. F., Palladium-catalyzed carboalkoxylation of aryl, benzyl, and vinylic halides. *The Journal of Organic Chemistry* **1974,** *39*, 3318-3326.
45. (a) Sergeev, A.; Spannenberg, A.; Beller, M., Palladium-catalyzed formylation of aryl bromides: Elucidation of the catalytic cycle of an industrially applied coupling reaction. *Journal of the American Chemical Society* **2008,** *130*, 15549-15563; (b) Ben-David, Y.; Portnoy, M.; Milstein, D., Chelate-assisted, palladium-catalyzed efficient carbonylation of aryl chlorides. *J. Am. Chem. Soc.* **1989,** *111*, 8742-8744.
46. (a) Jimenez-Rodriguez, C.; Eastham, G. R.; Cole-Hamilton, D. J., The methoxycarbonylation of aryl chlorides catalysed by palladium complexes of bis(di-tert-butylphosphinomethyl)benzene. *Dalton Transactions* **2005**, 1826-1830; (b) Lagerlund, O.; Larhed, M., Microwave-Promoted Aminocarbonylations of Aryl Chlorides Using Mo(CO)6 as a Solid Carbon Monoxide Source. *Journal of Combinatorial Chemistry* **2006,** *8*, 4-6; (c) Lundgren, R. J.; Peters, B. D.; Alsabeh, P. G.; Stradiotto, M., A P,N-Ligand for Palladium-Catalyzed Ammonia Arylation: Coupling of Deactivated Aryl Chlorides, Chemoselective Arylations, and Room Temperature Reactions. *Angewandte Chemie International Edition* **2010,** *49*, 4071-4074; (d) Martinelli, J. R.; Clark, T. P.; Watson, D. A.; Munday, R. H.; Buchwald, S. L., Palladium-catalyzed aminocarbonylation of aryl chlorides at atmospheric pressure: The dual role of sodium phenoxide. *Angewandte Chemie International Edition* **2007,** *46*, 8460-8463.
47. Wang, J. Y.; Strom, A. E.; Hartwig, J. F., Mechanistic Studies of Palladium-Catalyzed Aminocarbonylation of Aryl Chlorides with Carbon Monoxide and Ammonia. *J. Am. Chem. Soc.* **2018,** *140*, 7979-7993.
48. Miloserdov, F. M.; McMullin, C. L.; Belmonte, M. M.; Benet-Buchholz, J.; Bakhmutov, V. I.; Macgregor, S. A.; Grushin, V. V., The challenge of palladium-catalyzed aromatic azidocarbonylation: From mechanistic and catalyst deactivation studies to a highly efficient process. *Organometallics* **2014,** *33*, 736-752.
49. (a) Wu, X.-F.; Neumann, H.; Beller, M., Development of a Second Generation Palladium Catalyst System for the Aminocarbonylation of Aryl Halides with CO and Ammonia. *Chemistry - An Asian Journal* **2010,** *5*, 2168-2172; (b) Alsabeh, P. G.; Stradiotto, M.; Neumann, H.; Beller, M., Aminocarbonylation of (Hetero)aryl bromides with ammonia and amines using a palladium/dalphos catalyst system. *Advanced Synthesis and Catalysis* **2012,** *354*, 3065-3070; (c) Xu, T.; Alper, H., Palladium-catalyzed aminocarbonylation of aryl iodides using aqueous ammonia. *Tetrahedron Letters* **2013,** *54*, 5496-5499.
50. (a) Schnyder, A.; Beller, M.; Mehltretter, G.; Nsenda, T.; Studer, M.; Indolese, A. F., Synthesis of primary aromatic amides by aminocarbonylation of aryl halides using formamide as an ammonia synthon. *J. Org. Chem.* **2001,** *66*, 4311-4315; (b) Wan, Y.; Alterman, M.; Larhed, M.; Hallberg, A., Formamide as a Combined Ammonia Synthon and Carbon Monoxide Source in Fast Palladium-Catalyzed Aminocarbonylations of Aryl Halides. *Journal of Combinatorial Chemistry* **2003,** *5*, 82-84; (c) Wu, X.; Wannberg, J.; Larhed, M., Hydroxylamine as an ammonia equivalent in microwave-enhanced aminocarbonylations. *Tetrahedron* **2006,** *62*, 4665-4670.

51. Klinkenberg, J. L.; Hartwig, J. F., Catalytic Organometallic Reactions of Ammonia. *Angewandte Chemie International Edition* **2011,** *50*, 86-95.
52. Ozawa, F.; Soyama, H.; Yanagihara, H.; Aoyama, I.; Takino, H.; Izawa, K.; Yamamoto, T.; Yamamoto, A., Palladium-catalyzed double carbonylation of aryl halides to give α-keto amides. Mechanistic studies. *J. Am. Chem. Soc.* **1985,** *107*, 3235-3245.

CHAPTER 2

MECHANISTIC STUDIES OF PALLADIUM-CATALYZED AMINOCARBONYLATION OF ARYL CHLORIDES WITH CARBON MONOXIDE AND AMMONIA

2.1 Introduction

Palladium-catalyzed carbonylation reactions of aryl halides and pseudohalides furnish aromatic ketones,[53] aldehydes,[54] amides,[46d, 55] esters,[44, 56] and other carboxylic acid derivatives.[43e, 57] These processes have been used in industry to create pharmaceuticals, agrochemicals, and dyes.[43b, 43c] For example, lazabemide, a monoamine oxidase B inhibitor, was prepared in one step by the palladium-catalyzed aminocarbonylation of 2,5-dichloropyridine.[58] An intermediate in the synthesis of a GPIIb/IIa receptor antagonist was also synthesized by palladium-catalyzed aminocarbonylation of a highly functionalized aryl iodide on a 40 kg scale.[59] Finally, the reductive carbonylation of aryl halides with a palladium catalyst has been conducted on a >100 kg scale.[60]

Despite the broad scope and utility of palladium-catalyzed carbonylations of aryl halides, most of the steps of these reactions are poorly defined (Figure 2.1).[45a, 48, 61] The migratory insertion of CO into square planar arylpalladium halide complexes is fast and has been proposed to occur via a five-coordinate intermediate,[62] but few studies on the mechanism for oxidative addition of aryl halides in the presence of CO have been reported,[48] few studies on the reactions of amines with acylpalladium complexes have been published,[63] and no examples of the reactions of ammonia with acylpalladium complexes have been described. Pd(0) carbonyl complexes have been proposed as intermediates when reactions are conducted in the presence of carbon monoxide, but often such compounds containing ligands used for these carbonylation reactions have not been isolated and examples of the reactions of Pd(0) carbonyl complexes with aryl halides are limited.[52, 64, 65] The mechanism of oxidative addition of aryl halides in the presence of CO has been proposed to be distinct from the mechanism of oxidative addition of the same aryl halide during palladium-catalyzed coupling in the absence of CO. This difference results from the unproductive equilibria between active Pd(0) complexes lacking CO and inactive Pd(0) carbonyl adducts or clusters.[45a, 64] Although bidentate phosphines often have been used as ancillary ligands to discourage aggregation of Pd(0) compounds, monomeric Pd(0) complexes of these ligands in the presence of CO can contain one or two CO ligands, and they can associate to form bimetallic dimers containing a bridging CO moiety.[66] It is unclear which of these compounds undergo oxidative addition of the aryl halide. In one of the few studies on the oxidative additions of aryl halides to Pd(0)-carbonyl complexes, Grushin conducted the oxidative addition of aryl iodides to (Xantphos)$Pd(CO)_2$[48] to form a phenacyl Pd(II) iodide complex. However, experimental studies to reveal the Pd(0) species that reacts with the aryl halide were not reported; the mechanism of this oxidative addition was only explored computationally.

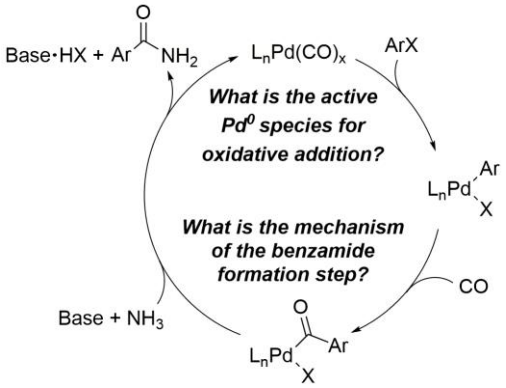

Figure 2.1. Simplified catalytic cycle for the aminocarbonylation of aryl halides with Pd and ammonia including questions about mechanistic details .

Data on the mechanism of the catalytic carbonylation of aryl chlorides and data on the oxidative addition of aryl chlorides to Pd(0) in the presence of CO are particularly scarce.[43c] Catalytic carbonylations of aryl chlorides are attractive because aryl chlorides are more commercially available and less expensive than other aryl halides.[10b, 67] However, the oxidative addition of aryl chlorides to Pd(0) in the presence of CO and the overall carbonylation of aryl chlorides is likely to be slow because the oxidative addition of aryl chlorides occurs most rapidly with low-coordinate, electron-rich Pd(0) species and the binding of CO makes the electron density lower and the coordination number higher than those in homoleptic Pd(0) phosphine complexes.[26e, 43c] Indeed, many methods for the carbonylation of aryl or heteroaryl chlorides require high temperatures ($\geq$ 100 °C),[46a, 46b, 64, 68] presumably to cause dissociation of CO from Pd(0) or separation of Pd(0) carbonyl clusters. Thus, an improved understanding of the identity of the palladium complex that reacts with the aryl chloride could enable the discovery of new carbonylations and catalysts that induce milder carbonylations of aryl chlorides.

In addition to the ambiguity about the mechanism of the oxidative addition of aryl halides to Pd(0) in the presence of CO, the mechanism of the reaction of acylpalladium complexes with nucleophiles is unclear. The mechanism of the reaction of phenacylpalladium complexes with alcohols to generate phenyl esters has been examined,[69] but few studies of the analogous reactions with amines have been conducted.[52, 63] Alcohols are typically more acidic than amines; therefore, alkoxides can be generated *in situ* during catalysis under basic conditions, and either the alcohol or the alkoxide could serve as coupling partner. In contrast, anionic amides are unlikely to be generated. Moreover, the coordinating ability and nucleophilicity of alcohols and alkoxides is much different from that of amines, leading to differences between the mechanism for the reaction of acyl complexes with oxygen-based nucleophiles and the mechanism for reactions with nitrogen-based nucleophiles. For example, the formation of phenyl esters from *trans*-$(PPh_3)_2Pd(COPh)I$ was suggested by Yamamoto to involve displacement of PPh_3 by an alcohol.[70] Upon deprotonation of the bound alcohol and extrusion of iodide, $(PPh_3)Pd(COPh)(OR)$ underwent reductive elimination of an ester. In contrast, the formation of benzamide was proposed to occur by substitution of iodide from *trans*-$(PPh_2Me)_2Pd(Ar)I$ by CO to generate a cationic Pd(II) carbonyl species, nucleophilic attack of amine on the bound CO, deprotonation of the ammonium nitrogen to form an arylpalladium carbamoyl complex, and reductive elimination of benzamide by formation of a carbon-carbon bond.[52] The difference between the mechanisms proposed to be followed with an alcohol and amine and the required displacement of phosphine and iodide for these paths make it even less clear how the aminocarbonylation of an aryl chloride with a catalyst containing a bidentate ligand and ammonia as nucleophile would occur (Figure 2.1).

The synthesis of primary benzamides by palladium-catalyzed carbonylation of aryl halides with ammonia is one of the least explored versions of carbonylative couplings.[49a, 68c] Palladium-catalyzed carbonylation reactions to form primary benzamides are typically conducted with ammonia surrogates, followed by deprotection.[50] While procedures involving ammonia or ammonium salts to generate primary benzamides exist, they are limited in number.[43a, 49b, 49c] Reactions to form primary amides with ammonia may be particularly difficult to achieve, due to the low nucleophilicity of ammonia,[71] the slow reductive elimination from Pd(II) complexes containing unsubstituted amido groups (i.e. $-NH_2$),[24d] and the tendency of ammonia to poison transition metal catalysts.[51] Thus, the challenge of achieving the aminocarbonylation of aryl halides directly with ammonia prompted us to identify a system that catalyzes the aminocarbonylation of aryl halides with ammonia as the nucleophile.

Herein, we report the aminocarbonylation of aryl chlorides with ammonia to form primary benzamides catalyzed by a Pd(0) complex of 1,3-(dicyclohexylphosphino)propane (DCPP) and describe detailed mechanistic studies of the reaction. A series of intermediates in the catalytic cycle were prepared independently and demonstrated to be competent reaction intermediates. Aryl chlorides and bromides were shown to react with a three-coordinate Pd(0) complex bearing a bidentate phosphine and a carbonyl ligand generated by dissociation of CO from the more stable dicarbonyl complex. A primary ^{13}C kinetic isotope effect and a Hammett analysis of the effect of the electronic properties of aryl chlorides showed that the reaction of the chloroarene with the palladium complex is irreversible, involves cleavage of the carbon-halogen bond, and occurs by the same concerted, non-ionic C–Cl cleavage as the oxidative addition of aryl halides to lower-coordinate Pd(0) species. Our data show that benzamide forms from the resulting phenacylpalladium chloride intermediate by an inner-sphere pathway during which ammonia displaces chloride from a phenacylpalladium chloride complex to generate a cationic Pd(II) ammine complex. This ammine complex undergoes deprotonation to furnish a phenacyl Pd(II) amido complex, which reductively eliminates benzamide. Overall, the rate-limiting step of the aminocarbonylation of aryl chlorides with ammonia was found to be the oxidative addition of an aryl chloride to Pd(0). Finally, a catalyst deactivation pathway involving the protonation of a dicarbonyl Pd(0) complex ligated by DCPP with NH_4Cl to produce a cationic, dimeric Pd(I) complex was revealed. Thus, our studies provide a rare experimental foundation for deducing the full mechanism of a palladium-catalyzed carbonylation process as well as data on the individual steps for valuable carbonylations of aryl chlorides with ammonia.

2.2 Results and Discussion

Identification of a Reaction System for Studies on the Mechanism of Aminocarbonylation of Aryl Chlorides with Ammonia.

Table 2.1. Effect of reaction conditions on the aminocarbonylation of *p*-chlorotoluene.[a]

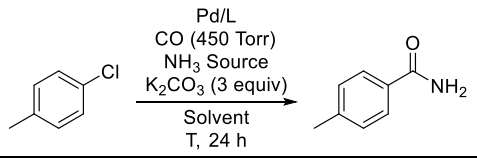

Entry	[Pd] (mol%)	L (mol %)	NH_3 Source (equiv)	Solvent	T (°C)	Yield (%)
1[b]	(DCPP)Pd(OAc)$_2$ (2)	-	NH_4Cl (1.1)	NMP	120	0
2	Pd(OAc)$_2$, (2.5)	DCPP·2HBF$_4$ (5)	NH_3 (4)	DMSO	120	50
3	Pd(OAc)$_2$, (2.5)	DCPP (5)	NH_3 (4)	DMSO	120	80
4	**1** (2.5)	-	NH_3 (4)	DMSO	110	91

[a]Reaction conditions: *p*-chlorotoluene (0.4 mmol), CO (450 Torr), K_2CO_3 (3 equiv), 0.5 mL solvent, 24 h, 25 mL Schlenk vessel. [b]760 Torr of CO. [c]Determined by NMR spectroscopy.

We chose to study the mechanism of palladium-catalyzed carbonylative couplings of chloroarenes with ammonia as the nucleophile because of the simplicity of these reagents and the synthetic value of the formation of primary benzamides. However, identifying a suitable system for mechanistic studies was not straightforward. Buchwald published aminocarbonylations of aryl halides with primary and secondary amines catalyzed by Pd(OAc)$_2$ and DCPP (1,3-bis(dicyclohexylphosphino)propane), but they showed that these reactions occur by phenoxycarbonylation of the aryl halide with the phenoxide base to form phenyl esters which subsequently react with amines to form amides. Thus, the catalytic process was not an

aminocarbonylation, and the insolubility of the phenoxide base would complicate mechanistic studies. Beller published the aminocarbonylations of aryl bromides with ammonia, but the analogous reactions of aryl chlorides, particularly those of electron-neutral aryl chlorides, occurred in low yield.[49a, 68c] Barnard published the most striking system for the aminocarbonylation of chloroarenes with ammonium chloride in a review. The reaction was reported to occur with 1 bar of CO at 100-120 °C with a catalyst generated from $Pd(OAc)_2$ and DCPP.[43a] The scope of the reaction in the review was limited to two examples of aryl chlorides, but the work by Buchwald suggested that (DCPP)Pd(0) complexes could catalyze the carbonylation of electron-rich and electron-poor aryl chlorides in the presence of 1 atm of CO.[46d] DCPP is similar to the 1,3-bis(diisopropyphosphino)propane ligand in some of the earliest publications by Milstein on palladium-catalyzed alkoxy- and aminocarbonylations of aryl chlorides with CO.[64]

Thus, we conducted studies to assess the scope of the aminocarbonylation of chloroarenes with ammonia catalyzed by DCPP complexes of palladium. We conducted initial studies on the reaction of *p*-chlorotoluene in the presence of ammonia or ammonium salts and low pressures of CO (Table 2.1) published by Barnard. The conditions for reactions of ammonium chloride did not form *p*-toluamide (Table 2.1, entry 1) in our hands, but reactions with gaseous ammonia afforded a measurable yield of the benzamide (entry 2). Reactions with a catalyst generated from the free base of DCPP (entry 3) formed *p*-toluamide in higher yields than those initiated with the HBF_4 salt of DCPP (entry 2). Ultimately, we found that reactions catalyzed by the ethylene complex **1** shown in Scheme 2.1 occurred in a high 91% yield (entry 4), even at 110 °C instead of 120 °C, with 450 Torr of CO.

Scheme 2.1. Synthesis of (DCPP)Pd(C_2H_4) (**1**) from Pd[P(^{t}Bu)$_3$]$_2$.

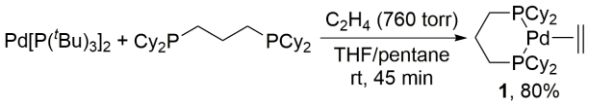

Ethylene complex **1** was synthesized by bubbling ethylene through a solution of Pd[P(^{t}Bu$_3$)]$_2$ and DCPP. Complex **1** was characterized by NMR spectroscopy, elemental analysis, and X-ray crystallography. We used complex **1** as a catalyst precursor because Bunel and Pörschke previously showed that the addition of CO to structurally analogous Pd ethylene complexes bearing bidentate phosphines rapidly formed (bisphosphine)$Pd(CO)_2$ complexes.[72] By starting with the ethylene complex, the carbonylation reactions would occur without induction periods that could result from reduction of Pd(II) to Pd(0).

A summary of our assessment of the scope of the aminocarbonylation is shown in Table 2.2. With 2.5 mol% of ethylene complex **1** as a precatalyst, 450 Torr of CO, and 4 equiv of ammonia, chlorobenzene (**2a**) formed benzamide (**3a**) in 83% yield. Electronically deactivated aryl chlorides **2b-d** underwent the aminocarbonylation process in good yields (75-89%). The sterically hindered and electron-rich aryl chloride **2e** underwent carbonylation, in a lower, but acceptable, yield of 62%. Reactions with electron-poor aryl chlorides **2f-j** afforded the corresponding benzamides **3f-j** in 60-100% yields, showing the compatibility of the reaction with a bulky ester (**2h**), cyano group (**2i**), and extended π systems (**2j**). Reactions with the heteroaryl chlorides 3-chloropyridine (**2k**) and 2-chlorothiophene (**2i**) generated the corresponding heteroaromatic benzamides **3k** and **3l** in 77% yield and 69% yield, respectively. Thus, complex **1**

catalyzes the aminocarbonylation of a broad set of aryl chlorides with ammonia, and mechanistic studies on this system, therefore, would involve a system that is synthetically valuable.

Table 2.2. Scope of palladium-catalyzed aminocarbonylation of aryl chlorides with ammonia.[a]

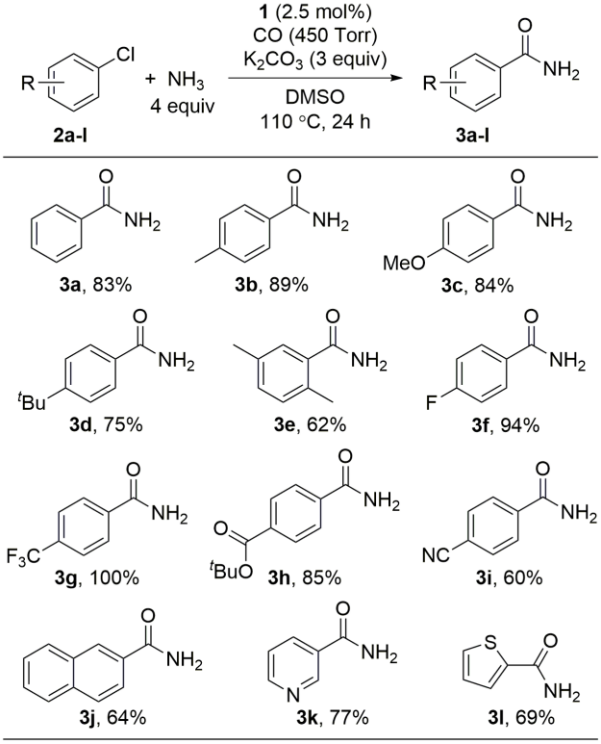

[a]Reactions were performed in a 25 mL Schlenk vessel on a 0.4 mmol scale in 0.5 mL of solvent, and yields are reported as isolated yields.

Identification of Pd(0) Carbonyl Adducts

To initiate our studies on the mechanism of the aminocarbonylation of chloroarenes with ammonia, we prepared the Pd(0) carbonyl compound ligated by DCPP. The stable carbonyl complex that would be present in the catalytic system was generated by the addition of 1000 Torr of CO to ethylene complex **1**. The dicarbonyl compound (DCPP)Pd(CO)$_2$ (**4**) was generated within 5 minutes in 98% yield. The ^{31}P NMR spectrum consisted of a singlet resonance at 20.8 ppm, and the ^{13}C NMR spectrum consisted of a broad resonance at 196.7 ppm for a carbonyl ligand. To determine the number and bonding mode of CO ligands bound to **4** under conditions relevant to the catalytic process, we measured solution-phase IR spectra of the (DCPP)Pd(0) carbonyl compound generated from **1** under 760 Torr of CO in a mixture of DMSO and toluene (1:1 v/v).[73] Two C–O stretches were observed at 1993 and 1949 cm^{-1} (see Supporting Information), which is consistent with the formulation of the Pd(0) species as a tetrahedral complex with C_{2v} symmetry containing two terminal carbonyl ligands. The solid-state structure of Pd(0) complex **4** was determined by X-ray crystallography (Figure 2.2). In the solid state, this complex displays a distorted tetrahedral geometry in which the propyl backbone of DCPP constrains the P1-Pd1-P2 angle to 98.84(3)° and the C1-Pd1-C2 angle is 110.98(6)°. The C1–O1 and C2–O2 bond distances (1.132(5) and 1.147(5) Å, respectively) are indicative of metal-to-ligand π-backbonding and are similar to those of other previously reported mononuclear Pd(0) complexes containing terminal

CO ligands.[48, 72a, 74] Dicarbonyl compound **4**, as a solid or in solution, is only briefly stable in the absence of CO.

Scheme 2.2. Synthesis of (DCPP)Pd(CO)$_2$ (**4**) from ethylene complex **1**.

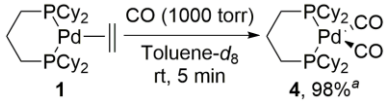

[a]Yield determined by ^{31}P NMR spectroscopy with PMes$_3$ as an internal standard.

To evaluate if dicarbonyl **4** remains intact at elevated temperatures, solution-IR spectra were obtained at 75 °C under 760 Torr of CO in a variable temperature IR cell. Two stretches at 1993 and 1949 cm^{-1} were detected, indicating that the Pd(0) complex retains both carbonyl ligands at elevated temperatures. To determine if the speciation of (DCPP)Pd(0) carbonyl compounds is dependent on CO pressure, the headspace of a solution of **4** was briefly flushed with nitrogen. The solution-IR spectrum of an aliquot of this solution contained the same two C–O stretches at 1993 and 1949 cm^{-1} at room temperature and stretches at 1994 and 1948 cm^{-1} at 75 °C (see Supporting Information). Thus, at both one atmosphere of CO and low pressures of CO, dicarbonyl compound **4** was the sole carbonyl compound observed.

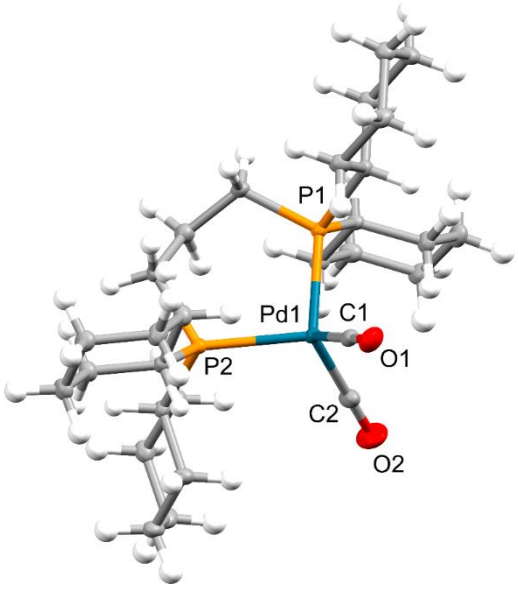

Figure 2.2. Solid state structure of (DCPP)Pd(CO)$_2$ (**4**) with ellipsoids set to 50%. Selected bond lengths (Å): P1-Pd1 2.3799(6), Pd1-C1 1.961(4), Pd1-C2 1.944(4), C1-O1 1.132(5), C2-O2 1.147(5). Selected bond angles (°): P1-Pd-P2 98.84(3), C1-Pd1-P1 110.98(6), C1-Pd1-P2 110.98(6), C1-Pd1-C2 113.83(16).

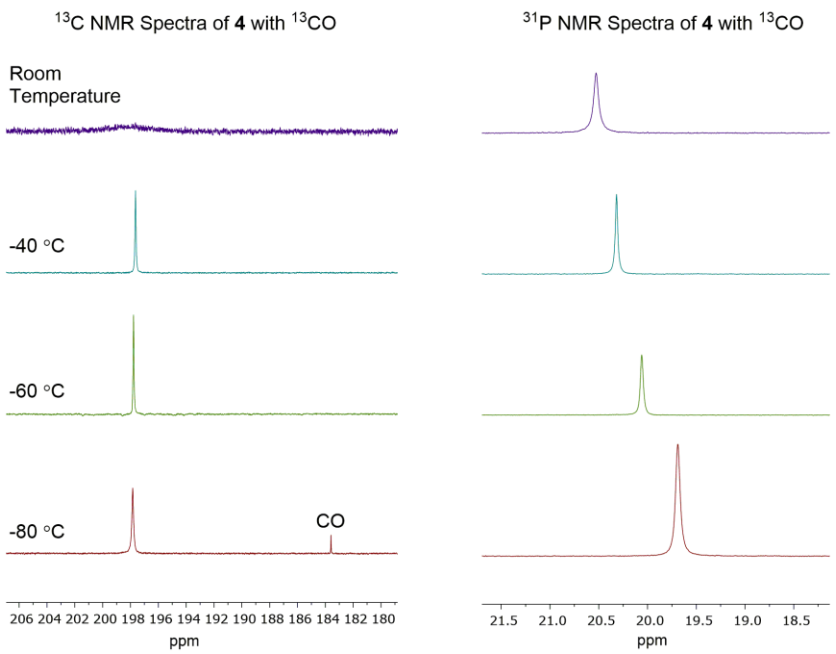

Figure 2.3. Variable temperature ^{13}C and ^{31}P NMR spectra of **4** under 600 Torr of ^{13}CO in toluene-d_8.

To complement the IR spectral data, NMR spectra of dicarbonyl compound **4** were obtained with 600 Torr of ^{13}CO in toluene-d_8 (Figure 2.3). Unfortunately, ^{31}P-^{13}C coupling between bound ^{13}CO and DCPP was not detected in either ^{13}C or ^{31}P NMR spectra; thus, the number of bound carbonyl ligands to **4** could not be determined by the multiplicity of the resonances observed in the ^{13}C or ^{31}P NMR spectra.[75] A broad resonance at 197 ppm was observed in the ^{13}C NMR spectrum of (DCPP)Pd(CO)$_2$ in toluene-d_8 at room temperature, and the resonance for unbound ^{13}CO was absent, indicating rapid exchange between bound and unbound ^{13}CO. The ^{13}C NMR spectrum at -40 °C contained a sharper resonance at 197 ppm, and a signal consistent with unbound ^{13}CO was observed at 184 ppm at -80 °C. Even at these temperatures, ^{31}P-^{13}C coupling was not observed in either the ^{13}C or ^{31}P NMR spectra. Due to the absence of phosphorus-carbon coupling, the number of CO ligands bound to **4** was determined by quantitative ^{13}C NMR spectroscopy with ^{13}CO and an internal ^{13}C enriched integration standard, 4-phenylanisole. At -40 °C with 1000 Torr of ^{13}CO, the number of CO ligands per palladium was determined to be 2.0. This value is consistent with the structure of dicarbonyl complex **4**.[76, 77]

Thus, IR and NMR spectroscopy along with X-ray crystallography showed that ethylene complex **1** is converted quantitatively to dicarbonyl complex **4** in the presence of CO. These methods also showed that complex **4** retains both CO ligands at elevated temperatures and under reduced pressures of CO. Therefore, we employed (DCPP)Pd(C_2H_4) (**1**) as a precursor to (DCPP)Pd(CO)$_2$ (**4**) for kinetic studies (*vide infra*).

Synthesis and Reactivity of Pd(II) Intermediates

To determine if Pd(II) aryl and phenacyl halide complexes bearing DCPP were catalytic intermediates, we synthesized (DCPP)Pd(II) aryl halide complexes **5a-j** and (DCPP)Pd(II) phenacyl halide complexes **6a-j**. Pd(II) aryl halide complexes (**5a-j)** ligated by DCPP were

synthesized by the reaction of $Pd(P^tBu_3)_2$ and an aryl halide in the presence of DCPP (Scheme 2.3). Phenacylpalladium chloride complexes **6a-b** and **6e-f** were obtained from the reaction of $Pd(PPh_3)_4$ with an acid chloride and subsequent ligand exchange with DCPP (Scheme 2.4a), whereas phenacylpalladium halide complexes **6c-d** (Scheme 2.4b) were generated by carbonylation of (DCPP)Pd(II) aryl halide complexes. Phenacylpalladium halide complexes (**6g-i**) were obtained by the reaction of dicarbonyl complex **4** (generated *in situ* from **1** and CO) with an aryl chloride or bromide in the presence of CO (Scheme 2.4c), demonstrating that **4** or compounds generated from **4** are capable of oxidative addition of aryl chlorides and bromides. Pd(II) phenacyl complexes **6a-i** are stable in solution and as solids and in the presence or absence of CO; they also do not undergo decarbonylation under vacuum at room temperature.

Scheme 2.3. Synthesis of Pd(II) aryl halide complexes.

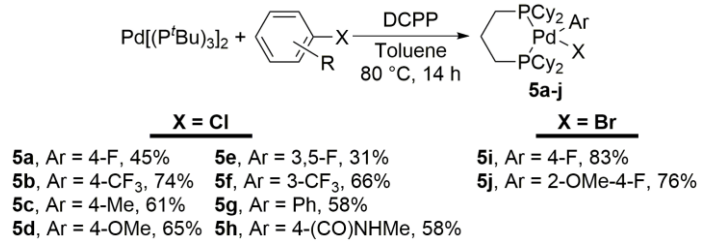

In contrast to complexes **6a-i**, phenacyl Pd(II) compound **6j** is only stable in solution in the presence of a CO atmosphere. Our attempts to isolate this compound resulted in the formation of decarbonylation product **5j**. Thus, characterization of **6j** was performed *in situ* by NMR spectroscopy under CO. After warming a solution of ethylene compound **1** and 1.5 equiv of 2-methoxy-4-fluoro-bromobenzene to 80 °C under 800 Torr of CO for 2.5 h, phenacylpalladium complex **6j** formed in 58% yield, and arylpalladium complex **5j** formed in 25% yield (Scheme 2.5). The ratio of **6j** to **5j** was approximately 2:1, respectively. Reaction for an additional 4 or 24 h at room temperature did not fully convert **5j** to **6j**, but the ratio of **6j** to **5j** increased to 3.7:1 after 4 h and 5:1 after 24 h. Thus, conversion of **5j** to **6j** is slow, but more data is required to assess if this partial conversion is actually an equilibrium.

Scheme 2.4. Synthesis of Pd(II) phenacyl complexes by oxidative addition or carbonylation.

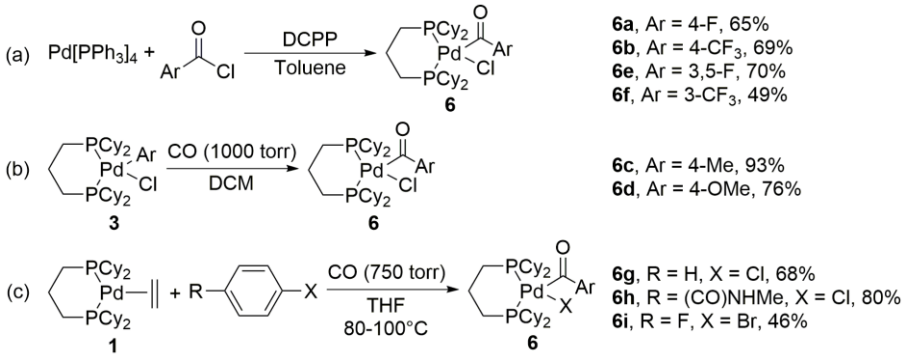

The reaction of phenacyl complex **6a** with excess ammonia in the presence of a soluble and hindered base, DBU, formed the corresponding primary benzamide in high yield (Scheme 2.6), indicating that these acyl complexes are chemically competent to be intermediates in the palladium-catalyzed aminocarbonylation reactions. Thus, by studying a series of stoichiometric

reactions of palladium complexes, we have provided strong evidence that compounds **5a-j** and **6a-j** are catalytic intermediates in palladium-catalyzed aminocarbonylation of aryl chlorides with ammonia.

Scheme 2.5. Synthesis of Pd(II) phenacyl bromide complex **6j** via oxidative addition of the corresponding aryl halide to in situ generated (DCPP)Pd(CO)$_2$ in the presence of CO.

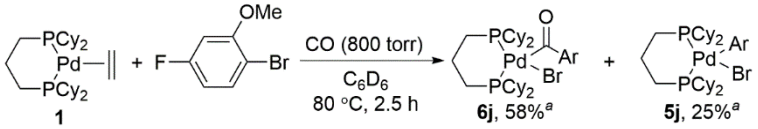

[a]Yield was determined by ^{1}H NMR spectroscopy with trimethoxybenzene as an internal standard.

Scheme 2.6. Pd(II) phenacyl chloride compound **6a** reductively eliminates in the presence of ammonia to form a primary benzamide.

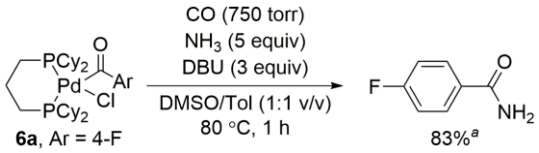

[a]Yield was determined by ^{1}H NMR spectroscopy with trimethoxybenzene as an internal standard.

The Mechanism of Oxidative Addition of Aryl Chlorides to (DCPP)Pd(CO)$_2$

The rate constants for the oxidative addition of 3,5-difluorochlorbenzene to (DCPP)Pd(CO)$_2$ (**4**) were measured by monitoring the appearance of the sum of the concentrations of arylpalladium halide complex **5e** and phenacylpalladium halide complex **6e** under pseudo-first order conditions of excess haloarene at 100 °C in a mixture of DMSO and toluene (1:1 v/v) (Scheme 2.7). Because dicarbonyl compound **4** is stable for only short times in the absence of CO, complex **4** was generated *in situ* from ethylene complex **1** prior to rate measurements.[78] The dependence of the rate of oxidative addition on CO pressure was determined to be inverse first order, based on the linear relationship between $1/k_{obs}$ and CO pressure (Figure 2.4a). The dependence of the rate on the concentration of 3,5-difluorochlorobenzene was determined to be first order based on the linear relationship between $1/k_{obs}$ and 1/[ArCl] (Figure 2.4b).

Scheme 2.7. Determination of pseudo-first order rate constants k_{obs} from the oxidative addition of 3,5-difluorochlorobenzene to (DCPP)Pd(CO)$_2$.

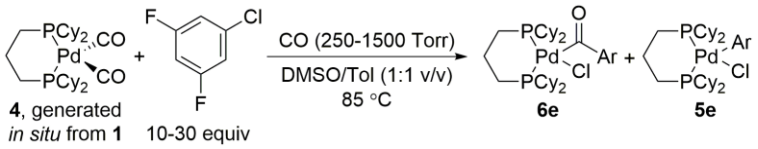

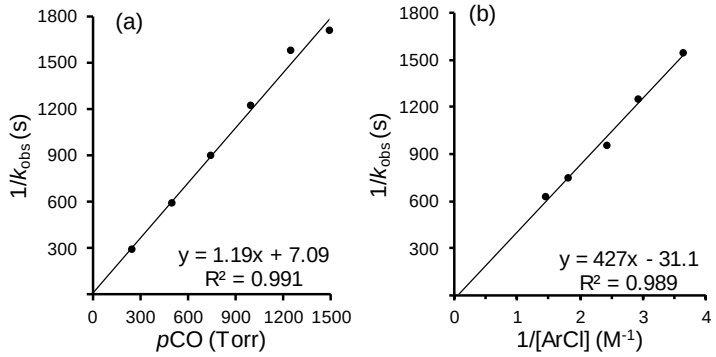

Figure 2.4. Dependence of the observed rate constant (k_{obs}) on (a) the pressure of CO (250-1500 Torr) with ArCl = 0.27 M and (b) the concentration ArCl (0.27-0.68 M) with *p*CO = 1000 Torr for the oxidative addition of 3,5-difluoro-chlorobenzene to (DCPP)Pd(CO)$_2$ (28 mM) in 1:1 v/v DMSO and toluene at 85 °C.

The observation of a first order dependence on the concentration of aryl chloride and an inverse first order dependence on the pressure of CO is consistent with the mechanisms of oxidative addition depicted in Figure 2.5. Path A involves reaction of the arene with the neutral, three-coordinate species to cleave the carbon-halogen bond and form a five-coordinate intermediate that undergoes rapid insertion of CO into the metal-aryl bond. This mechanism would be the simplest one that is consistent with our data. However, two alternative pathways are also consistent with the reaction orders. Path B involves the reaction of an aryl chloride with (κ^2-DCPP)Pd(CO) after dissociation of one of the phosphino groups of the DCPP ligand in (κ^2-DCPP)Pd(CO) to form (κ^1-DCPP)Pd(CO), followed by oxidative addition. Path C involves rate-limiting displacement of the CO ligand in (κ^2-DCPP)Pd(CO) by the haloarene to form (κ^2-DCPP)Pd(ArX). Carbon-halogen bond cleavage would then occur in this arene complex to form a four-coordinate, arylpalladium halide complex that would insert CO to form the phenacylpalladium halide species. Paths B and C occur without formation of a five-coordinate addition product from a neutral, three-coordinate Pd(0) complex.

We differentiated between these oxidative addition pathways for reactions of aryl chlorides to (DCPP)Pd(CO) by a combination of ^{13}C kinetic isotope effects (*vide infra)* and calculations by DFT (see Supporting Information). Our computational studies strongly suggested that the reaction did not occur by Path B involving partial dissociation of the bisphosphine ligand. The overall barrier for the oxidative addition of an aryl chloride to (κ^1-DCPP)Pd(CO) was computed to be 15 kcal/mol higher than the experimental barrier at standard state conditions, and it was calculated to be 12 kcal/mol higher than the experimental barrier at the temperature and concentrations of the reaction.[79] This high barrier for reaction by path B is consistent with the importance of chelating ligands to observe the carbonylation of aryl chlorides.[46a, 46d, 64, 68b] In contrast, the difference in energy between the highest-energy transition state – the transition state for oxidative addition of an aryl chloride – via path A and the computed energy of the experimentally determined resting state (DCPP)Pd(CO)$_2$ at concentrations close to those of the catalytic reaction was higher than the experimentally measured barrier by only 4 kcal/mol. The computed barrier for reaction by path C is ambiguous because we were unable to locate a transition state for the ligand substitution process, but this computed barrier is likely several kcal/mol lower than the experimental barrier based on the ground-state energies and transition state for oxidative addition to the (DCPP)Pd fragment. Although the transition state for carbon-chlorine bond cleavage was located for path C, this bond

cleavage event cannot be rate limiting because our kinetic data show an inverse first order dependence on pressure of CO. Thus, computation did not clearly show whether the reaction occurs by path A or C.

Instead, reaction by path A or C was distinguished by measuring the ^{13}C kinetic isotope effect (KIE) of the reaction of an aryl chloride with the Pd(0) dicarbonyl complex **4**. Path A involves irreversible reaction of the haloarene, followed by carbon-halogen bond cleavage. This addition could occur with or without initial, reversible formation of an arene complex, but cleavage of the carbon-halogen bond would occur in the irreversible step. Therefore, this pathway would be expected to occur with a primary kinetic isotope effect at the carbon *ipso* to chlorine. In contrast, reaction by pathway C involves irreversible displacement of CO to form an arene complex; because the irreversible step of the arene does not involve cleavage of the carbon-chlorine bond, this pathway would not give rise to a primary ^{13}C KIE at the carbon *ipso* to chlorine. Thus, the presence or absence of a primary ^{13}C KIE at the carbon *ipso* to chlorine would distinguish between these pathways.

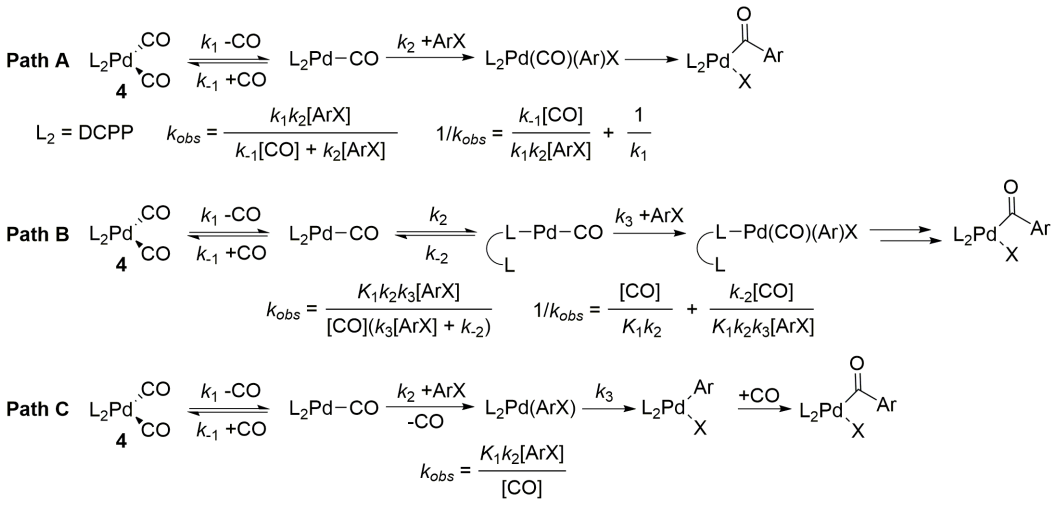

Figure 2.5. Proposed oxidative addition mechanisms of aryl halides to dicarbonyl compound **4**.

Measurement of a ^{13}C KIE for the Oxidative Addition of 4-chloro-N-methylbenzamide to (DCPP)Pd(CO)$_2$

Scheme 2.8. Determination of ^{13}C KIE of the oxidative addition of 4-chloro-*N*-methylbenzamide to **4**.

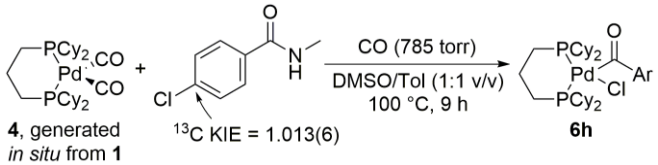

The ^{13}C KIE for the oxidative addition reaction of an aryl chloride to dicarbonyl **4** was obtained by the NMR spectroscopic method pioneered by Singleton.[80] A primary ^{13}C KIE of 1.013(6) was measured at the carbon *ipso* to chlorine for the oxidative addition of 4-chloro-*N*-methylbenzamide to complex **4** (Scheme 2.8). The ^{13}C KIEs at the carbonyl carbon was 0.993(8) and for the carbon atoms *ortho*, *meta* and *para* to chlorine were 0.994(5), 0.998(5), and 0.992(8),

respectively. 4-Chloro-*N*-methylbenzamide was chosen as the substrate in this study for its ease of isolation and the carbon of the *N*-methyl group was used at the standard. This ^{13}C KIE indicates that C-Cl bond cleavage is irreversible. Thus, our data are inconsistent with reaction by path C and are consistent with oxidative addition of the aryl chloride to a three-coordinate Pd(0) complex (path A, Figure 2.5).[81] Oxidative addition of an aryl chloride to a neutral, three-coordinate Pd(0) complex has not been documented previously. It is possible that the transition state for this oxidative addition reaction could involve concomitant dissociation of CO from (DCPP)Pd(CO) and cleavage of a C-Cl bond to avoid formation of a five-coordinate product.

Hammett Analysis of the Oxidative Addition of Aryl Chlorides to (DCPP)Pd(CO)$_2$

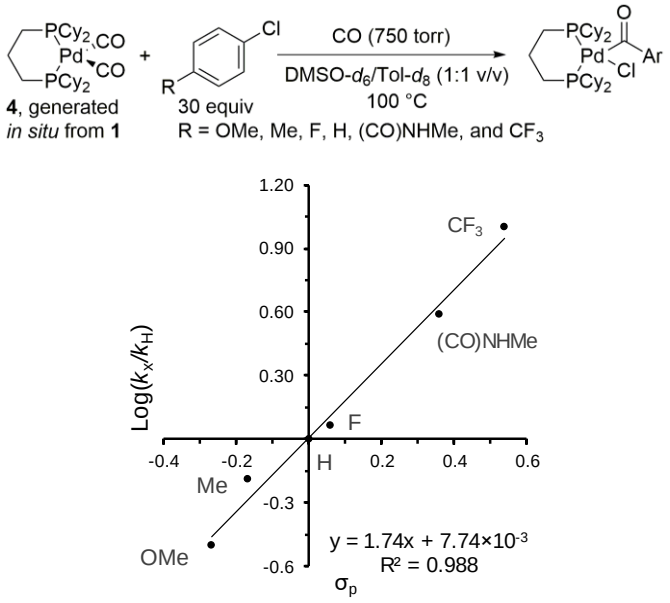

Figure 2.6. Hammett plot of the oxidative addition of *para*-substituted aryl chlorides (0.56 M) to (DCPP)Pd(CO)$_2$ (28 mM) with *p*CO = 750 Torr in DMSO-d_6/toluene-d_8 (1:1 v/v) at 100 °C.

Because our data indicate that the oxidative addition of aryl chlorides to dicarbonyl **4** may occur via a three-coordinate Pd(0) center bearing a bidentate ligand, we investigated whether this unusual oxidative addition of an aryl chloride proceeds by a concerted cleavage of the C-Cl bond or by a stepwise S_NAr-type mechanism. The oxidative addition of aryl halides to Pd(0) compounds bearing bidentate ligands have been proposed in prior publications to occur by an S_NAr type process on the basis of computational findings and a Hammett analysis of the electronic effects of aryl halides on oxidative addition to $L_2Pd(0)$ species.[10a, 82] In contrast, the accepted mechanism for oxidative addition of aryl halides to Pd(0) complexes containing one or two dative ligands is a concerted cleavage of the carbon-halogen bond of the aryl halide.[26c, 83]

To gain additional insight into the oxidative addition of aryl chlorides to dicarbonyl complex **4**, the electronic effects of the aryl group on the rate of the reaction were measured. A linear correlation between the σ parameter and the rate of oxidative addition was observed with a ρ value of 1.74 (Figure 2.6).[84] This ρ value indicates negative charge build-up at the carbon *ipso* to chlorine during the transition state of oxidative addition of aryl chlorides to **4**. A similar ρ value of 1.7 was measured by Yamamoto in the double carbonylation of aryl bromides with

$Pd(PPh_2Me)_2Cl_2$.[52] In addition, the ρ value of 1.74 obtained from our Hammett analysis is comparable to ρ values of oxidative addition of aryl iodides (ρ = 2) and triflates (ρ = 2.55) to $Pd(PPh_3)_4$, which are proposed to occur via concerted cleavage of the carbon-halogen or carbon-triflate bond.[26c, 83] Conversely, the oxidative addition of 2-bromo and 2-chloropyridines with substituents in the 5 position to $Pd(PPh_3)_4$ exhibit larger ρ values (4.4 and 4.3, respectively), and the oxidative addition of these heteroaryl halides have been proposed to occur by an S_NAr type process.[85] Thus, on the basis of our Hammett analysis, a ρ value of 1.74 is inconsistent with oxidative addition by an S_NAr mechanism.

In addition, the ^{13}C KIE measured for the oxidative addition of an aryl chloride to dicarbonyl **4** is distinct from ^{13}C KIE values reported for S_NAr reactions. The ^{13}C KIE values for the S_NAr reaction of the chlorine in atrazine with hydroxide are between 1.03–1.04.[86] Although the ^{13}C KIE value for the S_NAr reaction of atrazine involves different nucleophiles and electrophiles than in our organometallic system, we propose on the basis of our ^{13}C KIE measurements, kinetic studies, and a Hammett analysis, that the C-Cl bond cleavage by reaction with (DCPP)Pd(CO) occurs by a concerted process, not by an S_NAr-type reaction.

Mechanism of Oxidative Addition of Aryl Bromides to (DCPP)Pd(CO)$_2$

Scheme 2.9. Determination of pseudo-first order rate constants k_{obs} from the oxidative addition of 2-methoxy-4-fluoro-bromobenzene to $(DCPP)Pd(CO)_2$.

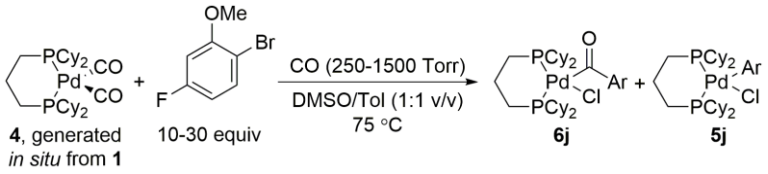

Because the carbonylative functionalization of aryl chlorides by Pd(0) in the presence of CO is less common than the analogous functionalization of aryl bromides and iodides, we performed mechanistic studies on the oxidative addition of aryl bromides to $(DCPP)Pd(CO)_2$. This study would reveal whether the mechanism of oxidative addition of aryl bromides to **4** differs from the mechanism of the reaction of aryl chlorides. The dependence of the rate of oxidative addition on the concentration of aryl bromide and on the pressure of CO was determined for reactions in a mixture of DMSO and toluene (1:1 v/v) under pseudo-first order conditions. Ethylene complex **1** served as a precursor to dicarbonyl compound **4**, and the sterically hindered and electronically deactivated aryl bromide 2-methoxy-4-fluoro-bromobenzene was selected for this study because oxidative addition of this substrate occurs at elevated temperatures with rates that are convenient to measure. The observed rate exhibited an inverse first order dependence on the pressure of CO (Figure 2.7a) and a first order dependence on the concentration of aryl bromide (Figure 2.7b). As such, these experiments suggest that aryl bromides and aryl chlorides react by similar pathways under these reaction conditions, wherein the haloarene reacts irreversibly with (DCPP)Pd(CO) to cleave the carbon-halogen bond. These results also agree with the computational studies performed by Grushin on the oxidative addition of aryl iodides to $(Xantphos)Pd(CO)_2$ discussed in the introduction.

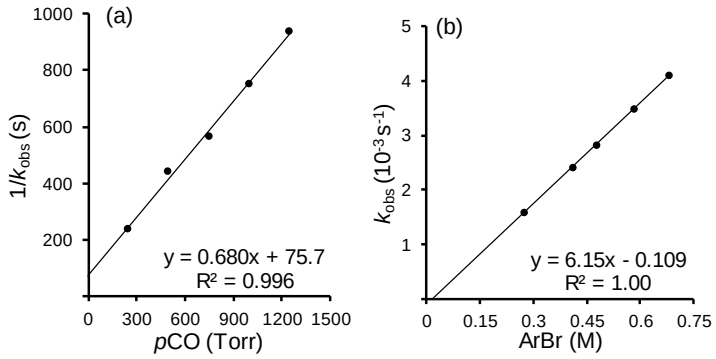

Figure 2.7. Dependence of the observed rate constant (k_{obs}) on (a) the pressure of CO (250-1500 Torr) with ArBr = 0.27 M at 75 °C and (b) the concentration of ArBr (0.27-0.68 M) with *p*CO = 1000 Torr at 70 °C for the oxidative addition of 2-methoxy-4-fluoro-bromobenzene to (DCPP)Pd(CO)$_2$ (28 mM) in DMSO and toluene (1:1 v/v).

Potential Mechanisms for the Formation of Benzamide from a Phenacylpalladium Chloride Intermediate

Scheme 2.10. Reaction to assess whether phenacylpalladium complex **6a** reductively eliminates 4-fluorobenzoyl chloride.

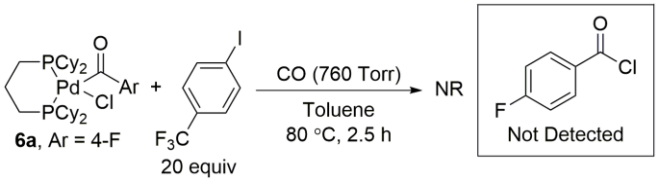

The formation of benzamide from phenacylpalladium chloride complexes ligated by DCPP could occur by reductive elimination of benzoyl chloride, followed by reaction of this acid chloride with ammonia and base, or it could occur by direct reaction of ammonia and base with the phenacylpalladium chloride complex. Although most mechanisms proposed for carbonylative couplings of aryl halides involve reaction of the nucleophile with an acylpalladium halide complex, phenacylpalladium chloride complexes have been reported recently to undergo reductive elimination to generate benzoyl chloride as part of a catalytic synthesis of benzoyl chlorides from aryl halides, CO and chloride salts.[43e, 61a, 87] This synthesis of benzoyl chlorides occurs with palladium catalysts containing bulky, monophosphine ligands, not bidentate phosphines like those in our current study. Nevertheless, we conducted experiments to test whether this reductive elimination occurs in the catalytic aminocarbonylation. To do so, DCPP-ligated phenacyl complex **6a** was heated at 80 °C for 2.5 h in the presence of 20 equiv of 4-iodobenzotrifluoride and 760 torr of CO (Scheme 2.10). This temperature and time corresponds to those at which **6a** reacts with ammonia and DBU to form 4-fluorobenzamide (Scheme 2.6). If **6a** reductively eliminated 4-fluorobenzoyl chloride, the iodoarene would trap the Pd(0) resulting from the reductive elimination. Under these conditions, 4-fluorobenzoyl chloride was not detected by ^{19}F NMR spectroscopy. Thus, we conclude that the reductive elimination of benzoyl chloride is not a likely pathway in the formation of benzamide from DCPP-ligated phenacyl complexes, and we conducted detailed studies to distinguish between pathways for the formation of benzamide by reaction of ammonia and base with the phenacylpalladium complex (Figure 2.8).

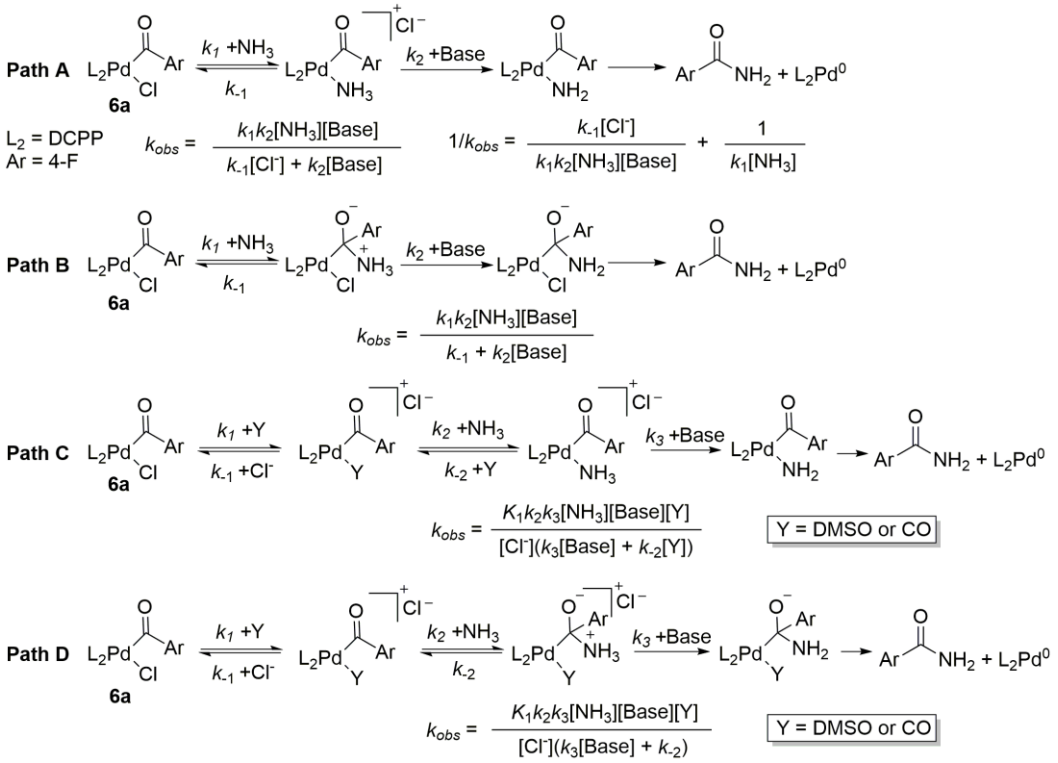

Figure 2.8. Proposed mechanisms for the formation of benzamide from (DCPP)Pd(II) phenacyl chloride complexes with ammonia and base.

Four potential pathways for formation of benzamide from phenacyl compound **6a** are shown in Figure 2.8. Path A occurs by reversible exchange of chloride by ammonia, deprotonation of the coordinated amine to form a Pd(II) acyl amido species, and reductive elimination to generate a primary benzamide. The exchange of amine for chloride could occur by any of the known pathways for ligand substitution on square-planar compounds. Path A is reminiscent of the inner-sphere reductive elimination of esters from acyl Pd(II) aryloxy complexes or the reaction of cationic acyl palladium(II) complexes with alcohols.[69] Path B involves an outer-sphere attack of ammonia at the carbonyl group of compound **6a**, followed by deprotonation of the resulting intermediate. Subsequent collapse of the anionic intermediate and loss of chloride produces the products of reductive elimination. Such pathways involving outer-sphere attack on an acyl group have been discussed for palladium-catalyzed alkoxycarbonylation reactions under basic conditions.[44, 88] Paths C and D involve displacement of chloride by either DMSO or CO to generate a cationic Pd(II) species. This cationic Pd(II) species could be more prone to nucleophilic attack by ammonia than a neutral compound. Path C involves displacement of chloride by DMSO or CO and subsequent displacement of the bound DMSO or CO by ammonia. The reductive elimination products would then be generated by deprotonation and reductive elimination. Path C is equivalent to Path A if the first two steps are fully reversible before deprotonation of the bound amine. Path D is the outer sphere variant of path C, in which ammonia attacks the acyl carbonyl group of a cationic Pd(II)-DMSO or Pd(II)-CO complex. After deprotonation and collapse of the resulting anionic intermediate, Pd(0) and a primary benzamide are generated.

Paths A, C, and D can be differentiated from path B by the order in chloride. Paths A, C, and D would be inverse first order in chloride, whereas path B would be zero order in chloride. If

k_1 in paths A, C, and D were not reversible, then reactions by these pathways would also be zero order in chloride and more sophisticated methods to differentiate the reaction by pathways A, B, C, and D would be needed. The order of the reaction in chloride and ammonia for path A would be the same as that for paths C and D, except that reaction by path D would be first order in DMSO or CO and reaction by path C would be first order in DMSO and CO at low amounts of DMSO or CO and zero order at high amounts of DMSO or CO. To elucidate the mechanism by which the phenacyl complex reacts with ammonia, we measured the dependence of the rate of formation of benzamide from acyl complex **6a** on the concentration of ammonia, chloride, base, DMSO, and pressure of CO (Scheme 2.11).

Determination of the Mechanism for the Formation of Benzamide

Scheme 2.11. Determination of initial rates and pseudo-first order rate constants for the formation of 4-fluorobenzamide from Pd(II) phenacyl chloride compound **6a**.

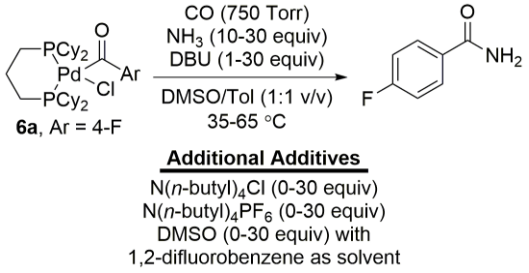

The rate of formation of benzamide from compound **6a** was determined by obtaining pseudo-first order rate constants from the decay of **6a** by ^{31}P NMR spectroscopy (Scheme 2.11) with 10-30 equiv of ammonia. All experiments were performed under 750 Torr of CO to capture the Pd(0) generated from reductive elimination as (DCPP)Pd(CO)$_2$ and were conducted with DBU as base. DBU was chosen as a substitute for K_2CO_3 to create homogeneous reaction conditions. Because DBU is a hindered base, it does not act as a nucleophile and generate side products.

The rate of formation of benzamide was determined to be first order in ammonia (Figure 2.9a) and inverse first order in N(*n*-butyl)$_4$Cl (Figure 2.9b, black trace). The inverse first order dependence on the concentration of N(*n*-butyl)$_4$Cl, a soluble source of chloride, is consistent with reaction by paths A, C, and D. The reaction of **6a** with ammonia was approximately zero order in N(*n*-butyl)$_4$PF$_6$ (Figure 2.9b, red trace), indicating that the inverse first order dependence on added chloride did not result from a salt effect or increase of solvent polarity from the salt.[89]

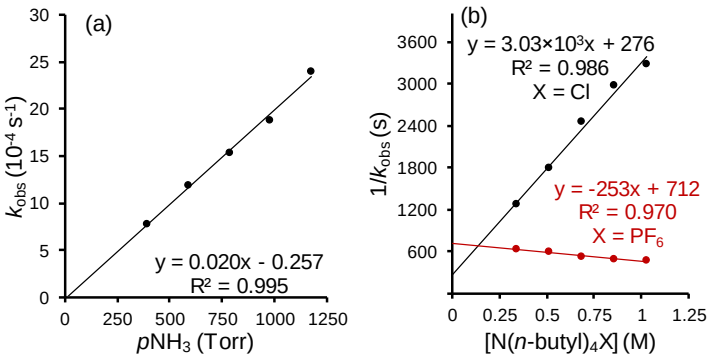

Figure 2.9. Dependence of the observed rate constant (k_{obs}) on (a) pNH$_3$ (392−1177 Torr, 10−30 equiv) with pCO = 750 Torr and [DBU] = 0.34 M and on (b) [N(n-butyl)$_4$Cl] (0.34−1.0 M, black trace) or [N(n-butyl)$_4$PF$_6$] (0.34−1.0 M, red trace) with pCO = 750 Torr, [DBU] = 0.34 M, and pNH$_3$ = 785 Torr (20 equiv) for the rate of formation of 4-fluorobenzamide from **6a** (34 mM) in 1:1 v/v DMSO and toluene at 35 °C. The pressure of CO is the pressure added to a J. Young tube at −196 °C.

The dependence of the reaction rate on the concentration of DBU was found to be first order at low concentrations of DBU and zero order at high concentrations of DBU. When initial rates were measured with 1-5 equiv of DBU (0.0342 M to 0.171 M), the rate of formation of benzamide was first order in DBU (Figure 10a). The reaction of **6a** with ammonia and 10-30 equiv (0.342-1.03 M) of DBU occurred with an approximately zero-order dependence on the concentration of DBU (Figure 2.10a). These results indicate that deprotonation is the rate limiting step at low concentrations of base and that attack of **6a** by ammonia is rate limiting at high concentrations of base. To explore the effects of base on reaction rate further, we determined the order of the reaction in base in the presence of 10 equiv of N(n-butyl)$_4$Cl (0.342 M). A first-order dependence of the rate on base was observed under these conditions (Figure 2.10c).

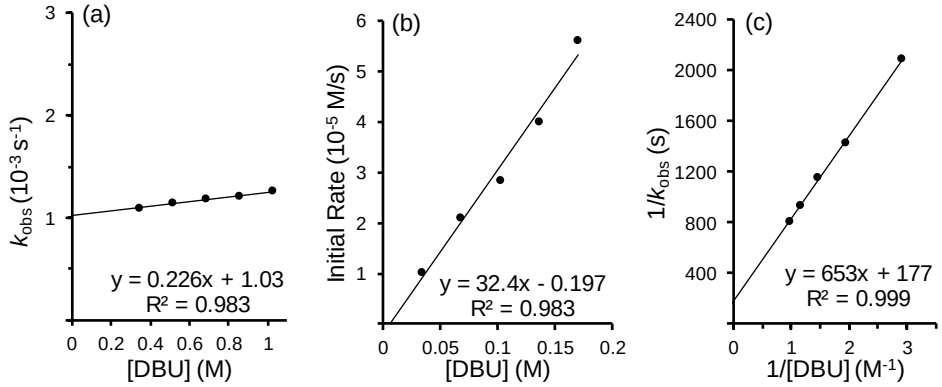

Figure 2.10. Dependence of the initial rate on (a) [DBU] (0.034−0.17 M) with pCO = 750 Torr and pNH3 = 588 Torr (15 equiv) at 60 °C for the rate of formation of 4-fluorobenzamide from **6a** (34 mM) in DMSO and toluene (1:1 v/v). Dependence of the observed rate constant (k_{obs}) on (b) [DBU] (0.34−1.0 M) with pCO = 750 Torr and pNH3= 392 Torr (10 equiv) at 35 °C for the rate of formation of 4-fluorobenzamide from **6a** (34 mM) in DMSO and toluene (1:1 v/v). Dependence of the observed rate constant (k_{obs}) on (c) [DBU] (0.34−1.0 M) with pCO = 750 Torr, pNH3= 392 Torr (10 equiv), and [N(n-butyl)$_4$Cl] = 0.34 M at 35 °C for the formation of p-

fluorobenzamide from **6a** (34 mM) in DMSO and toluene (1:1 v/v). The pressure of CO is the pressure added to a J. Young tube at −196 °C.

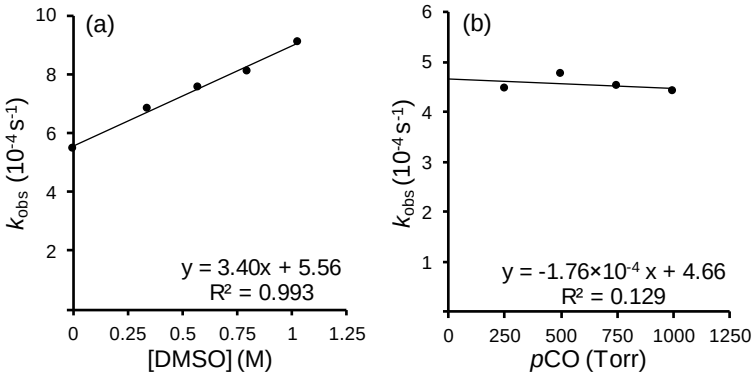

Figure 2.11. Dependence of the observed rate constant (k_{obs}) on (a) the concentration of DMSO (0.0-1.0 M) with pCO = 750 Torr, [DBU] = 0.34 M, and pNH$_3$ = 785 Torr (20 equiv) at 65 °C and (b) the pressure of CO (250-1000 Torr) with [DBU] = 0.34 M and pNH$_3$ = 785 Torr (20 equiv) at 65 °C for the rate of formation of *p*-fluorobenzamide from **6a** (34 mM) in 1,2-difluorobenzene. The pressure of CO is the pressure added to a J. Young tube at -196 °C or at -95 °C.

The first order behavior in DBU at low concentrations of DBU and zero order behavior in DBU at high concentrations of DBU is consistent with paths A, C, and D. Therefore, to differentiate between paths A, C, and D, the effect of the concentration of DMSO (0.0-1.0 M, 0-30 equiv) and the pressure of CO (250-1000 Torr) on the rate of formation of benzamide was measured in 1,2-difluorobenzene, a polar but non-coordinating solvent.[90] A positive, fractional order in DMSO was observed (Figure 2.11a). This non-integer order in DMSO is likely due to an increase in polarity of the reaction mixture at higher concentrations of DMSO, which would lead to a higher concentration of ammonia. This lack of a clear first-order dependence on the concentration of DMSO is inconsistent with path D and is consistent with path A or path C with the first two steps fully reversible. A zero-order dependence of k_{obs} on the pressure of CO also was observed (Figure 2.11b). This absence of a first order dependence on the pressure of CO is inconsistent with path D and also is consistent with path A or path C with the first two steps fully reversible. At the same time, the formation of benzamide occurs in the absence of added DMSO (Figure 2.11a), and the addition of DMSO does not significantly alter the rate of formation of benzamide. Thus, it is unlikely that DMSO additive or solvent assists the exchange of ammonia for chloride. It is unlikely that CO assists in the exchange of ammonia, given that the lack of dependence of the rate of benzamide formation on high concentrations of DMSO, which is more nucleophilic than CO. In addition, the relatively hard property of cationic Pd(II), the known direct substitution of chloride by nitrogen Lewis bases,[46] and lack of dependence of the rate of benzamide formation on CO makes the inclusion of CO in the mechanism of benzamide formation unlikely. Thus, we favor the reaction by path A in the presence or absence of DMSO or CO in the system. Our kinetic data on the formation of benzamide from **6a** are all consistent with ligand substitution of chloride by ammonia, most likely by associative ligand substitution, followed by deprotonation of coordinated ammonia and reductive elimination from the resulting phenacylpalladium(II) amido species to obtain Pd(0) and a primary benzamide.

Formation of Benzamide from an Aryl Pd(II) Amido Complex

Scheme 2.12. Synthesis of Pd(II) aryl amido complex **7** and subsequent reactivity with CO.

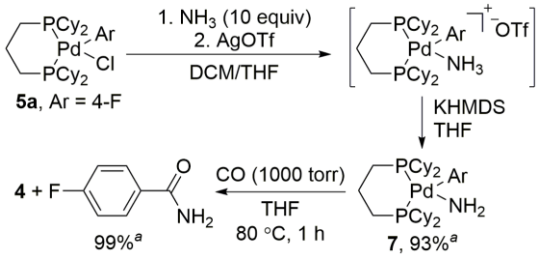

[a]Yields were obtained by ^{19}F NMR spectroscopy with OTf^- as an internal standard.

Decarbonylation of phenacyl Pd(II) halide species to the corresponding arylpalladium(II) halide species can occur during the catalytic process.[91] Such arylpalladium(II) halide intermediates were observed during our mechanistic studies of the oxidative addition of electron-poor aryl halides and of ortho-substituted aryl halides in the presence of CO. These complexes could result from reversible migratory insertion or slow migratory insertion of CO. Thus, ammonia could react with an arylpalladium(II) halide complex to form an arylpalladium(II) amido complex prior to migratory insertion of CO, to form aniline by reductive elimination as a side product, or to form a phenacylpalladium amido or arylpalladium carbamoyl complex by insertion of CO into the palladium-aryl or palladium-amido bond and subsequent formation of the organic amide.[46c, 92]

To explore the potential intermediacy of arylpalladium amido complexes, arylpalladium amido complex **7** was synthesized as shown in Scheme 2.12. Abstraction of chloride from **5a** with AgOTf in the presence of ammonia and subsequent deprotonation with KHMDS formed **7**. ^1H–^{15}N HSQC and ^{15}N DEPT experiments confirmed the presence of a mononuclear Pd-NH_2 amido species (see Supporting Information). Amido complex **7** slowly degrades in THF at room temperature. The onset of this decomposition can be detected by ^{31}P NMR spectroscopy after approximately 1.5 hours at room temperature and attempts to isolate **7** as a solid by crystallization led to decomposition. Thus, compound **7** was prepared *in situ* and was allowed to react with 1000 Torr of CO at 80 °C. After one hour, *p*-fluorobenzamide formed in 99% yield and compound **7** was fully consumed. The sole compound observed by ^{31}P NMR spectroscopy was dicarbonyl complex **4**. (Scheme 2.12). *p*-Fluoroaniline was not observed by ^{19}F NMR spectroscopy. These data imply that reductive elimination from a phenacyl Pd(II) amido complex or an aryl Pd(II) carbamoyl complex to generate the corresponding primary benzamide is faster than reductive elimination from an aryl Pd(II) amido complex to form aniline.

Identification of the Catalyst Resting State

To identify the major palladium complex in the catalytic reaction, the aminocarbonylation of 4-chlorofluorobenzene was monitored by ^{31}P NMR spectroscopy (Figure 2.12). Because dicarbonyl **4** is poorly soluble in DMSO alone, leading to weak signals, the catalytic reaction was monitored in a mixture of DMSO and toluene (1:1 v/v) to maintain the solubility of the palladium complexes. After 14 h at 100 °C, at which point 54% conversion of starting material occurred, the ^{31}P NMR spectrum consisted of a singlet at 20.3 ppm, which corresponds to dicarbonyl **4**, along with a second resonance at 15.6 ppm (Figure 2.12a). After 14 h at the lower temperature of 80 °C,

at which point 10% conversion of starting material occurred, the ^{31}P NMR spectrum contained only the resonance at 20.3 ppm for **4** (Figure 2.12b).

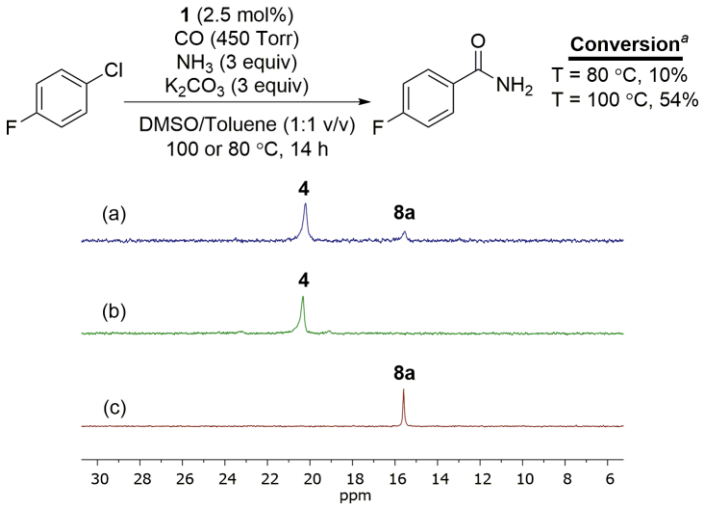

Figure 2.12. Room temperature ^{31}P NMR spectra of a catalytic reaction at partial conversion conducted at 100 (a) and 80 °C (b) after 14 h in DMSO and toluene (1:1 v/v) and of Pd(I) dimer **8a** in $CDCl_3$ at room temperature (c). [a]Conversion was determined with ^{19}F NMR spectroscopy with 4-fluorotoluene as an internal standard.

The second compound corresponding to the resonance at 15.6 ppm in Figure 2.12a is the dinuclear hydride complex **8a** in Scheme 2.13. This complex was prepared independently in 32% isolated yield by the addition of ammonium chloride to complex **4** at 100 °C for 45 min in the presence of CO. The ^{31}P NMR spectrum of **8a** at room temperature consists of a singlet at 15.6 ppm (Figure 2.12c), and the ^{1}H NMR spectrum contains a quintet at –5.28 ppm for the bridging hydride. Similar cationic Pd(I) dimers have been synthesized previously and proposed to be resting states in palladium-catalyzed alkoxycarbonylation reactions or have been isolated as by-products of palladium-catalyzed synthesis of hydrogen peroxide from carbon monoxide, oxygen, and water.[93] We hypothesized that this hydride complex forms in the catalytic cycle by protonation of dicarbonyl complex **4**.

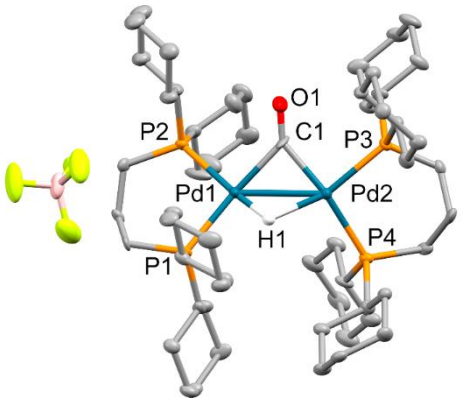

Figure 2.13. Solid state structure of Pd(I) dimer **8b** with ellipsoids set at 30% and selected hydrogen atoms omitted for clarity. Selected bond lengths (Å): Pd1-Pd2 2.749(1), Pd1-C1

2.09(1), Pd2-C1 2.02(2), C1-O1 1.15(2). Selected bond angles (°): P2-Pd1-P1 97.74(13), Pd1-C1-Pd2 83.9(6), P3-Pd2-P4 98.09(13).

Single crystals of **8b**, an analog of **8a** containing a tetrafluoroborate counterion, was obtained by addition of HBF_4 etherate to $(DCPP)Pd(CO)_2$, which was generated in situ from **4** and CO, and crystallization from a solution of THF and toluene (1.5:1 v/v). (Scheme 2.13). The ^1H and ^{31}P NMR spectrum of **8b** is identical to that of compound **8a**. The solid-state structure of complex **8b** consists of a dinuclear structure with two palladium centers that adopt distorted square-planar geometries. This geometry has been observed for other crystallographically characterized Pd(I) dimers bearing two bidentate ligands and a bridging carbonyl and hydride ligand.[93a, 94] The Pd-Pd distance is 2.749(1) Å, which is consistent with a metal-metal bond (Figure 2.13). In this structure, the two phosphorus atoms on each palladium are inequivalent, but a single ^{31}P NMR resonance is observed in solution at room temperature.

This equivalence of the phosphines in solution arises from a rapid, dynamic process, rather than a different structure in the solid state and in solution. Cooling **8b** to –99 °C in THF-d_8 caused the quintet of the bridging hydride in the ^1H NMR spectrum to partially coalesce to become a more complex, broad multiplet. Similarly, the ^{31}P NMR resonance of **8b** at –99 °C in THF-d_8 broadens and exhibits a multiplicity that is more complex than a singlet (see Supporting Information). The NMR spectra recorded of **8b** at –99 °C indicate that a dynamic process approaches but is not slower than the NMR timescale at –99 °C. In addition, due to the complexity of the spectra of **8b** at –99 °C, we were unable to determine the nature of the dynamic process leading to the equivalence of the phosphorus atoms of **8b** in solution at room temperature. This equivalence of the two phosphorus atoms has been previously reported for structurally analogous cationic Pd(I) dimers.[93c, 95] A rapid dissociation and association of either the bridging carbonyl or bridging hydride from one of the Pd atoms has been proposed as the cause for the equivalence of the phosphorus atoms at room temperature.[95]

Scheme 2.13. Synthesis of Pd(I) dimers **8a** and **8b**.

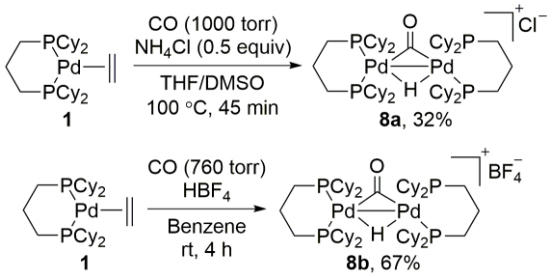

The reactivity of Pd(I) dimer **8a** was studied to assess its relevance to the mechanism of the catalytic aminocarbonylation. Compound **8a** was treated with an excess of DBU in the presence of 760 Torr of CO in DMSO at 100 °C. Over the course of 16 h, complex **8a** slowly reduced to dicarbonyl compound **4**. After this time, only 56% of **8a** converted to **4**, which precipitated as colorless crystals, along with Pd black (Scheme 2.14). Because the generation of **4** from **8a** is slower than the catalytic process, the formation of **8a** is a catalyst deactivation pathway, and we propose that **4** is the catalyst resting state.

Scheme 2.14. Reduction of Pd(I) dimer **8a** to Pd dicarbonyl complex **4** in the presence of CO and base.

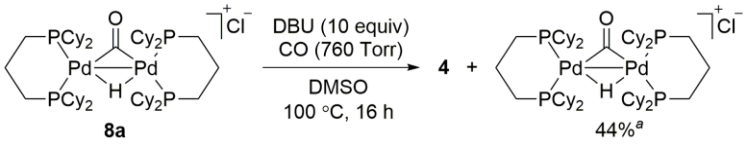

[a]Yield was determined with $PMes_3$ as an internal standard.

Identification of the Rate Limiting Step of the Catalytic Reaction

Based on our kinetic studies and identification of the major palladium complexes present in the catalytic reaction, the rate limiting step of the catalytic cycle is the oxidative addition of an aryl chloride to dicarbonyl compound **4**. In addition, the rate of the reduction of dimer **8a** to dicarbonyl **4** will affect the observed rate of the catalytic process. To identify the rate-determining step of the catalytic cycle, a time course of the reaction was measured with varying amounts of CO and ammonia (Figure 2.14). Qualitatively, the rate of the reaction conducted with 900 Torr of CO was less than the reaction conducted with 450 Torr of CO. This smaller rate is consistent with rate-limiting oxidative addition because dissociation of CO from compound **4** occurs prior to oxidative addition. The decrease in rate at higher concentrations of CO is inconsistent with rate-limiting reduction of **8a** to **4**, which would be expected to exhibit either zero or positive orders in CO pressure. Although doubling the amount of ammonia from 3 to 6 equiv increases the reaction rate slightly, the small size of that effect is inconsistent with rate-limiting formation of benzamide from reaction of the phenacyl complex with ammonia. We attribute this slight enhancement in rate to an increase in overall basicity of the reaction medium, which inhibits the formation of the inactive dimer **8a**. Thus, these data are consistent with oxidative addition as the rate-limiting step in the catalytic aminocarbonylation of aryl chlorides, as predicted from studies of the individual steps.

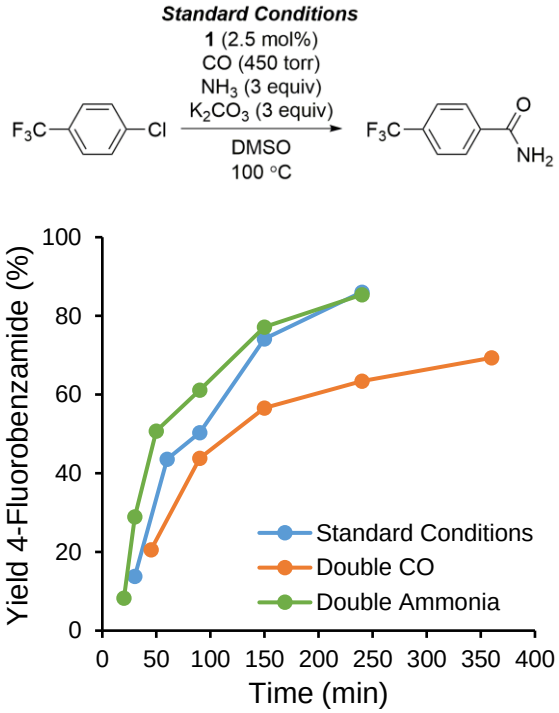

Figure 2.14. Time course of the palladium-catalyzed aminocarbonylation of 4-chlorobenzotrifluoride with varying amounts of CO and ammonia. [a]Yields were determined by GC.

2.3 Conclusion

The lack of studies on the oxidative addition and the formation of benzamide during the palladium-catalyzed aminocarbonylation of aryl chlorides has made the catalytic cycle of this process ambiguous. Our kinetic studies of the oxidative addition of the aryl halide and the formation of benzamide from a phenacylpalladium complex during the palladium-catalyzed aminocarbonylation of aryl chlorides with ammonia, as well as determination of the catalyst resting state and deactivation pathways, establish an experimental basis for the elementary steps that constitute the catalytic cycle of palladium-catalyzed aminocarbonylation. Our results indicate that the aminocarbonylation of aryl chlorides catalyzed by DCPP-ligated Pd(0) occurs by the mechanism summarized in Figure 2.15.

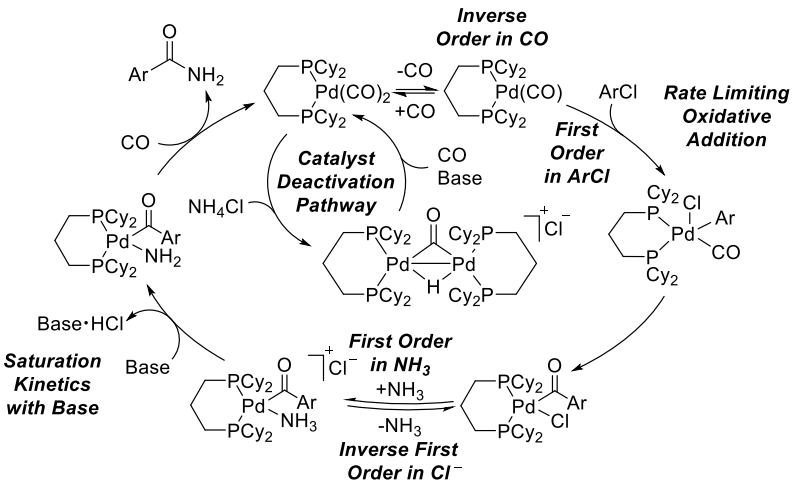

Figure 2.15. Proposed mechanism for palladium-catalyzed aminocarbonylation of aryl chlorides with ammonia.

The oxidative addition of a chloroarene and bromoarene to (DCPP)Pd(CO)$_2$ (**4**) was first-order in the concentration of aryl halide and inverse first-order in the pressure of CO, indicating that the haloarene reacts with a three-coordinate Pd complex bearing DCPP and one CO ligand (Figure 2.5, Path A). A primary ^{13}C KIE of 1.013(6) was measured for the carbon *ipso* to chlorine for the oxidative addition of 4-chloro-*N*-methylbenzamide to **4**, and a ρ value of 1.74 was obtained from a Hammett analysis of the effect of the electronic properties of the arene on the rate of oxidative addition. Together, these data are consistent with irreversible C–Cl bond cleavage during the reaction of the Pd(0) species with the haloarene by a concerted pathway, rather than an S_NAr type pathway. In addition, our ^{13}C KIE study discounts the possibility of irreversible ligand substitution of CO from (DCPP)Pd(CO) with an aryl chloride, wherein oxidative addition occurs at a two-coordinate (DCPP)Pd(0) complex, and implies that the oxidative addition of an aryl chloride occurs at a Pd(0) complex bearing DCPP and one CO ligand. Thus, we propose that the oxidative addition of aryl chlorides occurs at (DCPP)Pd(CO) by a concerted C–Cl bond cleavage event.

The rate of formation of benzamide from Pd(II) phenacyl compound **8a** was first order in ammonia and inverse order in chloride. A non-integer, positive order in the concentration of DMSO and pressure of CO was observed when the reaction was conducted in a non-coordinating solvent. These data are consistent with a mechanism for reaction of phenacyl compound **6a** with ammonia that involves an inner-sphere displacement of chloride by ammonia to form a cationic Pd(II) ammine complex as an intermediate (Figure 2.8, Path A). The rate of formation of benzamide was zero order in base at high concentrations of base and first order in base at low concentrations of base. These reaction orders imply that the rate-limiting step of benzamide formation is deprotonation at low concentrations of base and formation of an ammine complex at high concentrations of base. Moreover, the formation of benzamide does not occur directly from a cationic ammine intermediate. Instead, deprotonation generates an acyl Pd(II) amido species, which reductively eliminates to generate benzamide.

The rate limiting step of the overall catalytic reaction with an aryl chloride was determined by studying the dependence of the rate of the catalytic reaction on the pressure of ammonia and CO. Changes to the pressure of ammonia did not affect the rate of the reaction significantly,

whereas reactions at higher pressures of CO were slower than those at lower pressures of CO. Because the oxidative addition of an aryl chloride to **4** is inverse order in CO, the rate limiting step of the catalytic reaction is oxidative addition. The resting state of the catalytic reaction was determined to be dicarbonyl compound **4**, which is consistent with the observed dependence of the rate on CO pressure. A Pd(I) hydride dimer **8a** was also present in the catalytic system. This complex slowly reduces to dicarbonyl **4** in the presence of CO and base, and this slow rate of reentry into the catalytic cycle leads to the partial accumulation of this complex and reduction of the rate of the reaction. Future efforts in this area will be directed toward the development of palladium-catalyzed carbonylations that occur with additional classes of organic electrophiles.

2.4 Experimental

General Experimental Procedures

All manipulations were conducted under a nitrogen atmosphere in a glovebox or on a Schlenk manifold unless otherwise stated. ^{1}H, ^{19}F, ^{13}C, ^{15}N, and ^{31}P NMR spectra were recorded on a Bruker 400, 500, 600, or 900 MHz spectrometer. All ^{1}H chemical shifts are reported in parts per million relative to tetramethylsilane or residual protiated solvent as a reference, ^{13}C chemical shifts are reported in parts per million relative to the solvent as a reference, ^{31}P NMR chemical shifts are reported in parts per million relative to an 85% H_3PO_4 external standard, ^{19}F NMR chemical shifts are reported in parts per million relative to a $CFCl_3$ external standard, and all ^{15}N NMR chemical shifts are reported in parts per million relative to an NH_3 external standard. Elemental analyses were obtained at the Microanalytical Facility at the University of California, Berkeley. ESI-MS analyses and variable temperature IR spectra were obtained at the Lawrence Berkeley National Laboratory Catalysis Facility. X-ray crystal structures were obtained at the Small Molecule X-ray Crystallography Facility at the University of California, Berkeley. IR spectra were obtained on a Bruker Vertex80 Time-Resolved FTIR spectrometer.

$Pd(P(t\text{-}Bu)_3)_2$[96] and 4-chloro-*N*-methylbenzamide[97] were synthesized from previously reported procedures. All glassware was dried in an oven at 130 ºC for at least 6 hours. All other aryl halides were purchased from commercial sources, freeze-pump-thawed thrice, and stored over 4Å molecular sieves for 24 hours. $N(n\text{-butyl})_4Cl$ was recrystallized from acetone and diethyl ether and dried over P_2O_5 under dynamic vacuum for three days at ambient temperature. $N(n\text{-butyl})_4PF_6$ was recrystallized from ethanol and dried at 70 °C under dynamic vacuum for 12 hours. Trimethoxybenzene was purified by sublimation at 65 °C under static vacuum (100 mTorr). Anhydrous K_2CO_3 was purchased from a commercial source and dried under dynamic vacuum at 100 ºC for 12 hours. All other reagents were obtained from commercial sources and used as received. THF-d_8, DMSO-d_6, and 1,2-difluorobenzene were distilled from CaH_2, freeze-pump-thawed thrice, and stored over 4 Å or 3 Å molecular sieves for 24 hours. DMSO was vacuum distilled over CaH_2, freeze-pump-thawed thrice, and stored over 4 Å molecular sieves for 24 hours. All other deuterated solvents were freeze-pump-thawed thrice and stored over 4 Å molecular sieves for 24 hours. All other solvents were purchased from Sigma Aldrich, sparged with nitrogen for 45 minutes, and dried with a solvent purification system using a 1 m column containing activated alumina. ^{13}CO, $^{13}CH_3I$, and $^{15}NH_3$ (10 atom% ^{15}N) were purchased from commercial sources and used without further purification. Variable temperature solution cell IR spectra were obtained in a sealed CaF_2 cell, with a 0.5 mm lead spacer, held within a water heated jacket purchased from Specac.

Without exception, all DCPP bound Pd^{II} and Pd^{I} complexes synthesized in this work precipitate or crystallize as solvates, and the solvate molecules could not be removed even under prolonged exposure to vacuum. To quantify the amount of solvent per palladium complex and to simplify analysis by NMR spectroscopy, the Pd^{II} or Pd^{I} solvates were dissolved in DCM or benzene and dried in vacuo to afford DCM or benzene solvates. Quantification of the amount of DCM or benzene in each sample was determined by ^{1}H NMR spectroscopy in $CDCl_3$, and elemental analyses were submitted based on those measurements.

CAUTION: Carbon monoxide and ammonia are toxic, and all manipulations with CO and NH_3 *must* be performed in a well-ventilated and functioning fume hood.

*Synthesis of Primary Benzamides (**3a-l**)*

In a representative experiment, a 25 mL Schlenk vessel equipped with a Teflon stir bar was charged with **1** (5.7 mg, 1.0 µmol), aryl chloride (0.400 mmol), K_2CO_3 (166 mg, 1.20 mmol), and 0.50 mL of DMSO. The Schlenk vessel was exported from the glovebox and attached to a 61 mL gas addition bulb. The Schlenk vessel and the gas addition bulb were attached to a Schlenk line, and the vessel was cooled in liquid nitrogen. The headspace of the vessel was evacuated, and NH_3 (645 Torr, 1.60 mmol) was condensed directly into the vessel from the gas addition bulb. The Schlenk line was pressurized to 450 Torr of CO, and the plug valve of the vessel was quickly opened and rapidly closed. The reaction vessel was warmed to room temperature and placed into a 110 ºC oil bath. After the reaction mixture was stirred for 24 hours at this temperature, the Schlenk vessel was removed from the oil bath and opened in a well-ventilated fume hood.

The resulting suspension was diluted with ca. 2 mL of ethyl acetate and filtered through a silica gel plug. The plug was washed with 15 mL of ethyl acetate. The crude reaction mixture was concentrated and purified by silica gel chromatography to obtain a white solid.

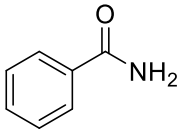

3a

3a was obtained as a white powder (40.0 mg, 83%). **^{1}H** NMR (500 MHz, DMSO-d_6) δ 8.00 (s, 1H), 7.92 – 7.86 (m, 2H), 7.53 (t, J = 7.3 Hz, 1H), 7.46 (t, J = 7.5 Hz, 2H), 7.39 (s, 1H). **^{13}C**{^{1}H} NMR (126 MHz, DMSO-d_6) δ 168.4, 134.7, 131.7, 128.7, 127.9. HRMS (ESI+) calcd for C_7H_8NO $[M+H]^+$: 122.0606. Found: 122.0602.

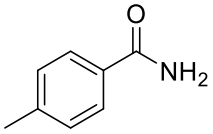

3b

3b was obtained as a white powder (48.1 mg, 89%). **^{1}H** NMR (400 MHz, DMSO-d_6) δ 7.87 (s, 1H), 7.80 – 7.64 (m, 2H), 7.25 (s, 1H), 7.21 (d, J = 8.0 Hz, 2H), 2.31 (s, 3H). **^{13}C**{^{1}H} NMR (126 MHz, DMSO-d_6) δ 168.2, 141.5, 131.9, 129.2, 128.0, 21.4. HRMS (ESI+) calcd for $C_8H_{10}NO$ $[M+H]^+$: 136.0762. Found: 136.0760.

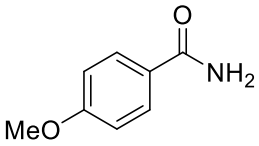

3c

3c was obtained as a white powder (50.5 mg, 84%). **^{1}H** NMR (500 MHz, DMSO-d_6) δ 8.13 – 7.57 (m, 3H), 7.21 (s, 1H), 6.98 (d, J = 8.9 Hz, 2H), 3.81 (s, 3H). **^{13}C**{^{1}H} NMR (126 MHz, DMSO-d_6) δ 167.9, 162.0, 129.8, 127.0, 113.8, 55.8. HRMS (ESI+) calcd for $C_8H_{10}NO_2$ $[M+H]^+$: 152.0711. Found: 152.0707.

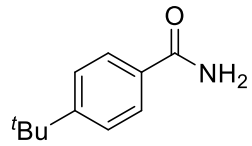

3d

3d was obtained as a white powder (53.3 mg, 75%). **^{1}H** NMR (500 MHz, DMSO-d_6) δ 7.92 (s, 1H), 7.86 – 7.75 (m, 2H), 7.53 – 7.39 (m, 2H), 7.30 (s, 1H), 1.30 (s, 9H). **^{13}C**{^{1}H} NMR (126 MHz, DMSO-d_6) δ 168.3, 154.4, 132.0, 127.8, 125.4, 35.1, 31.4. HRMS (ESI+) calcd for $C_{11}H_{16}NO$ $[M+H]^+$: 178.1232. Found: 178.1229.

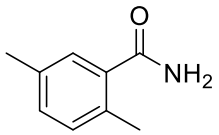

3e

3e was obtained as a white powder (36.8 mg, 62%). **^{1}H** NMR (500 MHz, DMSO-d_6) δ 7.67 (s, 1H), 7.32 (s, 1H), 7.18 (s, 1H), 7.15 – 7.08 (m, 2H), 2.31 (s, 3H), 2.28 (s, 3H). **^{13}C**{^{1}H} NMR (126 MHz, DMSO-d_6) δ 171.6, 137.4, 134.8, 132.4, 130.9, 130.2, 128.1, 20.9, 19.6. HRMS (ESI+) calcd for $C_9H_{12}NO$ $[M+H]^+$: 150.0919. Found: 150.0924.

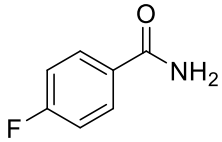

3f

3f was obtained as a white powder (52.5 mg, 94%). **^{1}H** NMR (500 MHz, Acetonitrile-d_3) δ 8.13 – 7.66 (m, 1H), 7.22 (t, J = 8.8 Hz, 1H), 6.77 (s, 1H), 6.04 (s, 1H). **^{13}C**{^{1}H} NMR (126 MHz, Acetonitrile-d_3) δ 167.5, 164.7 (d, J = 249.0 Hz), 130.4, 130.0 (d, J = 9.3 Hz), 115.2 (d, J = 22.1 Hz). **^{19}F** NMR (470 MHz, Acetonitrile-d_3) δ -110.67 (ddd, J = 14.1, 8.8, 5.2 Hz). HRMS (ESI+) calcd for C_7H_7FNO $[M+H]^+$: 140.0511. Found: 140.0513.

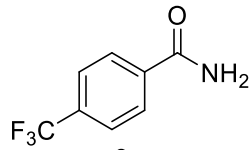

3g

3g was obtained as a white powder (75.4 mg, 100%). **^{1}H** NMR (500 MHz, DMSO-d_6) δ 8.22 (s, 1H), 8.07 (d, J = 8.1 Hz, 2H), 7.85 (d, J = 8.1 Hz, 2H), 7.66 (s, 1H). **^{13}C**{^{1}H} NMR (126 MHz, DMSO-d_6) δ 167.1, 138.5, 131.6 (q, J = 31.8 Hz), 128.8, 125.7 (q, J = 3.6 Hz), 124.4 (q, J = 272.4 Hz). **^{19}F** NMR (470 MHz, DMSO-d_6) δ -61.33. HRMS (ESI+) calcd for $C_8H_7F_3NO$ $[M+H]^+$:

190.0479. Found: 190.0476.

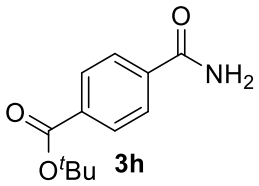

3h

3h was obtained as a white powder (75.3 mg, 85%). **^{1}H** NMR (500 MHz, DMSO-d_6) δ 8.15 (s, 1H), 8.02 – 7.88 (m, 4H), 7.58 (s, 1H), 1.56 (s, 9H). **^{13}C** NMR (126 MHz, DMSO-d_6) δ 167.6, 164.9, 138.5, 134.0, 129.4, 128.2, 81.6, 28.2. HRMS (ESI+) calcd for $C_{12}H_{16}NO_3$ $[M+H]^+$: 222.1130. Found: 222.1139.

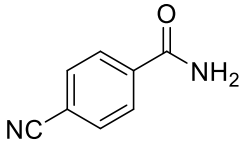

3i

3i was obtained as a white powder (35.1 mg, 60%). **^{1}H** NMR (500 MHz, DMSO-d_6) δ 8.23 (s, 1H), 8.03 (d, J = 8.4 Hz, 2H), 7.96 (d, J = 8.3 Hz, 2H), 7.70 (s, 1H). **^{13}C** NMR (126 MHz, DMSO-d_6) δ 166.9, 138.8, 132.9, 128.7, 118.9, 114.1. HRMS (ESI+) calcd for $C_8H_6N_2ONa$ $[M+Na]^+$:169.0378. Found: 169.0375.

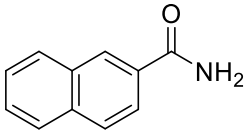

3j

3j was obtained as a white powder (44.1 mg, 64%). **^{1}H** NMR (500 MHz, DMSO-d_6d) δ 8.51 (s, 1H), 8.17 (s, 1H), 8.04 – 7.95 (m, 4H), 7.64 – 7.57 (m, 2H), 7.51 (s, 1H). **^{13}C** NMR (126 MHz, DMSO-d_6) δ 168.4, 134.6, 132.6, 132.1, 129.4, 128.3, 128.3, 128.1, 128.0, 127.1, 124.9. HRMS (ESI+) calcd for $C_{11}H_9NONa$ $[M+Na]^+$: 194.0582. Found: 194.0586.

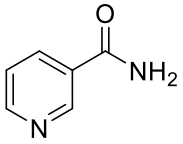

3k

3k was obtained as a white powder (37.9 mg, 77%). **^{1}H** NMR (500 MHz, DMSO-d_6) δ 9.04 (d, J = 2.4 Hz, 1H), 8.71 (dd, J = 4.8, 1.7 Hz, 1H), 8.30 – 8.10 (m, 2H), 7.63 (s, 1H), 7.51 (dd, J = 7.9, 4.8 Hz, 1H). **^{13}C**{^{1}H} NMR (126 MHz, DMSO-d_6) δ 166.9, 152.4, 149.2, 135.6, 130.1, 123.9. HRMS (ESI+) calcd for $C_6H_7N_2O$ [M+H]$^+$: 123.0558. Found: 123.0555.

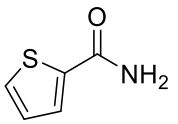

3l

3l was obtained as a white powder (35.2 mg, 69%). **^{1}H** NMR (500 MHz, DMSO-d_6) δ 7.98 (s, 1H), 7.77 – 7.72 (m, 2H), 7.40 (s, 1H), 7.14 (dd, J = 4.8, 3.8 Hz, 1H). **^{13}C** NMR (126 MHz, DMSO-d_6) δ 163.3, 140.8, 131.5, 129.1, 128.4. HRMS (ESI+) calcd for C_5H_5NOSNa [M+Na]$^+$: 149.9990. Found: 149.9984.

Synthesis of Palladium Complexes

*(DCPP)Pd(C_2H_4) (**1**)*

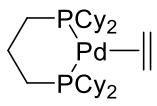

1

A 50 mL Schlenk flask equipped with a Teflon-coated stir bar was charged with Pd[P(^{t}Bu)$_3$]$_2$ (488 mg, 0.954 mmol), DCPP (500 mg, 1.12 mmol), 14 mL of THF, and 22 mL of pentane. This yellow solution was capped with a septum and stirred for 2 h. While under a flow of nitrogen, a vent needle attached to a bubbler was pierced through the septum. The flow of nitrogen through the bubbler was stopped, and ethylene was immediately flushed through the side arm of the Schlenk flask into the bubbler. The reaction mixture was stirred vigorously under a continuous flow of ethylene for 45 min to obtain a white precipitate. The resulting suspension was imported into a glovebox, and the precipitate was isolated on a fritted glass funnel, washed with ether (3 x 2 mL), and dried under vacuum to obtain ethylene complex **1** (434.4 mg, 80%, white powder). Colorless, single crystals of ethylene complex **1** were obtained by slow diffusion of pentane into a concentrated solution of **1** in toluene at -15 °C under 760 Torr of ethylene. Anal. Calc'd for $C_{29}H_{54}P_2Pd$: C, 60.99; H, 9.53. Found: C, 60.82; H, 9.42. **^{1}H** NMR (400 MHz, Benzene-d_6) δ 3.02 (s, 4H), 2.11-1.09 (m, 50). **^{31}P** NMR (162 MHz, Benzene-d_6) δ 21.6.

*(DCPP)Pd(CO)$_2$ (**4**)*

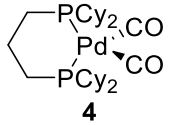

4

A J. Young tube was charged with ethylene complex **1** (30.0 mg, 0.0525 mmol) and 0.500 mL of benzene-d_6. The resulting white suspension was cooled in liquid nitrogen, and the headspace was evacuated under vacuum. The NMR tube was warmed to room temperature and pressurized with 1000 Torr of CO. The suspension was shaken (ca. 40 s) and re-pressurized to 1000 Torr, and this process was repeated until a colorless, homogenous solution was obtained. **^{1}H** NMR (600 MHz, Benzene-d_6, 1000 Torr CO) δ 1.90 (d, J = 12.8 Hz, 4H), 1.79-1.04 (m, 46H).**^{13}C** NMR (151 MHz, Benzene-d_6, 1000 Torr CO) δ 196.7 (br. s), 35.9 (dd, J = 6.7, 4.5 Hz), 28.7 (d, J = 9.1 Hz), 27.6 (d, J = 3.0 Hz), 27.2 – 27.0 (m), 26.45, 23.9 (t, J = 8.8 Hz), 22.2 (d, J = 6.5 Hz). **^{31}P**{^{1}H} NMR (243 MHz, Benzene-d_6, 1000 Torr CO) δ 20.8. IR (DMSO and toluene 1:1 v/v): ν_{CO} = 1993, 1949 cm^{-1}.

Determination of Yield

A J. Young tube was charged with ethylene complex **1** (10.0 mg, 0.0175 mmol), trimesitylphosphine (7.5 mg, 0.019 mmol) and 0.6 mL of toluene. The resulting white suspension

was cooled in liquid nitrogen, and the headspace was evacuated under vacuum. The NMR tube was warmed to room temperature and pressurized with 1000 Torr of CO. The suspension was shaken (ca. 40 s) and re-pressurized to 1000 Torr, and this process was repeated until a colorless, homogenous solution was obtained. By ^{31}P NMR spectroscopy, the yield of **1** was determined to be 98% relative to trimesitylphosphine.

*Single Crystals of **4***

A J. Young tube was charged with ethylene complex **1** (8.0 mg, 0.014 mmol), 0.25 mL of DMSO, and 0.25 mL of toluene. The resulting white suspension was cooled in liquid nitrogen, and the headspace was evacuated under vacuum. The NMR tube was warmed to room temperature and pressurized with 1000 Torr of CO. The suspension was shaken (ca. 40 s) and re-pressurized to 1000 Torr of CO, and this process was repeated until a colorless, homogenous solution was obtained. This clear solution was left to sit at room temperature to obtain colorless crystals of **4**. Upon removal from a CO atmosphere, crystals of **4** slowly decomposed at room temperature, likely from the dissociation of CO.

General Procedure for the Synthesis of Pd^{II} Aryl Halide Complexes (5a-j)

In a representative experiment, a 20 mL vial equipped with a Teflon stir bar was charged with Pd[P(^{t}Bu)$_3$]$_2$ (80.0 mg, 0.157 mmol), DCPP (68.4 mg, 0.157 mmol), and 5 mL of toluene. The resulting yellow solution was stirred for 1 h at room temperature. The aryl halide (1.25 mmol) was added to this solution, which was warmed to 80 °C and stirred for 15 h. Pentane (10 mL) was added to the reaction mixutre, and the resulting suspension was cooled to 0 °C for at least 5 h to obtain a white precipitate. The precipitate was isolated on a fritted glass funnel and washed with pentane (3 x 2 mL). The resulting powder was dissolved in 3 mL of DCM and dried under vacuum. The powder was re-dissolved in 3 mL of DCM and dried once more to obtain the product as a DCM solvate.

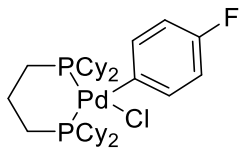

5a

The reaction to obtain complex **5a** was performed with 60.0 mg of Pd[(P^{t}Bu)$_3$]$_2$, 51.3 mg of DCPP, and 25.0 µL of 4-fluoro-chlorobenzene. Compound **5a** was obtained as a 1.5 DCM solvate (42.7 mg, 45%, white powder). **^{1}H** NMR (400 MHz, Chloroform-*d*) δ 7.33 (q, *J* = 7.3 Hz, 2H), 6.84 (t, *J* = 8.3 Hz, 2H), 2.43-0.88 (m, 50H). **^{19}F** NMR (376 MHz, Chloroform-*d*) δ -121.94 (t, *J* = 8.6 Hz). **^{31}P**{^{1}H} NMR (162 MHz, Chloroform-*d*) δ 24.8 (d, *J* = 39.6 Hz), 5.7 (dd, *J* = 39.6, 1.6 Hz). Anal. Calcd for $C_{34.5}H_{57}Cl_4FP_2Pd$: C, 51.73; H, 7.17. Found: C, 52.10; H, 7.11.

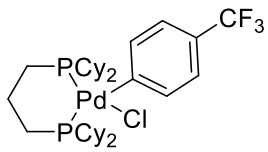

5b

The reaction to obtain complex **5b** was performed with 60.0 mg of Pd[(P^{t}Bu)$_3$]$_2$, 51.3 mg of DCPP, and 31.4 µL of 4-trifluoromethyl-chlorobenzene. Compound **5b** was obtained as a 0.43 DCM solvate (66.8 mg, 74%, white powder). **^{1}H** NMR (400 MHz, Chloroform-*d*) δ 7.56 (t, *J* = 7.5 Hz, 2H), 7.29 (d, *J* = 6.9 Hz, 2H), 2.43-0.92 (m, 50H). **^{19}F** NMR (376 MHz, Chloroform-*d*) δ -60.96. **^{31}P**{^{1}H} NMR (162 MHz, Chloroform-*d*) δ 24.7 (d, *J* = 39.7 Hz), 5.9 (d, *J* = 39.7 Hz). Anal. Calcd for $C_{34.43}H_{54.86}Cl_{1.86}F_3P_2Pd$: C, 54.40; H, 7.27. Found: C, 54.29; H, 7.33.

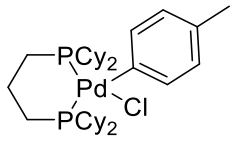

5c

Complex **5c** was obtained as a 1.5 DCM solvate (76.6 mg, 61%, white powder). **^{1}H** NMR (500 MHz, Methylene Chloride-d_2) δ 7.26 (t, J = 7.4 Hz, 2H), 6.92 (d, J = 5.6 Hz, 2H), 2.34-2.19 (m, 9H), 2.06-1.01 (m, 44 H). **^{31}P**{^{1}H} NMR (162 MHz, Chloroform-d) δ 25.1 (d, J = 41.4 Hz), 5.0 (d, J = 41.4 Hz). Anal. Calcd for $C_{35.5}H_{60}Cl_4P_2Pd$: C, 53.50; H, 7.59. Found: C, 53.33; H, 7.41.

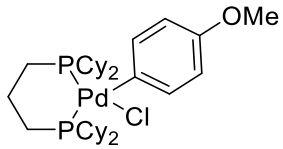

5d

Complex **5d** was obtained as a 1.1 DCM solvate (81.7 mg, 65%, white powder). **^{1}H** NMR (600 MHz, Methylene Chloride-d_2) δ 7.23 (t, J = 7.6 Hz, 2H), 6.70 (d, J = 7.8 Hz, 2H), 3.75 (s, 3H), 2.38-0.98 (m, 50H). **^{31}P**{^{1}H} NMR (162 MHz, Chloroform-d) δ 25.1 (d, J = 40.3 Hz), 5.2 (d, J = 40.2 Hz). Anal. Calcd for $C_{36.1}H_{59.2}Cl_{3.2}OP_2Pd$: C, 53.72; H, 7.39. Found: C, 53.56; H, 7.49.

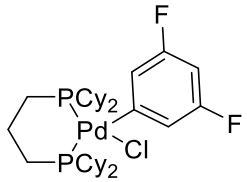

5e

Complex **5e** was obtained as a 1.65 DCM solvate (39.6 mg, 31%, white powder). **^{1}H** NMR (400 MHz, Chloroform-d) δ 6.98 (t, J = 7.2 Hz, 2H), 6.39 (tt, J = 9.5, 2.3 Hz, 1H), 2.40-0.92 (m, 50H). **^{19}F** NMR (376 MHz, Chloroform-d) δ -113.58 (q, J = 8.6 Hz). **^{31}P**{^{1}H} NMR (162 MHz, Chloroform-d) δ 24.8 (d, J = 38.3 Hz), 6.7 (dt, J = 38.2, 8.8 Hz). Anal. Calcd for $C_{34.65}H_{56.3}Cl_{4.3}F_2P_2Pd$: C, 50.04; H, 6.82. Found: C, 50.27; H, 6.79.

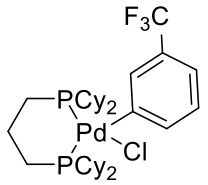

5f

Complex **5f** was obtained as a 0.36 DCM solvate (79.6 mg, 66%, white powder). **^{1}H** NMR (400 MHz, Chloroform-d) δ 7.69 (t, J = 6.9 Hz, 1H), 7.63 (d, J = 7.9 Hz, 1H), 7.22 – 7.13 (m, 2H), 2.42-0.81 (m, 50H). **^{19}F** NMR (376 MHz, Chloroform-d) δ -60.89. **^{31}P**{^{1}H} NMR (162 MHz, Chloroform-d) δ 24.4 (d, J = 39.9 Hz), 5.7 (d, J = 39.9 Hz). Anal. Calcd for $C_{34.36}H_{54.72}Cl_{1.72}F_3P_2Pd$: C, 54.72; H, 7.31. Found: C, 54.42; H, 7.37.

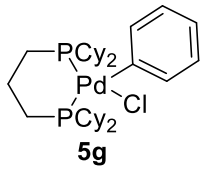

5g

Complex **5g** was obtained as a 2.0 DCM solvate (75.3 mg, 58%, white powder). **^{1}H** NMR (500 MHz, Chloroform-d) δ 7.43 (t, J = 7.6 Hz, 2H), 7.08 (td, J = 7.2, 1.9 Hz, 2H), 6.97 – 6.90 (m, 1H), 2.42 – 2.18 (m, 6H), 2.07 –1.90 (m, 2H), 1.87 – 1.12 (m, 40H), 1.07 – 0.94 (m, 2H). **^{31}P**{^{1}H} NMR (162 MHz, Chloroform-d) δ 24.6 (d, J = 41.5 Hz), 5.1 (d, J = 41.7 Hz). Anal. Calcd for $C_{35}H_{59}Cl_5P_2Pd$: C, 50.93; H, 7.20. Found: C, 51.06; H, 7.12.

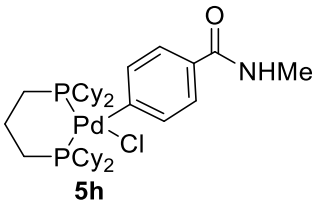

5h

Complex **5h** was obtained as a 1.5 DCM solvate (76.6 mg, 58%, white powder). **^{1}H** NMR (500 MHz, Chloroform-d) δ 7.55 (t, J = 7.4 Hz, 2H), 7.49 – 7.43 (m, 2H), 6.10 (d, J = 5.1 Hz, 1H), 3.00 (d, J = 4.8 Hz, 3H), 2.40 – 2.16 (m, 6H), 2.06-1.91 (m, 2H), 1.88 – 0.95 (m, 42H). **^{31}P**{^{1}H} NMR (162 MHz, Chloroform-d) δ 25.0 (d, J = 40.0 Hz), 5.6 (d, J = 40.3 Hz). Anal. Calcd for $C_{36.5}H_{61}Cl_4NOP_2Pd$: C, 52.19; H, 7.32; N, 1.67. Found: C, 52.36; H, 7.29; N, 1.72.

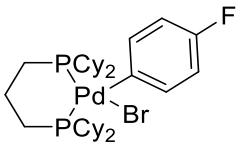

5i

The reaction to obtain complex **5i** was performed with 50.0 mg of $Pd[(P^tBu)_3]_2$, 47.0 mg of DCPP, and 43.0 µL of 4-fluorobromobenzene. **5i** was obtained as a 2.0 DCM solvate (72.3 mg, 83%, white powder). **^{1}H** NMR (400 MHz, Chloroform-*d*) δ 7.33 (q, *J* = 7.2 Hz, 2H), 6.84 (ddd, *J* = 10.2, 8.5, 1.9 Hz, 2H), 2.40 – 2.28 (m, 4H), 2.28 – 2.15 (m, 2H), 1.79 (s, 44H). **^{19}F** NMR (376 MHz, Chloroform-*d*) δ -122.18. **^{31}P**{^{1}H} NMR (162 MHz, Chloroform-*d*) δ 23.0 (d, *J* = 39.7 Hz), 4.2 (d, *J* = 40.1 Hz). Anal. Calcd for $C_{35}H_{58}BrCl_4FP_2Pd$: C, 47.34; H, 6.58. Found: C, 47.72; H, 6.64.

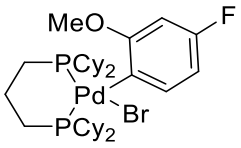

5j

Complex **5j** was obtained as a 0.62 DCM solvate (94.6 mg, 76%, white powder). **^{1}H** NMR (400 MHz, Chloroform-*d*) δ 7.00 (q, *J* = 8.0 Hz, 1H), 6.56 – 6.46 (m, 1H), 6.37 (dt, *J* = 12.1, 2.8 Hz, 1H), 3.76 (s, 3H), 2.86 – 0.49 (m, 50H). **^{19}F** NMR (376 MHz, Chloroform-*d*) δ -120.22. **^{31}P**{^{1}H} NMR (162 MHz, Chloroform-*d*) δ 21.4 (d, *J* = 37.2 Hz), 5.8 (d, *J* = 37.0 Hz). Anal. Calcd for $C_{34.62}H_{57.24}BrCl_{1.24}FOP_2Pd$: C, 51.93; H, 7.21. Found: C, 52.20; H, 7.41.

*General Procedure for the Synthesis of Pd^{II} Phenylacyl Complexes from Acid Chlorides (**6a-b, 6e-f**)*

The following procedure was adapted from Koide et al.[98] In a representative experiment, a 20 mL vial equipped with a Teflon-coated stir bar was charged with $Pd(PPh_3)_4$ (200 mg, 0.173 mmol), a substituted benzoyl chloride (0.208 mmol), and 8 mL of toluene. The vial was sealed with a Teflon lined cap and wrapped with electrical tape to exclude light. The reaction mixture was stirred at ambient temperature for 12 h. Pentane (10 mL) was added to precipitate a yellow powder, which was isolated on a fritted glass funnel and washed with pentane (3 x 2 mL). Without further purification, the yellow powder was suspended in a solution of DCPP (83.2 mg, 0.190 mmol) in 10 mL of toluene. The resulting suspension was stirred for 14 h at room temperature, and 10 mL of pentane was added to this solution, which was cooled to 0 °C for 12 h to precipitate the desired product. The precipitate was isolated on a fritted glass funnel and washed with pentane (3 x 2 mL). The resulting powder was dissolved in 3 mL of DCM and dried under vacuum. The powder was re-dissolved in 3 mL of DCM and dried once more to obtain the product as a DCM solvate.

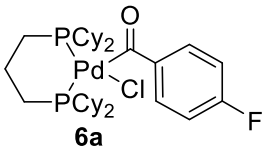

6a

Complex **6a** was obtained as a 0.65 DCM solvate (46.0 mg, 35%, yellow powder). **^{1}H** NMR (400 MHz, Chloroform-*d*) δ 8.17 (dd, *J* = 8.6, 5.8 Hz, 2H), 7.07 (t, *J* = 8.6 Hz, 2H), 2.33–0.74 (m, 50H).**^{19}F** NMR (376 MHz, Chloroform-*d*) δ -108.83. **^{31}P**{^{1}H} NMR (162 MHz, Chloroform-*d*) δ 21.8 (d, *J* = 63.2 Hz), 1.2 (d, *J* = 63.2 Hz). Anal. Calcd for $C_{34.64}H_{55.3}Cl_{2.3}FOP_2Pd$: C, 54.99; H, 7.37. Found: C, 54.98; H, 7.02.

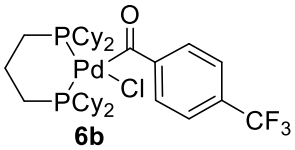

6b

Complex **6b** was obtained as a 0.50 DCM solvate (94.5 mg, 69%, yellow powder). **^{1}H** NMR (500 MHz, Chloroform-*d*) δ 8.28 (d, *J* = 8.0 Hz, 2H), 7.70 (d, *J* = 8.1 Hz, 2H), 2.35–0.83 (m, 50H). **^{19}F** NMR (470 MHz, Chloroform-*d*) δ -62.62. **^{31}P**{^{1}H} NMR (162 MHz, Chloroform-*d*) δ 22.4 (d, *J* = 61.9 Hz), 1.9 (d, *J* = 62.1 Hz). Anal. Calcd for $C_{35.5}H_{55}Cl_2F_3OP_2Pd$: C, 53.70; H, 6.98. Found: C, 54.04; H, 6.80.

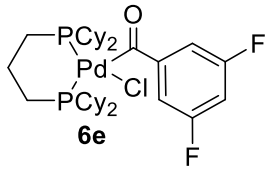

6e

Complex **6e** was obtained as a 0.75 DCM solvate (94.9 mg, 70%, orange powder). **^{1}H** NMR (500 MHz, Chloroform-*d*) δ 7.72 (m, 2H), 6.87 (ddt, *J* = 8.3, 4.9, 2.5 Hz, 1H), 2.32–0.85 (m, 50H). **^{19}F** NMR (376 MHz, Chloroform-*d*) δ -109.23. **^{31}P**{^{1}H} NMR (162 MHz, Chloroform-*d*) δ 22.6 (d, *J* = 61.0 Hz), 2.4 (d, *J* = 61.1 Hz). Anal. Calcd for $C_{34.75}H_{54.5}Cl_{2.5}F_2OP_2Pd$: C, 53.28; H, 7.01. Found: C, 53.52; H, 6.93.

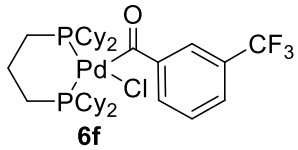

6f

Complex **6f** was obtained as a 0.10 DCM solvate (64.7 mg, 49%, orange powder). **^{1}H** NMR (500 MHz, Chloroform-*d*) δ 8.82 (s, 1H), 8.11 (d, *J* = 7.7 Hz, 1H), 7.67 (d, *J* = 7.7 Hz, 1H), 7.52 (t, *J* = 7.7 Hz, 1H), 2.39–0.56 (m, 50H). **^{19}F** NMR (470 MHz, Chloroform-*d*) δ -62.55. **^{31}P**{^{1}H} NMR (162 MHz, Chloroform-*d*) δ 22.5 (d, *J* = 61.6 Hz), 2.0 (d, *J* = 61.7 Hz). Anal. Calcd for $C_{35.1}H_{54.2}Cl_{1.2}F_3OP_2Pd$: C, 55.46; H, 7.19. Found: C, 55.37; H, 7.08.

*Synthesis of Pd^{II} Phenylacyl Complexes Obtained by Carbonylation of Pd^{II} Aryl Halide Complexes (**6c-d**)*

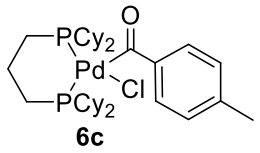

6c

A 0.5 mL solution of **5c** (48.7 mg, 0.0611 mmol) in DCM was transferred into a J. Young NMR tube. The J. Young NMR tube was cooled in liquid nitrogen, and the headspace was evacuated. The NMR tube was warmed to room temperature and backfilled to 1000 Torr of CO. The NMR tube was shaken (ca. 40 s), refilled with CO to 1000 Torr, and shaken again to obtain a yellow solution. The yellow solution was left to sit at room temperature for one hour, at which point it was imported into a glovebox and dried in vacuo to obtain **6c** as a 0.5 DCM solvate (42.0 mg, 93%, yellow solid). **^{1}H** NMR (400 MHz, Chloroform-*d*) δ 8.06 (d, *J* = 8.0 Hz, 2H), 7.19 (d, *J* = 7.9 Hz, 2H), 2.68–0.46 (m, 53 H). **^{31}P**{^{1}H} NMR (162 MHz, Chloroform-*d*) δ 21.7 (d, *J* = 64.3 Hz), 1.2 (d, *J* = 64.5 Hz). Anal. Calcd for $C_{35.5}H_{58}Cl_2OP_2Pd$: C, 57.61; H, 7.90. Found: C, 57.90; H, 7.70.

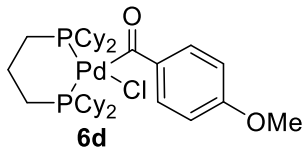

6d

A 0.5 mL solution of **5d** (24.7 mg, 0.0360 mmol) in DCM was transferred into a J. Young NMR tube. The J. Young NMR tube was cooled in liquid nitrogen, and the headspace was evacuated. The NMR tube was warmed to room temperature and backfilled to 1000 Torr of CO. The NMR was tube was shaken (ca. 40 s), refilled with CO to 1000 Torr, and shaken again to obtain a yellow solution. After sitting at room temperature for 20 minutes, the yellow solution was imported into a glovebox and dried in vacuo to obtain crude **6d**. Crude **6d** was dissolved in 3 mL benzene and dried under vacuum. This process was repeated once more to obtain **6d** as a 0.25 benzene solvate (20.2 mg, 76%, yellow solid). **^{1}H** NMR (400 MHz, Chloroform-*d*) δ 8.14 (d, *J* = 8.4 Hz, 2H), 6.90 (d, *J* = 8.3 Hz, 2H), 3.85 (s, 3H), 2.41–0.43 (m, 50H). **^{31}P**{^{1}H} NMR (162 MHz, Chloroform-*d*) δ 21.7 (d, *J* = 64.6 Hz), 1.1 (d, *J* = 64.0 Hz). Anal. Calcd for $C_{36.5}H_{58.5}ClO_2P_2Pd$: C, 59.79; H, 8.04. Found: C, 59.51; H, 8.21.

*Synthesis of Pd^{II} Phenylacyl Complexes Obtained by Oxidative Addition of an Aryl Halide under CO Atmosphere (**6g-j**)*

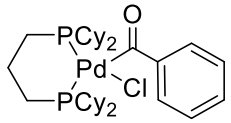

6g

A J. Young NMR tube was charged with ethylene complex **1** (30.0 mg, 0.0525 mmol), chlorobenzene (58.2 µL, 0.525 mmol), and 1 mL of THF. The resulting white suspension was cooled in liquid nitrogen, and the headspace was evacuated. The NMR tube was warmed to room temperature and backfilled with 750 Torr of CO. The NMR was tube was shaken (ca. 40 s) and refilled with CO to 750 Torr, and this process was repeated until a colorless, homogeneous solution was obtained. The NMR tube was warmed to 90 °C for 20 h and imported into a glovebox. The desired product was precipitated by the addition of 4 mL of pentane to obtain a yellow powder, which was isolated on a fritted glass funnel and washed with pentane (3 x 3 mL). The powder was dissolved in DCM and dried under vacuum. This process was repeated once more to obtain **6g** as a 0.38 DCM solvate (25.5 mg, 68%, yellow solid). **^{1}H** NMR (500 MHz, Chloroform-*d*) δ 8.34–8.00 (m, 2H), 7.40 (m, 3H), 2.66–0.61 (m, 50H). **^{31}P**{^{1}H} NMR (162 MHz, Chloroform-*d*) δ 21.7 (d, *J* = 64.2 Hz), 1.3 (d, *J* = 64.1 Hz). HRMS (ESI+) calcd for $C_{34}H_{55}ClNaOP_2Pd$ $[M+Na]^+$: 707.2348. Found: 707.2348.

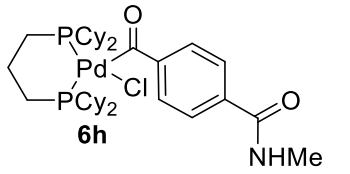

6h

A J. Young NMR tube was charged with ethylene complex **1** (30.0 mg, 0.0525 mmol), 4-chloro-N-methylbenzamide (22.1 mg, 0.130 mmol), 0.5 mL of 2-MeTHF, and 0.5 mL of THF. The resulting white suspension was cooled in liquid nitrogen, and the headspace was evacuated. The NMR tube was warmed to room temperature and backfilled with 750 Torr of CO. The NMR was tube was shaken (ca. 40 s) and refilled with CO to 750 Torr, and this process was repeated until a colorless, homogeneous solution was obtained. The NMR tube was warmed to 100 °C for 14 h and left to sit at room temperature for 4 h. The NMR tube was imported into a glovebox, and the crude reaction mixture was dried in vacuo. The resulting yellow solid was suspended in 7 mL of ether and stirred for 45 minutes. The solid was collected on a glass fiber filter paper plug, washed with ether (3 x 3 mL), and washed through the plug with DCM. The yellow DCM filtrate was concentrated under vacuum, dissolved in 2 mL DCM, and dried in vacuo to obtain **6h** as a 0.50 DCM solvate (32.8 mg, 80%, yellow solid). **^{1}H** NMR (600 MHz, Chloroform-*d*) δ 8.20 (d, *J* = 8.0 Hz, 2H), 7.79 (d, *J* = 8.0 Hz, 2H), 6.17 (d, *J* = 5.2 Hz, 1H), 3.02 (d, *J* = 4.8 Hz, 3H), 2.40–0.09 (m, 50H). **^{31}P**{^{1}H} NMR (243 MHz, Chloroform-*d*) δ 22.4 (d, *J* = 62.9 Hz), 1.8 (d, *J* = 62.7 Hz). Anal. Calcd for $C_{36.5}H_{59}Cl_2NO_2P_2Pd$: C, 55.98; H, 7.59; N, 1.79. Found: C, 55.73; H, 7.54; N, 1.73

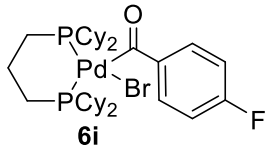

6i

A J. Young NMR tube was charged with ethylene complex **1** (30.0 mg, 0.0525 mmol), 4-bromo-fluorobenzene (46.2 µL, 0.420 mmol), and 1 mL of THF. The resulting white suspension was cooled in liquid nitrogen and the headspace was evacuated. The NMR tube was warmed to room temperature and backfilled with 750 Torr of CO. The NMR was tube was shaken (ca. 40 s) and refilled with CO to 750 Torr, and this process was repeated until a colorless, homogeneous solution was obtained. The NMR tube was warmed to 80 °C for 1.3 h and left to sit at room temperature for 40 min. The NMR tube was imported into a glovebox, and the 10 mL of pentane was added to the crude reaction mixture, which was cooled to 0 °C for four days. The mother liquor was removed and crystals of **6i** was washed with 2 mL of pentane and ether (2 x 2 mL). The crystals were suspended in 8 mL of ether, stirred for 12 h, and isolated on

a fritted glass funnel. The obtained yellow solid was dissolved in 3 mL of DCM and dried in vacuo. This process was repeated once more with DCM, and twice more with benzene to obtain **6i** as a 1.17 benzene and 0.20 DCM mixed solvate (19.0 mg, 46%, yellow powder). **^{1}H** NMR (400 MHz, Chloroform-*d*) δ 8.30 – 8.15 (m, 2H), 7.11 (t, *J* = 8.4 Hz, 2H), 2.88–0.50 (m, 50H). **^{19}F** NMR (376 MHz, Chloroform-*d*) δ -109.49. **^{31}P**{^{1}H} NMR (162 MHz, Chloroform-*d*) δ 20.0 (d, *J* = 63.7 Hz), 0.3 (d, *J* = 63.8 Hz). Anal. Calcd for $C_{34.4}H_{54.8}Cl_{0.8}BrOP_2Pd$: C, 52.97; H, 7.08. Found: C, 52.93; H, 6.91.

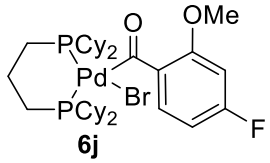

6j

A J. Young NMR tube was charged with ethylene complex **1** (16.0 mg, 0.028 mmol) and 0.6 mL of a C_6D_6 solution containing 2-methoxy-4-fluoro-bromobenzene (5.5 µL, 0.042 mmol). The resulting white suspension was cooled in liquid nitrogen, and the headspace was evacuated. The NMR tube was warmed to room temperature and backfilled with 800 Torr of CO. The NMR was tube was shaken (ca. 40 s) and refilled with CO to 800 Torr, and this process was repeated until a colorless, homogeneous solution was obtained. The NMR tube was warmed to 80 °C for 2.5 h and left to sit at room temperature for 30 minutes. NMR spectra were obtained on this sample which was determined to be a mixture of **5j** and **6j** in a ratio of 0.18:1, respectively. The yield was determined by quickly weighing trimethoxybenzene into the NMR tube while inside a glovebox. The NMR tube was cooled in liquid nitrogen, the headspace was evacuated, and while frozen, the tube was quickly pressurized to 800 Torr of CO. The tube was thawed to room temperature, and a ^{1}H NMR spectrum was collected. Based on integrations of the product relative to trimethoxybenzene, **6j** was obtained in 53% yield. **^{1}H** NMR (600 MHz, Benzene-d_6, 800 Torr CO) δ 8.69 (t, *J* = 8.1 Hz, 1H), 6.56-6.51 (m, 1H), 6.34 (dd, *J* = 11.1, 2.4 Hz, 1H), 3.32 (s, 3H), proton resonances of ligated DCPP could not be unambiguously assigned. **^{19}F** NMR (470 MHz, Benzene-d_6, 800 Torr CO) δ -108.28 (q, *J* = 8.9 Hz).**^{31}P**{^{1}H} NMR (243 MHz, Benzene-d_6, 800 Torr CO) δ 17.0 (d, *J* = 69.4 Hz), 0.5 (d, *J* = 69.5 Hz).

*Synthesis of (DCPP)Pd(4-fluorophenyl)(NH$_2$) (**7**)*

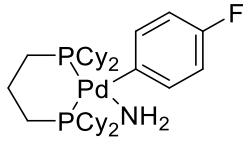

7

A 25 mL Schlenk vessel equipped with a Teflon stir bar was charged with Pd^{II} aryl chloride complex **5a** (40.5 mg, 0.0532 mmol) and 3 mL of DCM. The resulting colorless solution was frozen in liquid nitrogen, and the headspace was evacuated. While frozen, ammonia (250 Torr, 0.0532 mmol, non-isotopically enriched or 10 atom% ^{15}N) was condensed from a 61 mL gas bulb into the Schlenk vessel. The vessel was warmed to room temperature and imported into a glovebox. A solution of AgOTf (13.7 mg, 0.0532 mmol) in 2 mL THF was dispensed into the Schlenk vessel to immediately precipitate AgCl as a white powder. The vessel was sealed, and the resulting white suspension was stirred for 25 minutes and filtered through a glass fiber filter paper plug. The colorless filtrate was dried in vacuo to obtain a white powder. A solution of KHMDS (10.6 mg, 0.0532 mmol) in 0.8 mL of THF-d_8 was added to this solution to obtain a pale-yellow solution. **7** was synthesized in 93 % yield as determined by ^{19}F NMR against OTf anion. ^{15}N DEPT spectra of **7** were obtained by first collecting a DEPT-45 spectrum of **7**. Then, the same experimental parameters (i.e. number of scans, phasing, receiver gain, line broadening, etc.) were applied to subsequent DEPT-90 and DEPT-135 spectra. **^{1}H** NMR (600 MHz, THF-d_8) δ 7.35 (q, *J* = 7.1 Hz, 2H), 6.71 (t, *J* = 9.0 Hz, 2H), 2.32 – 2.21 (m, 2H), 2.08 – 1.90 (m, 7H), 1.86 – 1.78 (m, 8H), 1.72 – 1.62 (m, 14H), 1.58 – 1.48 (m, 8H), 1.36 – 1.16 (m, 11H), -0.51 (s, 2H or d, J_{NH} = 56.5 Hz with ^{15}N NH_3). **^{15}N** NMR (61 MHz, THF-d_8) δ 22.3 (dd, *J*

= 28.7, 3.1 Hz). **^{31}P**{^{1}H} NMR (243 MHz, THF-d_8) δ 10.7 (d, J = 40.6 Hz), 5.8 (d, J = 40.6 Hz). With $^{15}NH_3$, **^{31}P**{^{1}H} NMR (243 MHz, THF-d_8) δ 10.7 (dd, J = 40.5, 28.8 Hz), 5.8 (d, J = 40.6 Hz). **^{19}F** NMR (376 MHz, THF-d_8) δ -126.11.

*Synthesis of Pd^{I} Dimers (**8a-b**)*

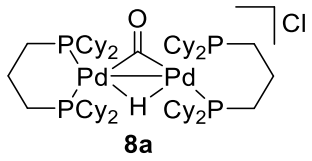

8a

A J. Young NMR tube was charged with ethylene complex **1** (35.0 mg, 0.0613 mmol), NH_4Cl (1.7 mg, 0.032 mmol), 600 µL THF, and 400 µL of DMSO. The resulting white suspension was frozen in liquid nitrogen, and the headspace was evacuated. The NMR tube was warmed to room temperature and backfilled with 1000 Torr of CO. The NMR was tube was shaken (ca. 40 s) and refilled back to a pressure of 1000 Torr CO, and this process was repeated 5 times to obtain a white suspension. The J. Young tube was warmed to 100 °C for 45 minutes to obtain an orange solution which turns pink upon cooling to room temperature. The J. Young tube was imported into a glovebox and transferred into a 20 mL vial. The tube was washed with 2 mL of THF, and the washings were combined. Ether (8 ml) and pentane (8 ml) were added to the pink THF solution, which was left to cool in a -35 °C freezer for 5 minutes to yield a pink precipitate. The precipitate was isolated on a glass fiber filter paper plug, washed with pentane (3 x 2 mL) and 2 mL of diethyl ether. The precipitate was washed through the plug with THF, and the pink filtrate was concentrated in vacuo. The resulting solid was dissolved in benzene and dried under vacuum, and this process was repeated once more to obtain **8a** as 0.67 benzene and 0.33 DMSO solvate. (pink powder, 23.8 mg, 32%). ATR-IR analysis was performed on the solid obtained after dissolving the mixed DMSO/benzene solvate of **8a** in THF and concentrating in vacuo. Repeated attempts at elemental analysis failed to produce acceptable results. **^{1}H** NMR (600 MHz, Methylene Chloride-d_2) δ 2.14-1.58 (m, 60H), 1.39 – 1.04 (m, 40H), -5.28 (p, J = 41.6 Hz, 1H). **^{31}P**{^{1}H} NMR (243 MHz, Methylene Chloride-d_2) δ 15.6. HRMS (ES+) Calcd for $C_{55}H_{101}O_1P_4{}^{106}Pd{}^{108}Pd$: 1115.4871, found: 1115.4890. ATR-IR: νCO = 1788 cm^{-1}.

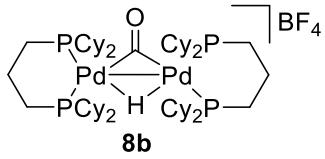

8b

A J. Young NMR tube was charged with ethylene complex **1** (100 mg, 0.175 mmol) and 1 mL of benzene. The resulting white suspension was frozen in liquid nitrogen, and the headspace was evacuated. The NMR tube was warmed to room temperature and backfilled with 760 Torr of CO. The NMR was tube was shaken (ca. 40 s) and refilled with CO to 760 Torr, and this process was repeated until a colorless, homogeneous solution was obtained. The J. Young tube was imported into a glovebox, transferred to a 20 mL vial equipped with a Teflon-coated stir bar, and diluted with 3 mL of benzene. HBF_4 (12.5 µL, 0.0919 mmol) was added all at once to this solution, and a pink solution was immediately obtained. The reaction mixture was stirred for 4 h to obtain a pink suspension. Ether (5 mL) was added to this suspension, and the precipitate was isolated on a fritted glass funnel and washed with ether (3 x 1 mL). The resulting pink powder was dissolved in 4 mL of benzene and dried under vacuum. This process was repeated once more to obtain **8b** as a 0.67 benzene solvate (73.3 mg, 67%, pink powder). Single crystals of **8b** were obtained by vapor diffusion of pentane into a concentrated solution of **8b** in a 1.5:1 v/v solution of THF and toluene. ATR-IR analysis was performed on the solid obtained from dissolving the benzene solvate of **8b** in THF and concentrating in vacuo. **^{1}H** NMR (500 MHz, Chloroform-d) δ 2.18–1.67 (m, 60H), 1.40–1.04 (m, 40H), -5.26 (p, J = 40.9 Hz, 1H). **^{19}F** NMR (376 MHz, Chloroform-

d) δ -153.80. **^{31}P**{^{1}H} NMR (162 MHz, Chloroform-*d*) δ 15.6. HRMS (ES+) Calcd for $C_{55}H_{101}O_1P_4{}^{106}Pd{}^{108}Pd$: 1115.487. Found: 1115.4907. ATR-IR: ν_{CO} = 1793 cm^{-1}. Anal. Calcd for $C_{59}H_{105}BF_4OP_4Pd_2$: C, 56.51; H, 8.44. Found: C, 56.34; H, 8.47.

Synthesis of ^{13}C Labelled 4-Phenylanisole

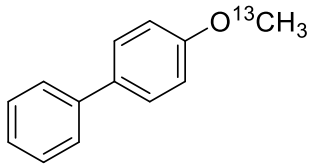

To a 15 mL solution of 4-phenylphenol (1.083 g, 6.360 mmol) in dimethylformamide was added NaOH (267.1 mg, 6.678 mmol). The solution was stirred for 1.5 hours. $^{13}CH_3I$ (1.0 g, 7.0 mmol, 99% ^{13}C), was added to the resulting white suspension, which was stirred for 45 minutes. The resulting colorless suspension was diluted with 3 mL of brine and extracted twice with ethyl acetate. The ethyl acetate extracts were combined and washed twice with aqueous 1 M NaOH and thrice with water. The ethyl acetate extracts were dried with anhydrous magnesium sulfate and concentrated via rotary evaporation to obtain 855.0 mg (66% yield, 99% ^{13}C incorporation) of the title compound as a white powder. ^{13}C incorporation was determined from the ^{13}C decoupled ^{1}H NMR spectrum of the product. **^{1}H** NMR (500 MHz, Benzene-d_6) δ 7.46 (d, *J* = 7.4 Hz, 2H), 7.40 (d, *J* = 11.4 Hz, 2H), 7.22 (t, *J* = 7.8 Hz, 2H), 7.12 (t, *J* = 7.4 Hz, 1H), 6.81 (dq, *J* = 7.4, 2.4 Hz, 2H), 3.30 (d, *J* = 143.7 Hz, 3H). **^{13}C**{^{1}H} NMR (126 MHz, Benzene-d_6) δ 159.4 (d, *J* = 2.4 Hz), 141.1, 133.8, 128.7, 128.2, 126.8, 126.5, 114.2 (d, *J* = 4.2 Hz), 54.46. m.p.: 85.3–87.0 ºC. HRMS (EI+) calcd for $C_{12}{}^{13}CH_{12}O$: 185.0922. Found: 185.0925.

Reactivity of 7 with CO

A J. Young tube containing a solution of **7** was cooled in liquid nitrogen, and the headspace was evacuated. The NMR tube was warmed to room temperature and backfilled with 1000 Torr of CO. The NMR tube was shaken (ca. 15 s), refilled with CO, and this process was repeated once more. The colorless solution was warmed to 80 °C for one hour, and product formation was analyzed by ^{19}F NMR spectroscopy and OTf anion was utilized as an internal reference.

Kinetic Studies

All samples for kinetic studies were prepared such that the total volume of the reaction mixture was 500 µL, and NMR spectrometer temperatures were calibrated with an ethylene glycol temperature standard. All samples were prepared and stored in a dry ice-acetone bath to avoid reactivity prior to data acquisition. Prior to data acquisition, the NMR spectrometers were shimmed on a dummy sample containing the aryl halide of interest in deuterated solvent for studies on oxidative addition (OA), or a solution of **6a** in deuterated solvent for studies on the formation of benzamide. All prepared samples were warmed to room temperature in a water bath (ca. 30 seconds), inserted into a pre-heated NMR spectrometer, and data acquisition was immediately started. A minimum of the first 40 seconds of data were discarded during data analysis to avoid sampling a temperature equilibration period, and a minimum of 3.5 half-lives worth of data was collected. Concentrations were determined by integration relative to a fluorine or phosphorus containing internal standard.

To obtain the observed rate constant (k_{obs}) during studies on oxidative addition, the concentration of oxidative addition products vs. time was fit to $y = A' - Ae^{(-k_{obs})t}$ with least squares fitting, and during studies on the formation of benzamide, the concentration of starting material vs. time was fit to $y = Ae^{(-k_{obs})t} + C$ with least squares fitting.

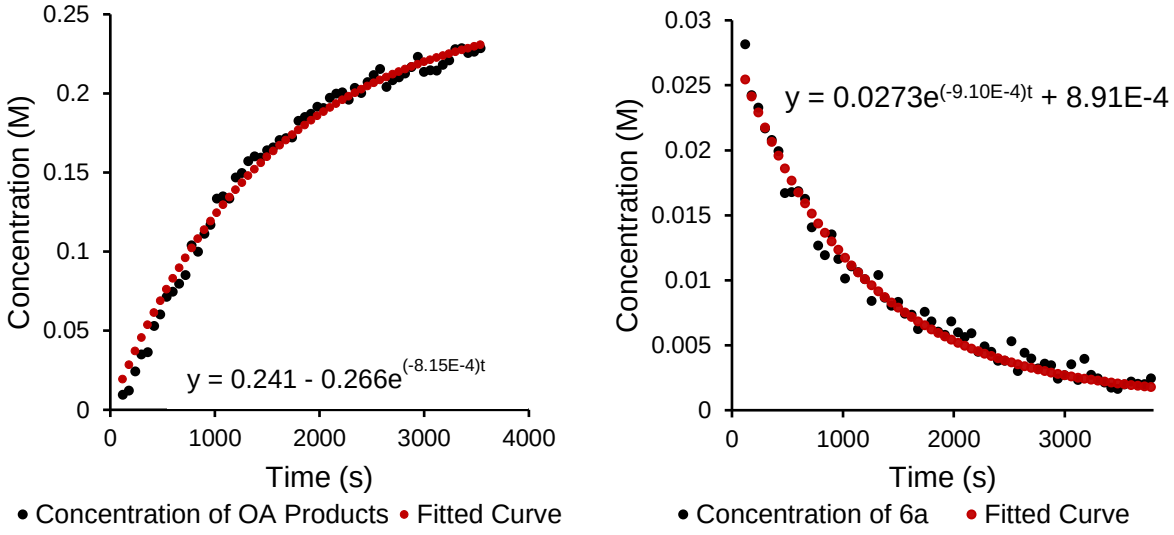

Figure S1. Representative curve fittings for oxidative addition (left) and formation of benzamide (right) kinetic studies.

Oxidative Addition Studies with 3,5-difluoro-chlorobenzene

Order in ArCl in 1:1 v/v DMSO and toluene

Inside a glovebox, a J. Young tube was charged with (DCPP)Pd(C_2H_4) (7.8 mg, 0.014 mmol), a corresponding amount of a 0.68 M stock solution of 3,5-difluoro-chlorobenzene in 1:1 v/v DMSO and toluene, 150 µL of a 91.0 mM stock solution of 4-fluorotoluene as an internal standard in 1:1 v/v DMSO and toluene, and a corresponding amount of 1:1 v/v DMSO and toluene to reach a total volume of 500 µL. The J. Young tube was exported from a glovebox, freeze-pump-thawed, and backfilled with 1000 Torr of CO. The J. Young tube was shaken until a homogeneous solution was obtained, and the tube was backfilled with CO to 1000 Torr. The tube was cooled in a dry ice-acetone bath until data acquisition commenced.

The NMR spectrometer was warmed to 85 °C, and the temperature was calibrated with an ethylene glycol temperature standard. The spectrometer was shimmed to a dummy sample containing a 500 µL solution of 4-fluorotoluene (0.28 M) and 3,5-difluoro-chlorobenzene (0.028 M) in 1:1 v/v DMSO-d_6 and toluene upon temperature equilibration. The J. Young tube was warmed to room temperature in a water bath and inserted into the NMR spectrometer, and data acquisition was commenced with a data point collected every minute.

Table S1. k_{obs} for the oxidative addition of 3,5-difluorochlorobenzene to **2** at 85 °C with varying concentrations of 3,5-difluorochlorobenzene in 1:1 v/v DMSO and toluene

Concentration of ArCl (M)	k_{obs} (10^{-4} s^{-1})
0.273	6.48
0.342	8.03
0.410	10.5
0.546	13.5
0.683	15.9

Order in pCO with ArCl in 1:1 v/v DMSO and toluene

A J. Young tube was charged with (DCPP)Pd(C_2H_4) (7.8 mg, 0.014 mmol) and 500 µL of a solution containing 0.27 M of 3,5-difluoro-chlorobenzene and 0.027 M of 4-fluorotoluene in 1:1 v/v DMSO and toluene. The J. Young tube was exported from a glovebox, freeze-pump-thawed once, and backfilled with the desired amount of CO (250-1500 Torr). The J. Young tube was shaken until a homogeneous solution was obtained and backfilled to the desired pressure of CO. The tube was cooled in a dry ice-acetone bath until data acquisition commenced.

The NMR spectrometer was warmed to 85 °C, and the temperature was calibrated with an ethylene glycol temperature standard. The spectrometer was shimmed to a dummy sample containing a 500 µL solution of 4-fluorotoluene (0.028 M) and 3,5-difluoro-chlorobenzene (0.28 M) in 1:1 v/v DMSO-d_6 and toluene upon temperature equilibration. The J. Young tube was warmed to room temperature in a water bath and inserted into the NMR spectrometer, and data acquisition was commenced with a data point collected every minute.

Table S2. k_{obs} for the oxidative addition of 3,5-difluorochlorobenzene to **2** at 85 °C with varying pressures of CO.

CO Pressure (Torr)	k_{obs} (10^{-4} s^{-1})
250	34.7
500	17.1
750	11.2
1000	8.19
1250	6.36
1500	5.86

Studies of the Oxidative Addition of 4-fluorobromobenzene

Order in ArBr in 1:1 v/v DMSO and toluene

A J. Young tube was charged with (DCPP)Pd(C_2H_4) (8.0 mg, 0.014 mmol), a corresponding amount of a 0.91 M stock solution of 2-bromo-5-fluoroanisole in 1:1 v/v DMSO and toluene, 125 µL solution of 4-fluorotoluene as an internal standard in 1:1 v/v DMSO and toluene, and a corresponding amount of 1:1 v/v DMSO and toluene to reach a total volume of 500 µL. The J. Young tube was exported from a glovebox, freeze-pump-thawed, and backfilled with 1000 Torr of CO. The J. Young tube was shaken until a homogeneous solution was obtained, and the tube was backfilled with CO to 1000 Torr. The tube was cooled in a dry ice-acetone bath until data acquisition commenced.

The NMR spectrometer was warmed to 75 °C, and the temperature was calibrated with an ethylene glycol temperature standard. The spectrometer was shimmed to a dummy sample containing a 500 µL solution of 4-fluorotoluene (0.028 M) and 2-bromo-5-fluoroanisole (0.28 M)

in 1:1 v/v DMSO-d_6 and toluene upon temperature equilibration. The J. Young tube was warmed to room temperature in a water bath and inserted into the NMR spectrometer, and data acquisition was commenced with a data point collected every minute.

Table S3. k_{obs} for the oxidative addition of 2-bromo-5-fluoroanisole to **2** at 75 °C with varying concentrations of 2-bromo-5-fluoroanisole in 1:1 v/v DMSO and toluene.

Concentration of ArBr (M)	k_{obs} (10^{-3} s^{-1})
0.273	1.58
0.410	2.40
0.478	2.82
0.584	3.48
0.683	4.10

Order in pCO with ArBr

A J. Young tube was charged with (DCPP)Pd(C_2H_4) (8.0 mg, 0.014 mmol) and 500 µL of a solution containing 0.27 M of 2-bromo-5-fluoroanisole and 0.027 M of 4-fluorotoluene in 1:1 v/v DMSO and toluene. The J. Young tube was exported from a glovebox, freeze-pump-thawed, and backfilled with the desired amount of CO (250-1500 Torr). The J. Young tube was shaken until a homogeneous solution was obtained, and the tube was backfilled with the desired amount of CO. The tube was cooled in a dry ice-acetone bath until data acquisition commenced.

The NMR spectrometer was warmed 75 °C, and the temperature was calibrated with an ethylene glycol temperature standard. The spectrometer was shimmed to a dummy sample containing a 500 µL solution of 4-fluorotoluene (0.028 M) and 2-bromo-5-fluoroanisole (0.28 M) in 1:1 v/v DMSO-d_6 and toluene upon temperature equilibration. The J. Young tube was warmed to room temperature in a water bath and inserted into the NMR spectrometer, and data acquisition was commenced with a data point collected every minute.

Table S4. k_{obs} for the oxidative addition of 2-bromo-5-fluoroanisole to **2** at 75 °C with varying pressures of CO in 1:1 v/v DMSO and toluene.

CO Pressure (Torr)	k_{obs} (10^{-3} s^{-1})
250	4.27
500	2.33
750	1.82
1000	1.56
1250	1.22
1500	1.11

Hammett Analysis

A J. Young tube was charged with (DCPP)Pd(C_2H_4) (8.0 mg, 0.014 mmol) and 500 µL of a solution containing 0.56 M of an aryl chloride and 70 mM of trimethoxybenzene or trimesitylphosphine in 1:1 v/v DMSO-d_6 and toluene-d_8. The J. Young tube was exported from a glovebox, freeze-pump-thawed, and backfilled with 1000 Torr of CO. The J. Young tube was shaken until a homogeneous solution was obtained, and the tube was backfilled with CO until it was under 1000 Torr of CO. The tube was cooled in a dry ice-acetone bath until data acquisition commenced.

The NMR spectrometer was preheated to 100 °C, and the temperature was calibrated with an ethylene glycol temperature standard. The spectrometer was shimmed to a dummy sample containing the same aryl chloride as above (0.56 M) in 1:1 v/v DMSO-d_6 and toluene upon temperature equilibration. The J. Young tube was warmed to room temperature in a water bath and inserted into the NMR spectrometer, and data acquisition commenced with a ^{1}H or ^{31}P spectrum collected every three minutes.

Table S5. k_{obs} for the oxidative addition of *para* substituted aryl chlorides to **2** at 100 °C.

Substituent	δ	k_{obs} (10^{-4} s^{-1})
H	0	4.58
F	0.06	5.29
Me	-0.17	2.95
(CO)NHMe	0.36	17.7
CF_3	0.54	45.7
OMe	-0.27	1.44

Studies on the Formation of Benzamide by reaction of NH_3 with 6a

Note: In this section, the pressure of CO added refers to the final pressure of the headspace of a J. Young tube while the tube is submerged in a cooling bath.

Order in NH_3

A J. Young tube was charged with **6a** (12.0 mg, 0.0171 mmol) and 500 µL of a solution containing 0.34 M DBU and 0.017 M $PMes_3$ in 1:1 v/v DMSO and toluene. The J. Young tube was exported from a glovebox, warmed briefly (ca. 20 s) in a 50 °C aluminum heating block to completely dissolve **6a**, and attached to an 8.0 mL gas addition bulb. The J. Young tube was cooled in a liquid nitrogen bath, and the headspace of the J. Young tube was evacuated. While frozen and under static vacuum, the desired amount of NH_3 was condensed directly into the J. Young tube (10-30 equivalents relative to **6a**), followed by 750 Torr of CO. The J. Young tube was stored in a Dewar containing dry ice and acetone until data acquisition commenced.

The NMR spectrometer was warmed to 35 °C, and the temperature was calibrated with an ethylene glycol temperature standard. The spectrometer was shimmed to a dummy sample containing **6a** (34 mM) in 1:1 v/v DMSO-d_6 and toluene upon temperature equilibration. The J. Young tube was warmed to room temperature in a water bath, shaken briefly, and inserted into the NMR spectrometer, and data acquisition was commenced with a spectrum collected every minute.

Table S6. k_{obs} for the formation of 4-fluorobenzamide from **6a** with varying concentrations of NH_3 at 35 °C.

NH_3 (Torr in 8.0 mL gas bulb)	NH_3 (equiv)	k_{obs} (10^{-4} s^{-1})
392	10	7.70
588	15	11.8
785	20	15.4
981	25	18.9
1177	30	24.0

Order in Base (Pseudo-First Order Conditions)

A J. Young tube was charged with **6a** (12.0 mg, 0.0171 mmol), a corresponding amount of a 1.71 M solution of DBU in 1:1 v/v DMSO and toluene, 200 µL of a 42.8 mM solution of $PMes_3$ in 1:1 v/v DMSO and toluene, and a corresponding amount of 1:1 v/v DMSO and toluene to obtain

a total volume of 500 µL. The J. Young tube was exported from a glovebox, warmed briefly (ca. 20 s) in a 50 °C aluminum heating block to completely dissolve **6a**, and attached to an 8.0 mL gas addition bulb. The J. Young tube was cooled in a liquid nitrogen bath, and the headspace of the J. Young tube was evacuated. While frozen and under static vacuum, 392 torr of NH_3 (10 equiv) was condensed directly into the J. Young tube, followed by 750 Torr of CO. The J. Young tube was stored in a dewar containing dry ice and acetone until data acquisition commenced.

The NMR spectrometer was warmed to 35 °C, and the temperature was calibrated with an ethylene glycol temperature standard. The spectrometer was shimmed to a dummy sample containing **6a** (34 mM) in 1:1 v/v DMSO-d_6 and toluene upon temperature equilibration. The J. Young tube was warmed to room temperature in a water bath, shaken briefly, and inserted into the NMR spectrometer, and data acquisition was commenced with a spectrum collected every minute.

Table S7. k_{obs} for the formation of 4-fluorobenzamide from **6a** with varying concentrations of DBU at 35 °C.

DBU (M)	k_{obs} (10^{-3} s^{-1})
0.342	1.10
0.513	1.15
0.684	1.19
0.855	1.21
1.03	1.26

Order in Base (Initial Rates)

A J. Young tube was charged with **6a** (12.0 mg, 0.0171 mmol), a corresponding amount of a 0.342 M solution of DBU 1:1 v/v DMSO and toluene, 250 µL of a 34.2 mM solution of $PMes_3$ in 1:1 v/v DMSO and toluene, and a corresponding amount of 1:1 v/v DMSO and toluene was dispensed into the J. Young tube to obtain a total volume of 500 µL. The J. Young tube was exported from a glovebox, warmed briefly (ca. 20 s) in a 50 °C aluminum heating block to completely dissolve **6a**, and attached to an 8.0 mL gas addition bulb. The J. Young tube was cooled in a liquid nitrogen bath, and the headspace of the J. Young tube was evacuated. While frozen and under static vacuum, 588 Torr of NH_3 (15 equiv) was condensed directly into the J. Young tube, followed by 750 Torr of CO. The J. Young tube was stored in a dewar containing dry ice and acetone until data acquisition commenced.

The NMR spectrometer was warmed to 60 °C, and the temperature was calibrated with an ethylene glycol temperature standard. The spectrometer was shimmed to a dummy sample containing **6a** (34 mM) in 1:1 v/v DMSO-d_6 and toluene upon temperature equilibration. The J. Young tube was warmed to room temperature in a water bath, shaken briefly, and inserted into the NMR spectrometer, and data acquisition was commenced with a spectrum collected every minute.

Table S8. Rates for the formation of 4-fluorobenzamide from **6a** with varying concentrations of DBU at 60 °C.

DBU (M)	Rate (10^{-5} M/s)
0.0342	1.025
0.0684	2.117
0.103	2.854
0.133	4.022
0.171	5.611

Order in Base (Pseudo-First Order Conditions with 10 equiv of N(n-butyl)$_4$Cl

A J. Young tube was charged with **6a** (12.0 mg, 0.0171 mmol), a corresponding amount of a 1.71 M solution of DBU in 1:1 v/v DMSO and toluene, 200 µL of a solution containing 0.855 M of N(*n*-butyl)$_4$Cl and 21.4 mM of PMes$_3$ in 1:1 v/v DMSO and toluene, and a corresponding amount of 1:1 v/v DMSO and toluene to reach a total volume of 500 µL. The J. Young tube was exported from a glovebox, warmed briefly (ca. 20 s) in a 50 °C aluminum heating block to completely dissolve **6a**, and attached to an 8.0 mL gas addition bulb. The J. Young tube was cooled in a liquid nitrogen bath, and the headspace of the J. Young tube was evacuated. While frozen and under static vacuum, 785 Torr of NH_3 (20 equiv) was condensed directly into the J. Young tube, followed by 750 Torr of CO. The J. Young tube was stored in a dewar containing dry ice and acetone until data acquisition commenced.

The NMR spectrometer was warmed to 35 °C, and the temperature was calibrated with an ethylene glycol temperature standard. The spectrometer was shimmed to a dummy sample containing **6a** (34 mM) and N(*n*-butyl)$_4$Cl (0.34 M) in 1:1 v/v DMSO-d_6 and toluene upon temperature equilibration. The J. Young tube was warmed to room temperature in a water bath, shaken briefly, and inserted into the NMR spectrometer, and data acquisition was commenced with a spectrum collected every minute.

Table S9. k_{obs} for the formation of 4-fluorobenzamide from **6a** with varying concentrations of DBU in the presence of 0.34 M N(*n*-butyl)$_4$Cl at 35 °C.

DBU (M)	k_{obs} (10^{-4} s^{-1})
0.342	4.78
0.513	7.00
0.684	8.68
0.855	10.7
1.03	12.3

Order in N(n-butyl)$_4$Cl

A J. Young tube was charged with **6a** (12.0 mg, 0.0171 mmol), 100 µL of a solution containing 1.71 M of DBU and 42.8 mM of PMes$_3$ in 1:1 v/v DMSO and toluene, and a corresponding amount of a solution containing 1.28 M of N(*n*-butyl)$_4$Cl in 1:1 v/v DMSO and toluene. Additional 1:1 v/v DMSO and toluene was added to the tube to obtain a total volume of 500 µL. The J. Young tube was exported from a glovebox, warmed briefly (ca. 20 s) in a 50 °C aluminum heating block to completely dissolve **6a**, and attached to an 8.0 mL gas addition bulb. The J. Young tube was cooled in a liquid nitrogen bath, and the headspace of the J. Young tube was evacuated. While frozen and under static vacuum, 785 Torr of NH_3 (20 equiv) was condensed directly into the J. Young tube, followed by 750 Torr of CO. The J. Young tube was stored in a dewar containing dry ice and acetone until data acquisition commenced.

The NMR spectrometer was warmed to 35 °C, and the temperature was calibrated with an ethylene glycol temperature standard. The spectrometer was shimmed to a dummy sample containing **6a** (34 mM) and N(*n*-butyl)$_4$Cl (0.34 M) in 1:1 v/v DMSO-d_6 and toluene upon temperature equilibration. The J. Young tube was warmed to room temperature in a water bath, shaken briefly, and inserted into the NMR spectrometer, and data acquisition was commenced with a spectrum collected every minute.

Table S10. k_{obs} for formation of 4-fluorobenzamide from **6a** with varying concentrations of N(*n*-butyl)$_4$Cl at 35 °C.

N(*n*-butyl)$_4$Cl (M)	k_{obs} (10^{-4} s^{-1})
0.342	7.90
0.513	5.56
0.684	4.07
0.855	3.36
1.03	3.06

Order in N(n-butyl)$_4$PF$_6$

A J. Young tube was charged with **6a** (12.0 mg, 0.0171 mmol), 100 µL of a solution containing 1.71 M of DBU and 42.8 mM of $PMes_3$ in 1:1 v/v DMSO and toluene, and a corresponding amount of a solution containing 1.28 M of N(*n*-butyl)$_4$PF$_6$ in 1:1 v/v DMSO and toluene. Additional 1:1 v/v DMSO and toluene was added to the tube to obtain a total volume of 500 µL. The J. Young tube was exported from a glovebox, warmed briefly (ca. 20 s) in a 50 °C aluminum heating block to completely dissolve **6a**, and attached to an 8.0 mL gas addition bulb. The J. Young tube was cooled in a liquid nitrogen bath, and the headspace of the J. Young tube was evacuated. While frozen and under static vacuum, 392 Torr of NH_3 (10 equiv) was condensed directly into the J. Young tube, followed by 750 Torr of CO. The J. Young tube was stored in a dewar containing dry ice and acetone until data acquisition commenced.

The NMR spectrometer was warmed to 35 °C, and the temperature was calibrated with an ethylene glycol temperature standard. The spectrometer was shimmed to a dummy sample containing **6a** (34 mM) and N(*n*-butyl)$_4$PF$_6$ (0.34 M) in 1:1 v/v DMSO-d_6 and toluene upon temperature equilibration. The J. Young tube was warmed to room temperature in a water bath, shaken briefly, and inserted into the NMR spectrometer, and data acquisition was commenced with a spectrum collected every minute.

Table S11. k_{obs} for the formation of 4-fluorobenzamide from **6a** with varying concentrations of N(*n*-butyl)$_4$PF$_6$ at 35 °C.

N(*n*-butyl)$_4$PF$_6$ (M)	k_{obs} (10^{-3} s^{-1})
0.342	1.58
0.513	1.70
0.684	1.90
0.855	2.07
1.03	2.14

Order in DMSO

A J. Young tube was charged with **6a** (12.0 mg, 0.0171 mmol), 200 µL of a solution containing 0.855 M DBU and 42.8 mM of $PMes_3$ in 1,2-difluorobenzene, a corresponding amount of a solution containing 1.71 M DMSO in 1,2-difluorobenzene, and a corresponding amount of 1,2-difluorobenzene was dispensed into the J. Young tube to obtain a total volume of 500 µL. The J. Young tube was exported from a glovebox and attached to an 8.0 mL gas addition bulb. The J. Young tube was cooled in a liquid nitrogen bath, and the headspace of the J. Young tube was evacuated. While frozen and under static vacuum, 785 Torr of NH_3 (20 equiv) was condensed directly into the J. Young tube, followed by 750 Torr of CO. The J. Young tube was stored in a dewar containing dry ice and acetone until data acquisition commenced.

The NMR spectrometer was warmed to 65 °C, and the temperature was calibrated with an ethylene glycol temperature standard. The spectrometer was shimmed to a dummy sample containing **6a** (34 mM) in 1:1 v/v 1,2-difluorobenzene/benzene-d_6 upon temperature equilibration. The J. Young tube was warmed to room temperature in a water bath, shaken briefly, and inserted into the NMR spectrometer, and data acquisition was commenced with a spectrum collected every minute.

Table S12. k_{obs} for the formation of 4-fluorobenzamide from **6a** with varying concentrations of DMSO at 65 °C.

DMSO (M)	k_{obs} (10^{-4} s^{-1})
0	5.50
0.342	6.83
0.570	7.57
0.798	8.12
1.03	9.10

Order in Pressure of CO

A J. Young tube was charged with **6a** (12.0 mg, 0.0171 mmol) and 500 µL of a solution containing 0.342 M DBU and 17.1 mM of $PMes_3$ in 1,2-difluorobenzene. The J. Young tube was exported from a glovebox and attached to a 8.0 mL gas addition bulb. The J. Young tube was cooled in a liquid nitrogen bath, and the headspace of the J. Young tube was evacuated. While frozen and under static vacuum, 785 Torr of NH_3 (20 equiv) was condensed directly into the J. Young tube, followed by the desired amount of CO. In order to accurately measure the order in pressure of CO, reactions with 750 and 1000 Torr of CO were cooled in a bath consisting of toluene and liquid nitrogen during reaction setup instead of liquid nitrogen. Unlike liquid nitrogen, the toluene and liquid nitrogen cooling bath is sufficiently cool to condense ammonia but not cool enough to condense CO. The J. Young tube was stored in a dewar containing dry ice and acetone until data acquisition commenced.

The NMR spectrometer was warmed to 65 °C, and the temperature was calibrated with an ethylene glycol temperature standard. The spectrometer was shimmed to a dummy sample containing **6a** (34 mM) in 1:1 v/v 1,2-difluorobenzene/benzene-d_6 upon temperature equilibration. The J. Young tube was warmed to room temperature in a water bath, shaken briefly, and inserted into the NMR spectrometer, and data acquisition was commenced with a spectrum collected every minute.

Table S13. k_{obs} for the formation of 4-fluorobenzamide from **6a** with varying pressures of CO at 65 °C.

CO (Torr)	k_{obs} (10^{-4} s^{-1})
250	4.48
500	4.70
750	4.52
1000	4.42

^{13}C KIE Experiments

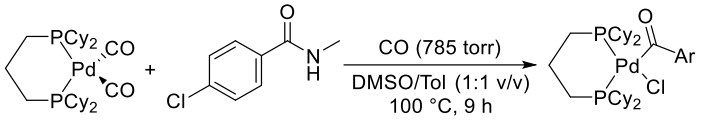

Scheme S1. ^{13}C KIE experiment on oxidative addition of an aryl chloride to (DCPP)Pd(CO)$_2$ with 4-chloro-*N*-methylbenzamide.

A 100 mL Schlenk vessel equipped with a Teflon-coated stir bar was charged with (DCPP)Pd(C_2H_4) (800.0 mg, 1.400 mmol), 4-chloro-*N*-methylbenzamide (237.6 mg, 1.400 mmol), trimethoxybenzene (16.8 mg, 1.00 mmol), and 50 mL of 1:1 v/v DMSO and toluene. The Schlenk vessel was freeze-pump-thawed and backfilled with 785 Torr of CO. The solution was stirred while under 785 Torr of CO until a homogenous solution was obtained (ca. 45 min). The resulting solution was warmed to 100 °C and stirred vigorously for 9 hours to obtain an orange solution. After cooling to room temperature, the reaction mixture was opened to air and aliquots of this solution were taken to obtain conversion by GC. Then. 2.8 g of NaOH in 5 mL of H_2O was added to this solution, which was stirred under air for 2 hours at ambient temperature. The resulting black suspension was filtered through Celite and washed with ether (30 mL). The filtrate was diluted with 10 mL H_2O and extracted with ether (3 x 20 mL). The combined ether extracts were washed with brine (10 ml), dried with $MgSO_4$, and concentrated in vacuo. The resulting precipitate was dissolved in ethyl acetate and pushed through a silica plug followed by ethyl acetate (3 x 10 mL). The filtrate was dried in vacuo, and the resulting crude material was loaded onto a preparative TLC plate containing a 500-micron thick layer of silica gel. Authentic 4-chloro-N-methylbenzamide was spotted alongside the crude reaction as a reference. 4-chloro-*N*-methylbenzamide from the crude reaction was isolated on the TLC plate with 3:1 ethyl acetate and hexanes, respectively, and the band corresponding to 4-chloro-N-methylbenzamide was scraped off, washed with ethyl acetate (3 x 15 mL), and concentrated in vacuo. This isolated material was loaded onto another preparative TLC plate and re-isolated with 1:1 ethyl acetate and hexanes. The band corresponding to 4-chloro-*N*-methylbenzamide was scraped off, washed with ethyl acetate (3 x 15 mL), and concentrated in vacuo to obtain 4-chloro-*N*-methylbenzamide.

^{13}C NMR spectra were obtained in $CDCl_3$ with inverse gated decoupling and a recycle delay of 40 seconds on a 900 MHz NMR spectrometer equipped with a cryoprobe. Integrations were obtained with an integral centered at each peak and an integral width of 4× peak width. The signal corresponding to the methyl group of 4-chloro-*N*-methylbenzamide was chosen as the internal integration standard, and its integration was set as 1.000. ^{13}C KIE values were obtained from the following equation, wherein F is the fractional conversion and R and R_0 are the integrations for recovered starting material and the natural abundance standard, respectively.

$$KIE = \frac{\ln(1-F)}{\ln[(1-F)\,R/R_0]}$$

The table below lists the conversion of starting material, average integration for each peak of the starting material, the corresponding standard deviation, and n, the total number of spectra obtained.

Table S14. Average ^{13}C NMR integrations of recovered 4-chloro-*N*-methylbenzamide and ^{13}C natural abundance 4-chloro-N-methylbenzamide.

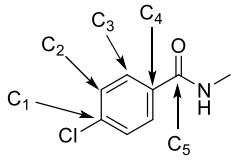

	Conversion (%)	C_1	C_2	C_3	C_4	C_5	n
Recovered Material	93.6(6)	1.149(16)	2.143(17)	2.175(29)	1.056(17)	1.127(27)	4
Natural Abundance Standard	n/a	1.110(9)	2.166(19)	2.176(18)	1.076(15)	1.123(10)	7

Table S15. R/R_0 and ^{13}C KIE values for each carbon atom determined from recovered 4-chloro-*N*-methylbenzamide.

	C_1	C_2	C_3	C_4	C_5
R/R_0	1.035(16)	0.984(12)	0.993(15)	0.976(21)	0.980(21)
^{13}C KIE	1.013(6)	0.994(5)	0.998(5)	0.992(8)	0.993(8)

Low Temperature Quantitative ^{13}C NMR Spectroscopic Experiments

A J. Young tube was charged with ^{13}C labelled 4-phenylanisole (15.6 mg, 0.0842 mmol), ethylene complex **1** (12.0 mg, 0.0210 mmol), and 600 µL of toluene-d_8. The tube was cooled in liquid nitrogen and the headspace was evacuated. The tube was pressurized with 1000 Torr ^{13}CO, shaken, and re-pressurized to 1000 Torr until a homogenous, colorless solution was obtained. The tube was inserted into an NMR spectrometer and cooled to -40 °C. Upon temperature equilibration, an inversion relaxation experiment was performed to obtain the T_1 values of all ^{13}C resonances at this temperature. A quantitative ^{13}C NMR spectroscopic experiment was performed with a D_1 of 10 times the longest T_1 and inverse-gated decoupling to determine the amount of CO bound to Pd carbonyl compound **2**.

Variable Temperature IR Spectroscopic Studies

A dry 50 mL round-bottom flask was charged with (DCPP)Pd(C_2H_4) (24.0 mg, 0.0420 mmol), a Teflon-coated stir bar, and 4 mL of 1:1 v/v DMSO and toluene. The suspension was stirred, and CO was bubbled into the reaction mixture until a homogeneous solution was obtained, indicating the formation of (DCPP)Pd($CO)_2$. A solution IR cell was purged with N_2, and an aliquot of the reaction mixture was quickly injected into the IR cell until the cell was entirely filled by the reaction mixture. The ports of the IR cell were sealed with NMR septa. The IR cell was placed into a water-heated jacket, and an IR spectrum was collected at room temperature. The cell was warmed to 75 °C by pumping hot water through the water-heated jacket. Upon temperature equilibration (ca. 7 minutes), an IR spectrum was obtained at this temperature. Spectra of 1:1 v/v DMSO and toluene were also collected at room temperature and 75 °C and subtracted from the above spectra to obtain IR spectra of **4**.

For analyses at low CO concentration, the headspace of the (DCPP)Pd($CO)_2$ solution was briefly purged with N_2 (20 seconds), stirred under this atmosphere for 10 minutes, and aliquots of this solution were taken for analysis at room temperature and at 75 °C following the same procedure described above.

Determination of Catalyst Resting State

In a representative experiment, a 25 mL Schlenk vessel equipped with a Teflon stir bar was charged with (DCPP)Pd(C_2H_4) (5.7 mg, 1.0 μmol), 4-fluorochlorobenzene (53 μL, 0.40 mmol), K_2CO_3 (166 mg, 1.20 mmol), 4-fluorotoluene (44 μL, 0.40 mmol) and 0.5 mL of 1:1 v/v DMSO and toluene. The Schlenk vessel was exported from the glovebox and attached to a 61 mL gas addition bulb. The Schlenk vessel was cooled in liquid nitrogen, the headspace of the Schlenk vessel was evacuated, and NH_3 (484 Torr, 1.2 mmol) was condensed directly into the vessel followed by 450 Torr of CO. The reaction vessel was placed into an oil bath preheated to the desired temperature (80 or 100 °C). After 14 hours, the Schlenk vessel was removed from the oil bath and opened in a well-ventilated fume hood. The resulting suspension was filtered into an NMR tube for yield determination by ^{19}F NMR spectroscopy and analysis by ^{31}P NMR spectroscopy.

Time Course Studies

In a representative experiment, a 25 mL Schlenk vessel equipped with a Teflon stir bar was charged with (DCPP)Pd(C_2H_4) (5.7 mg, 1.0 μmol), 4-chlorobenzotrifluoride (53 μL, 0.40 mmol), K_2CO_3 (166 mg, 1.20 mmol), dodecane (91 μL, 0.40 mmol), and 0.5 mL of DMSO. This process was repeated four more times to obtain a total of 5 reactions. The Schlenk vessels were exported from the glovebox and attached to a 61 mL gas addition bulb. A Schlenk vessel was cooled in liquid nitrogen, the headspace of the vessel was evacuated, and NH_3 (484 Torr, 1.2 mmol or 968 Torr, 2.4 mmol) was condensed directly into the vessel followed by 450 or 900 Torr of CO. This process was repeated for the other Schlenk vessels. After gas condensation, all vessels were cooled in a dry ice-acetone bath. The reaction vessels were placed into an oil bath preheated to 100 °C and stirred at 850 rpm. At the desired time, a Schlenk vessel was removed from the oil bath and cooled to room temperature in a water bath. The vessel was opened in a well-ventilated fume hood and 4 mL of toluene was added to the crude reaction mixture, which was capped and shaken. An aliquot of this suspension was filtered into a GC vial for yield determination via GC.

Table S16. Time Course Study Yields vs. Time

Standard Conditions		900 Torr of CO		6 equiv of NH_3 (968 Torr)	
Time (min)	Yield (%)	Time (min)	Yield (%)	Time (min)	Yield (%)
30	13.78	45	20.55	20	8.32
60	43.61	90	43.83	30	28.95
90	50.36	150	56.57	50	50.77
150	74.19	240	63.43	90	61.14
240	86.07	360	69.35	150	77.17
				240	85.39

DFT Calculations

Computational Methods

All DFT calculations were performed using the BP86 functional for geometry optimizations and the M06 functional for single point energy calculations as implemented in Gaussian 09. The D3 version of Grimme's dispersion was added to both functionals. The effective core potential and associated double ζ basis sets of LANL2DZ were utilized for palladium atoms in geometry optimizations. The effective core potential and associated triple ζ basis sets of LANL2TZ were utilized for palladium atoms in single point energy calculations. For the palladium atom, an f polarization function was added to the basis set during single point energy calculations. The 6-311G** basis set was utilized for all other atoms. Thermal corrections from the geometry optimizations were added to the energies found in single point energy calculations to find values for Gibbs free energy. All geometries are fully optimized and confirmed as minima or saddle points by analytical frequency calculations at the same level. CPCM was used to account for solvation effects in single point energy calculations.

Computed Reaction Pathways at STP

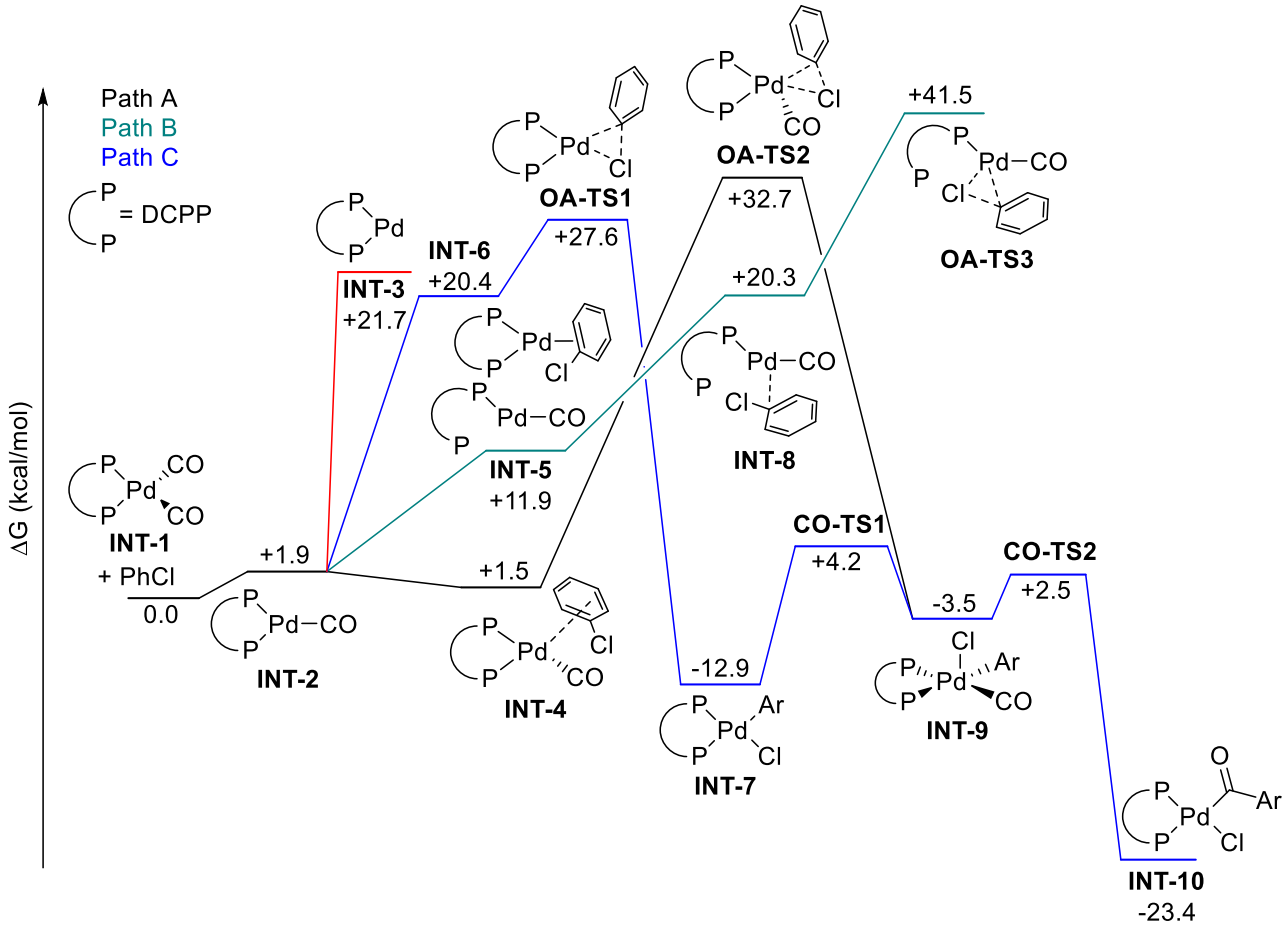

Figure S2. Computed reaction pathway for the oxidative addition of chlorobenzene in DMSO at STP.

2.5 References

Adapted with permission from Wang, J. Y.; Strom, A. E.; Hartwig, J. F. Mechanistic Studies of Palladium-Catalyzed Aminocarbonylation of Aryl Chlorides with Carbon Monoxide and Ammonia. *J. Am. Chem. Soc.* **2018**, *140*, 7979-7993. Copyright 2018 American Chemical Society.

1. (a) Johansson Seechurn, C. C. C.; Kitching, M. O.; Colacot, T. J.; Snieckus, V., Palladium-Catalyzed Cross-Coupling: A Historical Contextual Perspective to the 2010 Nobel Prize. *Angew. Chem. Int. Ed.* **2012,** *51*, 5062-5085; (b) Diccianni, J. B.; Diao, T., Mechanisms of Nickel-Catalyzed Cross-Coupling Reactions. *Trends in Chemistry* **2019,** *1*, 830-844.
2. Dorel, R.; Grugel, C. P.; Haydl, A. M., The Buchwald–Hartwig Amination After 25 Years. *Angew. Chem. Int. Ed.* **2019,** *58*, 17118-17129.
3. (a) Hartwig, J. F., Evolution of a Fourth Generation Catalyst for the Amination and Thioetherification of Aryl Halides. *Acc. Chem. Res.* **2008,** *41*, 1534-1544; (b) Yang, J.; Chen, T.; Han, L.-B., C–P Bond-Forming Reactions via C–O/P–H Cross-Coupling Catalyzed by Nickel. *J. Am. Chem. Soc.* **2015,** *137*, 1782-1785; (c) Wauters, I. D., W.; Stevens, C. V., Preparation of phosphines through C–P bond formation. *Beilstein J. Org. Chem.* **2014,** *10*, 1064-1096; (d) Sather, A. C.; Buchwald, S. L., The Evolution of Pd0/PdII-Catalyzed Aromatic Fluorination. *Acc. Chem. Res.* **2016,** *49*, 2146-2157.
4. Ruiz-Castillo, P.; Buchwald, S. L., Applications of Palladium-Catalyzed C–N Cross-Coupling Reactions. *Chem. Rev.* **2016,** *116*, 12564-12649.
5. Kosugi, M.; Kameyama, M.; Migita, T., Palladium-Catalyzed Aromatic Amination of Aryl Bromides with N,N-Di-Ethylamino-tributyltin. *Chem. Lett.* **1983,** *12*, 927-928.
6. Hartwig, J. F., Carbon−Heteroatom Bond-Forming Reductive Eliminations of Amines, Ethers, and Sulfides. *Acc. Chem. Res.* **1998,** *31*, 852-860.
7. Louie, J.; Hartwig, J. F., Palladium-catalyzed synthesis of arylamines from aryl halides. Mechanistic studies lead to coupling in the absence of tin reagents. *Tetrahedron Lett.* **1995,** *36*, 3609-3612.
8. Guram, A. S.; Rennels, R. A.; Buchwald, S. L., A Simple Catalytic Method for the Conversion of Aryl Bromides to Arylamines. *Angew. Chem. Int. Ed. Engl.* **1995,** *34*, 1348-1350.
9. (a) Driver, M. S.; Hartwig, J. F., A Second-Generation Catalyst for Aryl Halide Amination: Mixed Secondary Amines from Aryl Halides and Primary Amines Catalyzed by (DPPF)PdCl2. *J. Am. Chem. Soc.* **1996,** *118*, 7217-7218; (b) Wolfe, J. P.; Wagaw, S.; Buchwald, S. L., An Improved Catalyst System for Aromatic Carbon−Nitrogen Bond Formation: The Possible Involvement of Bis(Phosphine) Palladium Complexes as Key Intermediates. *J. Am. Chem. Soc.* **1996,** *118*, 7215-7216.
10. (a) Senn, H. M.; Ziegler, T., Oxidative Addition of Aryl Halides to Palladium(0) Complexes: A Density-Functional Study Including Solvation. *Organometallics* **2004,** *23*, 2980-2988; (b) Littke, A. F.; Fu, G. C., Palladium-Catalyzed Coupling Reactions of Aryl Chlorides. *Angew. Chem. Int. Ed.* **2002,** *41*, 4176-4211.
11. Beller, M.; Riermeier, T. H.; Reisinger, C.-P.; Herrmann, W. A., First palladium-catalyzed aminations of aryl chlorides. *Tetrahedron Lett.* **1997,** *38*, 2073-2074.
12. (a) Muci, A. R.; Buchwald, S. L., Practical Palladium Catalysts for C-N and C-O Bond Formation. In *Cross-Coupling Reactions: A Practical Guide*, Miyaura, N., Ed. Springer Berlin Heidelberg: Berlin, Heidelberg, 2002; pp 131-209; (b) Stambuli, J. P.; Kuwano, R.; Hartwig, J. F., Unparalleled Rates for the Activation of Aryl Chlorides and Bromides:

Coupling with Amines and Boronic Acids in Minutes at Room Temperature. *Angew. Chem. Int. Ed.* **2002,** *41*, 4746-4748; (c) Kataoka, N.; Shelby, Q.; Stambuli, J. P.; Hartwig, J. F., Air Stable, Sterically Hindered Ferrocenyl Dialkylphosphines for Palladium-Catalyzed C−C, C−N, and C−O Bond-Forming Cross-Couplings. *J. Org. Chem.* **2002,** *67*, 5553-5566; (d) Marion, N.; Nolan, S. P., Well-Defined N-Heterocyclic Carbenes−Palladium(II) Precatalysts for Cross-Coupling Reactions. *Acc. Chem. Res.* **2008,** *41*, 1440-1449.

13. (a) Shen, Q.; Ogata, T.; Hartwig, J. F., Highly Reactive, General and Long-Lived Catalysts for Palladium-Catalyzed Amination of Heteroaryl and Aryl Chlorides, Bromides, and Iodides: Scope and Structure–Activity Relationships. *J. Am. Chem. Soc.* **2008,** *130*, 6586-6596; (b) Shen, Q.; Shekhar, S.; Stambuli, J. P.; Hartwig, J. F., Highly Reactive, General, and Long-Lived Catalysts for Coupling Heteroaryl and Aryl Chlorides with Primary Nitrogen Nucleophiles. *Angew. Chem. Int. Ed.* **2005,** *44*, 1371-1375.
14. Uehling, M. R.; King, R. P.; Krska, S. W.; Cernak, T.; Buchwald, S. L., Pharmaceutical diversification via palladium oxidative addition complexes. *Science* **2019,** *363*, 405-408.
15. Wolfe, J. P.; Buchwald, S. L., Nickel-Catalyzed Amination of Aryl Chlorides. *J. Am. Chem. Soc.* **1997,** *119*, 6054-6058.
16. Brenner, E.; Fort, Y., New efficient nickel(0) catalysed amination of aryl chlorides. *Tetrahedron Lett.* **1998,** *39*, 5359-5362.
17. Manolikakes, G.; Gavryushin, A.; Knochel, P., An Efficient Silane-Promoted Nickel-Catalyzed Amination of Aryl and Heteroaryl Chlorides. *J. Org. Chem.* **2008,** *73*, 1429-1434.
18. Ge, S.; Green, R. A.; Hartwig, J. F., Controlling First-Row Catalysts: Amination of Aryl and Heteroaryl Chlorides and Bromides with Primary Aliphatic Amines Catalyzed by a BINAP-Ligated Single-Component Ni(0) Complex. *J. Am. Chem. Soc.* **2014,** *136*, 1617-1627.
19. (a) Chen; Yang, L.-M., Ni(II)−(σ-Aryl) Complex: A Facile, Efficient Catalyst for Nickel-Catalyzed Carbon−Nitrogen Coupling Reactions. *J. Org. Chem.* **2007,** *72*, 6324-6327; (b) Omar-Amrani, R.; Thomas, A.; Brenner, E.; Schneider, R.; Fort, Y., Efficient Nickel-Mediated Intramolecular Amination of Aryl Chlorides. *Org. Lett.* **2003,** *5*, 2311-2314; (c) Desmarets, C.; Schneider, R.; Fort, Y., Nickel-catalysed synthesis of 3-chloroanilines and chloro aminopyridines via cross-coupling reactions of aryl and heteroaryl dichlorides with amines. *Tetrahedron Lett.* **2001,** *42*, 247-250; (d) Park, N. H.; Teverovskiy, G.; Buchwald, S. L., Development of an Air-Stable Nickel Precatalyst for the Amination of Aryl Chlorides, Sulfamates, Mesylates, and Triflates. *Org. Lett.* **2014,** *16*, 220-223.
20. (a) Green, R. A.; Hartwig, J. F., Nickel-Catalyzed Amination of Aryl Chlorides with Ammonia or Ammonium Salts. *Angew. Chem.* **2015,** *127*, 3839-3843; (b) Borzenko, A.; Rotta-Loria, N. L.; MacQueen, P. M.; Lavoie, C. M.; McDonald, R.; Stradiotto, M., Nickel-Catalyzed Monoarylation of Ammonia. *Angew. Chem. Int. Ed.* **2015,** *54*, 3773-3777.
21. (a) Tassone, J. P.; England, E. V.; MacQueen, P. M.; Ferguson, M. J.; Stradiotto, M., PhPAd-DalPhos: Ligand-Enabled, Nickel-Catalyzed Cross-Coupling of (Hetero)aryl Electrophiles with Bulky Primary Alkylamines. *Angew. Chem. Int. Ed.* **2019,** *58*, 2485-2489; (b) Clark, J. S. K.; Ferguson, M. J.; McDonald, R.; Stradiotto, M., PAd2-DalPhos Enables the Nickel-Catalyzed C−N Cross-Coupling of Primary Heteroarylamines and (Hetero)aryl Chlorides. *Angew. Chem. Int. Ed.* **2019,** *58*, 6391-6395.
22. (a) Li, C.; Kawamata, Y.; Nakamura, H.; Vantourout, J. C.; Liu, Z.; Hou, Q.; Bao, D.; Starr, J. T.; Chen, J.; Yan, M.; Baran, P. S., Electrochemically Enabled, Nickel-Catalyzed

Amination. *Angew. Chem. Int. Ed.* **2017,** *56*, 13088-13093; (b) Kawamata, Y.; Vantourout, J. C.; Hickey, D. P.; Bai, P.; Chen, L.; Hou, Q.; Qiao, W.; Barman, K.; Edwards, M. A.; Garrido-Castro, A. F.; deGruyter, J. N.; Nakamura, H.; Knouse, K.; Qin, C.; Clay, K. J.; Bao, D.; Li, C.; Starr, J. T.; Garcia-Irizarry, C.; Sach, N.; White, H. S.; Neurock, M.; Minteer, S. D.; Baran, P. S., Electrochemically Driven, Ni-Catalyzed Aryl Amination: Scope, Mechanism, and Applications. *J. Am. Chem. Soc.* **2019,** *141*, 6392-6402.

23. Lim, C.-H.; Kudisch, M.; Liu, B.; Miyake, G. M., C–N Cross-Coupling via Photoexcitation of Nickel–Amine Complexes. *J. Am. Chem. Soc.* **2018,** *140*, 7667-7673.
24. (a) Paul, F.; Patt, J.; Hartwig, J. F., Palladium-catalyzed formation of carbon-nitrogen bonds. Reaction intermediates and catalyst improvements in the hetero cross-coupling of aryl halides and tin amides. *J. Am. Chem. Soc.* **1994,** *116*, 5969-5970; (b) Driver, M. S.; Hartwig, J. F., Energetics and Mechanism of Alkylamine N−H Bond Cleavage by Palladium Hydroxides: N−H Activation by Unusual Acid−Base Chemistry. *Organometallics* **1997,** *16*, 5706-5715; (c) Shekhar, S.; Ryberg, P.; Hartwig, J. F.; Mathew, J. S.; Blackmond, D. G.; Strieter, E. R.; Buchwald, S. L., Reevaluation of the Mechanism of the Amination of Aryl Halides Catalyzed by BINAP-Ligated Palladium Complexes. *J. Am. Chem. Soc.* **2006,** *128*, 3584-3591; (d) Klinkenberg, J. L.; Hartwig, J. F., Slow Reductive Elimination from Arylpalladium Parent Amido Complexes. *J. Am. Chem. Soc.* **2010,** *132*, 11830-11833; (e) Brusoe, A. T.; Hartwig, J. F., Palladium-Catalyzed Arylation of Fluoroalkylamines. *J. Am. Chem. Soc.* **2015,** *137*, 8460-8468; (f) Arrechea, P. L.; Buchwald, S. L., Biaryl Phosphine Based Pd(II) Amido Complexes: The Effect of Ligand Structure on Reductive Elimination. *J. Am. Chem. Soc.* **2016,** *138*, 12486-12493.
25. Diccianni, J. B.; Katigbak, J.; Hu, C.; Diao, T., Mechanistic Characterization of (Xantphos)Ni(I)-Mediated Alkyl Bromide Activation: Oxidative Addition, Electron Transfer, or Halogen-Atom Abstraction. *J. Am. Chem. Soc.* **2019,** *141*, 1788-1796.
26. (a) Roy, A. H.; Hartwig, J. F., Reductive Elimination of Aryl Halides from Palladium(II). *J. Am. Chem. Soc.* **2001,** *123*, 1232-1233; (b) Portnoy, M.; Milstein, D., Mechanism of aryl chloride oxidative addition to chelated palladium(0) complexes. *Organometallics* **1993,** *12*, 1665-1673; (c) Amatore, C.; Pfluger, F., Mechanism of oxidative addition of palladium(0) with aromatic iodides in toluene, monitored at ultramicroelectrodes. *Organometallics* **1990,** *9*, 2276-2282; (d) Barrios-Landeros, F.; Hartwig, J. F., Distinct Mechanisms for the Oxidative Addition of Chloro-, Bromo-, and Iodoarenes to a Bisphosphine Palladium(0) Complex with Hindered Ligands. *J. Am. Chem. Soc.* **2005,** *127*, 6944-6945; (e) Barrios-Landeros, F.; Carrow, B. P.; Hartwig, J. F., Effect of Ligand Steric Properties and Halide Identity on the Mechanism for Oxidative Addition of Haloarenes to Trialkylphosphine Pd(0) Complexes. *J. Am. Chem. Soc.* **2009,** *131*, 8141-8154.
27. (a) Tsou, T. T.; Kochi, J. K., Mechanism of oxidative addition. Reaction of nickel(0) complexes with aromatic halides. *J. Am. Chem. Soc.* **1979,** *101*, 6319-6332; (b) Bajo, S.; Laidlaw, G.; Kennedy, A. R.; Sproules, S.; Nelson, D. J., Oxidative Addition of Aryl Electrophiles to a Prototypical Nickel(0) Complex: Mechanism and Structure/Reactivity Relationships. *Organometallics* **2017,** *36*, 1662-1672.
28. Yamashita, M.; Hartwig, J. F., Synthesis, Structure, and Reductive Elimination Chemistry of Three-Coordinate Arylpalladium Amido Complexes. *J. Am. Chem. Soc.* **2004,** *126*, 5344-5345.
29. Wang, Y.; Shi, Y.-F.; Chen, Y.-B.; Wu, L.-M., Hydrazine reduction of metal ions to porous submicro-structures of Ag, Pd, Cu, Ni, and Bi. *J. Solid State Chem.* **2012,** *191*, 19-26.

30. Niemeier, J. K.; Kjell, D. P., Hydrazine and Aqueous Hydrazine Solutions: Evaluating Safety in Chemical Processes. *Org. Process Res. Dev.* **2013,** *17*, 1580-1590.
31. (a) DeAngelis, A.; Wang, D.-H.; Buchwald, S. L., Mild and Rapid Pd-Catalyzed Cross-Coupling with Hydrazine in Continuous Flow: Application to the Synthesis of Functionalized Heterocycles. *Angew. Chem. Int. Ed.* **2013,** *52*, 3434-3437; (b) Lundgren, R. J.; Stradiotto, M., Palladium-Catalyzed Cross-Coupling of Aryl Chlorides and Tosylates with Hydrazine. *Angew. Chem. Int. Ed.* **2010,** *49*, 8686-8690.
32. Schlummer, B.; Scholz, U., Palladium-Catalyzed C–N and C–O Coupling–A Practical Guide from an Industrial Vantage Point. *Adv. Synth. Catal.* **2004,** *346*, 1599-1626.
33. Katrizky, A. R.; Pozharskii, A. F., *Handbook of Heterocyclic Chemistry*. 2nd ed.; Pergamon: Oxford, 2000.
34. Karrouchi, K.; Radi, S.; Ramli, Y.; Taoufik, J.; Mabkhot, Y. N.; Al-aizari, F. A.; Ansar, M. h., Synthesis and Pharmacological Activities of Pyrazole Derivatives: A Review. *Molecules* **2018,** *23*, 134.
35. Potts, K. T., The Chemistry of 1,2,4-Triazoles. *Chem. Rev.* **1961,** *61*, 87-127.
36. Habeeb, A. G.; Praveen Rao, P. N.; Knaus, E. E., Design and Synthesis of Celecoxib and Rofecoxib Analogues as Selective Cyclooxygenase-2 (COX-2) Inhibitors: Replacement of Sulfonamide and Methylsulfonyl Pharmacophores by an Azido Bioisostere. *J. Med. Chem.* **2001,** *44*, 3039-3042.
37. Kotagiri, V. K.; Suthrapu, S.; Mukunda Reddy, J.; Prasad Rao, C.; Bollugoddu, V.; Bhattacharya, A.; Bandichhor, R., An Improved Synthesis of Rimonabant: Anti-Obesity Drug. *Org. Process Res. Dev.* **2007,** *11*, 910-912.
38. Hamprecht, G.; Witschel, M.; Hawkes, T. R.; Edmunds, A. J. F.; Morris, J. A.; van Almsick, A., Herbicides with Bleaching Properties. In *Modern Crop Protection Compounds*, Wiley-VCH Verlag & Co. KGaA: Weinheim, Germany, 2011; pp 197-276.
39. Theodoridis, G.; Liebl, R.; Zagar, C., Protoporphyrinogen IX Oxidase Inhibitors. In *Modern Crop Protection Compounds*, Wiley-VCH Verlag & Co. KGaA: Weinheim, Germany, 2011; pp 163-195.
40. Schirmann, J.-P.; Bourdauducq, P., Hydrazine. In *Ullmann's Encylopedia of Industrial Chemistry*, John Wiley and Sons: New York, 2001.
41. (a) Charier, S.; Ruel, O.; Baudin, J.-B.; Alcor, D.; Allemand, J.-F.; Meglio, A.; Jullien, L., An Efficient Fluorescent Probe for Ratiometric pH Measurements in Aqueous Solutions. *Angew. Chem.* **2004,** *116*, 4889-4892; (b) Sánchez, B.; Calderón, C.; Tapia, R. A.; Contreras, R.; Campodónico, P. R., Activation of Electrophile/Nucleophile Pair by a Nucleophilic and Electrophilic Solvation in a SNAr Reaction. *Front. Chem.* **2018,** *6*; (c) Wilsily, A.; Mennen, S. M.; Cosbie, A.; Milne, J. E., Synthesis of the Hydrazinyl Pyridine Intermediate: Phase-Appropriate Delivery. *Org. Process Res. Dev.* **2017,** *21*, 1286-1293; (d) Cho, H.-J.; Um, I.-H., The α-Effect in SNAr Reaction of 1-Fluoro-2,4-dinitrobenzene with Hydrazine: Ground-State Destabilization versus Transition-State Stabilization. *Bull. Korean Chem. Soc.* **2014,** *35*, 2371-2374; (e) Cho, H.-J.; Kim, M.-Y.; Um, I.-H., The α-Effect in SNAr Reaction of Y-Substituted-Phenoxy-2,4-Dinitrobenzenes with Amines: Reaction Mechanism and Origin of the α-Effect. *Bull. Korean Chem. Soc.* **2014,** *35*, 2448-2452.
42. (a) Siva Kumar, K.; Mahesh Kumar, P.; Sreenivasa Rao, V.; Jafar, A. A.; Meda, C. L. T.; Kapavarapu, R.; Parsa, K. V. L.; Pal, M., A new cascade reaction: concurrent construction of six and five membered rings leading to novel fused quinazolinones. *Org. Biomol. Chem.*

2012, *10*, 3098-3103; (b) Liu, X.; Barry, M.; Tsou, H.-R., Palladium-catalyzed arylation of N,N-dialkylhydrazines and the subsequent conversion to anilines. *Tetrahedron Lett.* **2007,** *48*, 8409-8412; (c) Cacchi, S.; Fabrizi, G.; Goggiamani, A.; Sgalla, S., Palladium-Catalyzed N-Arylation of N,N-Dialkylhydrazines with Aryl Chlorides. *Adv. Synth. Catal.* **2007,** *349*, 453-458; (d) Cacchi, S.; Fabrizi, G.; Goggiamani, A.; Licandro, E.; Maiorana, S.; Perdicchia, D., Synthesis of N,N-Dialkyl-N'-arylhydrazines via Palladium-Catalyzed N-Arylation by Using N,N-Dialkylhydrazines/2LiCl Adducts. *Org. Lett.* **2005,** *7*, 1497-1500.

43. (a) Barnard, C. F. J., Palladium-catalyzed carbonylation - A reaction come of age. *Organometallics* **2008,** *27*, 5402-5422; (b) Magano, J.; Dunetz, J. R., Large-Scale Applications of Transition Metal-Catalyzed Couplings for the Synthesis of Pharmaceuticals. *Chem. Rev.* **2011,** *111*, 2177-2250; (c) Brennführer, A.; Neumann, H.; Beller, M., Palladium-Catalyzed Carbonylation Reactions of Aryl Halides and Related Compounds. *Angew. Chem. Int. Ed.* **2009,** *48*, 4114-4133; (d) Quesnel, J. S.; Kayser, L. V.; Fabrikant, A.; Arndtsen, B. A., Acid Chloride Synthesis by the Palladium-Catalyzed Chlorocarbonylation of Aryl Bromides. *Chem. Eur. J.* **2015,** *21*, 9550-9555; (e) Quesnel, J. S.; Arndtsen, B. A., A Palladium-Catalyzed Carbonylation Approach to Acid Chloride Synthesis. *J. Am. Chem. Soc.* **2013,** *135*, 16841-16844.
44. Schoenberg, A.; Bartoletti, I.; Heck, R. F., Palladium-catalyzed carboalkoxylation of aryl, benzyl, and vinylic halides. *J. Org. Chem.* **1974,** *39*, 3318-3326.
45. (a) Sergeev, A.; Spannenberg, A.; Beller, M., Palladium-catalyzed formylation of aryl bromides: Elucidation of the catalytic cycle of an industrially applied coupling reaction. *J. Am. Chem. Soc.* **2008,** *130*, 15549-15563; (b) Ben-David, Y.; Portnoy, M.; Milstein, D., Chelate-assisted, palladium-catalyzed efficient carbonylation of aryl chlorides. *J. Am. Chem. Soc.* **1989,** *111*, 8742-8744.
46. (a) Jimenez-Rodriguez, C.; Eastham, G. R.; Cole-Hamilton, D. J., The methoxycarbonylation of aryl chlorides catalysed by palladium complexes of bis(di-tert-butylphosphinomethyl)benzene. *Dalton Trans.* **2005**, 1826-1830; (b) Lagerlund, O.; Larhed, M., Microwave-Promoted Aminocarbonylations of Aryl Chlorides Using $Mo(CO)_6$ as a Solid Carbon Monoxide Source. *J. Comb. Chem.* **2006,** *8*, 4-6; (c) Lundgren, R. J.; Peters, B. D.; Alsabeh, P. G.; Stradiotto, M., A P,N-Ligand for Palladium-Catalyzed Ammonia Arylation: Coupling of Deactivated Aryl Chlorides, Chemoselective Arylations, and Room Temperature Reactions. *Angewandte Chemie International Edition* **2010,** *49*, 4071-4074; (d) Martinelli, J. R.; Clark, T. P.; Watson, D. A.; Munday, R. H.; Buchwald, S. L., Palladium-catalyzed aminocarbonylation of aryl chlorides at atmospheric pressure: The dual role of sodium phenoxide. *Angew. Chem. Int. Ed.* **2007,** *46*, 8460-8463.
47. Wang, J. Y.; Strom, A. E.; Hartwig, J. F., Mechanistic Studies of Palladium-Catalyzed Aminocarbonylation of Aryl Chlorides with Carbon Monoxide and Ammonia. *J. Am. Chem. Soc.* **2018,** *140*, 7979-7993.
48. Miloserdov, F. M.; McMullin, C. L.; Belmonte, M. M.; Benet-Buchholz, J.; Bakhmutov, V. I.; Macgregor, S. A.; Grushin, V. V., The challenge of palladium-catalyzed aromatic azidocarbonylation: From mechanistic and catalyst deactivation studies to a highly efficient process. *Organometallics* **2014,** *33*, 736-752.
49. (a) Wu, X. F.; Neumann, H.; Beller, M., Selective palladium-catalyzed aminocarbonylation of aryl halides with CO and ammonia. *Chem. Eur. J.* **2010,** *16*, 9750-9753; (b) Alsabeh, P. G.; Stradiotto, M.; Neumann, H.; Beller, M., Aminocarbonylation of (Hetero)aryl bromides

with ammonia and amines using a palladium/dalphos catalyst system. *Adv. Synth. Catal.* **2012,** *354*, 3065-3070; (c) Xu, T.; Alper, H., Palladium-catalyzed aminocarbonylation of aryl iodides using aqueous ammonia. *Tetrahedron Lett.* **2013,** *54*, 5496-5499.

50. (a) Schnyder, A.; Beller, M.; Mehltretter, G.; Nsenda, T.; Studer, M.; Indolese, A. F., Synthesis of primary aromatic amides by aminocarbonylation of aryl halides using formamide as an ammonia synthon. *J. Org. Chem.* **2001,** *66*, 4311-4315; (b) Wan, Y.; Alterman, M.; Larhed, M.; Hallberg, A., Formamide as a Combined Ammonia Synthon and Carbon Monoxide Source in Fast Palladium-Catalyzed Aminocarbonylations of Aryl Halides. *J. Comb. Chem.* **2003,** *5*, 82-84; (c) Wu, X.; Wannberg, J.; Larhed, M., Hydroxylamine as an ammonia equivalent in microwave-enhanced aminocarbonylations. *Tetrahedron* **2006,** *62*, 4665-4670.
51. Klinkenberg, J. L.; Hartwig, J. F., Catalytic Organometallic Reactions of Ammonia. *Angew. Chem. Int. Ed.* **2011,** *50*, 86-95.
52. Ozawa, F.; Soyama, H.; Yanagihara, H.; Aoyama, I.; Takino, H.; Izawa, K.; Yamamoto, T.; Yamamoto, A., Palladium-catalyzed double carbonylation of aryl halides to give α-keto amides. Mechanistic studies. *J. Am. Chem. Soc.* **1985,** *107*, 3235-3245.
53. (a) Wu, X.-F.; Neumann, H.; Spannenberg, A.; Schulz, T.; Jiao, H.; Beller, M., Development of a General Palladium-Catalyzed Carbonylative Heck Reaction of Aryl Halides. *J. Am. Chem. Soc.* **2010,** *132*, 14596-14602; (b) Wu, X.-F.; Neumann, H.; Beller, M., Palladium-Catalyzed Coupling Reactions: Carbonylative Heck Reactions To Give Chalcones. *Angew. Chem. Int. Ed.* **2010,** *49*, 5284-5288.
54. (a) Schoenberg, A.; Heck, R. F., Palladium-catalyzed formylation of aryl, heterocyclic, and vinylic halides. *J. Am. Chem. Soc.* **1974,** *96*, 7761-7764; (b) Klaus, S.; Neumann, H.; Zapf, A.; Strübing, D.; Hübner, S.; Almena, J.; Riermeier, T.; Groß, P.; Sarich, M.; Krahnert, W.-R.; Rossen, K.; Beller, M., A General and Efficient Method for the Formylation of Aryl and Heteroaryl Bromides. *Angew. Chem. Int. Ed.* **2006,** *45*, 154-158.
55. (a) Schoenberg, A.; Heck, R. F., Palladium-catalyzed amidation of aryl, heterocyclic, and vinylic halides. *J. Org. Chem.* **1974,** *39*, 3327-3331; (b) Martinelli, J. R.; Freckmann, D. M. M.; Buchwald, S. L., Convenient Method for the Preparation of Weinreb Amides via Pd-Catalyzed Aminocarbonylation of Aryl Bromides at Atmospheric Pressure. *Org. Lett.* **2006,** *8*, 4843-4846; (c) Wu, X.-F.; Neumann, H.; Beller, M., Selective Palladium-Catalyzed Aminocarbonylation of Aryl Halides with CO and Ammonia. *Chem. Eur. J.* **2010,** *16*, 9750-9753.
56. (a) Mägerlein, W.; Beller, M.; Indolese, A. F., Palladium-catalyzed carbonylation of aryl halides — a detailed investigation of the alkoxycarbonylation of 4-bromoacetophenone. *J. Mol. Catal. A: Chem.* **2000,** *156*, 213-221; (b) Munday, R. H.; Martinelli, J. R.; Buchwald, S. L., Palladium-Catalyzed Carbonylation of Aryl Tosylates and Mesylates. *J. Am. Chem. Soc.* **2008,** *130*, 2754-2755.
57. (a) Wu, X.-F.; Neumann, H.; Beller, M., Palladium-catalyzed carbonylative coupling reactions between Ar-X and carbon nucleophiles. *Chem. Soc. Rev.* **2011,** *40*, 4986-5009; (b) Miloserdov, F. M.; Grushin, V. V., Palladium-Catalyzed Aromatic Azidocarbonylation. *Angew. Chem. Int. Ed.* **2012,** *51*, 3668-3672.
58. Schmid, R., Homogeneous Catalysis with Metal Complexes in a Pharmaceuticals' and Vitamins' Company: Why, What for, and Where to Go? *Chimia* **1996,** *50*, 110-113.
59. Atkins, R. J.; Banks, A.; Bellingham, R. K.; Breen, G. F.; Carey, J. S.; Etridge, S. K.; Hayes, J. F.; Hussain, N.; Morgan, D. O.; Oxley, P.; Passey, S. C.; Walsgrove, T. C.; Wells,

A. S., The Development of a Manufacturing Route for the GPIIb/IIIa Receptor Antagonist SB-214857-A. Part 2: Conversion of the Key Intermediate SB-235349 to SB-214857-A. *Org. Process Res. Dev.* **2003,** *7*, 663-675.

60. Torborg, C.; Beller, M., Recent Applications of Palladium-Catalyzed Coupling Reactions in the Pharmaceutical, Agrochemical, and Fine Chemical Industries. *Adv. Synth. Catal.* **2009,** *351*, 3027-3043.
61. (a) Quesnel, J. S.; Moncho, S.; Ylijoki, K. E.; Torres, G. M.; Brothers, E. N.; Bengali, A. A.; Arndtsen, B. A., Computational Study of the Palladium-Catalyzed Carbonylative Synthesis of Aromatic Acid Chlorides: The Synergistic Effect of PtBu3 and CO on Reductive Elimination. *Chem. Eur. J.* **2016,** *22*, 15107-15118; (b) Torres, G. M.; Quesnel, J. S.; Bijou, D.; Arndtsen, B. A., From Aryl Iodides to 1,3-Dipoles: Design and Mechanism of a Palladium Catalyzed Multicomponent Synthesis of Pyrroles. *J. Am. Chem. Soc.* **2016,** *138*, 7315-7324.
62. Garrou, P. E.; Heck, R. F., The mechanism of carbonylation of halo(bis ligand)organoplatinum(II), -palladium(II), and -nickel(II) complexes. *J. Am. Chem. Soc.* **1976,** *98*, 4115-4127.
63. Lin, Y.-S.; Yamamoto, A., Studies Relevant to Palladium-Catalyzed Carbonylation Processes. Mechanisms of Formation of Esters and Amides from Benzylpalladium and (Phenylacetyl)palladium Complexes on Reactions with Alcohols and Amines. *Organometallics* **1998,** *17*, 3466-3478.
64. Ben-David, Y.; Portnoy, M.; Milstein, D., Chelate-assisted, palladium-catalyzed efficient carbonylation of aryl chlorides. *J. Am. Chem. Soc.* **1989,** *111*, 8742-8744.
65. (a) Koji, K.; Michito, S.; Masanobu, H.; Yasuzo, U., Oxidative Additions of Alkyl Halides to Palladium(0) Carbonyl Complex. *Bull. Chem. Soc. Jpn.* **1973,** *46*, 2820-2822; (b) Stille, J. K.; Lau, K. S. Y., Oxidative addition of alkyl halides to zero-valent palladium complexes. Mechanisms. *J. Am. Chem. Soc.* **1976,** *98*, 5841-5849; (c) Lau, K. S. Y.; Wong, P. K.; Stille, J. K., Oxidative addition of benzyl halides to zero-valent palladium complexes. Inversion of configuration at carbon. *J. Am. Chem. Soc.* **1976,** *98*, 5832-5840; (d) Bloome, K. S.; McMahen, R. L.; Alexanian, E. J., Palladium-Catalyzed Heck-Type Reactions of Alkyl Iodides. *J. Am. Chem. Soc.* **2011,** *133*, 20146-20148; (e) Sargent, B. T.; Alexanian, E. J., Palladium-Catalyzed Alkoxycarbonylation of Unactivated Secondary Alkyl Bromides at Low Pressure. *J. Am. Chem. Soc.* **2016,** *138*, 7520-7523.
66. (a) Stromnova, T.; Moiseev, I., Palladium carbonyl complexes. *Russ. Chem. Rev.* **1998,** *67*, 485-514; (b) Crabtree, R. H.; Mingos, D. M. P., 8.04.1 Carbonyl Complexes. In *Comprehensive Organometallic Chemistry III, Volumes 1 - 13*, Elsevier: pp 197-210.
67. Grushin, V. V.; Alper, H., Transformations of Chloroarenes, Catalyzed by Transition-Metal Complexes. *Chem. Rev.* **1994,** *94*, 1047-1062.
68. (a) Huser, M.; Youinou, M.-T.; Osborn, J. A., Chlorocarbon Activation: Catalytic Carbonylation of Dichloromethane and Chlorobenzene. *Angew. Chem. Int. Ed. Engl.* **1989,** *28*, 1386-1388; (b) Mägerlein, W.; Indolese, A. F.; Beller, M., A More Efficient Catalyst for the Carbonylation of Chloroarenes. *Angew. Chem. Int. Ed.* **2001,** *40*, 2856-2859; (c) Wu, X.-F.; Neumann, H.; Beller, M., Development of a Second Generation Palladium Catalyst System for the Aminocarbonylation of Aryl Halides with CO and Ammonia. *Chem. Asian J.* **2010,** *5*, 2168-2172.
69. (a) Komiya, S.; Akai, Y.; Tanaka, K.; Yamamoto, T.; Yamamoto, A., Reductive elimination of aryl carboxylates from acyl(aryloxy)nickel(II) and -palladium(II)

complexes. *Organometallics* **1985,** *4*, 1130-1136; (b) van Leeuwen, P. W. N. M.; Zuideveld, M. A.; Swennenhuis, B. H. G.; Freixa, Z.; Kamer, P. C. J.; Goubitz, K.; Fraanje, J.; Lutz, M.; Spek, A. L., Alcoholysis of Acylpalladium(II) Complexes Relevant to the Alternating Copolymerization of Ethene and Carbon Monoxide and the Alkoxycarbonylation of Alkenes: the Importance of Cis-Coordinating Phosphines. *J. Am. Chem. Soc.* **2003,** *125*, 5523-5539.

70. Ozawa, F.; Kawasaki, N.; Okamoto, H.; Yamamoto, T.; Yamamoto, A., Mechanisms of double and single carbonylation reactions of aryl iodides catalyzed by palladium complexes to give .alpha.-keto esters and esters. *Organometallics* **1987,** *6*, 1640-1651.
71. (a) Seligson, A. L.; Trogler, W. C., Cone angles for amine ligands. X-ray crystal structures and equilibrium measurements for ammonia, ethylamine, diethylamine, and triethylamine complexes with the [bis(dimethylphosphino)ethane]methylpalladium(II) cation. *J. Am. Chem. Soc.* **1991,** *113*, 2520-2527; (b) Nigst, T. A.; Antipova, A.; Mayr, H., Nucleophilic Reactivities of Hydrazines and Amines: The Futile Search for the α-Effect in Hydrazine Reactivities. *J. Org. Chem.* **2012,** *77*, 8142-8155.
72. (a) Trebbe, R.; Goddard, R.; Rufińska, A.; Seevogel, K.; Pörschke, K.-R., Preparation and Structural Characterization of the Palladium(0)−Carbonyl Complexes (R2PC2H4PR2)Pd(CO)2 and {(R2PC2H4PR2)Pd}2(μ-CO). *Organometallics* **1999,** *18*, 2466-2472; (b) Perez, P. J.; Calabrese, J. C.; Bunel, E. E., Synthesis, Characterization, and Reactivity of [((^{i}Pr)$_2$P(CH$_2$)$_3$P(^{i}Pr)$_2$)(PCy$_3$)PdH][OR]. *Organometallics* **2001,** *20*, 337-345.
73. Due to the poor solubility of 4 in neat DMSO, a 1:1 v/v mixture of DMSO and toluene was chosen as a solvent mixture capable of dissolving 4.
74. (a) Grevin, J.; Kalck, P.; Daran, J. C.; Vaissermann, J.; Bianchini, C., Synthesis of a novel palladium(0) carbonyl complex containing a tridentate phosphorus ligand. X-ray crystal structure of [Pd(CO)(CH3C(CH2PPh2)3)]. *Inorg. Chem.* **1993,** *32*, 4965-4967; (b) Bellabarba, R. M.; Tooze, R. P.; Slawin, A. M. Z., Synthesis, X-ray characterisation and reactions of a trigonal planar palladium(0) carbonyl complex, (tbpx)PdCO. *Chem. Commun.* **2003**, 1916-1917.
75. Bunel also observed the absence of 31P-13C coupling in (DIPP)Pd(13CO) (DIPP = 1,3-bis(diisopropylphosphino) propane) under 13CO, which was attributed to rapid exchange between bound and unbound 13CO. See ref. 28b.
76. At this temperature and pressure of CO, a resonance at the chemical shift of free CO was observed suggesting that exchange between bound and unbound CO was no longer present at the NMR time scale.
77. Even with 1000 Torr of 13CO at –40 °C, phosphorus-carbon coupling was still not detected.
78. We monitored this reaction by 19F NMR spectroscopy because the concentration of 4 could not be determined accurately by 31P NMR spectroscopy at low pressures of CO (<500 Torr) and elevated temperatures due to broad resonances.
79. The 12 kcal/mol barrier is given as the difference in energy between the transition state for oxidative addition and the computed energy of the experimentally determined resting state.
80. Singleton, D. A.; Thomas, A. A., High-Precision Simultaneous Determination of Multiple Small Kinetic Isotope Effects at Natural Abundance. *J. Am. Chem. Soc.* **1995,** *117*, 9357-9358.
81. It should be noted that the y-intercept of the fit of 1/kobs versus pressure of CO and the fit of 1/kobs versus 1/[ArCl] (Figure 4a) correspond to 1/k1 in the equation given for Path A

in Figure 5. However, the values of this intercept were too close to zero to deduce an accurate value. This small value of the y-intercept reflects rapid exchange of unbound CO with the CO bound to dicarbonyl 4 and fits with the rapid exchange observed at room temperature by 13C NMR spectroscopy (vide supra).

82. Portnoy, M.; Milstein, D., Mechanism of aryl chloride oxidative addition to chelated palladium(0) complexes. *Organometallics* **1993,** *12*, 1665-1673.
83. (a) Fauvarque, J.-F.; Pflüger, F.; Troupel, M., Kinetics of oxidative addition of zerovalent palladium to aromatic iodides. *J. Organomet. Chem.* **1981,** *208*, 419-427; (b) Jutand, A.; Mosleh, A., Rate and Mechanism of Oxidative Addition of Aryl Triflates to Zerovalent Palladium Complexes. Evidence for the Formation of Cationic (.sigma.-Aryl)palladium Complexes. *Organometallics* **1995,** *14*, 1810-1817.
84. Hansch, C.; Leo, A.; Taft, R. W., A survey of Hammett substituent constants and resonance and field parameters. *Chem. Rev.* **1991,** *91*, 165-195.
85. Maes, B.; Verbeeck, S.; Verhelst, T.; Ekomié, A.; von Wolff, N.; Lefèvre, G.; Mitchell, E.; Jutand, A., Oxidative Addition of Haloheteroarenes to Palladium(0): Concerted versus SNAr-Type Mechanism. *Chem. Eur. J.* **2015,** *21*, 7858-7865.
86. (a) Meyer, A.; Penning, H.; Elsner, M., C and N isotope fractionation suggests similar mechanisms of microbial atrazine transformation despite involvement of different enzymes (AtzA and TrzN). *Environ. Sci. Technol.* **2009,** *43*, 8079-8085; (b) Grzybkowska, A.; Kaminski, R.; Dybala-Defratyka, A., Theoretical predictions of isotope effects versus their experimental values for an example of uncatalyzed hydrolysis of atrazine. *PCCP* **2014,** *16*, 15164.
87. Quesnel, J. S.; Kayser, L. V.; Fabrikant, A.; Arndtsen, B. A., Acid Chloride Synthesis by the Palladium-Catalyzed Chlorocarbonylation of Aryl Bromides. *Chem. Eur. J.* **2015,** *21*, 9550-9555.
88. Moser, W. R.; Wang, A. W.; Kildahl, N. K., Mechanistic studies of the palladium-catalyzed reaction of methanol with bromobenzene and carbon monoxide to produce methyl benzoate. 1. Stoichiometric study. *J. Am. Chem. Soc.* **1988,** *110*, 2816-2820.
89. The small increase in rate with increasing N(n-butyl)4PF6 suggests the reaction of 6a with ammonia depends slightly on the polarity of the solvent.
90. O'Toole, T. R.; Younathan, J. N.; Sullivan, B. P.; Meyer, T. J., 1,2-Difluorobenzene: a relatively inert and noncoordinating solvent for electrochemical studies on transition-metal complexes. *Inorg. Chem.* **1989,** *28*, 3923-3926.
91. Tsuji, J., Palladium-Catalyzed Decarbonylation of Acyl Halides and Aldehydes. In *Handbook of Organopalladium Chemistry for Organic Synthesis*, John Wiley & Sons, Inc.: 2002; pp 2643-2653.
92. (a) Surry, D. S.; Buchwald, S. L., Selective Palladium-Catalyzed Arylation of Ammonia: Synthesis of Anilines as Well as Symmetrical and Unsymmetrical Di- and Triarylamines. *J. Am. Chem. Soc.* **2007,** *129*, 10354-10355; (b) Vo, G. D.; Hartwig, J. F., Palladium-Catalyzed Coupling of Ammonia with Aryl Chlorides, Bromides, Iodides, and Sulfonates: A General Method for the Preparation of Primary Arylamines. *J. Am. Chem. Soc.* **2009,** *131*, 11049-11061; (c) Green, R. A.; Hartwig, J. F., Palladium-Catalyzed Amination of Aryl Chlorides and Bromides with Ammonium Salts. *Org. Lett.* **2014,** *16*, 4388-4391.
93. (a) Portnoy, M.; Frolow, F.; Milstein, D., Methanol reduces an organopalladium(II) complex to a palladium(I) hydride. Crystallographic characterization of a hydrido-bridged palladium complex. *Organometallics* **1991,** *10*, 3960-3962; (b) Portnoy, M.; Milstein, D.,

A binuclear palladium(I) hydride. Formation, reactions, and catalysis. *Organometallics* **1994,** *13*, 600-609; (c) Toth, I.; Elsevier, C. J., Formation of Dinuclear Palladium(I) Hydride [Pd2(.mu.-H)(.mu.-CO){(S,S)-BDPP}2]Cl by Methanolysis or Hydrolysis of Pd(COMe)(Cl){(S,S)-BDPP} {(S,S)-BDPP = (2S,4S)-2,4-Bis(diphenylphosphino)pentane}. *Organometallics* **1994,** *13*, 2118-2122; (d) Sperrle, M.; Gramlich, V.; Consiglio, G., Synthesis and Characterization of Cationic Palladium (6,6'-Dimethoxybiphenyl-2,2'-diyl)bis(diphenylphosphine) Complexes. *Organometallics* **1996,** *15*, 5196-5201; (e) Macchioni, A.; Romani, A.; Zuccaccia, C.; Guglielmetti, G.; Querci, C., Experimental Evidence for the Aggregation of [(Phen)2Pd2(μ-H)(μ-CO)]+ in Solution. *Organometallics* **2003,** *22*, 1526-1533.

94. Chan, S.; Lee, S.-M.; Lin, Z.; Wong, W.-T., Syntheses, structures and reactivities of [Os6Pd(CO)18(bipy)] and [{(bipy)Pd}20s3(CO)12]: Crystal and molecular structures of [{(bipy)Pd}2(μ-H)(μ-CO)][H3Os4(CO)12] and [(C4H9)4N]2[Pd2I6]. *J. Organomet. Chem.* **1996,** *510*, 219-231.
95. (a) Siedle, A. R.; Newmark, R. A.; Gleason, W. B., Protonation of phosphine complexes of zerovalent nickel, palladium, platinum, and ruthenium with fluorocarbon acids. *Inorg. Chem.* **1991,** *30*, 2005-2009; (b) Minghetti, G.; Bandini, A. L.; Banditelli, G.; Bonati, F.; Szostak, R.; Strouse, C. E.; Knobler, C. B.; Kaesz, H. D., Synthesis and characterization of cationic dinuclear hydridoplatinum complexes: crystal and molecular structure of [Pt2(.mu.-H,.mu.-CO)(dpe)2][BF4] (dpe = 1,2-bis(diphenylphosphino)ethane). *Inorg. Chem.* **1983,** *22*, 2332-2338.
96. Li, H.; Grasa, G. A.; Colacot, T. J., A Highly Efficient , Practical , and General Route for the Synthesis of (R3P)2 Pd(0): Structural Evidence on the Reduction Mechanism of Pd (II) to Pd (0). *Org. Lett.* **2010,** *12*, 3332-3335.
97. Banks, M. R.; Hudson, R. F., The Reaction of N-Alkylhydroxamic Acids with Sulphinyl Chlorides. *J. Chem. Soc. Perkin II* **1986**, 121-1.
98. Koide, Y.; Bott, S. G.; Barron, A. R., Alumoxanes as cocatalysts in the palladium-catalyzed copolymerization of carbon monoxide and ethylene: genesis of a structure-activity relationship. *Organometallics* **1996,** *15*, 2213-2226.
99. Sumino, S.; Fusano, A.; Fukuyama, T.; Ryu, I., Carbonylation Reactions of Alkyl Iodides through the Interplay of Carbon Radicals and Pd Catalysts. *Acc. Chem. Res.* **2014,** *47*, 1563-1574.
100. (a) Sargent, B. T.; Alexanian, E. J., Cobalt-Catalyzed Aminocarbonylation of Alkyl Tosylates: Stereospecific Synthesis of Amides. *Angew. Chem. Int. Ed.* **2019,** *58*, 9533-9536; (b) Sargent, B. T.; Alexanian, E. J., Cobalt-Catalyzed Carbonylative Cross-Coupling of Alkyl Tosylates and Dienes: Stereospecific Synthesis of Dienones at Low Pressure. *J. Am. Chem. Soc.* **2017,** *139*, 12438-12440.
101. Choi, J.; Martín-Gago, P.; Fu, G. C., Stereoconvergent Arylations and Alkenylations of Unactivated Alkyl Electrophiles: Catalytic Enantioselective Synthesis of Secondary Sulfonamides and Sulfones. *J. Am. Chem. Soc.* **2014,** *136*, 12161-12165.
102. Luo, Y.-R., *Handbook of Bond Dissociation Energies in Organic Compounds*. CRC Press: 2003; p 380.
103. (a) Wei, C. S.; Davies, G. H. M.; Soltani, O.; Albrecht, J.; Gao, Q.; Pathirana, C.; Hsiao, Y.; Tummala, S.; Eastgate, M. D., The Impact of Palladium(II) Reduction Pathways on the Structure and Activity of Palladium(0) Catalysts. *Angew. Chem. Int. Ed.* **2013,** *52*, 5822-5826; (b) Grushin, V. V.; Alper, H., Alkali-induced disproportionation of palladium(II)

tertiary phosphine complexes, [L_2PdCl_2], to LO and palladium(90). Key intermediates in the biphasic carbonylation of ArX catalyzed by [L_2PdCl_2]. *Organometallics* **1993,** *12*, 1890-1901.

104. Hasanayn, F.; Nsouli, N. H.; Al-Ayoubi, A.; Goldman, A. S., Addition of Alkyl Radicals to Transition-Metal-Coordinated CO: Calculation of the Reaction of [Ru(CO)5] and Related Complexes and Relevance to Alkane Carbonylation. *J. Am. Chem. Soc.* **2008,** *130*, 511-521.
105. Barry, J. T.; Berg, D. J.; Tyler, D. R., Radical Cage Effects: The Prediction of Radical Cage Pair Recombination Efficiencies Using Microviscosity Across a Range of Solvent Types. *J. Am. Chem. Soc.* **2017,** *139*, 14399-14405.
106. Lee, E.; Hooker, J. M.; Ritter, T., Nickel-Mediated Oxidative Fluorination for PET with Aqueous [18F] Fluoride. *J. Am. Chem. Soc.* **2012,** *134*, 17456-17458.
107. Koo, K.; Hillhouse, G. L., Carbon-Nitrogen Bond Formation by Reductive Elimination from Nickel(II) Amido Alkyl Complexes. *Organometallics* **1995,** *14*, 4421-4423.
108. Mohadjer Beromi, M.; Banerjee, G.; Brudvig, G. W.; Charboneau, D. J.; Hazari, N.; Lant, H. M. C.; Mercado, B. Q., Modifications to the Aryl Group of dppf-Ligated Ni σ-Aryl Precatalysts: Impact on Speciation and Catalytic Activity in Suzuki–Miyaura Coupling Reactions. *Organometallics* **2018,** *37*, 3943-3955.
109. Truong, T.-T.; Coates, G. W.; Abruña, H. D., High power organic cathodes using thin films of electropolymerized benzidine polymers. *Chem. Commun.* **2015,** *51*, 14674-14677.
110. Kong, X.; Zhang, H.; Xiao, Y.; Cao, C.; Shi, Y.; Pang, G., Effective, transition metal free and selective C–F activation under mild conditions. *RSC Advances* **2015,** *5*, 7035-7048.
111. Bilke, J. L.; O'Brien, P., On the Two-Ligand Catalytic Asymmetric Deprotonation of N-Boc Pyrrolidine: Probing the Effect of the Stoichiometric Ligand. *J. Org. Chem.* **2008,** *73*, 6452-6454.
112. van Koten, G.; Noltes, J. G., Group IB organometallic chemistry: XIV. Intramolecular ring-closure reactions of novel arylcopper compounds RCuI2. Synthesis of 7,8-dihydrodibenzo[f,h][1,4]dioxecin and 7,8-dihydrodibenzo-6,9-dimethyl[f,h][1,4]diazecin. *J. Organomet. Chem.* **1976,** *104*, 127-138.

CHAPTER 3

PD-CATALYZED AMINOCARBONYLATION REACTIONS WITH ALKYL HALIDES

3.1 Introduction

Pd-catalyzed carbonylative cross-coupling reactions with aryl halides are commonly used to prepare aromatic carboxylic acid derivatives.[43a] The same types of carbonylative functionalization reactions with alkyl halides to form carbonyl containing functional groups are less common.[99] Classical methods for the carbonylation of alkyl halides have largely been limited to alkyl iodides, which undergo photolysis to generate an alkyl radical that undergoes addition to carbon monoxide (CO).[99] These methods typically require pressures of CO in excess of 40 atm.

In 2016, Alexanian reported a Pd-catalyzed alkoxycarbonylation of alkyl bromides.[65e] This protocol is more convenient than the photolysis of alkyl iodides because it requires only 2 atm of CO, and reactions can be performed thermally at 50 °C. Mechanistic studies performed by the Alexanian group implicated the intermediacy of an alkyl radical, and a single-electron pathway for oxidative addition of the alkyl bromide to Pd(0) was proposed. Additional work by this group on the carbonylative functionalization of alkyl electrophiles involves cobalt-catalyzed Heck and aminocarbonylation reactions with alkyl tosylates, which occur by an S_N2-type oxidative addition mechanism of the alkyl tosylates to an anionic Co complex.[100] Because of this oxidative addition mechanism, amides can be synthesized by aminocarbonylation of the alkyl tosylate with high enantiospecificity; however, sterically hindered alkyl tosylates do not undergo reaction. These cobalt-catalyzed methods also require high pressures of CO (40 atm).

Thus, aminocarbonylation reactions of hindered alkyl halides have not been reported. Reaction by an alkyl radical intermediate would likely allow sterically hindered secondary and tertiary alkyl halides to undergo this carbonylation reaction. Moreover, chiral ancillary ligands could promote stereoconvergent reactivity.[101] In this scenario, the stereochemical outcome of the reaction is controlled by the catalyst and not by the substrate. In addition, the direct synthesis of amides by the reaction of an alkyl halide, CO, and an amine is desirable because it can replace syntheses of amides that involve multiple synthetic steps, such as the preparation of an alkyl Grignard reagent and the reaction of that Grignard reagent with a carbamoyl chloride. Herein, we describe the development of a Pd-catalyzed method for the aminocarbonylation of alkyl bromides.

3.2 Results and Discussion

Previous work in our group demonstrated that Pd complexes ligated by 1,3-(dicyclohexylphosphino)propane (DCPP) catalyzed aminocarbonylation reactions of aryl chlorides with ammonia.[47] The scope of this reaction encompasses both electron rich and electron poor chloroarenes, and because only a limited number of palladium catalysts can promote such reactivity with chloroarenes, the mechanism of this transformation was extensively studied. Due to the generality of this reaction, we investigated if this palladium system would catalyze similar reactions with hindered alkyl halides. We also envisioned that these prior mechanistic studies would facilitate further investigations on reactions between this metal complex and alkyl halides.

Table 3.1. Survey of Reaction Conditions.[a]

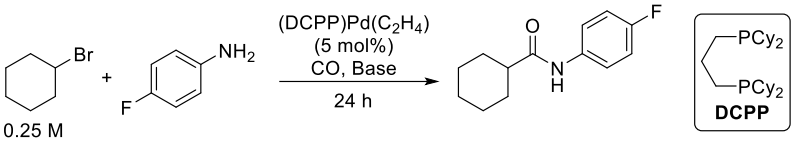

Entry	Solvent	Temperature (°C)	Base (equiv)	CO (Torr)	Yield (%)[b]
1	DMSO	100	K_2CO_3 (2)	450	21
2	Toluene	100	K_2CO_3 (2)	450	14
3	1,4-Dioxane	100	K_2CO_3 (2)	450	31
4	1,4-Dioxane	100	K_2CO_3 (2)	250	14
5	1,4-Dioxane	100	K_2C_3 (2)	760	43
6	1,4-Dioxane	100	K_2CO_3 (2)	1000	44
7	1,4-Dioxane	100	DBU (2)	760	0
8	1,4-Dioxane	100	DIPEA (2)	760	0
9	1,4-Dioxane	25	K_2CO_3 (2)	760	0
10	1,4-Dioxane	40	K_2CO_3 (2)	760	0
11	1,4-Dioxane	75	K_2CO_3 (2)	760	73
12[c]	1,4-Dioxane	75	K_2CO_3 (2)	760	0
13[d]	1,4-Dioxane	75	K_2CO_3 (2)	760	0
14[e]	1,4-Dioxane	75	K_2CO_3 (2)	760	53
15[f]	1,4-Dioxane	75	K_2CO_3 (2)	760	12

[a]Reactions were performed on a 0.123 mmol scale in 0.50 mL of solvent with 1.00 equiv of alkyl halide or tosylates and 1.00 equiv of aniline. [b]Yields were determined by GC analysis or by ^{19}F NMR spectroscopy. [c]Reaction with cyclohexyl chloride. [d]Reaction with cyclohexyl tosylate. [e]Reaction with cyclohexyl iodide. [f]Reaction with *t*-butyl bromide.

We began our studies on the aminocarbonylation of alkyl halides by conducting the reaction of cyclohexyl bromide with aniline and (DCPP)Pd(C_2H_4) as precatalyst. The results from these experiments are summarized in Table 3.1. Cyclohexyl bromide underwent aminocarbonylation with 4-fluoroaniline to give the amide product in low yield at 450 Torr of CO in either toluene, DMSO, or 1,4-dioxane at 100 °C for 24 h (Table 3.1, entries 1-3). Under these conditions, the reaction in 1,4-dioxane was the highest yielding (31%). Thus, subsequent reactions were performed in 1,4-dioxane.

The effect of the pressure of CO on the yield of the reaction was ascertained. The yield of the desired product decreased to 14% from reactions with a lower pressure of CO (Table 3.1 entry 4) that was 230 Torr, rather than 450 Torr in our initial conditions. However, the yield of the desired product increased to 43% and 44% when the pressure of CO was increased to 760 (entry 5) and 1000 Torr (entry 6), respectively. Thus, the yield of the reaction benefits from an increase in pressure of CO, but the yield of reactions with 760 Torr and 1000 Torr of CO were within experimental error of each other. The remainder of our study was conducted with 760 Torr of CO because reactions at this pressure do not necessitate the use of special reaction vessels.

Because K_2CO_3 is not soluble in 1,4-dioxane, we examined reaction conditions with DBU, or DIPEA as base. Previous mechanistic studies on this catalyst system for the aminocarbonylation of chloroarenes with ammonia showed that slow sequestration of a proton leads to the formation of a catalytically inactive Pd(I) dimer bridged by a carbonyl and hydride ligand.[47] Since DBU and DIPEA are freely soluble in dioxane, we hypothesized that an increase in concentration of base would inhibit this catalyst deactivation pathway and increase the yield of the reaction. However,

reactions with DBU or DIPEA as base did not yield the desired amide product (entries 7 and 8, respectively).

The effect of temperature on the yield of the reaction also was analyzed. Reactions at room temperature or 40 °C did not produce the desired product in a measurable quantity (entries 9 and 10). However, reactions at 75 °C gave yields (entry 11, 73%) higher than those at 100 °C.

Having identified conditions that lead to aminocarbonylation of cyclohexyl bromide in good yield, we examined the aminocarbonylation of other cyclohexyl halides and of cyclohexyl tosylate. Reactions with cyclohexyl chloride or tosylate did not furnish any of the desired product (entries 12 and 13, respectively), and reactions with cyclohexyl iodide occurred in a lower yield (entry 14, 56%) than the reaction with cyclohexyl bromide under similar conditions. The reduced yield for the reaction with cyclohexyl iodide is likely due to a side reaction prior to the start of the carbonylation reaction. When the reagents were combined in a reaction vessel prior to pressurization with CO, the Pd precatalyst changed color from colorless to yellow. We propose that the Pd precatalyst catalyzes a reaction that consumes cyclohexyl iodide in an unproductive fashion that leads to the deactivation of the palladium catalyst. However, more in depth studies are needed to support this claim. Overall, these trends in reactivity track with the bond dissociation energies of C-O, -Cl, -Br, and -I bonds.[102]

Scheme 3.1. Reaction between (DCPP)Pd(CO)$_2$ and cyclohexyl bromide.

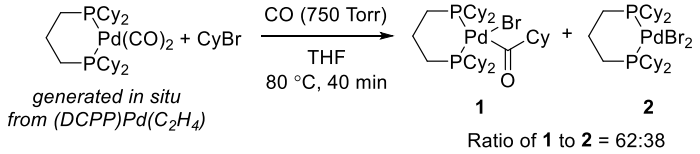

To further our understanding of the reactivity of the Pd catalyst with cyclohexyl bromide, we generated (DCPP)Pd(CO)$_2$ in situ and allowed it to react with cyclohexyl bromide in THF at 80 °C (Scheme 3.1). A ^{31}P NMR spectrum of the reaction revealed the complete consumption of (DCPP)Pd(CO)$_2$ and the formation of a compound exhibiting a pair of doublets at 19.1 and -3.5 ppm with a coupling constant of 74 Hz. This coupling constant is most consistent with an alkylacylpalladium(II) bromide complex **1**. We have previously synthesized a library of phenacylpalladium(II) halide complexes ligated by DCPP. The J_{PP} coupling constants of these acyl complexes are 60-70 Hz.[47] In comparison, the J_{PP} coupling constants of arylpalladium(II) halide complexes ligated by DCPP span 37-41 Hz. Based on these data, we propose that the doublets at 19.1 and -3.5 ppm correspond to alkyacyl complex **1**. An additional singlet was observed at 27.4 ppm in the ^{31}P NMR spectrum, which is consistent with the formation of (DCPP)PdBr$_2$ **2**. Based on these structural assignments, the ratio of acyl complex **1** to dibromide complex **2** was 62:38. We hypothesize that dibromide species **2** is catalytically inactive, and the formation of this complex sequesters catalytically active palladium complexes from the catalytic cycle. Palladium dihalide salts are often used as precatalysts for Pd-catalyzed cross coupling reactions, but these salts must be reduced to Pd(0) to initiate the catalytic reaction.[103] Thus, the formation of the dibromide species represents a pathway for the generation of an off-cycle Pd complex. Future studies in this area will involve the examination of the effect of CO and concentration of alkyl halide on the rate of formation of these Pd(II) species from (DCPP)Pd(CO)$_2$.

Additional mechanistic information can be gleaned from the catalytic reaction with a tertiary alkyl bromide. (DCPP)Pd(CO)$_2$ catalyzes the aminocarbonylation of *t*-butyl bromide with 4-fluoroaniline, albeit in a low yield of 12% (Table 3.1, entry 15). The steric hinderance of the *t*-butyl group strongly disfavors reaction by an S_N2 pathway. We propose that reaction by a concerted oxidative addition pathway, akin to the oxidative addition of aryl halides to Pd(0), is also disfavored because the steric hinderance of the *t*-butyl group inhibits a side-on coordination of a sterically hindered (DCPP)Pd(0) complex to the C-Br anti-bonding orbital. The formation of a Pd(0) complex with an η^2-bound aryl halide has been proposed to be an intermediate prior to the oxidative addition of the aryl halide to Pd(0).[10a] Because the analogous σ-complex of Pd(0) and *t*-butyl bromide is unlikely to form based on steric constraints, we propose that the mechanism of oxidative addition of alkyl halides to DCPP ligated Pd(0) is distinct from that of aryl halides and likely does not occur by a concerted, two-electron pathway. Moreover, the catalytic reaction is only capable of producing amide from cyclohexyl bromide and iodide, but not with cyclohexyl chloride or tosylate, and this trend tracks with the bond dissociation energy of the carbon-halide or -oxygen bond. Based on these preliminary data, we favor an oxidative addition pathway involving the intermediacy of an alkyl radical. However, further experiments are warranted to support this hypothesis, such as stoichiometric reactions of (DCPP)Pd(CO)$_2$ with alkyl bromides containing radical clocks or with a non-racemic alkyl bromide containing a stereogenic center at the α-halo position.

Scheme 3.2. Proposed mechanisms for the formation of acylpalladium(II) bromide complex **1** from Pd(0).

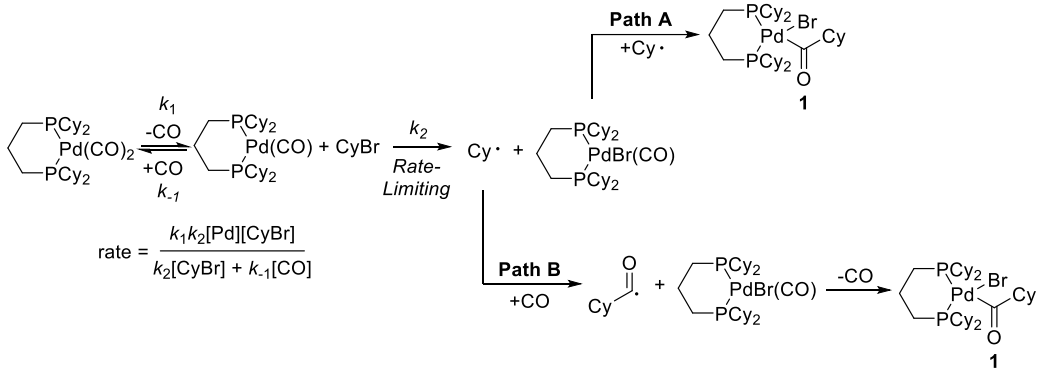

We propose the following possible mechanisms for the formation of acylpalladium(II) bromide intermediate **1** (Scheme 3.2). We hypothesize that the cleavage of the C-Br bond of cyclohexyl bromide by the palladium catalyst occurs at a more electron rich monocarbonyl complex, (DCPP)Pd(CO), rather than at the less electron poor and coordinatively saturated (DCPP)Pd(CO)$_2$. If the cleavage of the C-Br bond was rate limiting, then the rate of stoichiometric reactions involving the palladium catalyst would be inverse first order in the pressure of CO and first order in the concentration of cyclohexyl bromide. The rate of the stoichiometric reaction will also be zero order in the concentration of cyclohexyl bromide at high concentrations of this electrophile under the proposed mechanism. After scission of the C-Br bond, the cyclohexyl radical undergoes direct addition to a metal bound CO ligand at a Pd(I) monocarbonyl complex to furnish acylpalladium(II) bromide complex **1** (Path A, Scheme 3.2). The addition of alkyl radicals to metal-bound carbonyl ligands have been previously proposed as a viable reaction pathway in transition-metal catalyzed carbonylation reactions of alkanes.[104] Alternatively, the cyclohexyl

radical can undergo addition to exogenous CO and the resulting acyl radical undergoes direct addition to a Pd(I) bromide complex to give acylpalladium(II) complex **1** (Path B, Scheme 3.3). We postulate that the formation of (DCPP)$PdBr_2$ (**2**) observed in our preliminary mechanistic studies (Scheme 3.1) occurs by an additional bromine radical abstraction by a (DCPP)Pd(I) bromide complex.

These two pathways for the formation of acyl complex **1** after cleavage of the C-Br bond of cyclohexyl bromide can be distinguished by the effect of the pressure of CO on the outcome of the reaction. If the formation of acyl complex **1** occurs by Path B, then reaction at reduced pressures of CO would inhibit the formation of acyl complex **1**. At this low pressure of CO, the formation of acyl radical by the addition of cyclohexyl radical to CO will be inhibited and a larger ratio of (DCPP)$PdBr_2$ to acyl complex **1** will be observed. Additionally, in this low pressure of CO regime, the alkyl radical can either dimerize or abstract hydrogen radical from solvent to form alkane, and the correlation of the concentration of these organic compounds to the pressure of CO may indicate reaction by Path B. In contrast, this effect of the pressure of CO should not be as marked if reaction occurred by Path A. The cleavage of the C-Br bond and formation of acyl complex **1** likely occurs within a solvent cage, and unproductive side-reactions occur by the escape of cyclohexyl radical from this cage. The rates of these processes are expected to be unaffected by variations in the pressure of CO. Thus, varying the pressure of CO should not change the ratio of acyl complex **1** and (DCPP)$PdBr_2$ by Path A.

Based on previous studies of Pd-catalyzed aminocarbonylation reactions of aryl halides[47] and due to the steric hinderance of the acyl group bearing a secondary alkyl group, we propose that the formation of amide occurs by the reductive elimination of amide from an acylpalladium(II) amido species rather than a pathway involving nucleophilic attack of the amine at the carbonyl group of the acyl ligand (Scheme 3.3).

Scheme 3.3. Proposed mechanism for the formation of amide.

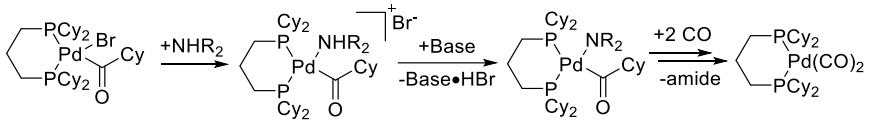

We then explored the effect of additives on the yield of the catalytic reaction based on our proposed mechanism and observations during our mechanistic studies. Similar to the results in Scheme 3.1, bisphosphine ligated Pd diiodide complexes formed during Pd-catalyzed azidocarbonylation of aryl iodides studied by Grushin.[48] The addition of polymethylhydrosiloxane (PMHS) was found to increase the yield of the desired product in the catalytic reaction; this increase was proposed to result from the reduction of the Pd(II) diiodide complex to Pd(0) by reaction with PMHS. We hypothesized that PMHS also could act as a reductant in our system to reduce (DCPP)$PdBr_2$ to Pd(0). Additionally, Tyler found that organometallic radical recombination reactions that occur in solvent cages were promoted in the presence of additives that increased the bulk viscosity of the reaction medium,[105] and we posited that PMHS can act as a reductant and increase the viscosity of the medium. Inspired by these reports, we performed the aminocarbonylation of cyclohexyl bromide in the presence of 0.25 equiv of PMHS (Scheme 3.4a); however, the yield of the desired amide product (60%) was lower than that of the reaction without PMHS. In addition, reactions in tetraglyme, which is a viscous, ethereal solvent, gave a 31% yield of the desired product, which is diminished in comparison to reactions

in 1,4-dioxane (Scheme 3.4b). We propose that PMHS acts as a source of hydrogen radical to quench the alkyl radical generated in the reaction to give an unreactive alkane. Tetraglyme can also act in a similar fashion due to the multiple weak C-H bonds in this solvent molecule that could undergo reaction with alkyl radicals.

Scheme 3.4. Aminocarbonylation reactions with PMHS or in tetraglyme.[a]

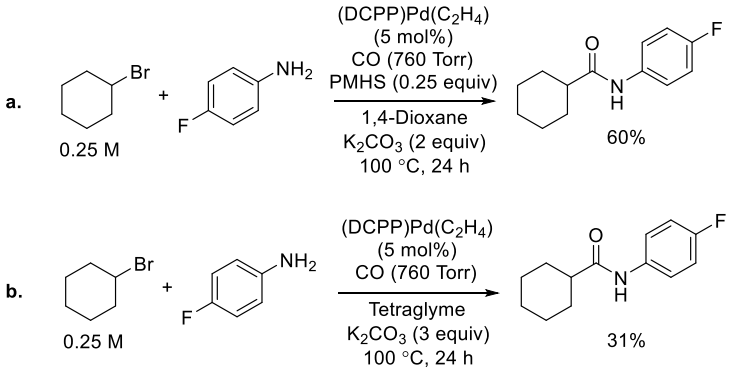

[a]Yields were determined by ^{19}F NMR spectroscopy.

3.3 Conclusion

In summary, we have uncovered a Pd-catalyst that is capable of undergoing an aminocarbonylation reaction with alkyl halides. Mechanistic studies on this system are incomplete but point towards a pathway for oxidative addition that occurs by the formation of an alkyl radical. This oxidative addition pathway also forms catalytically inactive Pd(II) dibromide. Future efforts could involve identification of reaction conditions to increase the yield and generality of this aminocarbonylation reaction, which will likely involve a survey of electrophiles, nucleophiles, and reductants. Moreover, the effect of chiral ligands on the stereochemical outcome of this reaction with alkyl halides containing α-halo stereocenters merits examination. Further mechanistic studies on this system will entail a more detailed investigation on the oxidative addition of alkyl halides to $(DCPP)Pd(CO)_2$ and the identification of the rate-limiting step of catalysis and the resting state of the catalyst.

3.4 Experimental

General Experimental Procedures

^1H, ^{19}F, ^{31}P NMR spectra were recorded on a Bruker 400, 500, or 600 MHz spectrometer. All ^1H chemical shifts are reported in parts per million relative to tetramethylsilane or residual protiated solvent as a reference, ^{31}P NMR chemical shifts are reported in parts per million relative to an 85% H_3PO_4 external standard, and ^{19}F NMR chemical shifts are reported in parts per million relative to a $CFCl_3$ external standard. All manipulations were performed in an inert atmosphere glovebox filled with nitrogen or on a Schlenk manifold. All liquid reagents were purchased from commercial sources and sparged briefly with nitrogen prior to use. $(DCPP)Pd(C_2H_4)$ was synthesized according to previously reported procedures.[47] Reagent grade carbon monoxide was purchased from Praxair. GC analyses were performed on an HP 6890 GC equipped with an HP-5 column (25 m x 0.20 mm x 0.33 μm film) and an FID detector.

Caution: Carbon monoxide is a highly toxic gas and should only be manipulated in a well-ventilated fume hood.

Survey of Reaction Conditions

In a representative experiment, a 25 mL Schlenk vessel was charged with a Teflon-coated stir bar, (DCPP)Pd(C_2H_4) (3.5 mg, 6.13 μmol), 0.500 mL of solvent, cyclohexyl halide or tosylate (0.123 mmol), 4-fluoroaniline (11.6 μL, 1.23 mmol), dodecane (27.9 μL) or fluorobenzene (11.5 μL, 0.123 mmol), and base (0.246 mmol) in an inert atmosphere glovebox. The Schlenk vessel was sealed with a Teflon stopper and exported from the glovebox. Then, the Schlenk vessel was cooled in liquid nitrogen, freeze-pump-thawed once, and then pressurized to the desired pressure of CO. The reaction mixture was warmed to the desired temperature with stirring for 24 h, vented in a well-ventilated fume hood, and cooled to room temperature. The yield of product was analyzed by gas chromatography or ^{19}F NMR spectroscopy.

Stoichiometric Reaction of (DCPP)Pd(CO)$_2$ with Cyclohexyl Bromide

In an inert atmosphere glovebox, a J. Young NMR tube was charged with (DCPP)Pd(C_2H_4) (8.0 mg, 0.014 mmol), cyclohexyl bromide (8.63 μL, 0.0700 mmol), and 0.500 mL of THF. The NMR tube was then exported from the box, freeze-pump-thawed once, and pressurized to 750 Torr of CO. The resulting white suspension was shaken by hand until a homogeneous, colorless solution was obtained (ca. 30 s). The NMR tube was warmed to 80 °C for 40 min to obtain a yellow solution, cooled to room temperature, and analyzed by ^{31}P NMR spectroscopy (Figure 3.1).

Figure 3.1. ^{31}P NMR spectrum of the reaction between $(DCPP)Pd(CO)_2$ and cyclohexyl bromide.

31P NMR (162 MHz, THF) δ 19.06 (d, *J* = 74.0 Hz), -3.48 (d, *J* = 73.6 Hz).

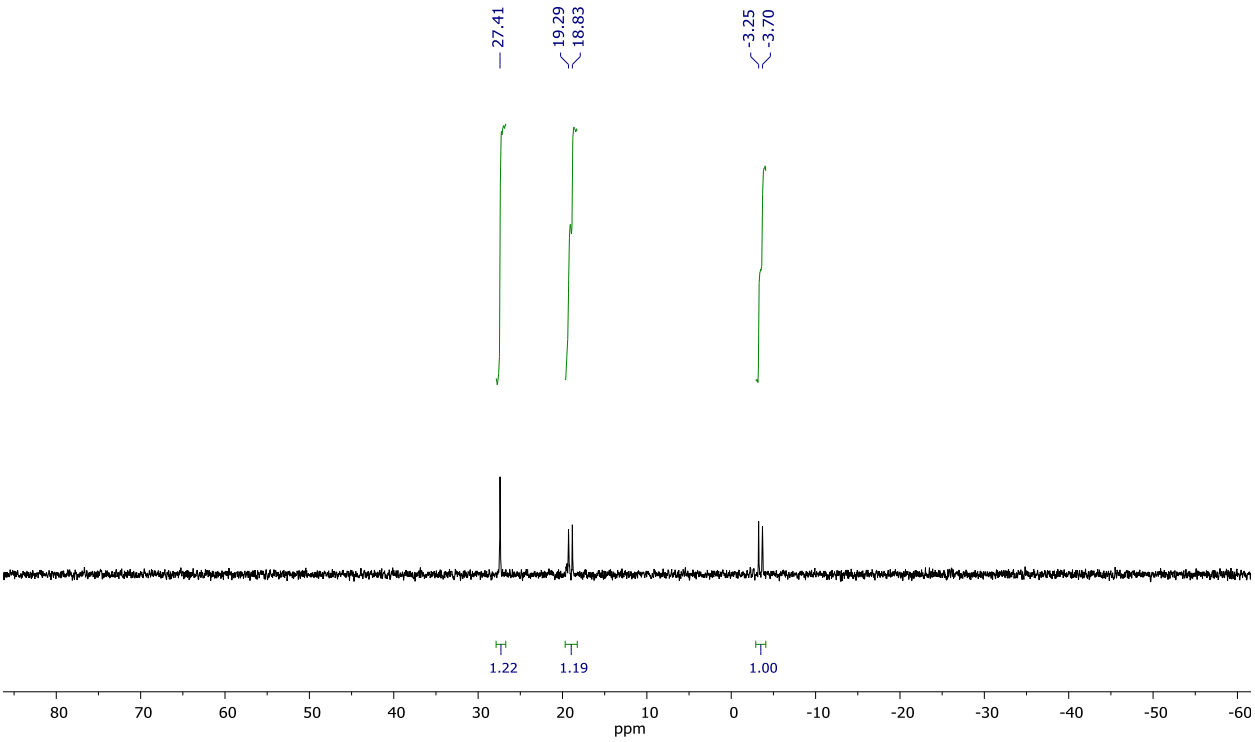

3.5 References

1. Barnard, C. F. J., Palladium-catalyzed carbonylation - A reaction come of age. *Organometallics* **2008,** *27*, 5402-5422.
2. Sumino, S.; Fusano, A.; Fukuyama, T.; Ryu, I., Carbonylation Reactions of Alkyl Iodides through the Interplay of Carbon Radicals and Pd Catalysts. *Acc. Chem. Res.* **2014,** *47*, 1563-1574.
3. Sargent, B. T.; Alexanian, E. J., Palladium-Catalyzed Alkoxycarbonylation of Unactivated Secondary Alkyl Bromides at Low Pressure. *J. Am. Chem. Soc.* **2016,** *138*, 7520-7523.
4. (a) Sargent, B. T.; Alexanian, E. J., Cobalt-Catalyzed Aminocarbonylation of Alkyl Tosylates: Stereospecific Synthesis of Amides. *Angew. Chem. Int. Ed.* **2019,** *58*, 9533-9536; (b) Sargent, B. T.; Alexanian, E. J., Cobalt-Catalyzed Carbonylative Cross-Coupling of Alkyl Tosylates and Dienes: Stereospecific Synthesis of Dienones at Low Pressure. *J. Am. Chem. Soc.* **2017,** *139*, 12438-12440.
5. Choi, J.; Martín-Gago, P.; Fu, G. C., Stereoconvergent Arylations and Alkenylations of Unactivated Alkyl Electrophiles: Catalytic Enantioselective Synthesis of Secondary Sulfonamides and Sulfones. *J. Am. Chem. Soc.* **2014,** *136*, 12161-12165.
6. Wang, J. Y.; Strom, A. E.; Hartwig, J. F., Mechanistic Studies of Palladium-Catalyzed Aminocarbonylation of Aryl Chlorides with Carbon Monoxide and Ammonia. *J. Am. Chem. Soc.* **2018,** *140*, 7979-7993.
7. Luo, Y.-R., *Handbook of Bond Dissociation Energies in Organic Compounds*. CRC Press: 2003; p 380.
8. (a) Wei, C. S.; Davies, G. H. M.; Soltani, O.; Albrecht, J.; Gao, Q.; Pathirana, C.; Hsiao, Y.; Tummala, S.; Eastgate, M. D., The Impact of Palladium(II) Reduction Pathways on the Structure and Activity of Palladium(0) Catalysts. *Angew. Chem. Int. Ed.* **2013,** *52*, 5822-5826; (b) Grushin, V. V.; Alper, H., Alkali-induced disproportionation of palladium(II) tertiary phosphine complexes, $[L_2PdCl_2]$, to LO and palladium(90). Key intermediates in the biphasic carbonylation of ArX catalyzed by $[L_2PdCl_2]$. *Organometallics* **1993,** *12*, 1890-1901.
9. Senn, H. M.; Ziegler, T., Oxidative Addition of Aryl Halides to Palladium(0) Complexes: A Density-Functional Study Including Solvation. *Organometallics* **2004,** *23*, 2980-2988.
10. Hasanayn, F.; Nsouli, N. H.; Al-Ayoubi, A.; Goldman, A. S., Addition of Alkyl Radicals to Transition-Metal-Coordinated CO: Calculation of the Reaction of [Ru(CO)5] and Related Complexes and Relevance to Alkane Carbonylation. *J. Am. Chem. Soc.* **2008,** *130*, 511-521.
11. Miloserdov, F. M.; McMullin, C. L.; Belmonte, M. M.; Benet-Buchholz, J.; Bakhmutov, V. I.; Macgregor, S. A.; Grushin, V. V., The challenge of palladium-catalyzed aromatic azidocarbonylation: From mechanistic and catalyst deactivation studies to a highly efficient process. *Organometallics* **2014,** *33*, 736-752.
12. Barry, J. T.; Berg, D. J.; Tyler, D. R., Radical Cage Effects: The Prediction of Radical Cage Pair Recombination Efficiencies Using Microviscosity Across a Range of Solvent Types. *J. Am. Chem. Soc.* **2017,** *139*, 14399-14405.

CHAPTER 4

SYNTHESIS AND REACTIVITY STUDIES OF ARYLNICKEL(II) AMIDO COMPLEXES

4.1 Introduction

Studies of the synthesis and reactivity of arylpalladium(II) amido complexes have elucidated mechanistic steps in the formation of arylamines in Pd-catalyzed C-N coupling reactions. As a result of these studies, the reductive eliminations of arylamines from these arylpalladium(II) amido complexes were directly observed, and the most widely accepted mechanisms for Pd-catalyzed C-N coupling reactions occur through an arylpalladium(II) amido intermediate.[2, 6] Moreover, kinetic studies of the reductive elimination of arylamines from arylpalladium(II) amido complexes have revealed that the electronic effects of both the aryl and amido groups largely control the rate of arylamine formation, wherein reductive elimination to produce arylamines from these compounds is facilitated by electron poor aryl groups and electron rich amido groups.[4, 6, 24f] Additional mechanistic studies on arylpalladium(II) amido complexes have revealed the origin of the selectivity for mono- versus polyarylation of ammonia, which was deduced from the relative stabilities of arylpalladium amido complexes bearing unsubstituted and aryl substituted amido groups.[24d] In turn, these mechanistic data have allowed for the rational selection of a catalyst system or reaction conditions for a given C-N coupling reaction.[4]

In contrast, the synthesis of arylnickel(II) amido complexes relevant to C-N coupling reactions have not been reported, even though these types of nickel complexes have been proposed as intermediates in these coupling reactions.[18, 22b] Although there is debate as to whether the arylnickel(II) amido species directly reductively eliminates arylamine or undergoes oxidation to an arylnickel(III) amido species prior to reductive elimination of arylamine,[18] these claims have not been experimentally tested, and the catalytic competency of arylnickel amido complexes in C-N coupling reactions has not been demonstrated. Thus, mechanistic studies on arylnickel(II) amido complexes can guide efforts to further the development of Ni-catalyzed C-N coupling reactions, which are more attractive than their Pd-catalyzed analogues because nickel is less expensive and more abundant than palladium.[1b] Herein, we describe the synthesis and reactivity of two arylnickel(II) amido complexes ligated by TMEDA or DPPF. These complexes display differing propensities to undergo reductive elimination in the presence and absence of an added oxidant. These studies set the stage for further studies on the synthesis and reactivity of arylnickel amido complexes.

4.2 Results and Discussion

The synthesis of TMEDA-ligated arylnickel(II) amido complexes was pursued at the outset of this study because TMEDA-ligated arylnickel(II) bromide complexes can be readily synthesized by the reaction of $Ni(COD)_2$ with a wide array of bromoarenes in the presence of TMEDA.[106] Thus, a library of arylnickel(II) halide complexes can be generated from these TMEDA-ligated complexes containing aryl groups with varying electronic and steric properties. Inspired by analogous studies on arylpalladium(II) amido complexes, we hypothesized that these TMEDA-ligated arylnickel(II) halide complexes could be converted into their corresponding arylnickel(II) amido complex by a reaction with an amide salt or with an amine and a base.[24b, 24d, 24f, 28] Substitution of TMEDA from these amido complexes with ligands used in Ni-catalyzed C-N coupling reactions would create a diverse collection of arylnickel(II)amido species (Scheme 4.1).

Scheme 4.1. Planned synthetic route for the synthesis of arylnickel(II) amido complexes.

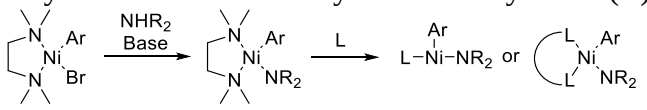

Scheme 4.2. Synthesis of TMEDA-ligated arylnickel(II) amido complex **2**.

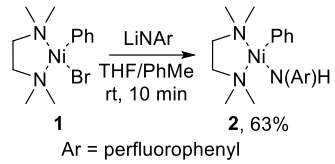

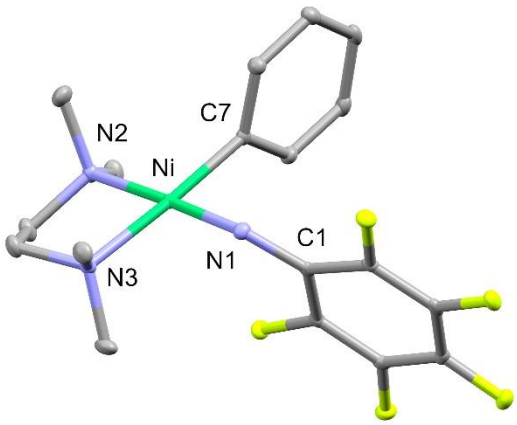

Figure 4.1. Solid-state structure of arylnickel(II) amido compound **2**. Thermal ellipsoids are set to the 30% probability level. Selected bond lengths (Å): N1-Ni 1.8842(12), N2-Ni 1.9748(12), N3-Ni 2.0549(12), and C7-Ni 1.8861(14). Selected bond angles (°): N1-Ni-C7 88.16(6), C7-Ni-N2 94.46(5), N1-Ni-N3 91.16(5), N2-Ni-N3 86.23(5), and C1-N1-Ni 127.01(10).

We postulated that the reactivity of arylnickel(II) amido complexes is similar to that of arylpalladium(II) amido complexes. Our group and others have demonstrated that arylpalladium(II) amido complexes bearing electron poor amido groups undergo reductive elimination more slowly than those with electron rich amido groups.[24f] We aimed to exploit this electronic effect to synthesize an arylnickel(II) amido compound that would be stable at room temperature (Scheme 4.1). Thus, the installation of a perfluorophenylamido group was chosen for this reaction because of the electron withdrawing property of the perfluorophenyl group. TMEDA-ligated phenylnickel(II) amido complex **2** was synthesized in 62% yield by the reaction of arylnickel(II) bromide complex **1** with lithium perfluorophenylamide to yield a diamagnetic arylnickel(II) amido species that was stable at room temperature (Scheme 4.2). This amido complex was crystallized by diffusion of pentane into a concentrated solution of **2** in THF and toluene, and its solid-state structure was determined by X-ray crystallography. Complex **2** is square planar, consistent with a low-spin Ni(II) complex (Figure 4.1).

The ability of amido complex **2** to undergo reductive elimination of arylamine was examined. The reaction of amido complex **2** at 80 °C for 1 h in the presence of PPh_3 fully consumed **2** and Ni black formed. However, no diarylamine product was observed by ^{19}F NMR spectroscopy of the crude reaction mixture (Scheme 4.3a). In contrast, the reaction of nickel complex **2** with 1 or 2 equiv of Ag(OTf) gave the diarylamine product and a black particulate, which likely contains a mixture of silver and nickel (Scheme 4.3b). Based on the mass balance measured by ^{19}F NMR

spectroscopy, the arylamine product formed in 96% and 70% yield from the reactions with 1 and 2 equiv of AgOTf, respectively. Because the yield of the arylamine product is higher from the reaction with 1 equiv of AgOTf, and both reactions with 1 or 2 equiv of AgOTf produce diarylamine in high yield, reductive elimination of arylamine from amido complex **2** in the presence of an oxidant likely occurs from a Ni(III) species, rather than at a Ni(IV) complex. The lower yield of diarylamine from the reaction with 2 equiv of AgOTf may be due to unproductive side reactions caused by consumption of the diarylamine product by excess AgOTf. The reductive elimination of alkylamine from an alkyl(II) amido complex has been reported to occur in higher yield in the presence of oxidants at room temperature than in the absence of oxidant at a more elevated temperature.[107]

Scheme 4.3. Reactivity of nickel amido complex **2**.

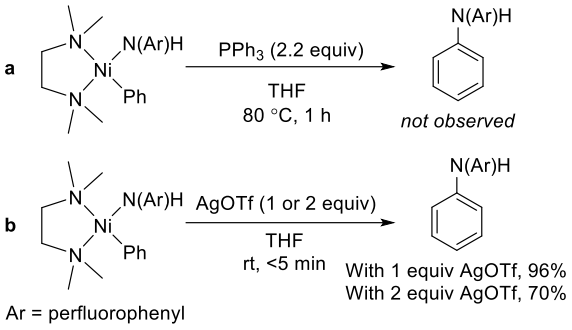

We attempted to synthesize derivatives of complex **2** bearing a series of bidentate L_2-type ligands. However, reaction of complex **2** with a suite of bisphosphine ligands did not yield any of the products from substitution of the TMEDA by bisphosphines. By ^{19}F NMR spectroscopy, the nickel amido complex remained (Scheme 4.4). Because complex **2** did not undergo these substitution reactions, we attempted to synthesize arylnickel(II) bromide complexes containing diamine ligands possessing more steric hinderance or larger bite angles than that of TMEDA. We posited that the steric hinderance or the larger bite angle of ligands **4**-**6** would make the resulting arylnickel(II) amido complex more susceptible to ligand substitution reactions than TMEDA-ligated complex **2**. However, reactions with $Ni(COD)_2$ and bromobenzene in the presence of these ligands did not furnish the desired arylnickel(II) complexes (Scheme 4.5). The ^1H NMR spectra of the crude reactions with these diamine ligands gave broad resonances, consistent with the formation of paramagnetic Ni species.

Scheme 4.4. Attempted synthesis of derivatives of amido complex **2** by ligand substitution reactions.

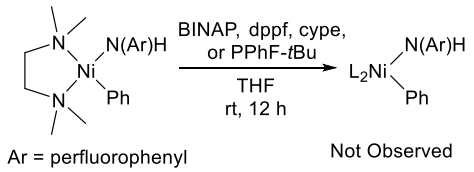

Scheme 4.5. Attempted synthesis of derivatives of TMEDA complex **2**.

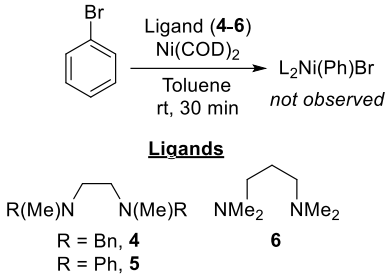

Scheme 4.6. Synthesis of DPPF-ligated nickel amido complex **7**.

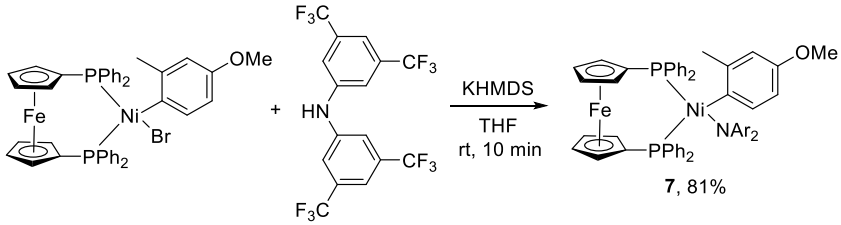

Because the substitution of TMEDA with a bisphosphine ligand from amido complex **7** did not occur, we synthesized bisphosphine-ligated amido complexes through another route. DPPF-ligated nickel amido complexes were pursued because of their proposed relevance to Ni-catalyzed amination reactions of aryl chlorides.[15] Arylnickel(II) complex **7** was synthesized by allowing (DPPF)Ni(2-methyl-4-methoxyphenyl)Br to react with KHMDS and bis(3,5-ditrifluoromethylphenyl)amine to yield arylnickel(II)amido complex **7** in 81% yield (Scheme 4.6). DPPF-ligated amido complex **7**, like TMEDA-ligated amido complex **2**, is diamagnetic and stable at room temperature. Due to this thermal stability, nickel complex **7** was crystallized by the slow diffusion of pentane into a concentrated solution of **7** in THF, and the solid-state structure was obtained by X-ray crystallography (Figure 4.2). The structure of **7** is square planar and is consistent with an arylnickel(II) amido complex.

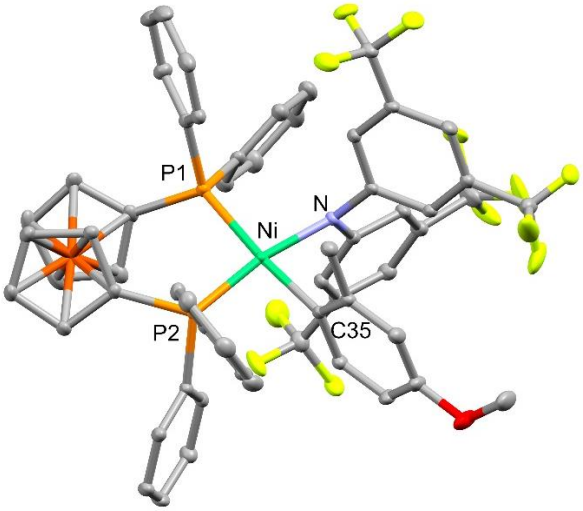

Figure 4.2. Solid state structure of DPPF-ligated amido complex **7**. Thermal ellipsoids are set to the 30% probability level. Selected bond lengths(Å): Ni-C35 1.949(2), Ni-N 1.9591(17), Ni-P2

2.1985(6), and Ni-P1 2.3149(6). Selected bond angles(°): C(35)-Ni1-N1 85.46(8), C35-Ni-P2 84.46(6), N-Ni-P1 87.36(5), and P2-Ni-P1 102.65(2).

We attempted to synthesize DPPF-ligated arylnickel(II) amido complexes with more electron rich amido ligands than that found in **7** by the method outlined in Scheme 4.6. Reaction of KHMDS with (DPPF)Ni(2-methyl-4-methoxyphenyl)Br and *p*-fluoroaniline in THF (Scheme 4.7) led to the immediate formation of a red solution followed by the formation of Ni black within 30 s at room temperature. Analysis of the crude reaction mixture by ^{31}P NMR spectroscopy did not reveal any resonances corresponding to an arylnickel(II) amido complex. However, GC/MS analysis of the crude reaction mixture revealed an ion signal consistent with the molecular ion of the diarylamine product. The same reaction with di-*p*-tolylamine in place of *p*-fluoroaniline led to the immediate formation of nickel black (Scheme 4.8). A ^{31}P NMR spectrum of the crude reaction also did not contain any resonances consistent with the formation of an arylnickel amido species. The triarylamine product that would result from reductive elimination was not observed by GC/MS analysis of the crude reaction mixture, and the primary nitrogen containing compound according to this analysis was di-*p*-tolylamine. We propose that the nickel amido complexes that result from the reactions in Schemes 4.7 and 4.8 are more temperature sensitive than amido complex **7**. Further studies on the synthesis of DPPF-ligated amido complexes involve the synthesis and characterization of these nickel complexes at low temperature to avoid decomposition at ambient temperature.

Scheme 4.7. Attempted Synthesis of DPPF ligated amido complexes with *p*-fluoroaniline.

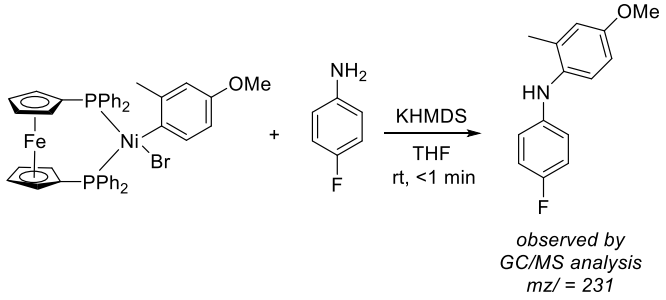

Scheme 4.8. Attempted Synthesis of DPPF ligated amido complexes with di-*p*-tolylamine.

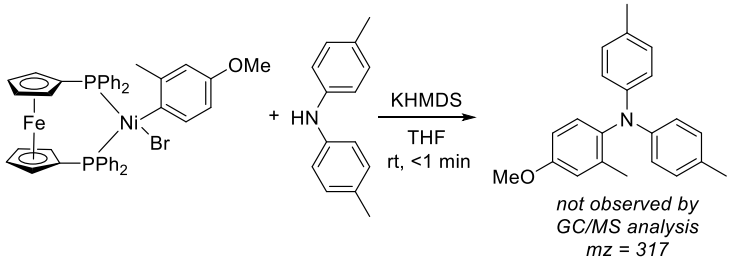

Scheme 4.8. Reaction of amido complex **7** in benzene at 65 °C.

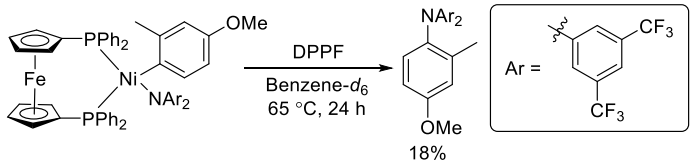

Scheme 4.9. Oxidation of amido complex **7** in THF at room temperature.

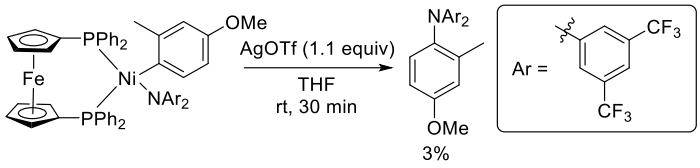

Reductive elimination of arylamine from nickel complex **7** was studied. NMR spectroscopic analysis of the reaction of **7** in the presence of PPh_3 at 65 °C in benzene-d_6 for 35 min revealed that **7** did not undergo reaction, and after 24 h at this temperature, the complete consumption of complex **7** was observed by ^{31}P and ^{19}F NMR spectroscopy to give a complex mixture of fluorine containing compounds (Scheme 4.8). Based on the ^{19}F NMR spectrum of the crude reaction, the desired triarylamine product was generated in 18% yield. This yield was estimated by integration of the resonance corresponding to the triarylamine product divided by the total integration of fluorine containing compounds. Thus, the arylnickel(II) amido complex **7** undergoes multiple reactions upon heating to give several organic products, and the product obtained from reductive elimination of arylamine from **7** is a minor pathway.

Reaction of bis(3,5-ditrifluoromethylphenyl)amine and 4-fluoro-chlorobenzene catalyzed by the combination of $Ni(COD)_2$ and DPPF did not give the desired triarylamine product by ^{19}F NMR spectroscopic analysis of the crude reaction (Scheme 4.10). Presumably, this catalytic reaction generates an arylnickel(II) amido complex with the same amido ligand as complex **7**, and as a consequence, these two amido complexes likely have similar reactivities. Thus, we hypothesize that the low yields of triarylamine in the catalytic (Scheme 4.9) and stoichiometric reactions (Schemes 4.7 and 4.8) are due to the high barrier for reductive elimination to form the C-N bond from arylnickel(II) amido complexes containing the same amido ligand as complex **7**. A structurally analogous DPPF-ligated arylpalladium(II) complex bearing the same amido group as complex **7** was synthesized by our group and was found to not undergo reductive elimination upon heating.[28]

Scheme 4.10. Attempted Ni-catalyzed C-N coupling reaction with bis(3,5-ditrifluoromethylphenyl)amine.

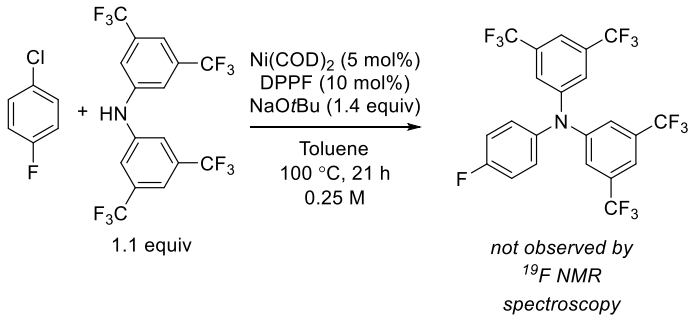

Unlike TMEDA-ligated amido complex **2**, DPPF-ligated amido species **7** does not undergo reductive elimination to produce the triarylamine by reaction with AgOTf cleanly. When complex **7** was allowed to react with 1.1 equiv of AgOTf at room temperature for 30 min, amido complex **7** underwent 70% conversion to give the desired triarylamine product in just 3% yield. (Scheme 4.9). The disparities in the reactions of amido complexes **2** and **7** (Scheme 4.11) may arise from

differences caused by N,N- versus P,P- ancillary ligands, monoarylamido versus diarylamido ligands, and electron neutral versus electron rich aryl ligands. Future efforts involving the reactivity of DPPF-ligated arylnickel(II) amido species will entail the synthesis of complexes containing aryl and amido groups possessing differing electronic and steric properties. The reductive elimination of arylamine from these compounds will be studied to determine if arylamine is produced in higher yield from an arylnickel(II) amido species or by an arylnickel(III) amido intermediate.

Scheme 4.11. Summary of reactivity of amido complexes **2** and **7**.

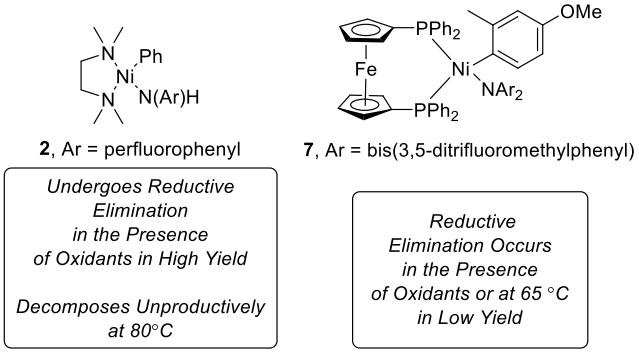

4.3 Conclusion and Future Directions

In summary, two arylnickel(II) amido complexes were synthesized and their abilities to generate aryl amine by reductive elimination was evaluated. TMEDA-ligated amido complex **2** does not undergo reductive elimination to furnish the desired diarylamine product upon heating, but in the presence of 1 equiv of AgOTf as oxidant, the desired diarylamine product was generated in 96% yield. In contrast, DPPF-ligated amido complex **7** undergoes reaction at 65 °C to produce the desired triarylamine product, but in a low yield of 18% and with several other unidentified fluorine containing compounds. We propose that these Ni compounds do not undergo reductive elimination entirely or cleanly upon heating, due to the highly electron withdrawing substituents of the amido groups contained in these complexes. Future studies will entail the synthesis and the study of the reactivity of a library of arylnickel(II) amido complexes with varying electronic properties at the aryl and amido groups by the methods outlined in this chapter. We showed that TMEDA-ligated amido complex **2** undergoes facile reductive elimination in the presence of 1 equiv of oxidant, which implies that reductive elimination to give aryl amine occurs at a Ni(III) intermediate. However, this observation cannot be applied to all arylnickel amido complexes, as DPPF-ligated amido complex **7** does not undergo reductive elimination to give arylamine in high yield in the presence of oxidant. Thus, additional studies will involve the reaction of amido complexes with oxidants with the aim of identifying differences or similarities in reactivity involving arylnickel amido complexes ligated by bidentate, N,N- and P,P-ligands which are used in Ni-catalyzed C-N coupling reactions. Moreover, the viability of forming a Ni(III) amido species in the context of a Ni-catalyzed C-N coupling reaction will be assessed.

4.4 Experimental

General Experimental Procedures

All manipulations were conducted under a nitrogen atmosphere in a glovebox or on a Schlenk manifold unless otherwise stated. All glassware was dried in an oven at 140 °C for at least

14 h prior to use. ^{1}H, ^{19}F, and ^{31}P NMR spectra were recorded on a Bruker 400, 500, or 6009 MHz spectrometer. All ^{1}H chemical shifts are reported in parts per million relative to tetramethylsilane or residual protiated solvent as a reference, ^{31}P NMR chemical shifts are reported in parts per million relative to an 85% H_3PO_4 external standard and all ^{19}F NMR chemical shifts are reported in parts per million relative to a $CFCl_3$ external standard. X-ray crystal structures were obtained at the Small Molecule X-ray Crystallography Facility at the University of California, Berkeley. (TMEDA)Ni(Ph)Br (**1**),[106] (DPPF)Ni(2-methyl-4-methoxyphenyl)Br,[108] diamine ligand **5**,[109] and bis(3,5-ditrifluoromethylphenyl)amine[28] were synthesized according to previously reported procedures. All deuterated NMR solvents were purchased from Cambridge Isotope Labs, freeze-pump-thawed thrice, and stored over 4Å molecular sieves for 24 h before use. All other reagents were purchased from commercial sources and used as received.

Synthesis of Lithium Perfluorophenylamide

A 20 mL vial was charged with perfluoroaniline (1.19 g, 6.50 mmol), LiHMDS (1.20 g, 7.15 mmol), 8 mL of toluene, and a Teflon-coated stir bar. The reaction mixture was stirred for 30 min to obtain a white suspension. The precipitated solids were collected on a fritted glass funnel and washed with pentane (4 x 15 mL) and dried under vacuum to obtain the title compound as a white powder (984 mg, 80%), which was soluble in THF and diethyl ether.

^{1}H NMR (400 MHz, THF-d_8) δ 2.78 (br. s, 1H).

^{19}F NMR (376 MHz, THF-d_8) δ -173.3 (m), -173.7 (br. s).

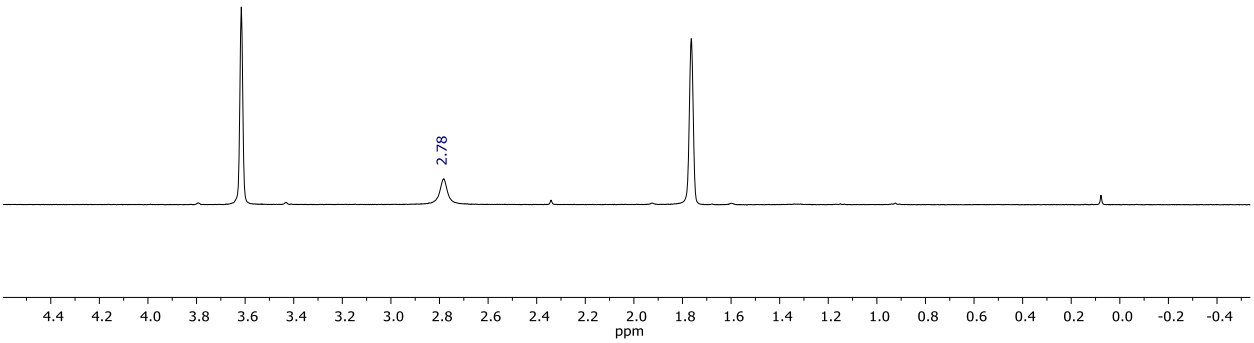

Figure 4.3. ^{1}H NMR spectrum of lithium perfluorophenylamide.

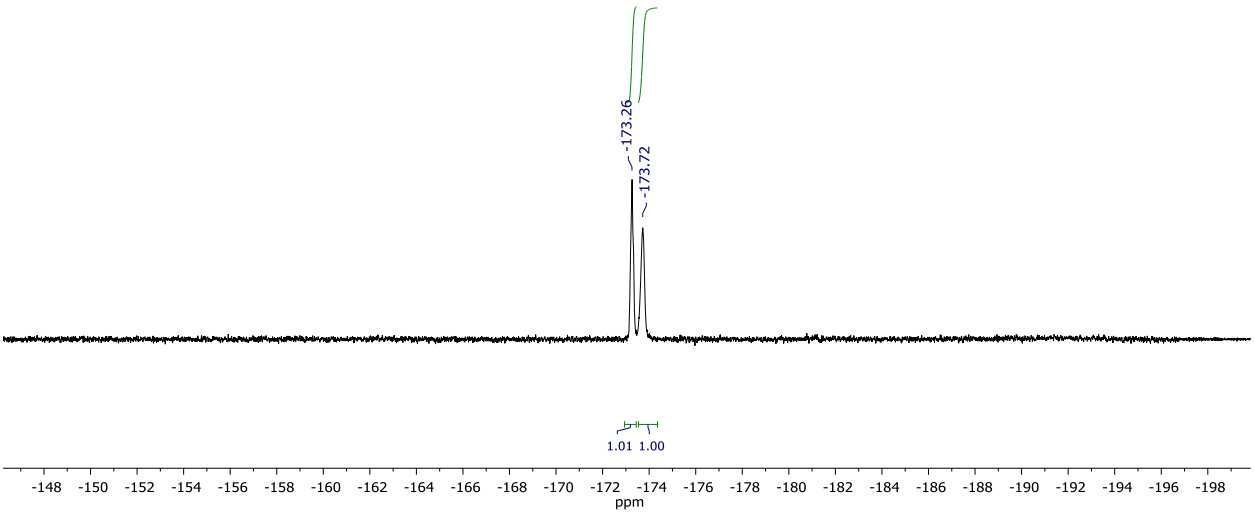

Figure 4.4. ^{19}F NMR spectrum of lithium perfluorophenylamide.

*Synthesis of Nickel Amido Complex **2***

A 20 mL vial was charged with (TMEDA)Ni(Ph)Br (**1**) (75.0 mg, 0.226 mmol), lithium perfluorophenylamide (44.9 mg, 0.237 mmol), 3 mL of toluene, 0.5 mL of THF, and a Teflon-coated stir bar. The reaction mixture was stirred for 10 min at room temperature and concentrated under vacuum to remove THF. The resulting mixture was filtered through a syringe filter, and the filtrate was layered with ca. 6 mL of pentane and cooled to -35 °C for 14 h to obtain dark orange solids of the title compound (62 mg, 63%). Crystals suitable for X-ray crystallographic analysis were grown by slow diffusion of pentane into a concentrated solution of **2** in a 1:2 v/v solution of THF and toluene, respectively, at -35 °C.

^{1}H NMR (400 MHz, THF-d_8) δ 7.48 (d, J = 6.4 Hz, 2H), 6.62 (t, J = 7.5 Hz, 2H), 6.49 (t, J = 7.2 Hz, 1H), 2.47 – 2.42 (m, 8H), 2.41 – 2.37 (m, 2H), 2.18 (s, 6H). ^{19}F NMR (376 MHz, THF-d_8) δ -165.2 (br. s), -171.1 (t, J = 23.1 Hz), -189.9 (tt, J = 23.0, 13.5 Hz).

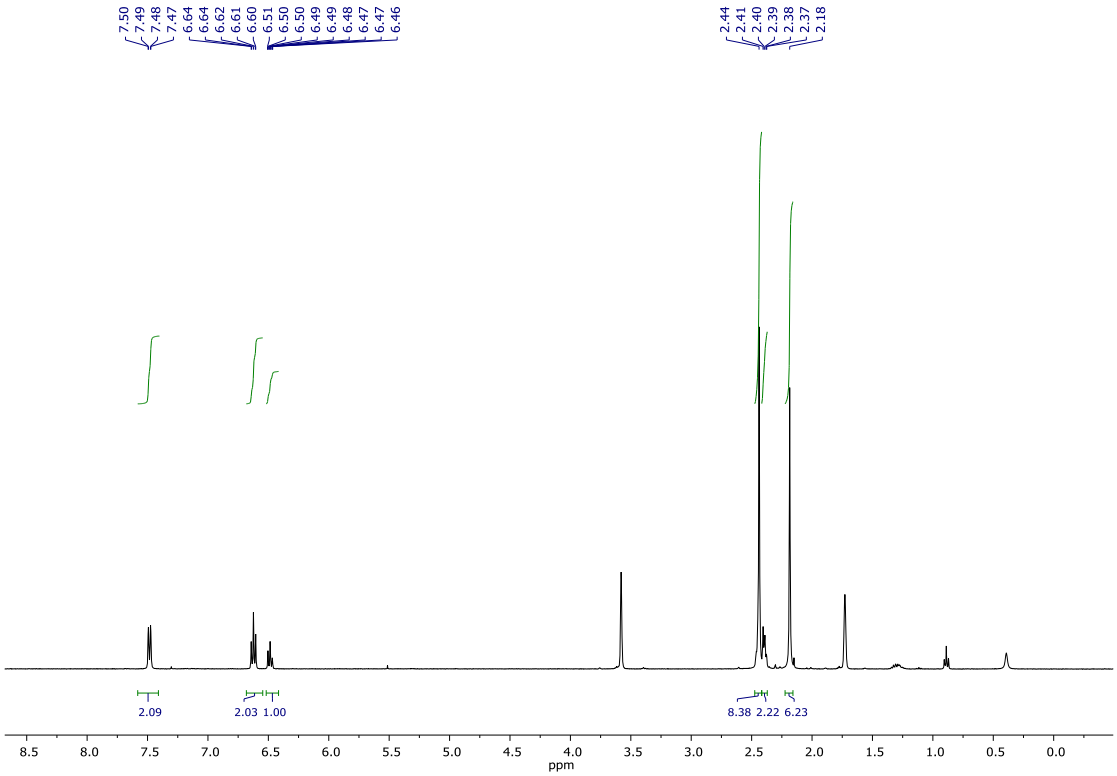

Figure 4.5. ^{1}H NMR spectrum of amido complex 2.

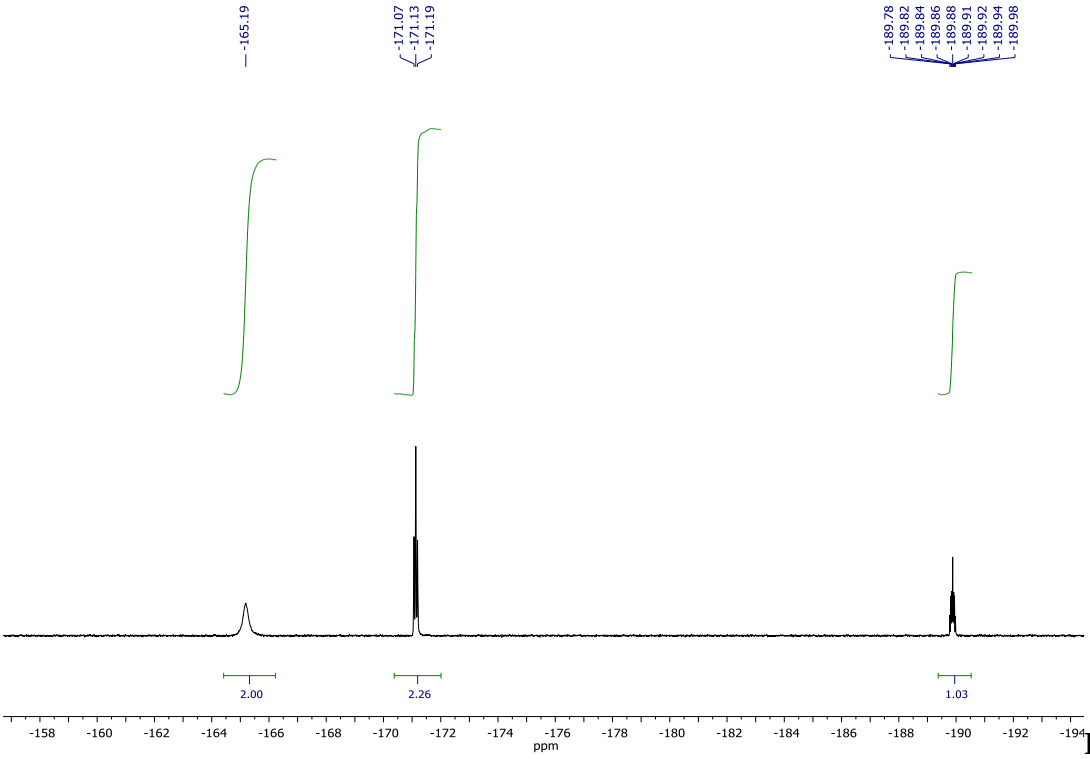

Figure 4.6. ^{19}F NMR spectrum of amido complex 2.

*Reaction of Amido Complex **2** at 50-80 °C*

A J. Young NMR tube was charged with (TMEDA)Ni(Ph)Br (**1**) (15.0 mg, 0.0452 mmol), lithium perfluorophenylamide (9.0 mg, 0.0475 mmol), and 0.600 mL THF-d_8. The reaction mixture was left to sit at room temperature, and complete conversion of starting materials to amido complex **2** was observed by NMR spectroscopy. PPh_3 (26.1 mg, 0.0994 mmol) was weighed into the J. Young NMR tube and the reaction mixture was warmed to 50 °C for 23 min, then to 65 °C for 25 min, and 80 °C for 1 h. The reaction was monitored by ^{31}P and ^{19}F NMR spectroscopy at each of those time and temperature intervals. No reaction was observed at 50 °C after 23 min. At 65 °C after 25 min, a few resonances were observed in the ^{19}F NMR spectrum but the amido complex **2** primarily remained unreacted (> 90% remained as **1** based on mass balance in the ^{19}F NMR spectrum). At 80 °C after 1 h, Ni black was obtained and the ^{19}F NMR spectrum contained a multitude of peaks, none of which were consistent with the ^{19}F NMR chemical shift of the desired diarylamine product (Figure 4.7). The expected diarylamine product has ^{19}F NMR shifts at (376 MHz, THF-d_8) δ -150.0 (d, J = 20.1 Hz), -165.5 (td, J = 21.9, 5.3 Hz), and -167.1 (t, J = 21.6 Hz). These chemical shifts in THF-d_8 were determined by the independent synthesis of 2,3,4,5,6-pentafluoro-N-phenylbenzenamine according to previously reported procedures.[110]

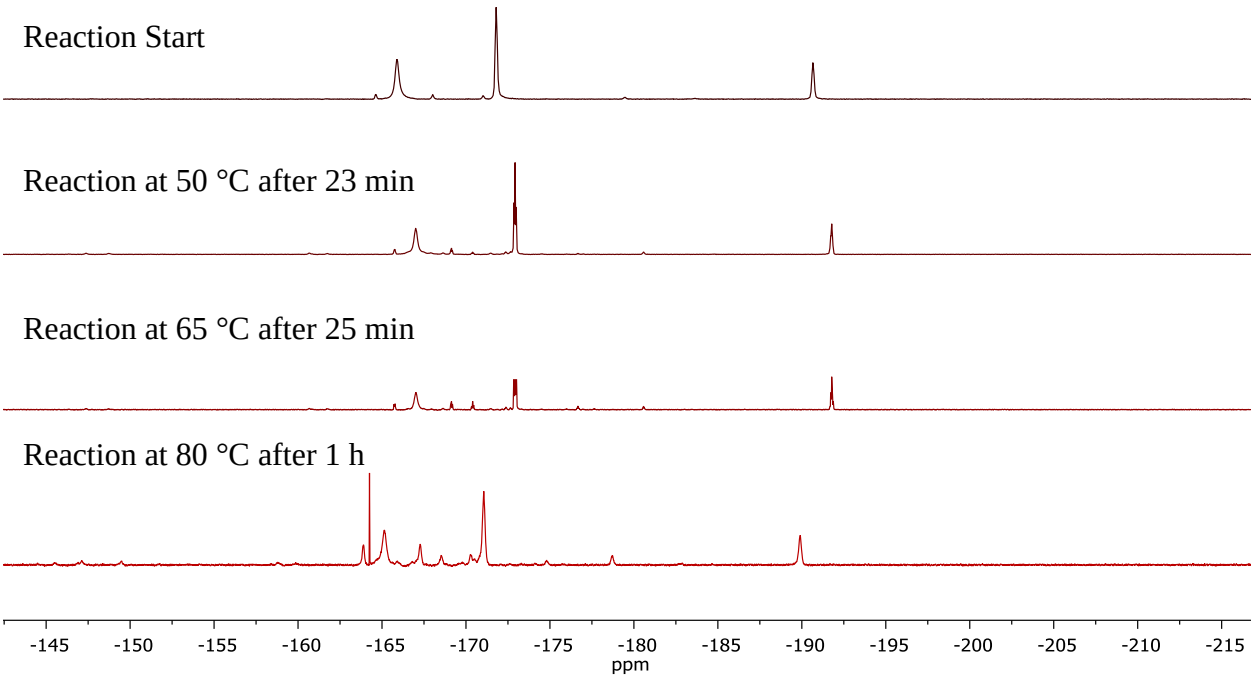

Figure 4.7. ^{19}F NMR spectra of the reaction of amido complex 1 in the presence of PPh_3.

*Oxidation of Amido Complex **2***

A 4 mL vial was charged with amido complex **2** (15.0 mg, 0.0346 mmol), AgOTf (8.9 mg, 0.0346 mmol or 17.8 mg, 0.0692 mmol), and 1 mL of THF. The vial was capped with a Teflon-lined cap and the contents were gently shaken for ca. 10 s to obtain a grey suspension. The reaction mixture was filtered to obtain an orange solution from the reaction with 1 equiv of AgOTf and a yellow solution from the reaction with 2 equiv of AgOTf. These crude reaction mixtures were analyzed by NMR spectroscopy (Figure 4.8). The desired diarylamine product was observed in both reactions by ^{19}F NMR spectroscopy.

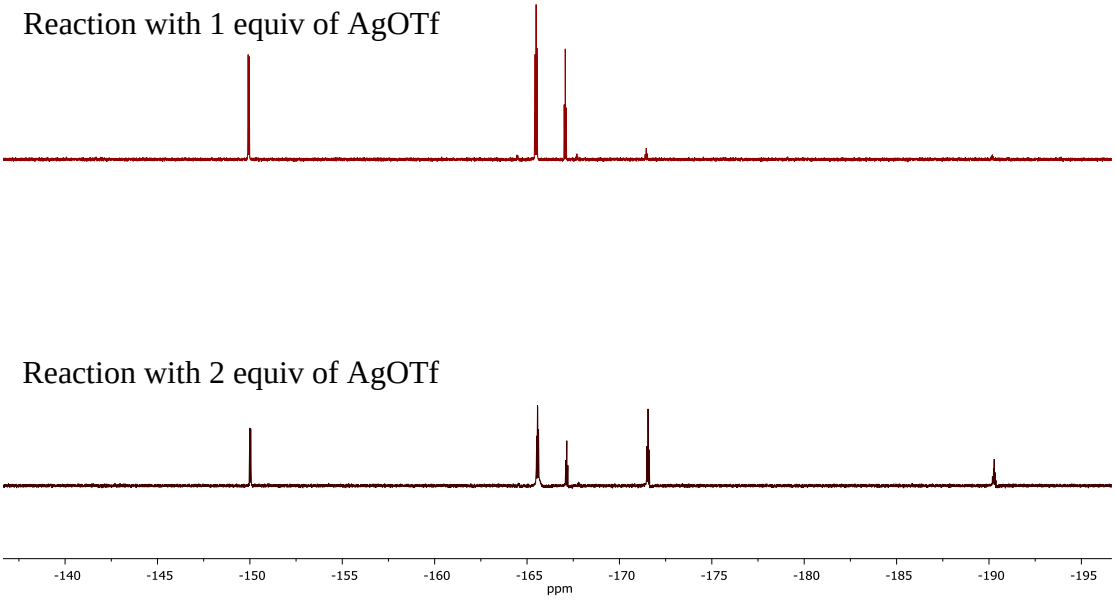

Figure 4.8. Oxidation of amido complex **2** with 1 or 2 equiv of AgOTf.

*Attempted Ligand Substitution Reactions with Amido Complex **2***

In a representative experiment, a 20 mL vial was charged with amido complex **2** (22.9 mg, 0.0527 mmol), bisphosphine ligand (0.0543 mmol), a Teflon-coated stir bar, and ca. 3 mL of THF. The reaction mixture was stirred for 12 h at room temperature, and the outcome of the reaction was assessed by ^{31}P and ^{19}F NMR spectroscopy. In all cases, only starting material was observed.

*Synthesis of Diamine Ligand **4***

The following procedure was adapted from a previously reported procedure.[111] A 25 mL round-bottom flask was charged with *N*,*N*′-dibenzylethylenediamine (2.26 mL, 11.75 mmol), formaldehyde (9.4 mL, 37% in H_2O), and a Teflon-coated stir bar. The reaction mixture was stirred at room temperature and formic acid (4.4 mL, 117 mmol) was added dropwise. The reaction mixture was refluxed for 16 h, cooled to room temperature, and concentrated by rotary evaporation. The crude reaction mixture was diluted with 50 mL of aqueous 2 M NaOH solution, and this mixture was extracted with chloroform (4 x 50 mL). The organic fractions were combined, washed with 100 mL of brine, dried with $MgSO_4$, filtered, and concentrated by rotary evaporation. The crude mixture was purified by automated column chromatography with a 0-30% gradient of EtOAc in hexanes. The title compound was obtained as a colorless liquid (1.58 g, 50%). The ^{1}H NMR spectrum of diamine **4** was consistent with those reported in the literature.[112]

^{1}H NMR (300 MHz, Chloroform-*d*) δ 7.49 – 7.11 (m, 10H), 3.55 (s, 4H), 2.61 (s, 4H), 2.25 (s, 6H).

*Reactions of Diamine Ligands **4**-**6** with Ni(COD)$_2$ and Bromobenzene.*

A 20 mL vial was charged with ligand (1.05 mmol), Ni(COD)$_2$ (275 mg, 1.00 mmol), 3 mL of toluene, and a Teflon-coated stir bar. Bromobenzene (157 µL) was then added to the resulting suspension with stirring at room temperature. After 10-30 min, Ni black or a Ni mirror formed. The ^{1}H NMR spectra of the filtered reaction mixture gave broad resonances consistent with the formation of paramagnetic species.

*Synthesis of Nickel Amido Complex **7***

A 20 mL vial was charged with (DPPF)Ni(2-methyl-4-methoxyphenyl)Br (130.8 mg, 0.1607 mmol), bis(3,5-ditrifluoromethylphenyl)amine (72.3 mg, 0.164 mmol), and ca. 3 mL of THF. KHMDS (32.7 mg, 0.164 mmol) was weighed into the resulting orange solution to immediately obtain a red solution, which was shaken briefly by hand (ca. 10 s) and left to sit at room temperature for 15 min. The reaction mixture was filtered through a glass pipette plugged with a glass fiber filter paper pad and layered with ca. 6 mL of pentane. The biphasic solution was then cooled to -35 °C for 14 h to obtain red cubes suitable for X-ray crystallographic analysis. The mother liquor was removed, and the solids were washed with pentane (3 x 4 mL) and dried under vacuum to obtain the title compound as a red powder (155.2 mg, 81%). Complex **7** was isolated as a solvate containing pentane and THF, and these residual solvent molecules could not be removed by extended dying under vacuum.

^{1}H NMR (400 MHz, Benzene-d_6) δ 9.32 – 8.44 (broad multiplet, 5H), 8.16 (br. s, 2H), 7.44 (t, *J* = 7.0 Hz, 3H), 7.35 – 7.26 (m, 6H), 7.25 – 7.12 (m, 3H), 6.95 (s, 1H), 6.87-6.73 (m, 3H), 6.72 – 6.64 (m, 5H), 6.00 (d, *J* = 8.3 Hz, 1H), 5.97 (s, 1H), 5.39 (s, 1H), 4.65 (s, 1H), 3.96 (s, 1H), 3.76 (s, 1H), 3.69 (d, *J* = 9.2 Hz, 2H), 3.20 (s, 3H), 1.66 (s, 3H). ^{31}P NMR (162 MHz, Benzene-d_6) δ 13.58 (d, *J* = 21.7 Hz), 12.67 (d, *J* = 21.5 Hz). ^{19}F NMR (376 MHz, Benzene-d_6) δ -62.5 (br. s), -62.6 (s).

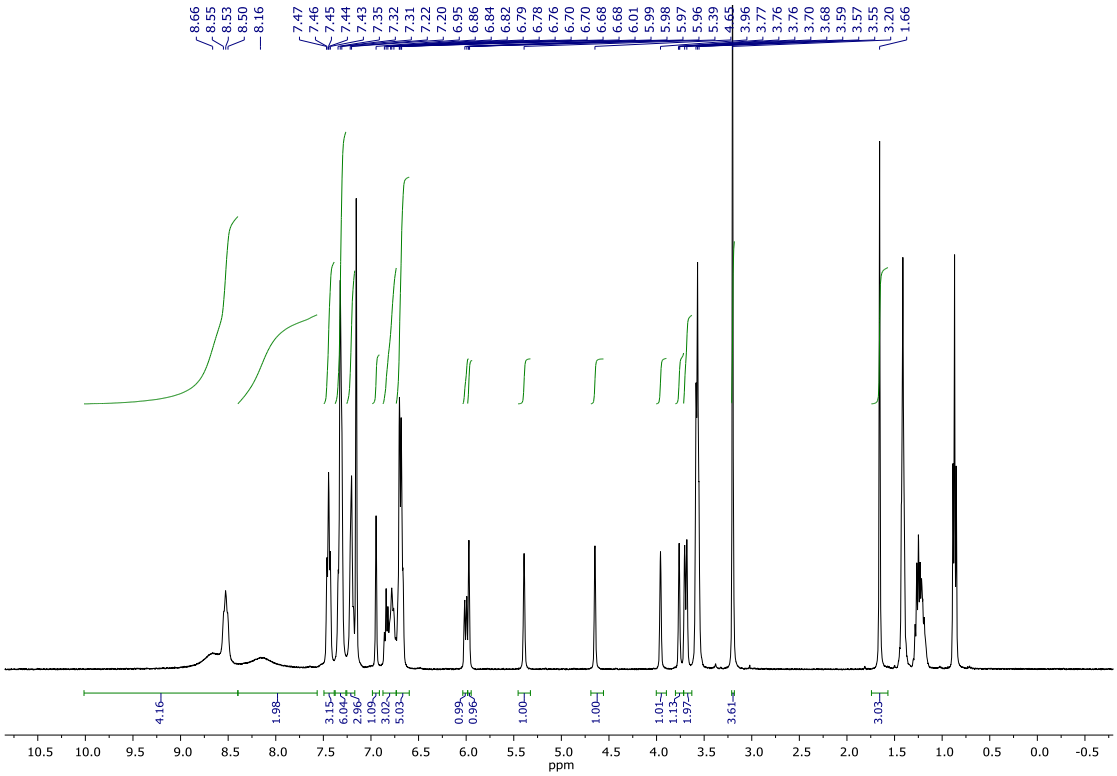

Figure 4.9. ^{1}H NMR spectrum of amido complex 7.

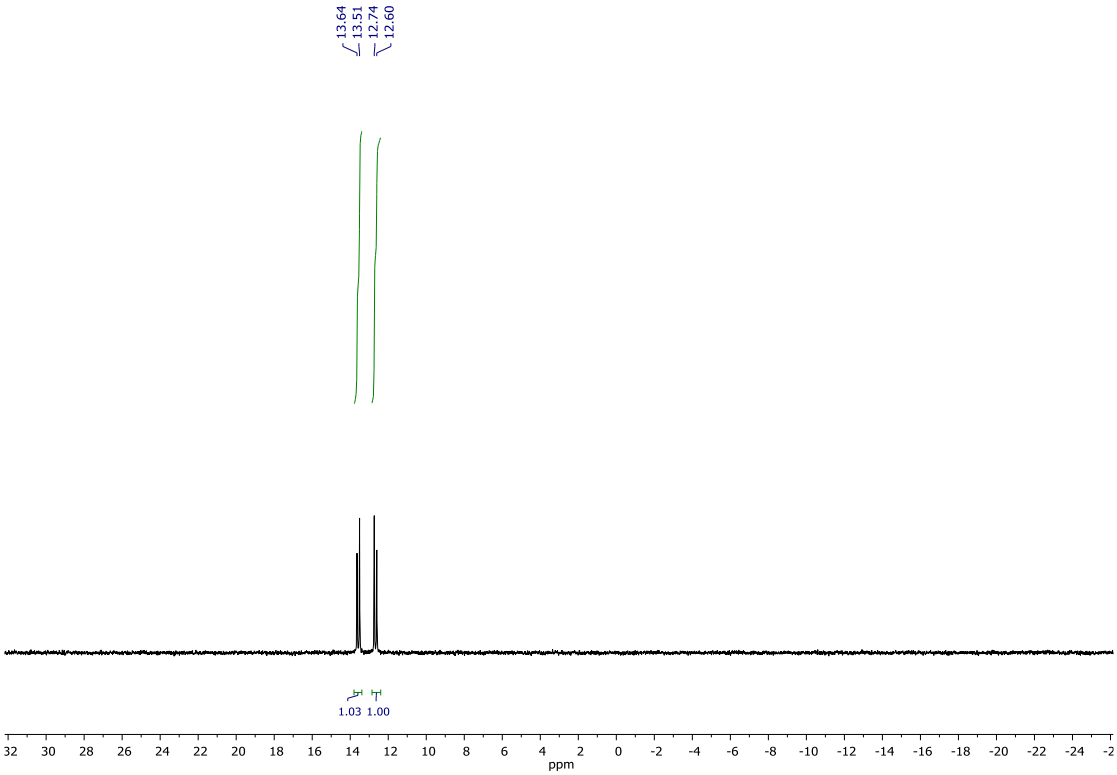

Figure 4.10. ^{31}P NMR spectrum of amido complex 7.

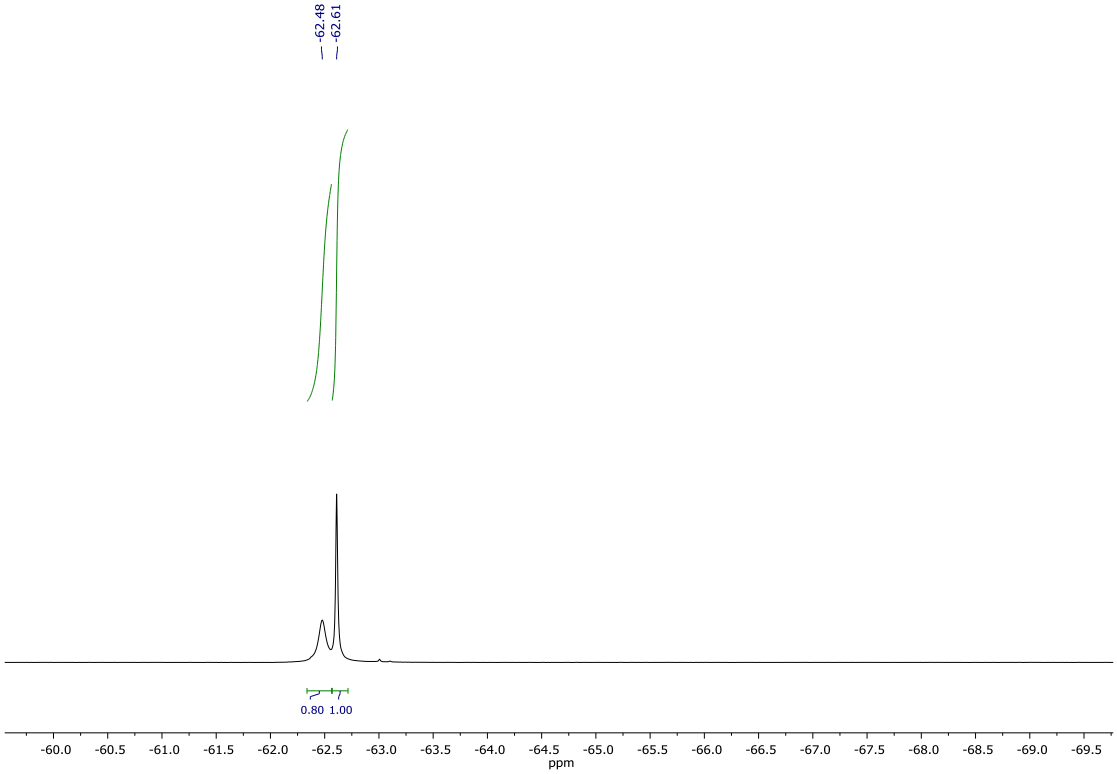

Figure 4.11 ^{19}F NMR spectrum of amido complex 7.

Independent Synthesis of N,N-bis(3,5-bis(trifluoromethyl)phenyl)-4-methoxy-2-methylaniline

A 20 mL vial was charged with 4-methoxyl-2-methylaniline (469 µL, 3.65 mmol), 3,5-ditrifluoromethyl-4-bromobenzene (1.57 mL, 9.13 mmol), $Pd(dba)_2$ (104.9 mg, 0.183 mmol), P*t*Bu_3 (73.8 mg, 0.365 mmol), a Teflon-coated stir bar, 5 mL of toluene, and 3 mL of THF. Then, NaO*t*Bu (878 mg, 9.13 mmol) was weighed directly into the reaction mixture, which was stirred at room temperature for 10 min and then warmed to 100 °C with stirring for 17.5 h. The reaction mixture was transferred into a separatory funnel along with 20 mL of water. The organic layer was diluted with 15 mL of EtOAc, and the aqueous layer was separated from this biphasic solution. The organic layer was washed with brine (20 mL) and water (20 mL), dried with $MgSO_4$, filtered, and concentrated by rotary evaporation until a red-orange solid was obtained. The title compound was obtained as an off-white solid (1.11 g, 54%) after column chromatography of the crude reaction in hexanes. Anal. Calculated for $C_{59}H_{46}F_{12}FeNiNOP_2$: C, 59.58; H, 3.90, N, 1.18. Found: C, 59.31, H, 3.74, N 0.98.

^{1}H NMR (400 MHz, Chloroform-*d*) δ 7.48 (s, 2H), 7.37 (s, 4H), 7.06 (d, *J* = 8.5 Hz, 1H), 6.89 (d, *J* = 2.9 Hz, 1H), 6.86 (dd, *J* = 8.5, 3.0 Hz, 1H), 3.87 (s, 3H), 2.03 (s, 3H).

^{19}F NMR (376 MHz, Chloroform-*d*) δ -62.5.

^{19}F NMR (376 MHz, Benzene-d_6) δ -62.1.

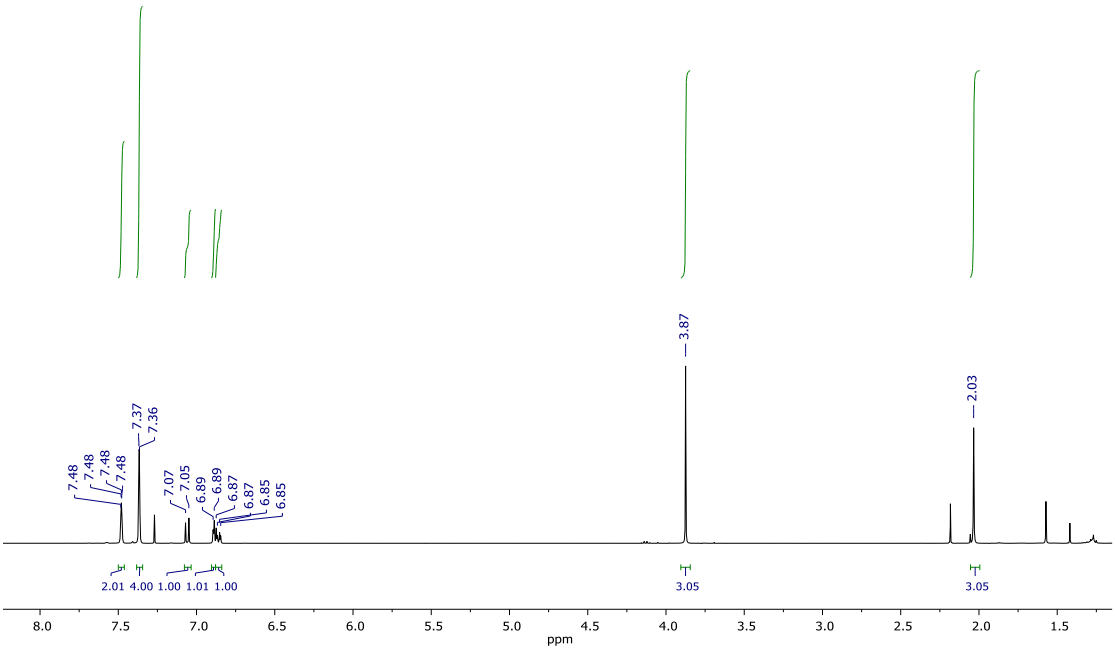

Figure 4.12 ^{1}H NMR spectrum of amido complex of N,N-bis(3,5-bis(trifluoromethyl)phenyl)-4-methoxy-2-methylaniline.

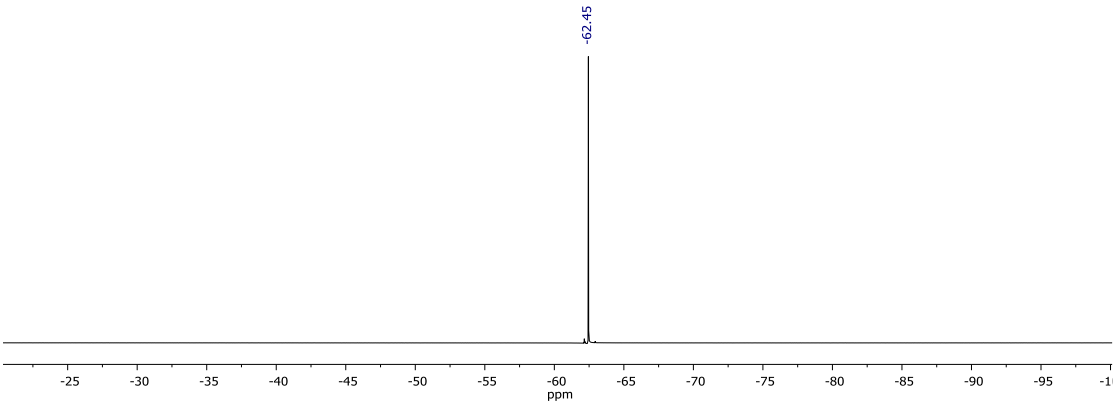

Figure 4.13 ^{19}F NMR spectrum of amido complex of N,N-bis(3,5-bis(trifluoromethyl)phenyl)-4-methoxy-2-methylaniline.

*Reaction of amido complex **7** at 65 °C*

A J. Young NMR tube was charged with amido complex **7** (15.0 mg, 0.0126 mmol), DPPF (10.0 mg, 0.0180 mmol), and 600 µL of benzene-d_6. The resulting red solution was warmed to 65 °C for 35 min and NMR spectra were obtained of the reaction mixture, which only revealed resonances corresponding to amido complex **7**. The NMR tube was then warmed to 65 °C for 24 h to obtain a dark red suspension. A ^{19}F NMR spectrum of the crude reaction (Figure 4.14) revealed the formation of *N*,*N*-bis(3,5-bis(trifluoromethyl)phenyl)-4-methoxy-2-methylaniline in 18% yield based on mass balance.

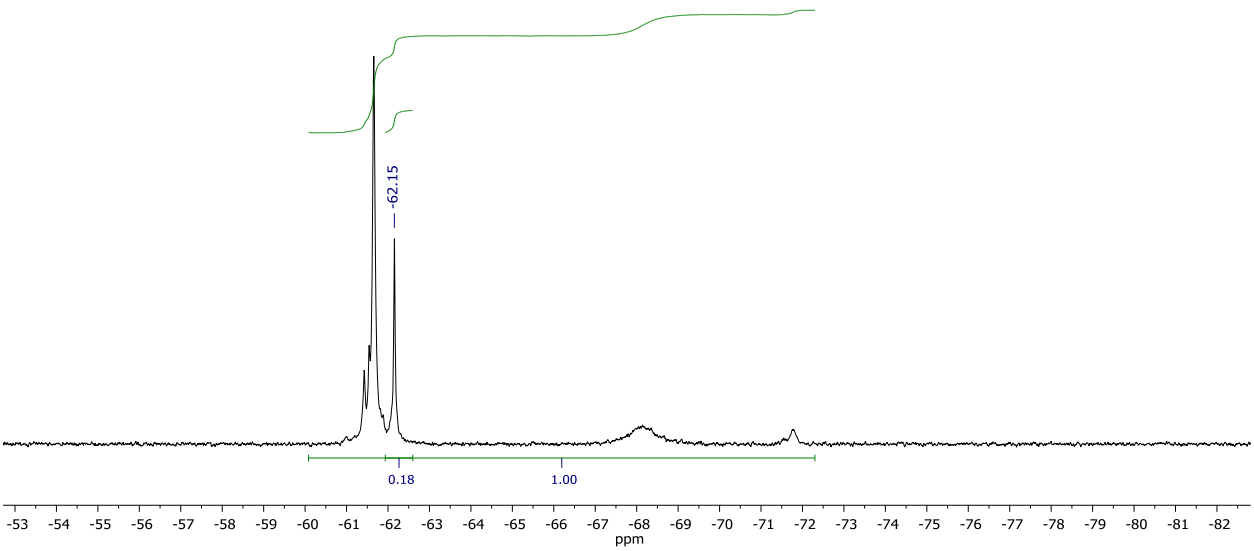

Figure 4.14. ^{19}F NMR spectrum of the reaction of amido complex 7 at 65 °C for 24 h.

*Oxidation of Amido Complex **7***

A 4 mL vial was charged with amido complex **7** (30.0 mg, 0.0252 mmol), AgOTf (7.1 mg, 0.027 mmol), and 1 mL of THF. The resulting brown suspension was shaken by hand for 1 minute and the suspension was left to sit at room temperature for 30 min. The reaction mixture was filtered through a syringe filter, and the filtrate was analyzed by ^{19}F NMR spectroscopy (Figure 4.15). The resonance for the desired amine product in the crude reaction mixture was assigned by spiking the reaction mixture with authentic amine product.

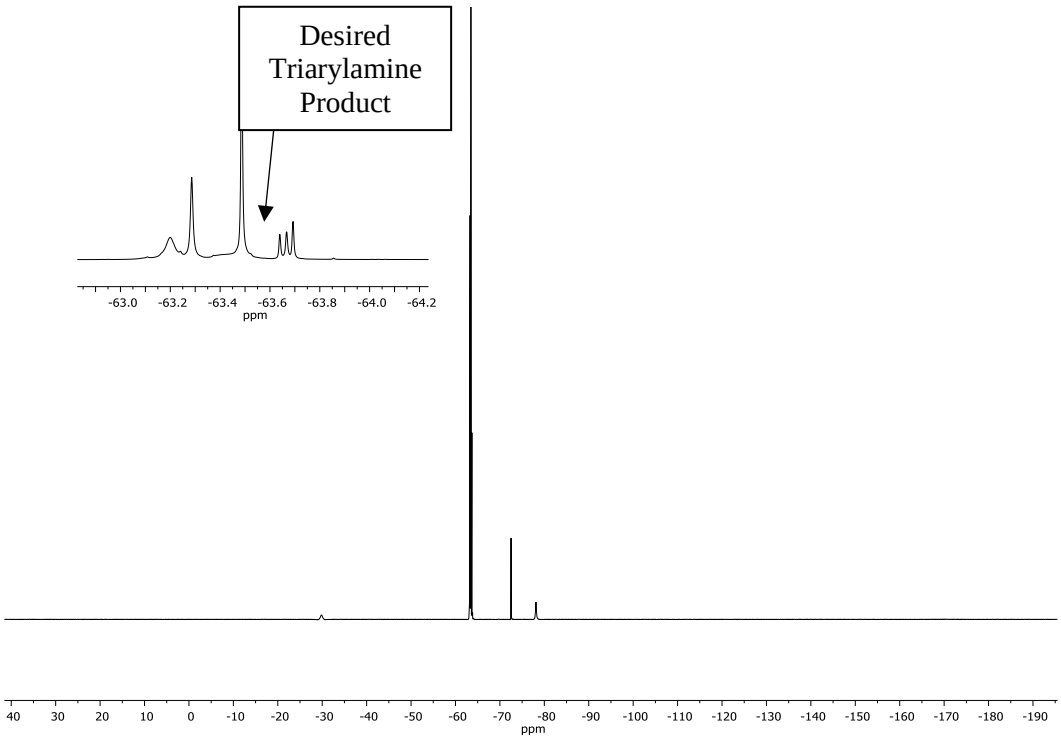

Figure 4.15. ^{19}F NMR spectrum of the oxidation of amido complex 7 with AgOTf.

Attempted Synthesis of DPPF-ligated Nickel Amido Complex with Di-p-tolylamine

A 20 mL vial was charged with (DPPF)Ni(2-methyl-4-methoxyphenyl)Br (30.0 mg, 0.0368 mmol), di-*p*-tolylamine (7.3 mg, 0.037 mmol), and ca. 3 mL of THF. KHMDS (7.4 mg, 0.037 mmol) was weighed into this solution, which was then shaken by hand (ca. 5 s) to obtain a black suspension. Analysis of the crude reaction mixture by ^{31}P NMR spectroscopy only detected the presence of free DPPF.

Attempted Synthesis of DPPF-ligated Nickel Amido Complex with p-fluoroaniline

A 20 mL vial was charged with (DPPF)Ni(2-methyl-4-methoxyphenyl)Br (30.0 mg, 0.0368 mmol), *p*-fluoroaniline (3.49 µL, 0.037 mmol), and ca. 3 mL of THF. KHMDS (7.4 mg, 0.037 mmol) was weighed into this solution, which was then shaken by hand (ca. 5 s) to obtain a red solution which quickly turned black within 30 s at room temperature. Analysis of the crude reaction mixture by GC/MS gave an m/z signal consistent with the molecular ion of N-(4-fluorophenyl)-4-methoxy-2-methylaniline (m/z =231).

X-Ray Crystallographic Data for Amido Complexes

*X-Ray Crystallographic Data for Amido Complex **2**.*

A yellow block 0.39 x 0.24 x 0.18 mm in size was mounted on a Cryoloop with Paratone oil. Data were collected in a nitrogen gas stream at 100(2) K using omega scans. Crystal-to-detector distance was 35 mm and exposure time was 0.50 seconds per frame using a scan width of 0.5°. Data collection was 100% complete to 26.366° in θ. A total of 19753 reflections were collected covering the indices -10<=h<=10, -11<=k<=11, -15<=l<=15. 3752 reflections were founded to be symmetry independent, with an R_{int} of 0.0454. Indexing and unit cell refinement indicated a primitive, triclinic lattice. The space group was found to be P -1 (No. 2). The data were integrated using the CrysAlis^{Pro} 1.171.40.45a software program and scaled using the SCALE3 ABSPACK scaling algorithm. Solution by intrinsic phasing (SHELXT-2015) produced a heavy-atom phasing model consistent with the proposed structure. All non-hydrogen atoms were refined anisotropically by full-matrix least-squares (SHELXL-2014). All hydrogen atoms were placed using a riding model. Their positions were constrained relative to their parent atom using the appropriate HFIX command in SHELXL-2014.

Table 1. Crystal data and structure refinement for amido complex **2**.

Identification code	Wang002_Hartwig	
Empirical formula	C18 H22 F5 N3 Ni	
Formula weight	434.09	
Temperature	100(2) K	
Wavelength	0.71073 Å	
Crystal system	Triclinic	
Space group	P -1	
Unit cell dimensions	a = 8.6178(3) Å	α= 87.958(2)°.
	b = 9.5455(2) Å	β= 70.939(2)°.
	c = 12.4595(3) Å	γ = 72.282(2)°.
Volume	920.47(5) $Å^3$	
Z	2	
Density (calculated)	1.566 Mg/m^3	
Absorption coefficient	1.110 mm^{-1}	
F(000)	448	
Crystal size	0.390 x 0.240 x 0.180 mm^3	
Theta range for data collection	2.881 to 26.366°.	
Index ranges	-10<=h<=10, -11<=k<=11, -15<=l<=15	
Reflections collected	19753	
Independent reflections	3752 [R(int) = 0.0454]	
Completeness to theta = 26.366°	99.8 %	
Absorption correction	Semi-empirical from equivalents	
Max. and min. transmission	1.00000 and 0.68535	
Refinement method	Full-matrix least-squares on F^2	
Data / restraints / parameters	3752 / 0 / 252	
Goodness-of-fit on F^2	1.044	
Final R indices [I>2sigma(I)]	R1 = 0.0237, wR2 = 0.0604	
R indices (all data)	R1 = 0.0250, wR2 = 0.0611	
Extinction coefficient	n/a	
Largest diff. peak and hole	0.326 and -0.216 e.$Å^{-3}$	

Table 2. Atomic coordinates (x 10^4) and equivalent isotropic displacement parameters ($Å^2$x 10^3) for wang002_hartwig. U(eq) is defined as one third of the trace of the orthogonalized U^{ij} tensor.

	x	y	z	U(eq)
C(1)	2650(2)	3705(2)	3364(1)	14(1)
C(2)	1422(2)	5066(2)	3348(1)	15(1)
C(3)	918(2)	6247(2)	4117(1)	16(1)
C(4)	1637(2)	6163(2)	4968(1)	17(1)
C(5)	2855(2)	4856(2)	5020(1)	16(1)
C(6)	3353(2)	3684(2)	4242(1)	14(1)
C(7)	6253(2)	2306(2)	1456(1)	15(1)
C(8)	7131(2)	2987(2)	1934(1)	18(1)
C(9)	7922(2)	3995(2)	1356(1)	22(1)
C(10)	7851(2)	4367(2)	281(1)	23(1)
C(11)	6968(2)	3730(2)	-206(1)	22(1)
C(12)	6184(2)	2724(2)	379(1)	18(1)
C(13)	8776(2)	-549(2)	1935(2)	26(1)
C(14)	7740(2)	-1189(2)	516(1)	27(1)
C(15)	6850(2)	-1999(2)	2440(1)	24(1)
C(16)	5088(2)	-2041(2)	2511(1)	23(1)
C(17)	3245(2)	-295(2)	4141(1)	26(1)
C(18)	2329(2)	-390(2)	2538(1)	22(1)
F(1)	637(1)	5194(1)	2548(1)	19(1)
F(2)	-302(1)	7498(1)	4048(1)	22(1)
F(3)	1122(1)	7304(1)	5747(1)	24(1)
F(4)	3551(1)	4724(1)	5858(1)	21(1)
F(5)	4538(1)	2431(1)	4365(1)	19(1)
N(1)	3048(2)	2519(1)	2648(1)	16(1)
N(2)	7252(2)	-763(1)	1743(1)	16(1)
N(3)	3849(2)	-540(1)	2885(1)	16(1)
Ni(1)	5129(1)	946(1)	2188(1)	12(1)

Table 3. Bond lengths [Å] and angles [°] for wang002_hartwig.

C(1)-N(1)	1.3527(19)
C(1)-C(2)	1.409(2)
C(1)-C(6)	1.4101(19)
C(2)-F(1)	1.3592(16)
C(2)-C(3)	1.372(2)
C(3)-F(2)	1.3510(16)
C(3)-C(4)	1.382(2)
C(4)-F(3)	1.3507(17)
C(4)-C(5)	1.380(2)
C(5)-F(4)	1.3481(16)
C(5)-C(6)	1.375(2)
C(6)-F(5)	1.3573(16)
C(7)-C(12)	1.401(2)
C(7)-C(8)	1.404(2)
C(7)-Ni(1)	1.8861(14)
C(8)-C(9)	1.392(2)
C(8)-H(8)	0.9500
C(9)-C(10)	1.390(2)
C(9)-H(9)	0.9500
C(10)-C(11)	1.387(2)
C(10)-H(10)	0.9500
C(11)-C(12)	1.390(2)
C(11)-H(11)	0.9500
C(12)-H(12)	0.9500
C(13)-N(2)	1.4824(19)
C(13)-H(13A)	0.9800
C(13)-H(13B)	0.9800
C(13)-H(13C)	0.9800
C(14)-N(2)	1.483(2)
C(14)-H(14A)	0.9800
C(14)-H(14B)	0.9800
C(14)-H(14C)	0.9800
C(15)-N(2)	1.4992(19)
C(15)-C(16)	1.504(2)
C(15)-H(15A)	0.9900
C(15)-H(15B)	0.9900
C(16)-N(3)	1.484(2)
C(16)-H(16A)	0.9900
C(16)-H(16B)	0.9900
C(17)-N(3)	1.4814(19)
C(17)-H(17A)	0.9800
C(17)-H(17B)	0.9800
C(17)-H(17C)	0.9800
C(18)-N(3)	1.4751(19)
C(18)-H(18A)	0.9800
C(18)-H(18B)	0.9800
C(18)-H(18C)	0.9800
N(1)-Ni(1)	1.8842(12)
N(1)-H(1)	0.87(2)
N(2)-Ni(1)	1.9748(12)
N(3)-Ni(1)	2.0549(12)
N(1)-C(1)-C(2)	123.48(13)
N(1)-C(1)-C(6)	123.51(13)
C(2)-C(1)-C(6)	112.92(13)
F(1)-C(2)-C(3)	118.06(12)
F(1)-C(2)-C(1)	117.68(13)
C(3)-C(2)-C(1)	124.19(13)
F(2)-C(3)-C(2)	119.84(13)
F(2)-C(3)-C(4)	119.62(13)
C(2)-C(3)-C(4)	120.53(13)
F(3)-C(4)-C(5)	121.13(13)
F(3)-C(4)-C(3)	121.10(13)
C(5)-C(4)-C(3)	117.73(13)
F(4)-C(5)-C(6)	119.55(13)
F(4)-C(5)-C(4)	119.30(13)
C(6)-C(5)-C(4)	121.15(13)
F(5)-C(6)-C(5)	117.34(12)
F(5)-C(6)-C(1)	119.16(13)
C(5)-C(6)-C(1)	123.45(13)
C(12)-C(7)-C(8)	116.24(13)
C(12)-C(7)-Ni(1)	119.43(11)
C(8)-C(7)-Ni(1)	124.30(11)
C(9)-C(8)-C(7)	121.71(14)
C(9)-C(8)-H(8)	119.1
C(7)-C(8)-H(8)	119.1
C(10)-C(9)-C(8)	120.49(14)
C(10)-C(9)-H(9)	119.8
C(8)-C(9)-H(9)	119.8
C(11)-C(10)-C(9)	119.09(14)
C(11)-C(10)-H(10)	120.5
C(9)-C(10)-H(10)	120.5
C(10)-C(11)-C(12)	119.90(14)
C(10)-C(11)-H(11)	120.1
C(12)-C(11)-H(11)	120.1
C(11)-C(12)-C(7)	122.56(14)
C(11)-C(12)-H(12)	118.7
C(7)-C(12)-H(12)	118.7
N(2)-C(13)-H(13A)	109.5
N(2)-C(13)-H(13B)	109.5
H(13A)-C(13)-H(13B)	109.5
N(2)-C(13)-H(13C)	109.5
H(13A)-C(13)-H(13C)	109.5
H(13B)-C(13)-H(13C)	109.5
N(2)-C(14)-H(14A)	109.5
N(2)-C(14)-H(14B)	109.5
H(14A)-C(14)-H(14B)	109.5
N(2)-C(14)-H(14C)	109.5
H(14A)-C(14)-H(14C)	109.5
H(14B)-C(14)-H(14C)	109.5
N(2)-C(15)-C(16)	109.51(12)
N(2)-C(15)-H(15A)	109.8
C(16)-C(15)-H(15A)	109.8
N(2)-C(15)-H(15B)	109.8
C(16)-C(15)-H(15B)	109.8
H(15A)-C(15)-H(15B)	108.2
N(3)-C(16)-C(15)	108.25(12)
N(3)-C(16)-H(16A)	110.0
C(15)-C(16)-H(16A)	110.0
N(3)-C(16)-H(16B)	110.0

C(15)-C(16)-H(16B)	110.0
H(16A)-C(16)-H(16B)	108.4
N(3)-C(17)-H(17A)	109.5
N(3)-C(17)-H(17B)	109.5
H(17A)-C(17)-H(17B)	109.5
N(3)-C(17)-H(17C)	109.5
H(17A)-C(17)-H(17C)	109.5
H(17B)-C(17)-H(17C)	109.5
N(3)-C(18)-H(18A)	109.5
N(3)-C(18)-H(18B)	109.5
H(18A)-C(18)-H(18B)	109.5
N(3)-C(18)-H(18C)	109.5
H(18A)-C(18)-H(18C)	109.5
H(18B)-C(18)-H(18C)	109.5
C(1)-N(1)-Ni(1)	127.01(10)
C(1)-N(1)-H(1)	108.6(13)
Ni(1)-N(1)-H(1)	114.4(13)
C(13)-N(2)-C(14)	107.77(12)
C(13)-N(2)-C(15)	106.72(12)
C(14)-N(2)-C(15)	109.95(12)
C(13)-N(2)-Ni(1)	116.05(10)
C(14)-N(2)-Ni(1)	109.00(9)
C(15)-N(2)-Ni(1)	107.26(9)
C(18)-N(3)-C(17)	107.87(12)
C(18)-N(3)-C(16)	109.12(12)
C(17)-N(3)-C(16)	110.64(12)
C(18)-N(3)-Ni(1)	113.22(9)
C(17)-N(3)-Ni(1)	108.47(9)
C(16)-N(3)-Ni(1)	107.53(9)
N(1)-Ni(1)-C(7)	88.16(6)
N(1)-Ni(1)-N(2)	177.38(5)
C(7)-Ni(1)-N(2)	94.46(5)
N(1)-Ni(1)-N(3)	91.16(5)
C(7)-Ni(1)-N(3)	175.82(5)
N(2)-Ni(1)-N(3)	86.23(5)

Symmetry transformations used to generate equivalent atoms:

Table 4. Anisotropic displacement parameters ($Å^2 x\ 10^3$)for wang002_hartwig. The anisotropic displacement factor exponent takes the form: $-2\pi^2[\ h^2 a^{*2} U^{11} + ... + 2\ h\ k\ a^*\ b^*\ U^{12}\ ]$

	U^{11}	U^{22}	U^{33}	U^{23}	U^{13}	U^{12}
C(1)	10(1)	16(1)	14(1)	3(1)	-3(1)	-6(1)
C(2)	12(1)	19(1)	14(1)	6(1)	-5(1)	-7(1)
C(3)	12(1)	14(1)	20(1)	6(1)	-2(1)	-4(1)
C(4)	16(1)	16(1)	17(1)	-1(1)	-1(1)	-7(1)
C(5)	14(1)	21(1)	13(1)	4(1)	-4(1)	-9(1)
C(6)	11(1)	15(1)	16(1)	5(1)	-4(1)	-3(1)
C(7)	12(1)	13(1)	17(1)	0(1)	-4(1)	-2(1)
C(8)	19(1)	18(1)	18(1)	-1(1)	-6(1)	-6(1)
C(9)	20(1)	18(1)	29(1)	-5(1)	-5(1)	-7(1)
C(10)	20(1)	14(1)	29(1)	2(1)	0(1)	-7(1)
C(11)	22(1)	21(1)	20(1)	6(1)	-5(1)	-5(1)
C(12)	17(1)	20(1)	18(1)	2(1)	-7(1)	-6(1)
C(13)	16(1)	23(1)	42(1)	4(1)	-15(1)	-5(1)
C(14)	27(1)	23(1)	24(1)	-5(1)	-5(1)	-1(1)
C(15)	22(1)	17(1)	34(1)	7(1)	-13(1)	-6(1)
C(16)	23(1)	17(1)	31(1)	6(1)	-11(1)	-8(1)
C(17)	35(1)	32(1)	16(1)	7(1)	-7(1)	-19(1)
C(18)	20(1)	24(1)	29(1)	5(1)	-12(1)	-11(1)
F(1)	17(1)	23(1)	19(1)	5(1)	-11(1)	-3(1)
F(2)	19(1)	15(1)	27(1)	5(1)	-5(1)	0(1)
F(3)	26(1)	19(1)	23(1)	-5(1)	-4(1)	-7(1)
F(4)	22(1)	27(1)	16(1)	1(1)	-9(1)	-9(1)
F(5)	18(1)	18(1)	20(1)	2(1)	-11(1)	0(1)
N(1)	14(1)	18(1)	16(1)	1(1)	-7(1)	-3(1)
N(2)	15(1)	15(1)	21(1)	2(1)	-7(1)	-4(1)
N(3)	16(1)	17(1)	16(1)	3(1)	-7(1)	-7(1)
Ni(1)	11(1)	12(1)	13(1)	2(1)	-5(1)	-4(1)

Table 5. Hydrogen coordinates (x 10^4) and isotropic displacement parameters ($Å^2$x 10^3) for wang002_hartwig.

	x	y	z	U(eq)
H(8)	7187	2753	2671	22
H(9)	8515	4431	1700	27
H(10)	8399	5049	-116	27
H(11)	6900	3980	-937	27
H(12)	5578	2304	35	21
H(13A)	9168	173	1426	39
H(13B)	9707	-1490	1778	39
H(13C)	8461	-187	2728	39
H(14A)	6755	-1344	365	40
H(14B)	8715	-2101	308	40
H(14C)	8073	-401	63	40
H(15A)	6880	-1852	3215	28
H(15B)	7728	-2947	2086	28
H(16A)	5106	-2356	1758	27
H(16B)	4738	-2752	3062	27
H(17A)	4235	-397	4395	39
H(17B)	2676	-1025	4487	39
H(17C)	2425	698	4372	39
H(18A)	1482	584	2813	34
H(18B)	1808	-1156	2864	34
H(18C)	2686	-498	1705	34
H(1)	2600(30)	2800(20)	2114(17)	27(5)

*X-Ray Crystallographic Data for Amido Complex **7.***

A red block 0.25 x 0.22 x 0.10 mm in size was mounted on a Cryoloop with Paratone oil. Data were collected in a nitrogen gas stream at 100(2) K using omega scans. Crystal-to-detector distance was 33.00 mm and exposure time was 15.00 seconds per frame using a scan width of 0.5°. Data collection was 100% complete to 26.372° in θ. A total of 62596 reflections were collected covering the indices -16<=h<=16, -19<=k<=19, -19<=l<=19. 12085 reflections were found to be symmetry independent, with an R_{int} of 0.0504. Indexing and unit cell refinement indicated a primitive, triclinic lattice. The space group was found to be P -1 (No. 2). The data were integrated using the CrysAlis^{Pro} 1.171.40.54a software program and scaled using the SCALE3 ABSPACK scaling algorithm. Solution by intrinsic phasing (SHELXT-2015) produced a heavy-atom phasing model consistent with the proposed structure. All non-hydrogen atoms were refined anisotropically by full-matrix least-squares (SHELXL-2014). All hydrogen atoms were placed using a riding model. Their positions were constrained relative to their parent atom using the appropriate HFIX command in SHELXL-2014. Electron density corresponding to a highly disordered THF molecule was treated using the SQUEEZE function as the second positions could not be found in the electron density map. The presence of the THF molecule is included in the empirical formula, formula weight and density calculated for the structure.

Table 1. Crystal data and structure refinement for JWang004_Hartwig.

Identification code	JWang004_Hartwig	
Empirical formula	C67 H63 F12 Fe N Ni O2 P2	
Formula weight	1318.76	
Temperature	100(2) K	
Wavelength	0.71073 Å	
Crystal system	Triclinic	
Space group	P -1	
Unit cell dimensions	a = 13.3225(4) Å	α= 75.675(2)°.
	b = 15.2669(4) Å	β= 71.512(3)°.
	c = 15.8909(5) Å	γ = 81.460(2)°.
Volume	2961.35(16) Å^3	
Z	2	
Density (calculated)	1.479 Mg/m^3	
Absorption coefficient	0.696 mm^{-1}	
F(000)	1280	
Crystal size	0.250 x 0.220 x 0.100 mm^3	
Theta range for data collection	2.766 to 26.372°.	
Index ranges	-16<=h<=16, -19<=k<=19, -19<=l<=19	
Reflections collected	62596	
Independent reflections	12085 [R(int) = 0.0504]	
Completeness to theta = 26.372°	99.8 %	
Absorption correction	Semi-empirical from equivalents	
Max. and min. transmission	1.00000 and 0.88272	
Refinement method	Full-matrix least-squares on F^2	
Data / restraints / parameters	12085 / 0 / 818	
Goodness-of-fit on F^2	1.032	
Final R indices [I>2sigma(I)]	R1 = 0.0391, wR2 = 0.0998	
R indices (all data)	R1 = 0.0479, wR2 = 0.1044	
Extinction coefficient	n/a	
Largest diff. peak and hole	1.022 and -0.569 e.Å^{-3}	

Table 2. Atomic coordinates (x 10^4) and equivalent isotropic displacement parameters ($Å^2$x 10^3) for jwang004_hartwig. U(eq) is defined as one third of the trace of the orthogonalized U^{ij} tensor.

	x	y	z	U(eq)
Ni(1)	2804(1)	2425(1)	2318(1)	19(1)
Fe(1)	5777(1)	906(1)	2222(1)	25(1)
P(2)	3656(1)	1521(1)	1394(1)	19(1)
P(1)	4032(1)	2508(1)	3045(1)	23(1)
F(5)	3511(1)	6025(1)	626(1)	49(1)
F(6)	3302(1)	6326(1)	1919(1)	45(1)
F(3B)	-1368(13)	6062(10)	2195(13)	49(1)
F(4)	2375(1)	7092(1)	1067(1)	52(1)
N(1)	1827(1)	3211(1)	3075(1)	22(1)
F(8B)	252(7)	121(4)	6176(5)	50(2)
F(10A)	-940(16)	3078(12)	6895(9)	64(4)
F(2B)	-930(20)	5352(18)	1330(30)	77(1)
F(7B)	1169(8)	20(3)	4812(3)	44(2)
F(1A)	-1645(2)	5050(2)	2829(2)	63(1)
O(1)	-1273(2)	2476(1)	1309(2)	65(1)
C(23)	3170(2)	391(1)	1747(2)	22(1)
C(35)	1626(2)	2401(1)	1848(2)	22(1)
C(10)	5066(2)	1200(1)	1222(1)	22(1)
F(12B)	-113(9)	4136(9)	6076(9)	55(2)
C(24)	3399(2)	-173(2)	1126(2)	25(1)
C(43)	1508(2)	4079(1)	2645(2)	22(1)
C(51)	1200(2)	2835(1)	3914(2)	23(1)
C(28)	2674(2)	41(1)	2659(2)	25(1)
C(9)	5882(2)	1806(2)	1025(2)	25(1)
C(29)	3615(2)	1888(1)	210(2)	23(1)
C(36)	858(2)	1774(1)	2337(2)	28(1)
C(45)	192(2)	5160(2)	2124(2)	27(1)
C(6)	5582(2)	297(2)	1284(2)	24(1)
C(17)	4891(2)	3441(2)	2476(2)	27(1)
C(44)	472(2)	4307(1)	2575(2)	24(1)
C(11)	3480(2)	2749(2)	4194(2)	27(1)
C(52)	1317(2)	1895(1)	4263(2)	24(1)
C(58)	488(2)	3350(2)	4513(2)	27(1)
C(30)	4428(2)	2352(2)	-453(2)	27(1)
C(1)	4951(2)	1540(2)	3235(2)	27(1)
C(41)	1407(2)	3063(1)	1137(2)	25(1)
C(7)	6680(2)	355(2)	1132(2)	28(1)
C(12)	3364(2)	2051(2)	4959(2)	34(1)
C(42)	2178(2)	3763(2)	545(2)	28(1)
C(34)	2749(2)	1721(2)	-34(2)	29(1)
C(50)	2239(2)	4737(1)	2237(2)	24(1)
C(26)	2679(2)	-1413(2)	2331(2)	34(1)
C(53)	768(2)	1502(2)	5135(2)	27(1)
C(5)	4668(2)	619(2)	3458(2)	31(1)
C(48)	1947(2)	5586(1)	1781(2)	26(1)
C(25)	3154(2)	-1065(2)	1417(2)	31(1)
C(8)	6866(2)	1278(2)	974(2)	30(1)
C(27)	2431(2)	-858(2)	2952(2)	32(1)
C(37)	-82(2)	1809(2)	2136(2)	36(1)
C(16)	3128(2)	3634(2)	4302(2)	33(1)
C(47)	926(2)	5815(1)	1720(2)	28(1)

C(31)	4390(2)	2646(2)	-1344(2)	34(1)
C(40)	447(2)	3099(2)	935(2)	33(1)
C(18)	4918(2)	3924(2)	1605(2)	29(1)
C(33)	2723(2)	2015(2)	-925(2)	36(1)
C(56)	-57(2)	2942(2)	5384(2)	31(1)
C(38)	-298(2)	2479(2)	1443(2)	39(1)
C(46)	-915(2)	5382(2)	2049(2)	35(1)
C(55)	64(2)	2013(2)	5720(2)	31(1)
C(49)	2780(2)	6256(2)	1349(2)	32(1)
C(22)	5510(2)	3688(2)	2934(2)	35(1)
C(4)	5593(2)	35(2)	3476(2)	41(1)
C(32)	3537(2)	2475(2)	-1580(2)	37(1)
C(54)	976(2)	511(2)	5490(2)	36(1)
C(2)	6067(2)	1500(2)	3123(2)	36(1)
C(13)	2896(2)	2229(2)	5822(2)	43(1)
C(15)	2669(2)	3805(2)	5167(2)	42(1)
C(21)	6146(2)	4403(2)	2520(2)	43(1)
C(19)	5556(2)	4650(2)	1196(2)	37(1)
F(9B)	1902(7)	334(3)	5712(7)	62(3)
C(20)	6164(2)	4882(2)	1661(2)	44(1)
C(3)	6445(2)	570(2)	3272(2)	45(1)
C(14)	2553(2)	3104(2)	5924(2)	45(1)
C(57)	-760(3)	3542(2)	5982(2)	49(1)
C(39)	-1669(2)	3233(2)	830(3)	56(1)
F(11A)	-1755(7)	3627(17)	5942(12)	88(5)
C(60A)	6417(7)	1980(6)	5142(5)	56(2)
C(63A)	5280(70)	4050(50)	6160(50)	111(5)
C(59A)	7523(8)	2202(11)	4455(9)	80(3)
C(62A)	5755(7)	3557(5)	5341(5)	73(2)
C(61A)	6003(7)	2594(5)	5787(5)	70(1)
C(61B)	6575(8)	3093(6)	5152(6)	70(1)
C(60B)	6841(11)	2218(8)	4842(8)	56(2)
C(62B)	5483(9)	3131(7)	5881(6)	73(2)
C(59B)	7938(11)	2251(15)	4138(11)	80(3)
C(63B)	5240(90)	4120(60)	6080(60)	111(5)
F(7A)	1611(8)	90(5)	4922(6)	48(2)
F(9A)	1373(9)	394(3)	6220(8)	58(2)
F(8A)	54(6)	94(5)	5896(8)	41(2)
F(12A)	-447(15)	4283(7)	5940(9)	82(4)
F(10B)	-1264(14)	3172(9)	6763(11)	81(5)
F(11B)	-1437(13)	4125(12)	5572(10)	97(4)
F(1B)	-1484(9)	4667(11)	2416(11)	63(1)
F(2A)	-1060(4)	5088(3)	1368(4)	77(1)
F(3A)	-1184(2)	6283(2)	1881(2)	49(1)

Table 3. Bond lengths [Å] and angles [°] for jwang004_hartwig.

Ni(1)-C(35)	1.949(2)
Ni(1)-N(1)	1.9591(17)
Ni(1)-P(2)	2.1985(6)
Ni(1)-P(1)	2.3149(6)
Fe(1)-C(1)	2.017(2)
Fe(1)-C(10)	2.023(2)
Fe(1)-C(9)	2.030(2)
Fe(1)-C(2)	2.030(2)
Fe(1)-C(6)	2.039(2)
Fe(1)-C(5)	2.040(2)
Fe(1)-C(3)	2.055(2)
Fe(1)-C(8)	2.055(2)
Fe(1)-C(7)	2.062(2)
Fe(1)-C(4)	2.069(3)
P(2)-C(10)	1.820(2)
P(2)-C(23)	1.824(2)
P(2)-C(29)	1.842(2)
P(1)-C(1)	1.803(2)
P(1)-C(17)	1.830(2)
P(1)-C(11)	1.846(2)
F(5)-C(49)	1.336(3)
F(6)-C(49)	1.336(3)
F(3B)-C(46)	1.159(17)
F(4)-C(49)	1.336(3)
N(1)-C(51)	1.365(3)
N(1)-C(43)	1.405(3)
F(8B)-C(54)	1.287(7)
F(10A)-C(57)	1.409(16)
F(2B)-C(46)	1.17(3)
F(7B)-C(54)	1.398(6)
F(1A)-C(46)	1.345(4)
O(1)-C(39)	1.354(4)
O(1)-C(38)	1.382(3)
C(23)-C(28)	1.392(3)
C(23)-C(24)	1.400(3)
C(35)-C(41)	1.392(3)
C(35)-C(36)	1.410(3)
C(10)-C(9)	1.439(3)
C(10)-C(6)	1.442(3)
F(12B)-C(57)	1.404(10)
C(24)-C(25)	1.379(3)
C(24)-H(24)	0.9500
C(43)-C(50)	1.394(3)
C(43)-C(44)	1.406(3)
C(51)-C(52)	1.410(3)
C(51)-C(58)	1.414(3)
C(28)-C(27)	1.387(3)
C(28)-H(28)	0.9500
C(9)-C(8)	1.423(3)
C(9)-H(9)	0.9500
C(29)-C(30)	1.385(3)
C(29)-C(34)	1.401(3)
C(36)-C(37)	1.378(3)
C(36)-H(36)	0.9500
C(45)-C(44)	1.382(3)
C(45)-C(47)	1.393(3)
C(45)-C(46)	1.499(3)
C(6)-C(7)	1.418(3)
C(6)-H(6)	0.9500
C(17)-C(18)	1.389(3)
C(17)-C(22)	1.401(3)
C(44)-H(44)	0.9500
C(11)-C(12)	1.387(4)
C(11)-C(16)	1.396(3)
C(52)-C(53)	1.375(3)
C(52)-H(52)	0.9500
C(58)-C(56)	1.379(3)
C(58)-H(58)	0.9500
C(30)-C(31)	1.390(3)
C(30)-H(30)	0.9500
C(1)-C(2)	1.434(3)
C(1)-C(5)	1.440(3)
C(41)-C(40)	1.404(3)
C(41)-C(42)	1.515(3)
C(7)-C(8)	1.414(3)
C(7)-H(7)	0.9500
C(12)-C(13)	1.391(4)
C(12)-H(12)	0.9500
C(42)-H(42A)	0.9800
C(42)-H(42B)	0.9800
C(42)-H(42C)	0.9800
C(34)-C(33)	1.385(3)
C(34)-H(34)	0.9500
C(50)-C(48)	1.386(3)
C(50)-H(50)	0.9500
C(26)-C(25)	1.388(4)
C(26)-C(27)	1.388(3)
C(26)-H(26)	0.9500
C(53)-C(55)	1.394(3)
C(53)-C(54)	1.496(3)
C(5)-C(4)	1.414(3)
C(5)-H(5)	0.9500
C(48)-C(47)	1.382(3)
C(48)-C(49)	1.502(3)
C(25)-H(25)	0.9500
C(8)-H(8)	0.9500
C(27)-H(27)	0.9500
C(37)-C(38)	1.377(4)
C(37)-H(37)	0.9500
C(16)-C(15)	1.389(4)
C(16)-H(16)	0.9500
C(47)-H(47)	0.9500
C(31)-C(32)	1.381(4)
C(31)-H(31)	0.9500
C(40)-C(38)	1.388(4)
C(40)-H(40)	0.9500
C(18)-C(19)	1.396(3)
C(18)-H(18)	0.9500
C(33)-C(32)	1.379(4)

C(33)-H(33)	0.9500	C(60B)-C(59B)	1.533(13)
C(56)-C(55)	1.391(3)	C(60B)-H(60C)	0.9900
C(56)-C(57)	1.493(3)	C(60B)-H(60D)	0.9900
C(46)-F(1B)	1.326(14)	C(62B)-C(63B)	1.59(10)
C(46)-F(2A)	1.345(5)	C(62B)-H(62C)	0.9900
C(46)-F(3A)	1.350(4)	C(62B)-H(62D)	0.9900
C(55)-H(55)	0.9500	C(59B)-H(59D)	0.9800
C(22)-C(21)	1.383(4)	C(59B)-H(59E)	0.9800
C(22)-H(22)	0.9500	C(59B)-H(59F)	0.9800
C(4)-C(3)	1.405(4)	C(63B)-H(63D)	0.9800
C(4)-H(4)	0.9500	C(63B)-H(63E)	0.9800
C(32)-H(32)	0.9500	C(63B)-H(63F)	0.9800
C(54)-F(7A)	1.258(7)	C(35)-Ni(1)-N(1)	85.46(8)
C(54)-F(9B)	1.359(5)	C(35)-Ni(1)-P(2)	84.46(6)
C(54)-F(8A)	1.362(8)	N(1)-Ni(1)-P(2)	169.88(5)
C(54)-F(9A)	1.383(6)	C(35)-Ni(1)-P(1)	172.29(7)
C(2)-C(3)	1.422(4)	N(1)-Ni(1)-P(1)	87.36(5)
C(2)-H(2)	0.9500	P(2)-Ni(1)-P(1)	102.65(2)
C(13)-C(14)	1.379(4)	C(1)-Fe(1)-C(10)	110.39(8)
C(13)-H(13)	0.9500	C(1)-Fe(1)-C(9)	108.02(9)
C(15)-C(14)	1.383(4)	C(10)-Fe(1)-C(9)	41.61(8)
C(15)-H(15)	0.9500	C(1)-Fe(1)-C(2)	41.51(9)
C(21)-C(20)	1.374(4)	C(10)-Fe(1)-C(2)	140.26(9)
C(21)-H(21)	0.9500	C(9)-Fe(1)-C(2)	110.44(10)
C(19)-C(20)	1.387(4)	C(1)-Fe(1)-C(6)	141.96(9)
C(19)-H(19)	0.9500	C(10)-Fe(1)-C(6)	41.57(8)
C(20)-H(20)	0.9500	C(9)-Fe(1)-C(6)	69.18(9)
C(3)-H(3)	0.9500	C(2)-Fe(1)-C(6)	176.52(9)
C(14)-H(14)	0.9500	C(1)-Fe(1)-C(5)	41.56(9)
C(57)-F(12A)	1.243(11)	C(10)-Fe(1)-C(5)	109.97(9)
C(57)-F(10B)	1.244(14)	C(9)-Fe(1)-C(5)	136.54(9)
C(57)-F(11A)	1.332(9)	C(2)-Fe(1)-C(5)	69.13(11)
C(57)-F(11B)	1.371(8)	C(6)-Fe(1)-C(5)	113.65(9)
C(39)-H(39A)	0.9800	C(1)-Fe(1)-C(3)	68.94(10)
C(39)-H(39B)	0.9800	C(10)-Fe(1)-C(3)	177.41(11)
C(39)-H(39C)	0.9800	C(9)-Fe(1)-C(3)	140.94(11)
C(60A)-C(61A)	1.483(11)	C(2)-Fe(1)-C(3)	40.74(11)
C(60A)-C(59A)	1.556(10)	C(6)-Fe(1)-C(3)	137.64(10)
C(60A)-H(60A)	0.9900	C(5)-Fe(1)-C(3)	67.79(11)
C(60A)-H(60B)	0.9900	C(1)-Fe(1)-C(8)	135.19(9)
C(63A)-C(62A)	1.57(8)	C(10)-Fe(1)-C(8)	69.31(9)
C(63A)-H(63A)	0.9800	C(9)-Fe(1)-C(8)	40.77(9)
C(63A)-H(63B)	0.9800	C(2)-Fe(1)-C(8)	109.10(10)
C(63A)-H(63C)	0.9800	C(6)-Fe(1)-C(8)	68.24(9)
C(59A)-H(59A)	0.9800	C(5)-Fe(1)-C(8)	176.52(9)
C(59A)-H(59B)	0.9800	C(3)-Fe(1)-C(8)	113.01(11)
C(59A)-H(59C)	0.9800	C(1)-Fe(1)-C(7)	175.36(10)
C(62A)-C(61A)	1.504(10)	C(10)-Fe(1)-C(7)	69.18(8)
C(62A)-H(62A)	0.9900	C(9)-Fe(1)-C(7)	68.43(9)
C(62A)-H(62B)	0.9900	C(2)-Fe(1)-C(7)	136.09(9)
C(61A)-H(61A)	0.9900	C(6)-Fe(1)-C(7)	40.45(8)
C(61A)-H(61B)	0.9900	C(5)-Fe(1)-C(7)	143.09(9)
C(61B)-C(60B)	1.492(15)	C(3)-Fe(1)-C(7)	111.70(10)
C(61B)-C(62B)	1.549(15)	C(8)-Fe(1)-C(7)	40.18(9)
C(61B)-H(61C)	0.9900	C(1)-Fe(1)-C(4)	68.91(10)
C(61B)-H(61D)	0.9900	C(10)-Fe(1)-C(4)	137.60(10)

C(9)-Fe(1)-C(4)	176.67(10)	C(37)-C(36)-C(35)	122.1(2)
C(2)-Fe(1)-C(4)	68.28(11)	C(37)-C(36)-H(36)	119.0
C(6)-Fe(1)-C(4)	112.30(10)	C(35)-C(36)-H(36)	119.0
C(5)-Fe(1)-C(4)	40.24(10)	C(44)-C(45)-C(47)	121.3(2)
C(3)-Fe(1)-C(4)	39.83(12)	C(44)-C(45)-C(46)	119.6(2)
C(8)-Fe(1)-C(4)	142.39(10)	C(47)-C(45)-C(46)	119.1(2)
C(7)-Fe(1)-C(4)	114.70(10)	C(7)-C(6)-C(10)	108.42(19)
C(10)-P(2)-C(23)	99.01(9)	C(7)-C(6)-Fe(1)	70.64(12)
C(10)-P(2)-C(29)	100.83(10)	C(10)-C(6)-Fe(1)	68.62(11)
C(23)-P(2)-C(29)	103.27(10)	C(7)-C(6)-H(6)	125.8
C(10)-P(2)-Ni(1)	120.63(7)	C(10)-C(6)-H(6)	125.8
C(23)-P(2)-Ni(1)	113.54(7)	Fe(1)-C(6)-H(6)	126.5
C(29)-P(2)-Ni(1)	116.73(7)	C(18)-C(17)-C(22)	119.5(2)
C(1)-P(1)-C(17)	103.55(11)	C(18)-C(17)-P(1)	121.05(17)
C(1)-P(1)-C(11)	101.54(10)	C(22)-C(17)-P(1)	119.45(19)
C(17)-P(1)-C(11)	100.69(10)	C(45)-C(44)-C(43)	120.66(19)
C(1)-P(1)-Ni(1)	118.98(7)	C(45)-C(44)-H(44)	119.7
C(17)-P(1)-Ni(1)	113.72(8)	C(43)-C(44)-H(44)	119.7
C(11)-P(1)-Ni(1)	115.93(7)	C(12)-C(11)-C(16)	119.1(2)
C(51)-N(1)-C(43)	118.31(17)	C(12)-C(11)-P(1)	120.62(17)
C(51)-N(1)-Ni(1)	119.62(14)	C(16)-C(11)-P(1)	120.21(19)
C(43)-N(1)-Ni(1)	118.19(14)	C(53)-C(52)-C(51)	121.8(2)
C(39)-O(1)-C(38)	119.1(2)	C(53)-C(52)-H(52)	119.1
C(28)-C(23)-C(24)	118.87(19)	C(51)-C(52)-H(52)	119.1
C(28)-C(23)-P(2)	120.22(16)	C(56)-C(58)-C(51)	121.0(2)
C(24)-C(23)-P(2)	120.50(17)	C(56)-C(58)-H(58)	119.5
C(41)-C(35)-C(36)	117.40(19)	C(51)-C(58)-H(58)	119.5
C(41)-C(35)-Ni(1)	123.20(15)	C(29)-C(30)-C(31)	120.9(2)
C(36)-C(35)-Ni(1)	118.58(16)	C(29)-C(30)-H(30)	119.6
C(9)-C(10)-C(6)	106.59(18)	C(31)-C(30)-H(30)	119.6
C(9)-C(10)-P(2)	126.23(16)	C(2)-C(1)-C(5)	106.9(2)
C(6)-C(10)-P(2)	127.16(16)	C(2)-C(1)-P(1)	129.75(19)
C(9)-C(10)-Fe(1)	69.43(12)	C(5)-C(1)-P(1)	123.08(17)
C(6)-C(10)-Fe(1)	69.81(12)	C(2)-C(1)-Fe(1)	69.72(13)
P(2)-C(10)-Fe(1)	124.27(11)	C(5)-C(1)-Fe(1)	70.07(13)
C(25)-C(24)-C(23)	120.5(2)	P(1)-C(1)-Fe(1)	120.93(11)
C(25)-C(24)-H(24)	119.8	C(35)-C(41)-C(40)	120.4(2)
C(23)-C(24)-H(24)	119.8	C(35)-C(41)-C(42)	122.56(19)
C(50)-C(43)-N(1)	120.10(19)	C(40)-C(41)-C(42)	117.1(2)
C(50)-C(43)-C(44)	117.71(19)	C(8)-C(7)-C(6)	108.37(19)
N(1)-C(43)-C(44)	122.13(18)	C(8)-C(7)-Fe(1)	69.64(13)
N(1)-C(51)-C(52)	120.05(19)	C(6)-C(7)-Fe(1)	68.91(12)
N(1)-C(51)-C(58)	123.48(19)	C(8)-C(7)-H(7)	125.8
C(52)-C(51)-C(58)	116.2(2)	C(6)-C(7)-H(7)	125.8
C(27)-C(28)-C(23)	120.6(2)	Fe(1)-C(7)-H(7)	127.2
C(27)-C(28)-H(28)	119.7	C(11)-C(12)-C(13)	120.5(2)
C(23)-C(28)-H(28)	119.7	C(11)-C(12)-H(12)	119.7
C(8)-C(9)-C(10)	108.23(19)	C(13)-C(12)-H(12)	119.7
C(8)-C(9)-Fe(1)	70.58(14)	C(41)-C(42)-H(42A)	109.5
C(10)-C(9)-Fe(1)	68.97(12)	C(41)-C(42)-H(42B)	109.5
C(8)-C(9)-H(9)	125.9	H(42A)-C(42)-H(42B)	109.5
C(10)-C(9)-H(9)	125.9	C(41)-C(42)-H(42C)	109.5
Fe(1)-C(9)-H(9)	126.1	H(42A)-C(42)-H(42C)	109.5
C(30)-C(29)-C(34)	118.7(2)	H(42B)-C(42)-H(42C)	109.5
C(30)-C(29)-P(2)	120.66(16)	C(33)-C(34)-C(29)	119.8(2)
C(34)-C(29)-P(2)	120.58(17)	C(33)-C(34)-H(34)	120.1

C(29)-C(34)-H(34)	120.1	C(37)-C(38)-C(40)	119.7(2)
C(48)-C(50)-C(43)	120.9(2)	O(1)-C(38)-C(40)	124.6(2)
C(48)-C(50)-H(50)	119.6	F(3B)-C(46)-F(2B)	106.4(15)
C(43)-C(50)-H(50)	119.6	F(3B)-C(46)-F(1B)	114.6(9)
C(25)-C(26)-C(27)	120.0(2)	F(2B)-C(46)-F(1B)	90.9(16)
C(25)-C(26)-H(26)	120.0	F(1A)-C(46)-F(2A)	109.1(3)
C(27)-C(26)-H(26)	120.0	F(1A)-C(46)-F(3A)	104.5(2)
C(52)-C(53)-C(55)	121.7(2)	F(2A)-C(46)-F(3A)	105.1(3)
C(52)-C(53)-C(54)	119.6(2)	F(3B)-C(46)-C(45)	119.7(9)
C(55)-C(53)-C(54)	118.6(2)	F(2B)-C(46)-C(45)	110.1(14)
C(4)-C(5)-C(1)	108.3(2)	F(1B)-C(46)-C(45)	111.1(5)
C(4)-C(5)-Fe(1)	70.98(15)	F(1A)-C(46)-C(45)	111.9(2)
C(1)-C(5)-Fe(1)	68.38(13)	F(2A)-C(46)-C(45)	113.0(3)
C(4)-C(5)-H(5)	125.9	F(3A)-C(46)-C(45)	112.7(2)
C(1)-C(5)-H(5)	125.9	C(56)-C(55)-C(53)	117.0(2)
Fe(1)-C(5)-H(5)	126.3	C(56)-C(55)-H(55)	121.5
C(47)-C(48)-C(50)	121.5(2)	C(53)-C(55)-H(55)	121.5
C(47)-C(48)-C(49)	120.6(2)	F(5)-C(49)-F(4)	106.7(2)
C(50)-C(48)-C(49)	117.9(2)	F(5)-C(49)-F(6)	106.4(2)
C(24)-C(25)-C(26)	120.1(2)	F(4)-C(49)-F(6)	106.32(19)
C(24)-C(25)-H(25)	119.9	F(5)-C(49)-C(48)	111.97(19)
C(26)-C(25)-H(25)	119.9	F(4)-C(49)-C(48)	112.7(2)
C(7)-C(8)-C(9)	108.38(19)	F(6)-C(49)-C(48)	112.3(2)
C(7)-C(8)-Fe(1)	70.18(13)	C(21)-C(22)-C(17)	120.1(3)
C(9)-C(8)-Fe(1)	68.65(13)	C(21)-C(22)-H(22)	120.0
C(7)-C(8)-H(8)	125.8	C(17)-C(22)-H(22)	120.0
C(9)-C(8)-H(8)	125.8	C(3)-C(4)-C(5)	108.2(2)
Fe(1)-C(8)-H(8)	126.9	C(3)-C(4)-Fe(1)	69.53(16)
C(28)-C(27)-C(26)	119.8(2)	C(5)-C(4)-Fe(1)	68.78(14)
C(28)-C(27)-H(27)	120.1	C(3)-C(4)-H(4)	125.9
C(26)-C(27)-H(27)	120.1	C(5)-C(4)-H(4)	125.9
C(38)-C(37)-C(36)	119.9(2)	Fe(1)-C(4)-H(4)	127.4
C(38)-C(37)-H(37)	120.1	C(33)-C(32)-C(31)	119.5(2)
C(36)-C(37)-H(37)	120.1	C(33)-C(32)-H(32)	120.2
C(15)-C(16)-C(11)	120.0(2)	C(31)-C(32)-H(32)	120.2
C(15)-C(16)-H(16)	120.0	F(8B)-C(54)-F(9B)	107.3(4)
C(11)-C(16)-H(16)	120.0	F(7A)-C(54)-F(8A)	110.8(5)
C(48)-C(47)-C(45)	117.9(2)	F(7A)-C(54)-F(9A)	108.2(4)
C(48)-C(47)-H(47)	121.0	F(8A)-C(54)-F(9A)	101.0(4)
C(45)-C(47)-H(47)	121.0	F(8B)-C(54)-F(7B)	106.7(4)
C(32)-C(31)-C(30)	120.0(2)	F(9B)-C(54)-F(7B)	102.0(3)
C(32)-C(31)-H(31)	120.0	F(7A)-C(54)-C(53)	115.2(4)
C(30)-C(31)-H(31)	120.0	F(8B)-C(54)-C(53)	117.0(4)
C(38)-C(40)-C(41)	120.5(2)	F(9B)-C(54)-C(53)	111.4(3)
C(38)-C(40)-H(40)	119.7	F(8A)-C(54)-C(53)	111.4(4)
C(41)-C(40)-H(40)	119.7	F(9A)-C(54)-C(53)	109.2(3)
C(17)-C(18)-C(19)	120.0(2)	F(7B)-C(54)-C(53)	111.3(3)
C(17)-C(18)-H(18)	120.0	C(3)-C(2)-C(1)	107.6(2)
C(19)-C(18)-H(18)	120.0	C(3)-C(2)-Fe(1)	70.56(14)
C(32)-C(33)-C(34)	121.0(2)	C(1)-C(2)-Fe(1)	68.77(12)
C(32)-C(33)-H(33)	119.5	C(3)-C(2)-H(2)	126.2
C(34)-C(33)-H(33)	119.5	C(1)-C(2)-H(2)	126.2
C(58)-C(56)-C(55)	122.3(2)	Fe(1)-C(2)-H(2)	126.0
C(58)-C(56)-C(57)	117.5(2)	C(14)-C(13)-C(12)	120.1(3)
C(55)-C(56)-C(57)	120.2(2)	C(14)-C(13)-H(13)	120.0
C(37)-C(38)-O(1)	115.7(2)	C(12)-C(13)-H(13)	120.0

C(14)-C(15)-C(16)	120.4(2)
C(14)-C(15)-H(15)	119.8
C(16)-C(15)-H(15)	119.8
C(20)-C(21)-C(22)	120.2(2)
C(20)-C(21)-H(21)	119.9
C(22)-C(21)-H(21)	119.9
C(20)-C(19)-C(18)	119.6(3)
C(20)-C(19)-H(19)	120.2
C(18)-C(19)-H(19)	120.2
C(21)-C(20)-C(19)	120.6(2)
C(21)-C(20)-H(20)	119.7
C(19)-C(20)-H(20)	119.7
C(4)-C(3)-C(2)	109.0(2)
C(4)-C(3)-Fe(1)	70.64(15)
C(2)-C(3)-Fe(1)	68.71(14)
C(4)-C(3)-H(3)	125.5
C(2)-C(3)-H(3)	125.5
Fe(1)-C(3)-H(3)	126.7
C(13)-C(14)-C(15)	119.9(2)
C(13)-C(14)-H(14)	120.1
C(15)-C(14)-H(14)	120.1
F(12A)-C(57)-F(11A)	112(2)
F(10B)-C(57)-F(11B)	109.5(8)
F(10B)-C(57)-F(12B)	106.8(11)
F(11B)-C(57)-F(12B)	102.3(13)
F(12A)-C(57)-F(10A)	105.4(11)
F(11A)-C(57)-F(10A)	98.5(8)
F(12A)-C(57)-C(56)	118.2(6)
F(10B)-C(57)-C(56)	117.4(7)
F(11A)-C(57)-C(56)	111.8(5)
F(11B)-C(57)-C(56)	112.4(4)
F(12B)-C(57)-C(56)	107.2(5)
F(10A)-C(57)-C(56)	108.8(7)
O(1)-C(39)-H(39A)	109.5
O(1)-C(39)-H(39B)	109.5
H(39A)-C(39)-H(39B)	109.5
O(1)-C(39)-H(39C)	109.5
H(39A)-C(39)-H(39C)	109.5
H(39B)-C(39)-H(39C)	109.5
C(61A)-C(60A)-C(59A)	113.9(8)
C(61A)-C(60A)-H(60A)	108.8
C(59A)-C(60A)-H(60A)	108.8
C(61A)-C(60A)-H(60B)	108.8
C(59A)-C(60A)-H(60B)	108.8
H(60A)-C(60A)-H(60B)	107.7
C(62A)-C(63A)-H(63A)	109.5
C(62A)-C(63A)-H(63B)	109.5
H(63A)-C(63A)-H(63B)	109.5
C(62A)-C(63A)-H(63C)	109.5
H(63A)-C(63A)-H(63C)	109.5
H(63B)-C(63A)-H(63C)	109.5
C(60A)-C(59A)-H(59A)	109.5
C(60A)-C(59A)-H(59B)	109.5
H(59A)-C(59A)-H(59B)	109.5
C(60A)-C(59A)-H(59C)	109.5
H(59A)-C(59A)-H(59C)	109.5
H(59B)-C(59A)-H(59C)	109.5
C(61A)-C(62A)-C(63A)	104(3)
C(61A)-C(62A)-H(62A)	111.1
C(63A)-C(62A)-H(62A)	111.1
C(61A)-C(62A)-H(62B)	111.1
C(63A)-C(62A)-H(62B)	111.1
H(62A)-C(62A)-H(62B)	109.0
C(60A)-C(61A)-C(62A)	113.6(6)
C(60A)-C(61A)-H(61A)	108.9
C(62A)-C(61A)-H(61A)	108.9
C(60A)-C(61A)-H(61B)	108.9
C(62A)-C(61A)-H(61B)	108.9
H(61A)-C(61A)-H(61B)	107.7
C(60B)-C(61B)-C(62B)	113.1(9)
C(60B)-C(61B)-H(61C)	109.0
C(62B)-C(61B)-H(61C)	109.0
C(60B)-C(61B)-H(61D)	109.0
C(62B)-C(61B)-H(61D)	109.0
H(61C)-C(61B)-H(61D)	107.8
C(61B)-C(60B)-C(59B)	108.4(13)
C(61B)-C(60B)-H(60C)	110.0
C(59B)-C(60B)-H(60C)	110.0
C(61B)-C(60B)-H(60D)	110.0
C(59B)-C(60B)-H(60D)	110.0
H(60C)-C(60B)-H(60D)	108.4
C(61B)-C(62B)-C(63B)	108(4)
C(61B)-C(62B)-H(62C)	110.0
C(63B)-C(62B)-H(62C)	110.0
C(61B)-C(62B)-H(62D)	110.0
C(63B)-C(62B)-H(62D)	110.0
H(62C)-C(62B)-H(62D)	108.4
C(60B)-C(59B)-H(59D)	109.5
C(60B)-C(59B)-H(59E)	109.5
H(59D)-C(59B)-H(59E)	109.5
C(60B)-C(59B)-H(59F)	109.5
H(59D)-C(59B)-H(59F)	109.5
H(59E)-C(59B)-H(59F)	109.5
C(62B)-C(63B)-H(63D)	109.5
C(62B)-C(63B)-H(63E)	109.5
H(63D)-C(63B)-H(63E)	109.5
C(62B)-C(63B)-H(63F)	109.5
H(63D)-C(63B)-H(63F)	109.5
H(63E)-C(63B)-H(63F)	109.5

Symmetry transformations used to generate equivalent atoms:

Table 4. Anisotropic displacement parameters ($Å^2 x\ 10^3$)for jwang004_hartwig. The anisotropic displacement factor exponent takes the form: $-2\pi^2[\ h^2a^{*2}U^{11} + ... + 2\ h\ k\ a^*\ b^*\ U^{12}\ ]$

	U^{11}	U^{22}	U^{33}	U^{23}	U^{13}	U^{12}
Ni(1)	17(1)	15(1)	27(1)	-8(1)	-7(1)	0(1)
Fe(1)	23(1)	26(1)	34(1)	-14(1)	-15(1)	6(1)
P(2)	17(1)	16(1)	26(1)	-8(1)	-8(1)	-1(1)
P(1)	21(1)	22(1)	30(1)	-11(1)	-10(1)	0(1)
F(5)	50(1)	37(1)	50(1)	-14(1)	9(1)	-19(1)
F(6)	40(1)	44(1)	57(1)	-11(1)	-15(1)	-22(1)
F(3B)	35(1)	25(1)	89(2)	-6(1)	-28(2)	6(1)
F(4)	46(1)	18(1)	88(1)	2(1)	-22(1)	-10(1)
N(1)	20(1)	17(1)	31(1)	-8(1)	-7(1)	1(1)
F(8B)	72(4)	32(2)	35(3)	-1(2)	-5(2)	-8(2)
F(10A)	98(10)	46(4)	31(3)	-22(2)	21(5)	-19(6)
F(2B)	66(2)	84(3)	130(2)	-77(3)	-73(2)	33(2)
F(7B)	71(4)	21(2)	33(2)	-5(1)	-9(2)	4(2)
F(1A)	20(1)	76(2)	75(2)	15(1)	-12(1)	-2(1)
O(1)	46(1)	38(1)	129(2)	0(1)	-60(1)	-7(1)
C(23)	18(1)	17(1)	33(1)	-8(1)	-8(1)	0(1)
C(35)	18(1)	19(1)	34(1)	-11(1)	-10(1)	0(1)
C(10)	20(1)	24(1)	25(1)	-10(1)	-9(1)	1(1)
F(12B)	49(4)	51(5)	69(4)	-47(4)	7(3)	-14(3)
C(24)	20(1)	25(1)	33(1)	-11(1)	-6(1)	-2(1)
C(43)	23(1)	16(1)	30(1)	-10(1)	-8(1)	0(1)
C(51)	20(1)	21(1)	31(1)	-9(1)	-9(1)	-1(1)
C(28)	23(1)	21(1)	34(1)	-10(1)	-10(1)	3(1)
C(9)	23(1)	24(1)	31(1)	-11(1)	-10(1)	-2(1)
C(29)	25(1)	19(1)	29(1)	-10(1)	-12(1)	2(1)
C(36)	25(1)	19(1)	39(1)	-6(1)	-11(1)	-1(1)
C(45)	25(1)	22(1)	38(1)	-11(1)	-12(1)	0(1)
C(6)	23(1)	24(1)	30(1)	-13(1)	-10(1)	1(1)
C(17)	21(1)	23(1)	40(1)	-13(1)	-7(1)	-2(1)
C(44)	21(1)	19(1)	34(1)	-9(1)	-8(1)	-3(1)
C(11)	22(1)	32(1)	35(1)	-18(1)	-11(1)	0(1)
C(52)	22(1)	20(1)	31(1)	-10(1)	-8(1)	2(1)
C(58)	26(1)	19(1)	38(1)	-12(1)	-9(1)	0(1)
C(30)	22(1)	30(1)	30(1)	-9(1)	-10(1)	2(1)
C(1)	28(1)	31(1)	28(1)	-15(1)	-14(1)	6(1)
C(41)	24(1)	20(1)	36(1)	-10(1)	-11(1)	-2(1)
C(7)	22(1)	31(1)	37(1)	-18(1)	-12(1)	6(1)
C(12)	36(1)	34(1)	37(1)	-15(1)	-13(1)	2(1)
C(42)	30(1)	21(1)	35(1)	-6(1)	-12(1)	-2(1)
C(34)	31(1)	21(1)	41(1)	-8(1)	-18(1)	-3(1)
C(50)	19(1)	20(1)	36(1)	-11(1)	-7(1)	0(1)
C(26)	34(1)	18(1)	50(2)	-9(1)	-10(1)	-4(1)
C(53)	30(1)	24(1)	29(1)	-7(1)	-10(1)	-2(1)
C(5)	39(1)	30(1)	26(1)	-9(1)	-13(1)	5(1)
C(48)	26(1)	18(1)	37(1)	-10(1)	-8(1)	-4(1)
C(25)	25(1)	25(1)	47(1)	-19(1)	-9(1)	-2(1)
C(8)	19(1)	35(1)	39(1)	-17(1)	-7(1)	-2(1)
C(27)	30(1)	24(1)	36(1)	-4(1)	-6(1)	-3(1)
C(37)	25(1)	23(1)	62(2)	-6(1)	-16(1)	-7(1)

C(16)	30(1)	32(1)	43(1)	-17(1)	-13(1)	2(1)
C(47)	30(1)	16(1)	40(1)	-6(1)	-13(1)	0(1)
C(31)	33(1)	37(1)	31(1)	-7(1)	-9(1)	1(1)
C(40)	35(1)	23(1)	49(2)	-8(1)	-24(1)	2(1)
C(18)	22(1)	25(1)	41(1)	-13(1)	-7(1)	1(1)
C(33)	45(2)	29(1)	48(2)	-11(1)	-31(1)	-1(1)
C(56)	28(1)	29(1)	37(1)	-16(1)	-4(1)	-3(1)
C(38)	30(1)	27(1)	68(2)	-10(1)	-27(1)	-3(1)
C(46)	32(1)	26(1)	52(2)	-7(1)	-22(1)	0(1)
C(55)	31(1)	31(1)	30(1)	-10(1)	-5(1)	-6(1)
C(49)	31(1)	21(1)	43(1)	-8(1)	-8(1)	-4(1)
C(22)	29(1)	38(1)	45(1)	-16(1)	-13(1)	-5(1)
C(4)	56(2)	33(1)	38(1)	-13(1)	-26(1)	16(1)
C(32)	49(2)	34(1)	33(1)	-8(1)	-22(1)	3(1)
C(54)	39(1)	31(1)	35(1)	-3(1)	-12(1)	2(1)
C(2)	32(1)	46(1)	43(1)	-26(1)	-23(1)	9(1)
C(13)	44(2)	49(2)	37(1)	-16(1)	-13(1)	4(1)
C(15)	38(1)	42(2)	53(2)	-30(1)	-15(1)	7(1)
C(21)	32(1)	45(2)	60(2)	-23(1)	-11(1)	-13(1)
C(19)	32(1)	28(1)	44(2)	-9(1)	-1(1)	0(1)
F(9B)	65(4)	42(2)	85(6)	10(2)	-49(4)	2(2)
C(20)	30(1)	35(1)	65(2)	-19(1)	2(1)	-12(1)
C(3)	45(2)	57(2)	48(2)	-28(1)	-33(1)	26(1)
C(14)	44(2)	59(2)	40(2)	-29(1)	-12(1)	9(1)
C(57)	52(2)	41(2)	49(2)	-24(1)	2(1)	-2(1)
C(39)	42(2)	41(2)	100(3)	-10(2)	-47(2)	0(1)
F(11A)	62(4)	115(10)	83(7)	-54(7)	-12(4)	45(5)
C(60A)	67(6)	62(4)	45(5)	-10(3)	-24(4)	-5(3)
C(63A)	152(8)	86(12)	93(11)	-47(8)	-27(7)	21(7)
C(59A)	58(8)	109(5)	78(9)	-25(7)	-20(6)	-10(7)
C(62A)	103(5)	67(4)	53(4)	-15(3)	-31(4)	9(3)
C(61A)	85(4)	64(4)	71(4)	-23(3)	-32(3)	2(3)
C(61B)	85(4)	64(4)	71(4)	-23(3)	-32(3)	2(3)
C(60B)	67(6)	62(4)	45(5)	-10(3)	-24(4)	-5(3)
C(62B)	103(5)	67(4)	53(4)	-15(3)	-31(4)	9(3)
C(59B)	58(8)	109(5)	78(9)	-25(7)	-20(6)	-10(7)
C(63B)	152(8)	86(12)	93(11)	-47(8)	-27(7)	21(7)
F(7A)	53(4)	23(2)	49(3)	-4(2)	3(3)	12(3)
F(9A)	63(5)	52(3)	60(5)	0(2)	-34(5)	9(2)
F(8A)	37(3)	23(2)	47(5)	2(3)	2(3)	-4(2)
F(12A)	104(9)	23(2)	74(5)	-23(3)	51(5)	-21(4)
F(10B)	81(7)	33(3)	87(8)	-27(5)	53(5)	-20(4)
F(11B)	97(7)	100(7)	87(6)	-52(6)	-30(5)	73(6)
F(1B)	20(1)	76(2)	75(2)	15(1)	-12(1)	-2(1)
F(2A)	66(2)	84(3)	130(2)	-77(3)	-73(2)	33(2)
F(3A)	35(1)	25(1)	89(2)	-6(1)	-28(2)	6(1)

Table 5. Hydrogen coordinates (x 10^4) and isotropic displacement parameters ($Å^2$x 10^3) for jwang004_hartwig.

	x	y	z	U(eq)
H(24)	3726	61	500	30
H(28)	2501	420	3085	30
H(9)	5781	2447	942	30
H(36)	992	1312	2821	33
H(6)	5244	-246	1405	29
H(44)	-42	3872	2841	29
H(52)	1788	1522	3885	29
H(58)	382	3988	4311	32
H(30)	5019	2470	-297	32
H(7)	7202	-142	1137	34
H(12)	3606	1447	4892	41
H(42A)	2792	3695	776	42
H(42B)	1824	4372	557	42
H(42C)	2415	3674	-80	42
H(34)	2181	1408	411	34
H(50)	2945	4601	2272	29
H(26)	2525	-2032	2531	41
H(5)	3977	435	3573	38
H(25)	3310	-1443	990	37
H(8)	7534	1507	853	35
H(27)	2094	-1092	3576	38
H(37)	-580	1372	2474	44
H(16)	3203	4118	3784	40
H(47)	729	6401	1412	34
H(31)	4952	2965	-1792	41
H(40)	306	3552	448	40
H(18)	4501	3760	1289	35
H(33)	2136	1897	-1087	44
H(55)	-316	1740	6321	37
H(22)	5492	3363	3531	42
H(4)	5631	-609	3605	49
H(32)	3510	2674	-2189	44
H(2)	6479	2003	2977	43
H(13)	2812	1746	6341	51
H(15)	2433	4408	5238	50
H(21)	6571	4564	2829	52
H(19)	5574	4983	601	45
H(20)	6598	5378	1383	53
H(3)	7158	347	3238	54
H(14)	2238	3226	6514	55
H(39A)	-1253	3321	188	84
H(39B)	-1631	3759	1066	84
H(39C)	-2410	3168	888	84
H(60A)	5904	2014	4799	68
H(60B)	6469	1349	5492	68
H(63A)	5151	4696	5930	166
H(63B)	5791	3954	6513	166
H(63C)	4616	3791	6552	166
H(59A)	7714	1812	4013	120
H(59B)	8056	2094	4783	120

H(59C)	7495	2839	4137	120
H(62A)	5230	3590	5009	88
H(62B)	6405	3831	4912	88
H(61A)	6535	2587	6106	84
H(61B)	5350	2361	6249	84
H(61C)	6573	3595	4621	84
H(61D)	7133	3184	5403	84
H(60C)	6302	2126	4568	68
H(60D)	6846	1707	5365	68
H(62C)	5499	2679	6444	88
H(62D)	4923	2991	5659	88
H(59D)	7991	2844	3717	120
H(59E)	8038	1774	3799	120
H(59F)	8487	2158	4448	120
H(63D)	5826	4278	6249	166
H(63E)	4581	4145	6582	166
H(63F)	5152	4560	5537	166

4.5 References

1. (a) Hartwig, J. F., Carbon−Heteroatom Bond-Forming Reductive Eliminations of Amines, Ethers, and Sulfides. *Acc. Chem. Res.* **1998,** *31*, 852-860; (b) Dorel, R.; Grugel, C. P.; Haydl, A. M., The Buchwald–Hartwig Amination After 25 Years. *Angew. Chem. Int. Ed.* **2019,** *58*, 17118-17129.
2. (a) Ruiz-Castillo, P.; Buchwald, S. L., Applications of Palladium-Catalyzed C–N Cross-Coupling Reactions. *Chem. Rev.* **2016,** *116*, 12564-12649; (b) Arrechea, P. L.; Buchwald, S. L., Biaryl Phosphine Based Pd(II) Amido Complexes: The Effect of Ligand Structure on Reductive Elimination. *J. Am. Chem. Soc.* **2016,** *138*, 12486-12493.
3. Klinkenberg, J. L.; Hartwig, J. F., Slow Reductive Elimination from Arylpalladium Parent Amido Complexes. *J. Am. Chem. Soc.* **2010,** *132*, 11830-11833.
4. (a) Ge, S.; Green, R. A.; Hartwig, J. F., Controlling First-Row Catalysts: Amination of Aryl and Heteroaryl Chlorides and Bromides with Primary Aliphatic Amines Catalyzed by a BINAP-Ligated Single-Component Ni(0) Complex. *J. Am. Chem. Soc.* **2014,** *136*, 1617-1627; (b) Kawamata, Y.; Vantourout, J. C.; Hickey, D. P.; Bai, P.; Chen, L.; Hou, Q.; Qiao, W.; Barman, K.; Edwards, M. A.; Garrido-Castro, A. F.; deGruyter, J. N.; Nakamura, H.; Knouse, K.; Qin, C.; Clay, K. J.; Bao, D.; Li, C.; Starr, J. T.; Garcia-Irizarry, C.; Sach, N.; White, H. S.; Neurock, M.; Minteer, S. D.; Baran, P. S., Electrochemically Driven, Ni-Catalyzed Aryl Amination: Scope, Mechanism, and Applications. *J. Am. Chem. Soc.* **2019,** *141*, 6392-6402.
5. Diccianni, J. B.; Diao, T., Mechanisms of Nickel-Catalyzed Cross-Coupling Reactions. *Trends in Chemistry* **2019,** *1*, 830-844.
6. Lee, E.; Hooker, J. M.; Ritter, T., Nickel-Mediated Oxidative Fluorination for PET with Aqueous [18F] Fluoride. *J. Am. Chem. Soc.* **2012,** *134*, 17456-17458.
7. (a) Yamashita, M.; Hartwig, J. F., Synthesis, Structure, and Reductive Elimination Chemistry of Three-Coordinate Arylpalladium Amido Complexes. *J. Am. Chem. Soc.* **2004,** *126*, 5344-5345; (b) Driver, M. S.; Hartwig, J. F., Energetics and Mechanism of Alkylamine N−H Bond Cleavage by Palladium Hydroxides: N−H Activation by Unusual Acid−Base Chemistry. *Organometallics* **1997,** *16*, 5706-5715.

8. Koo, K.; Hillhouse, G. L., Carbon-Nitrogen Bond Formation by Reductive Elimination from Nickel(II) Amido Alkyl Complexes. *Organometallics* **1995,** *14*, 4421-4423.
9. Wolfe, J. P.; Buchwald, S. L., Nickel-Catalyzed Amination of Aryl Chlorides. *J. Am. Chem. Soc.* **1997,** *119*, 6054-6058.
10. Mohadjer Beromi, M.; Banerjee, G.; Brudvig, G. W.; Charboneau, D. J.; Hazari, N.; Lant, H. M. C.; Mercado, B. Q., Modifications to the Aryl Group of dppf-Ligated Ni σ-Aryl Precatalysts: Impact on Speciation and Catalytic Activity in Suzuki–Miyaura Coupling Reactions. *Organometallics* **2018,** *37*, 3943-3955.
11. Truong, T.-T.; Coates, G. W.; Abruña, H. D., High power organic cathodes using thin films of electropolymerized benzidine polymers. *Chem. Commun.* **2015,** *51*, 14674-14677.
12. Kong, X.; Zhang, H.; Xiao, Y.; Cao, C.; Shi, Y.; Pang, G., Effective, transition metal free and selective C–F activation under mild conditions. *RSC Advances* **2015,** *5*, 7035-7048.
13. Bilke, J. L.; O'Brien, P., On the Two-Ligand Catalytic Asymmetric Deprotonation of N-Boc Pyrrolidine: Probing the Effect of the Stoichiometric Ligand. *J. Org. Chem.* **2008,** *73*, 6452-6454.
14. van Koten, G.; Noltes, J. G., Group IB organometallic chemistry: XIV. Intramolecular ring-closure reactions of novel arylcopper compounds RCuI2. Synthesis of 7,8-dihydrodibenzo[f,h][1,4]dioxecin and 7,8-dihydrodibenzo-6,9-dimethyl[f,h][1,4]diazecin. *J. Organomet. Chem.* **1976,** *104*, 127-138.

CHAPTER 5

CROSS-COUPLING BETWEEN HYDRAZINE AND ARYL HALIDES WITH HYDROXIDE BASE AT PPM LOADINGS OF PALLADIUM BY RATE-DETERMINING DEPROTONATION OF HYDRAZINE

5.1. Introduction

Aryl hydrazines are synthetic intermediates in the construction of a multitude of nitrogen-containing heterocycles,[33] such as indoles,[113] indazoles,[114] pyrazoles,[34] and triazoles.[35] For this reason, the preparation of a variety of pharmaceuticals and agrochemicals include aryl hydrazines as intermediates, including Celebrex,[36] Rimonabant,[37] Rizatriptan,[115] pyraclostrobin,[116] norflurazon,[38] ipfencarbazone,[117] and flufenpyr-ethyl.[39] Aryl hydrazines also serve as cross-coupling partners to form C−C or C−heteroatom bonds.[118] Aryl hydrazines are typically prepared by diazotization of aniline, followed by reduction with tin or metabisulfite salts, a process which generates explosive diazonium intermediates and large amounts of salt waste.[40] Nucleophilic aromatic substitution with hydrazine also can form aryl hydrazines, but this reaction is typically limited to arenes containing highly electron-withdrawing substituents or electrophilic heterocycles.[41, 119] Thus, a general and low-cost synthesis of aryl hydrazines would be synthetically valuable and industrially relevant.

Palladium-catalyzed C−N coupling reactions are a well-established means to generate alkyl and aryl amines.[3a, 4] However, the synthesis of aryl hydrazines by coupling aryl halides to hydrazine with palladium catalysts is much less developed.[31, 120] Although C−N coupling reactions with hydrazones are well-known, these reactions require an additional deprotection step to reveal the aryl hydrazine.[4] Palladium-catalyzed C−N coupling reactions with hydrazine are difficult to develop because hydrazine is a strong reductant and can reduce catalytically competent Pd(II) species to catalytically inactive Pd black.[29, 121] Moreover, hydrazine contains multiple N–H bonds and can undergo more than one C−N coupling reaction. For these reasons, few catalytic systems have coupled hydrazine with aryl halides to generate monoaryl hydrazine products. Although prior reports by Stradiotto[31b, 120] and Buchwald[31a] showed that the reaction can occur, these reactions have been conducted with NaO*t*Bu as base and high loadings of palladium catalyst (1-20 mol%). This base and these catalyst loadings create an expense that prohibits this reaction from being used to generate simple aryl hydrazines.[32] For palladium-catalyzed C−N coupling reactions with hydrazine to be conducted on large scale, this reaction must occur with low loadings of catalyst and must be conducted with hydrazine hydrate and with a simple base, such as hydroxide or carbonate salts.

Mechanistic studies that could guide the selection of catalysts and conditions for the coupling of hydrazine are sparse. No studies of the mechanism of C-N coupling reactions with hydrazine have been published. Thus, it is unclear how the unusual electronic properties and small size of hydrazine, in addition to the water in hydrazine hydrate, will affect the identity of the species in the catalytic system, the identity and rate of the turnover-limiting step, and pathways to catalyst decomposition. It is not known what catalytic intermediate is responsible for forming the C-N bond of the aryl hydrazine product. By drawing from related mechanistic studies in C-N cross-coupling reactions with palladium catalysts,[6, 122] it is plausible that an arylpalladium hydrazido intermediate could generate aryl hydrazine by reductive elimination; however, the synthesis of palladium hydrazido complexes and their reactivity is unknown. Reported C-N coupling reactions with hydrazine display a high selectivity for forming monoaryl hydrazine over diaryl hydrazine, and the basis for this selectivity is not understood. Thus, there are many aspects of the mechanism of C-N coupling with hydrazine that lack literature precedent.

Herein, we report the synthesis of aryl hydrazines from a diverse array of aryl chlorides or bromides by palladium-catalyzed coupling of hydrazine with loadings of catalyst as low as 100

ppm and potassium hydroxide as base and an accompanying mechanistic study that reveals an unusual resting state, characterization of a palladium parent hydrazido complex, and reductive elimination reactions from this complex. The resting state of the catalyst is a combination of an arylpalladium chloride complex and an arylpalladium hydroxide complex, and the rate-limiting step is the reaction of the arylpalladium chloride complex with hydrazine and hydroxide base to generate water and an arylpalladium hydrazido complex that reductively eliminates aryl hydrazine. The arylpalladium hydroxide complex reacts with hydrazine to generate the same arylpalladium hydrazido complex. Unlike the arylpalladium chloride complex, the aryl hydroxide complex is not selective for the formation of monoaryl hydrazine. Generation and studies of the reactivity of the hydrazido intermediate showed that reductive elimination is rapid.

5.2. Results and Discussion

Reaction Development

In prior work, our group has shown that the combination of the Josiphos ligand, (*R*)-1-[(*S*)-2-(dicyclohexylphosphino)ferrocenyl]ethyldi-*tert*-butylphosphine (CyPF-*t*Bu) and a palladium precursor catalyzes the reactions of aryl halides with small amines, ammonia, or thiols. The reactions of thiols and primary amines occurred with high turnover numbers and with catalyst loadings as low as 5 ppm,[13a, 123] and the reactions of aryl halides with ammonia and primary amines also occurred with high selectivity for the product from monoarylation.[13, 92c, 124] The steric bulk, chelation, and rigid backbone of CyPF-*t*Bu promotes reductive elimination and inhibits β-hydride elimination that would lead to protodehalogenation of the aryl halide. We considered that this system containing CyPF-*t*Bu and palladium could catalyze couplings of aryl halides with hydrazine to obtain monoaryl hydrazine products with similar turnovers and selectivities, and if the C-N coupling reactions of aryl chlorides with hydrazine could be conducted with an inexpensive base, preferably a hydroxide salt, then such arylations could be practical enough for commercial applications. Prior reactions catalyzed by CyPF-*t*Bu and palladium were previously conducted with hexamethyldisilazide or *t*-butoxide bases; only a few reactions have been conducted with this catalyst and carbonate or phosphate bases[13a] and none with hydroxide bases. Although Stradiotto reported the coupling of one aryl bromide with hydrazine, NaO*t*Bu was used as base, 3 mol% of CyPF-*t*Bu and palladium were used, and reactions of hydrazine with this catalyst were not conducted further.

Table 5.1. Survey of reaction conditions of C−N coupling with hydrazine.

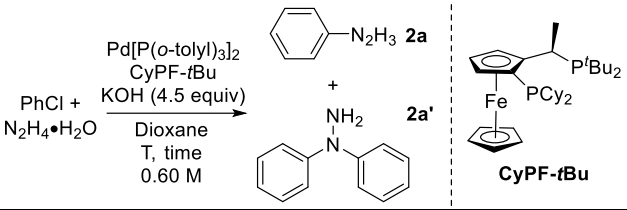

Entry	[Pd] and [L] (ppm)	$N_2H_4 \cdot H_2O$ (equiv)	T (°C)	Time (h)	Conv. (%)	Yield **2a** (%)[a]	**2a**:**2a'**
1[b,c]	100	3	110	24	26	26	>98:2
2[c,d]	100	3	110	24	55	55	>98:2
3[c,e]	100	3	110	24	44	44	>98:2
4[c,f]	100	3	110	24	22	22	>98:2
5[c,g]	100	3	110	24	67	63	94:6
6[c]	800	3	110	24	>99	>98	>98:2
7	800	3	110	24	95	93	95:5
8	400	3	110	24	75	70	94:6
9	400	3	110	65	91	85	96:4
10	200	3	110	24	56	53	95:5
11	0	3	100	24	0	0	n/a
12	800	3	100	24	>99	95	96:4
13	800	3	80	24	>99	93	93:7
14	800	3	65	24	>99	88	88:12
15	800	1.7	100	24	>99	82	94:6
16	800	2.3	100	24	>99	86	94:6
17	800	3	100	4	>99	96	96:4
18[f]	800	3	100	4	84	81	97:3

[a]Yield determined by ^{1}H NMR spectroscopy. [b]Reaction with $Pd(dba)_2$. [c]Reaction with NaO*t*Bu (4.5 equiv) instead of KOH. [d]Reaction with $[Pd(allyl)Cl]_2$. [e]Reaction with $[Pd(cinnamyl)Cl]_2$. [f]Reaction with $Pd(OAc)_2$. [g]Reaction with NaOH (4.5 equiv) instead of KOH. The values listed here are typically ± 3% between replicates.

To test whether the coupling aryl chlorides with hydrazine could occur with this type of catalyst with high turnovers, we investigated reactions with CyPF-*t*Bu as ligand and $Pd[P(o\text{-tolyl})_3]_2$ as the Pd(0) source (Table 5.1). Previously reported systems for C-N coupling reactions with palladium and CyPF-*t*Bu utilize a palladium(II) salt as a precatalyst and DME as solvent. Typically, the temperatures for these reactions were 10-35 °C above the boiling point of DME and these reactions were conducted in a closed system. Because hydrazine can undergo metal-catalyzed and thermal decomposition to generate gases, we opted to use a higher boiling ethereal analogue of DME, 1,4-dioxane, as solvent to mitigate the possibility of over pressurizing a closed system. We tested conditions that were inspired by previously reported, palladium-catalyzed C-N coupling reactions with CyPF-*t*Bu as ligand and assessed the yields of these reactions by ^{1}H NMR spectroscopy. With 100 ppm of palladium and CyPF-*t*Bu, we examined various commonly used palladium precursors. Reactions with commercially available palladium(II) salts and $Pd(dba)_2$ with NaO*t*Bu as base resulted in low yields (22-44%, Table 5.1, entries 1-4) of the *N*-aryl hydrazine product; however, reactions with $Pd[P(o\text{-tolyl})_3]_2$ resulted in a higher yield (63%, Table 5.1, entry 5) of the *N*-aryl hydrazine product, albeit a small amount of 1,1-diphenyl hydrazine was observed in 4% yield. To address the modest yields of these reactions, we pursued conditions with $Pd[P(o\text{-tolyl})_3]_2$ that increase the yield of phenyl hydrazine. By varying the loading of palladium and ligand from 100 to 800 ppm, we found that the combination of $Pd[P(o\text{-tolyl})_3]_2$ and CyPF-*t*Bu catalyzed the reaction between chlorobenzene and hydrazine with NaO*t*Bu as base to generate phenyl

hydrazine in high yield (>98%) with only 800 ppm (0.08 mol%) of catalyst (entry 6). Unlike many couplings of amines, this reaction also occurred in a similar fashion with potassium hydroxide (entry 7) as base, as long as potassium hydroxide was a finely ground powder. We chose to use potassium hydroxide for the remainder of our study because it is at least an order of magnitude less expensive than *t*-butoxide salts.[32] Reactions with a catalyst loading below 800 ppm of palladium and ligand occurred to lower conversion and yield (entries 7-8 and 10-11); however, they occurred in slightly higher yield and conversion with 400 ppm of catalyst when the reaction time was increased from 24 to 65 h (entry 9). The remainder of our study was conducted with 800 ppm of catalyst because reactions with this loading reached completion within 24 h and in high yield.

Hydroxide bases are rarely used in C−N coupling reactions. Most of the existing C-N coupling reactions with hydroxide bases have been conducted with a phase-transfer catalyst or water as solvent or co-solvent;[125] however, these additives were not required for the reaction of hydrazine to occur with our system. The only side-products detected by ^{1}H NMR spectroscopy during the course of this study were 1,1-diphenyl hydrazine and benzene. Typically, benzene was observed in <1% yield; however, reactions of aryl halides that occurred with high conversion but with low to modest yields of phenyl hydrazine or 1,1-phenylhydrazine (*vide supra*) formed benzene as the remainder of the mass balance.

At 100 °C, both the yield and the conversion of the reaction were higher, 95% and >99%, respectively, (entry 12) than at 110 °C. This result indicates that the catalyst lifetime is shorter at the higher temperature. However, the yield of phenyl hydrazine from reactions conducted at temperatures below 100 °C were lower than 95%, and the selectivity for monoarylation decreased (entries 13 and 14). The reactions conducted with less than 3 equiv of hydrazine occurred in lower yield than those with 3 equiv, but selectivity for the monoarylation of hydrazine was unaffected (entries 15-16). The length of time required for the reaction to obtain >99% conversion could be reduced from 24 to 4 h. At 100 °C, the reaction reached completion within 4 h with 800 ppm of catalyst and KOH as base (entry 17).When KOH was substituted with NaOH under these conditions, a reduction in yield and conversion was observed, 81% and 84%, respectively (entry 18).

Reaction Scope

The scope of the reaction of hydrazine with aryl and heteroaryl chlorides and bromides is summarized in Scheme 5.1. Because of the air sensitivity of aryl hydrazines, we reacted the aryl hydrazines with acetylacetone (acac) in a one-pot procedure alongside KOH and palladium catalyst to obtain 3,5-dimethyl-N-arylpyrazoles, which are more stable than aryl hydrazines towards air and can be isolated and purified by column chromatography. To test if our system could catalyze the C-N coupling reaction between 3,5-dimethylpyrazole and an aryl halide, thereby providing a false positive result, a control reaction with 3,5-dimethylpyrazole, instead of hydrazine, and chlorobenzene was performed (see Supporting Information for details), and the *N*-aryl pyrazole was not detected by ^{1}H NMR spectroscopy or GC-MS analysis. Thus, the pyrazoles formed by the reactions in Scheme 5.1 result from the condensation of the aryl hydrazine with acetylacetone and not by a C−N coupling reaction between an aryl halide and 3,5-dimethylpyrazole.

A majority of the reactions of hydrazine with aryl and heteroaryl chlorides occurred with low loadings of catalyst (800 ppm or 0.08 mol%) and with KOH as base. However, 1600 ppm (0.16 mol%) of catalyst was required to couple hydrazine with the more hindered 2-chlorotoluene to form the *o*-Me substituted pyrazole **3k** in 71% yield. Although this loading was higher than for the unhindered chloroarenes, previously reported couplings of hydrazine with *o*-methyl substituted haloarenes required 1-5 mol% of palladium catalyst to obtain reactions that generated the desired product in 74-88% yield.[31, 120] The reaction between hydrazine and chlorobenzene reached completion within 4 h, but the reactions of most aryl halides required 5-24 h to reach high conversion. Ethers, thioethers, *t*-butyl esters, alcohols, amines, amides, hindered ketones, nitriles, additional halides, and terminal olefins were tolerated in the aryl halide in this reaction. The reaction of 1,4-dichlorobenzene with hydrazine to generate 4-chloroaryl hydrazine by reaction at one chloride selectively even occurred with only 100 ppm (0.01 mol%) of palladium catalyst. Substrates containing heteroaryl moieties, such as pyridine, quinoline, benzothiophene, imidazo[1,2-*a*]pyridine, and benzopyrazine units, underwent the reaction in 64-97% isolated yield.

In a few cases, the reactions required NaO*t*Bu as base to achieve high yields. For example, the reaction of electron-rich chloroarene **1d** with KOH as base resulted in a low yield of 4-methoxyphenyl hydrazine (29% by ^{1}H NMR spectroscopy). However, the same reaction with NaO*t*Bu as base proceeded in 84% isolated yield. In a few other cases the pyrazoles were isolated in modest yield, but the yield of the C−N coupling reaction was high. For example, pyrazoles **3e-f**, **3ab**, and **3ae** were isolated in 45-69% yield, but the yields of the C−N coupling reactions with the corresponding aryl chlorides determined by NMR spectroscopy were 75-81%. The disparity in these yields is likely due to the hydrolysis of the ester, nitrile, or amide functional groups in **1f**, **1ab**, and **1ae**, respectively, or by the condensation of hydrazine onto the ketone in **1e** under basic conditions during the course of the reaction of the hydrazine product and acetylacetone.[126]

Scheme 5.1. Scope of C−N coupling reaction with hydrazine and (hetero)aryl chlorides or bromides.

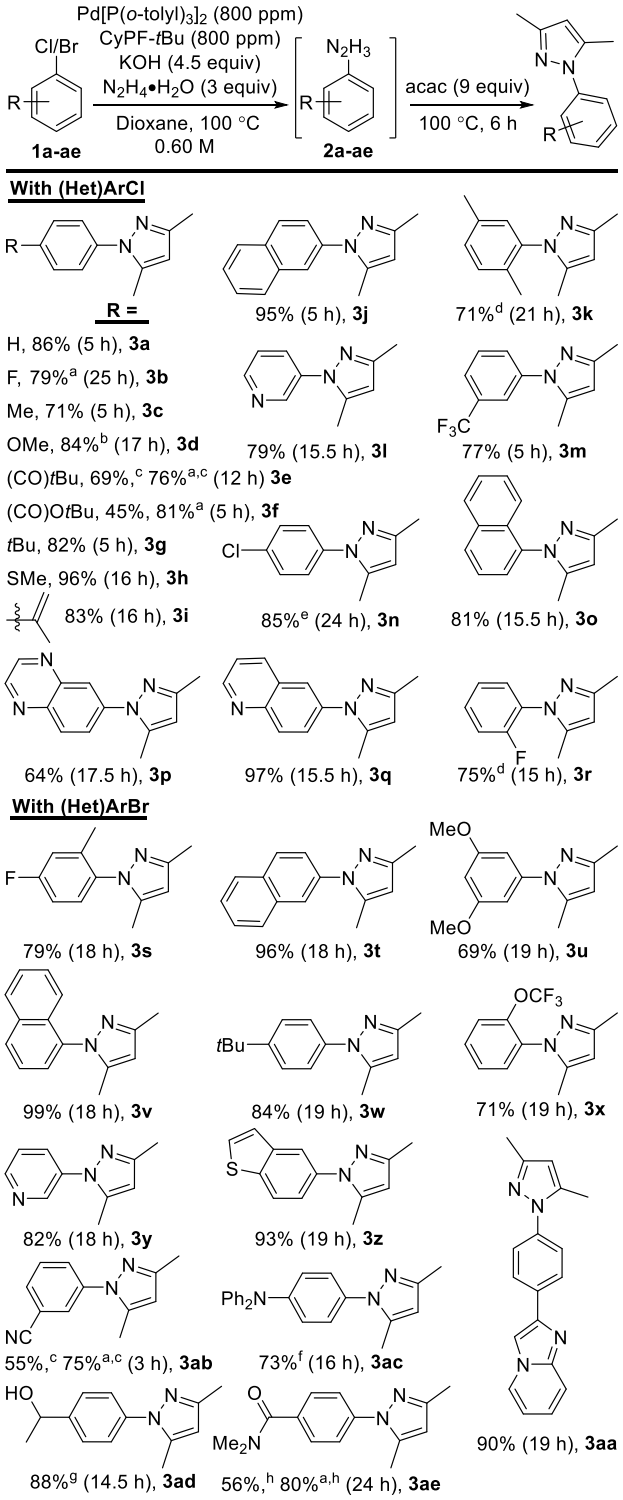

All yields are isolated yields unless stated otherwise. [a]Yield of aryl hydrazine determined by ^{1}H NMR spectroscopy. [b]4.5 equiv NaO*t*Bu instead of KOH. [c]1 mol% Pd[P(*o*-tolyl$_3$)]$_2$, 1 mol% CyPF-*t*Bu, and 4.5 equiv of NaO*t*Bu at rt. [d]0.16 mol% Pd[P(*o*-tolyl$_3$)]$_2$ and 0.16 mol% CyPF-*t*Bu. [e]0.01 mol% Pd[P(*o*-tolyl$_3$)]$_2$ and 0.01 mol% CyPF-*t*Bu.[f]0.12 mol%

Pd[P(*o*-tolyl$_3$)]$_2$, 0.12 mol% CyPF-*t*Bu, and 4.5 equiv of NaO*t*Bu. [g]Isolated as a 2:1 mixture of 3,5-dimethylpyrazole and **3z**, respectively. [h]0.2 mol% Pd[P(*o*-tolyl$_3$)]$_2$, 0.2 mol% CyPF-*t*Bu, and 4.5 equiv of NaO*t*Bu at rt.

During prior published work on palladium-catalyzed C−N cross-coupling reactions with hydrazine, the reactions of aryl bromides occurred in much lower yields than those of aryl chlorides, and the scope of these reactions with these catalysts occurring in useful yields were limited to chloroarenes and aryl tosylates.[31] This trend in reactivity of the aryl electrophiles is unusual because aryl bromides are more reactive than aryl chlorides in other palladium-catalyzed cross-coupling reactions of nitrogen nucleophiles with aryl halides, and reactions involving aryl bromides typically require lower catalyst loadings and lead to higher yields.[3a, 10b, 127] In contrast to the previously published couplings of hydrazine with aryl bromides, these reactions occurred in high yield with our catalyst system, which was generated from CyPF-*t*Bu and Pd[P(*o*-tolyl)$_3$]$_2$. Thus, our methodology is well suited to the reaction of a wide range of aryl and heteroaryl chlorides and bromides and is compatible for the synthesis of biologically active molecules containing aryl hydrazine intermediates.

Mechanistic Studies on C−N Cross-Coupling with Hydrazine

Scheme 5.2. Determination of catalyst resting state by analyzing the catalytic reaction at partial conversion by ^{31}P NMR spectroscopy (a) ^{31}P NMR spectrum of catalytic reaction analyzed at 52% conversion, (b) ^{31}P NMR spectrum of (CyPF-*t*Bu)Pd(*p*-tolyl)(OH) (**5**) in 1,4-dioxane, and (c) ^{31}P NMR spectrum of (CyPF-*t*Bu)Pd(*p*-tolyl)Cl (**4**) in 1,4-dioxane.

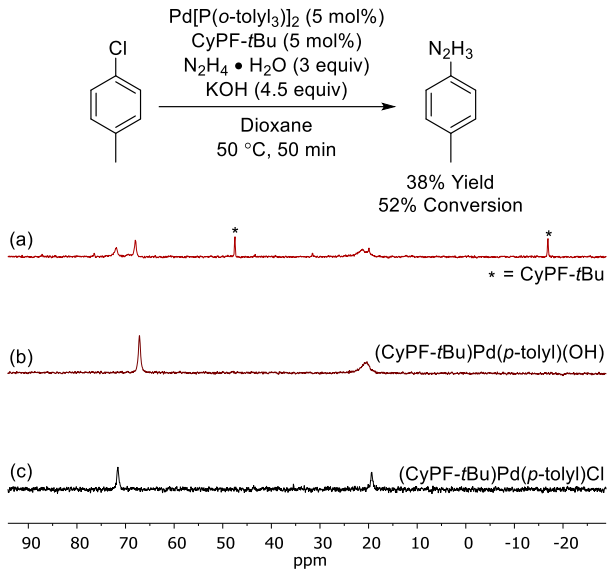

Due to high synthetic value of the palladium-catalyzed C−N coupling reactions of hydrazine and the absence of mechanistic data on this process with any catalyst, we conducted a detailed analysis of the palladium complexes in the system and the rates of the individual steps of the process. We began our mechanistic studies by identifying the resting state of the catalyst, which was determined by analyzing the catalytic reaction of 4-chlorotoluene at partial conversion by ^{31}P NMR spectroscopy. With 4-chlorotoluene as the substrate and at 52% conversion with 5 mol% of catalyst, two palladium species were detected in a 1:1 ratio by ^{31}P NMR spectroscopy (Scheme 5.2). One of these species is the arylpalladium chloride complex resulting from oxidative addition of the chloroarene to CyPF-*t*Bu-ligated Pd(0), (CyPF-*t*Bu)Pd(*p*-tolyl)Cl (**4**), while the other

species was determined to be the aryl hydroxide species **5**, which was synthesized independently (Scheme 5.3). This experiment implies that oxidative addition of the chloroarene to Pd(0) is not the rate-limiting step of the catalytic reaction; rather, the reaction between hydrazine and one or both of these Pd(II) species could be rate-limiting or the reductive elimination of aryl hydrazine from a Pd(II) center after reversible generation of an arylpalladium hydrazido complex could be rate-limiting.

Measurements of the initial rates of the catalytic reaction were conducted with varying concentrations of palladium catalyst, hydrazine monohydrate, and chloroarene. It should be noted that these reactions contain KOH, which acts as a heterogenous base. The catalytic reaction was found to be zero-order in chloroarene and first-order in palladium catalyst and first-order in hydrazine monohydrate. (Figure 5.1). These data also indicate that the oxidative addition of the chloroarene to palladium is not rate-limiting.

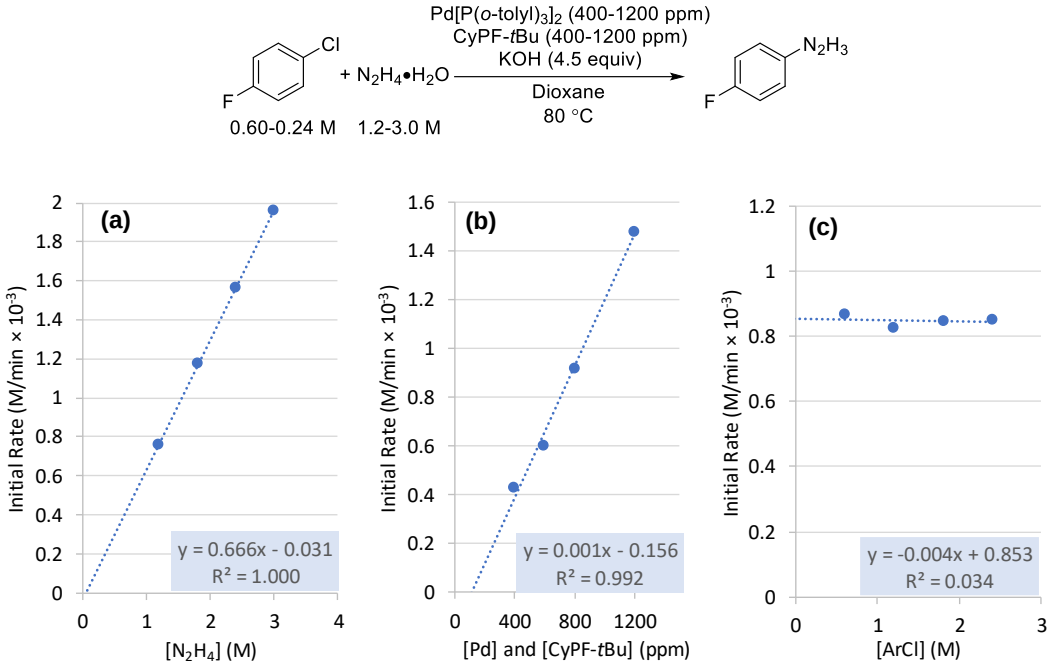

Figure 5.1. (a) Dependence of initial rate on [N_2H_4] (1.2-3.0 M) with [ArCl] = 0.60 M and [Pd] and [CyPF-*t*Bu] = 800 ppm. (b) Dependence of initial rate on [Pd] and [CyPF-*t*Bu] (400-1200 ppm) with [ArCl] = 0.60 M and [N_2H_4] = 1.8 M. (c) Dependence of initial rate on [ArCl] (0.60-2.4 M) with [N_2H_4] = 1.8 M and [Pd] and [CyPF-*t*Bu] = 800 ppm.

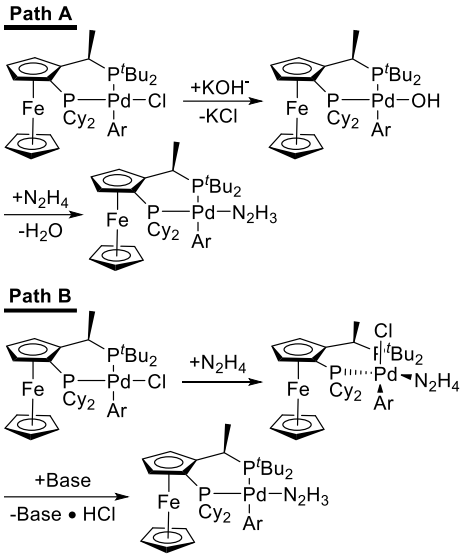

Figure 5.2. Proposed mechanisms for the rate-limiting step of the catalytic reaction.

The rate-limiting step could involve an association between hydrazine and an arylpalladium(II) chloride complex to generate a five-coordinate compound that undergoes deprotonation (Figure 5.2, Path A), an acid-base reaction between hydrazine and an arylpalladium(II) hydroxide compound to generate an arylpalladium(II) hydrazido complex and water (Figure 5.2, Path B), or a combination of these pathways occurring concurrently. All of these scenarios lead to the formation of an arylpalladium(II) hydrazido species that we propose undergoes reductive elimination to give aryl hydrazine. To examine these possible scenarios, we synthesized *p*-tolyl and phenyl palladium(II) hydroxide complexes **5** and **6** by allowing CyPF-*t*Bu to react with $[Pd(PPh)_3(\mu\text{-}OH)(Ar)]_2$ (Ar = *p*-Tol or Ph) (Scheme 5.3). *p*-Tolyl complex **5** reacted with 10 equivalents of hydrazine monohydrate at 65 °C in the presence of PPh_3 to generate (CyPF-*t*Bu)Pd(PPh_3) in quantitative yield, along with *p*-tolyl hydrazine in 85% yield after 45 min (Scheme 5.4). Thus, the aryl hydroxide species generates aryl hydrazine and is catalytically competent. The acid-base reaction between the aryl hydroxide complex and hydrazine to generate an arylpalladium(II) hydrazido complex that undergoes reductive elimination mirrors similar reactions between transition metal hydroxide complexes and amines or thiols to generate water and the corresponding metal amido or thiolate complexes which have been reported by our group and others.[24b, 128]

Scheme 5.3. Synthesis of palladium aryl hydroxide complexes **5** and **6**.

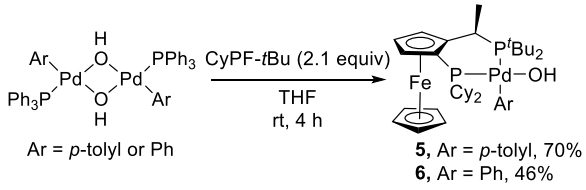

Scheme 5.4. Reaction of arylpalladium(II) hydroxide complex **5** with hydrazine.

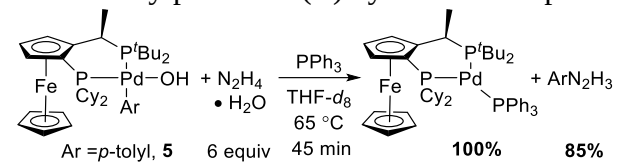

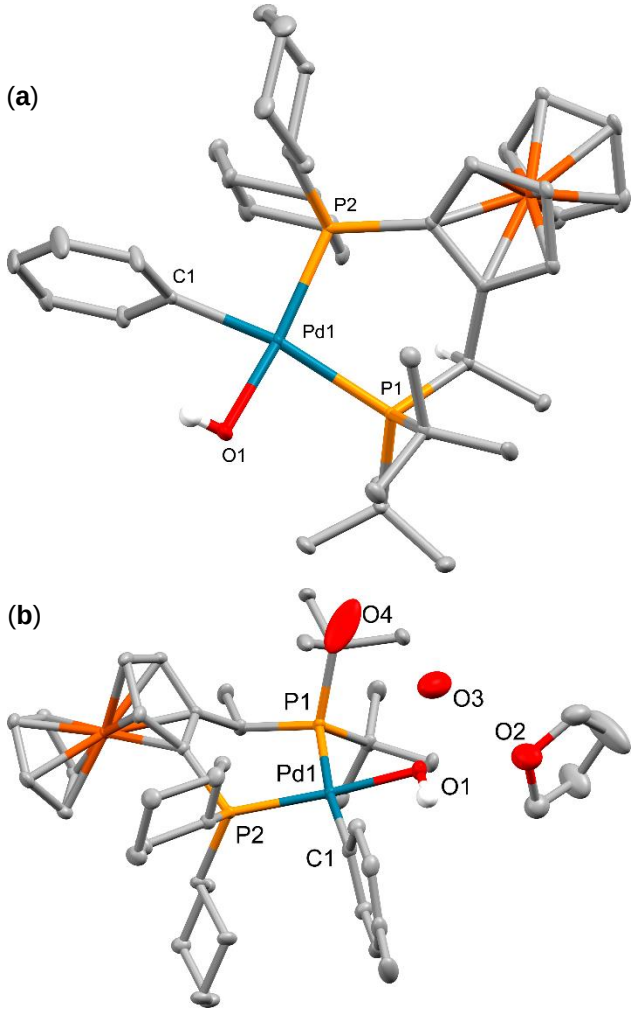

Figure 5.3. (a) ORTEP drawing of (CyPF-tBu)Pd(Ph)(OH) (**6**) with ellipsoids set at 30% and selected hydrogen atoms omitted for clarity. Selected bond lengths (Å): C1-Pd1 2.044(4), O1-Pd1 2.049(4), P1-Pd1 2.3882(11), and P2-Pd1 2.2708(12). Selected bond angles (°): C1-Pd1-O1 82.90(17), C1-Pd1-P2 91.90(13), O1-Pd1-P1 88.71(13), P2-Pd1-P1 97.39(4), O1-Pd1-P2 168.91(12), and C1-Pd1-P1 169.61(12). (b) ORTEP drawing of (CyPF-tBu)Pd(*p*-tolyl)(OH) (**5**) with ellipsoids set at 50% and selected hydrogen atoms omitted for clarity. Selected bond lengths (Å): C1-Pd1 2.055(2), O1-Pd1 2.0571(18), P1-Pd1 2.4156(6), P2-Pd1 2.2808(6), O1-O3 2.819(4), O2-O3 3.062(4), and O3-O4 2.61(2). Selected bond angles (°): C1-Pd1-O1 82.96(9), C1-Pd1-P2 91.42(7), O1-Pd1-P1 90.23(6), P2-Pd1-P1 95.51(2), O1-Pd1-P2 168.91(12), and C1-Pd1-P1 169.61(12).

Monomeric aryl hydroxide palladium complexes bearing CyPF-*t*Bu as ligand have been previously synthesized by our group,[128b] but were not crystallographically characterized. Single

crystals of phenyl hydroxide complex **6** were grown by slow diffusion of pentane into a concentrated solution of **6** in THF at −15 °C. The solid-state structure of aryl hydroxide complex **6** confirms that **6** is a monomeric, square planar complex with a terminal hydroxide ligand. the *p*-tolyl hydroxide complex **5** was crystallized by the diffusion of pentane into a solution of **5** in THF in the presence of 24 equiv of water, and the solid-state structure of complex **5** contains a hydrogen bonding network consisting of one water molecule (O3) interacting with the palladium bound hydroxide group (O1). The Pd-O distance in **5** is a longer 2.057(2) with an O1-O3 distance of 2.819(4) Å (Figure 5.3b). A THF molecule (O2) and an additional water molecule (O4) with 25% occupancy are present in this hydrogen bonding network. The O2-O3 distance is 3.062(4) Å and the O3-O4 distance is 2.61(2) Å. These oxygen-oxygen distances are consistent with hydrogen bonding interactions.[129]

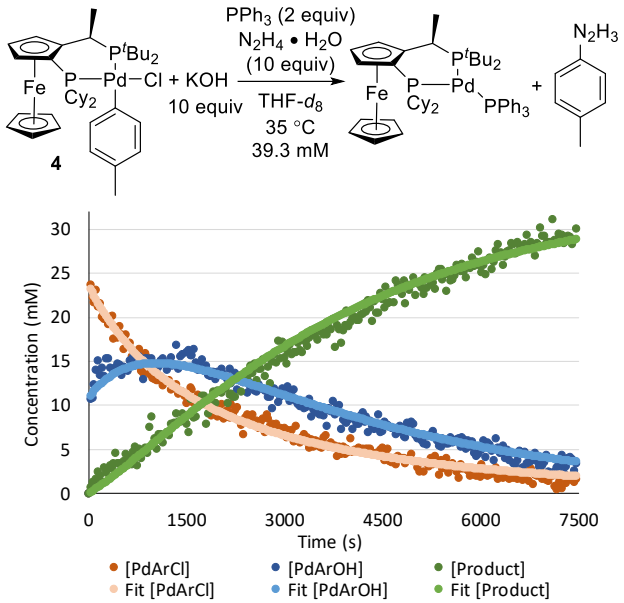

Figure 5.4. Time course of reaction between (CyPF-*t*Bu)Pd(*p*-tolyl)Cl (**4**), hydrazine monohydrate, and KOH monitored by ^{31}P NMR spectroscopy with $PMes_3$ as an internal standard and fitted curves obtained from COPASI. The trace in orange corresponds to the concentration of (CyPF-*t*Bu)Pd(*p*-tolyl)Cl , the trace in blue corresponds to the concentration of (CyPF-*t*Bu)Pd(*p*-tolyl)OH, and the trace in green corresponds to the concentration of (CyPF-*t*Bu)Pd(PPh_3).

We conducted further studies to determine if aryl hydrazine could be generated by reaction between hydrazine and chloride complex **4** by path A or B (Figure 5.2), or a combination of these pathways. We studied the viability of these pathway by conducting stoichiometric reactions with arylpalladium chloride complex **4** with hydrazine monohydrate in the presence of KOH.

It should be noted that the conversion of chloride complex **4** to aryl hydroxide complex **5** does not reach equilibrium at the beginning of these stoichiometric reactions due to the heterogeneous reaction between a soluble palladium complex and an insoluble hydroxide salt. Consistent with this proposal, the stoichiometric reaction between chloride complex **4** and tetrabutylammonium (TBA) hydroxide, a soluble source of hydroxide anion, quantitatively generates aryl hydroxide complex **5** at room temperature within 5 minutes in THF (Scheme 5.5a). However, when chloride complex **4** is mixed with 10 equiv of KOH and 10 equiv of hydrazine monohydrate at room temperature, chloride complex **4** is converted to aryl hydroxide complex **5**

more slowly (Scheme 5.5b). A time course of this reaction by ^{31}P NMR spectroscopy indicated that complete conversion of chloride complex **4** to aryl hydroxide species **5** was obtained after 23 min (see Supporting Information). However, aryl hydroxide complex **5** does not react with 5 equiv of TBA(Cl) at room temperature, and chloride complex **4** was not detected after 1 h by ^{31}P NMR spectroscopy under these conditions (Scheme 5.5c). Thus, the formation of aryl hydroxide complex **5** from chloride complex **4** is faster than the reverse of that reaction, and the equilibrium between chloride complex **4** and aryl hydroxide **5** favors the aryl hydroxide complex **5**. At room temperature, aryl hydrazine was not formed in these experiments. We propose that this salt metathesis reaction is possible in organic solvent because hydrazine and water aids in the solvation of potassium hydroxide through dipole-ion interactions. Our group has previously demonstrated that arylpalladium(II) hydroxide compounds react reversibly with soluble halide salts to generate arylpalladium(II) halide complexes.[130]

Scheme 5.5. Reactions of arylpalladium(II) chloride complex **4** with hydroxide sources and reactions of arylpalladium(II) hydroxide complex **5** with KCl.

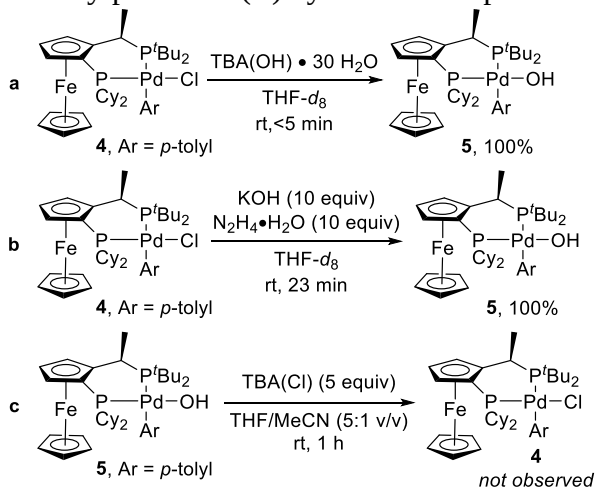

The reaction between chloride complex **4**, hydrazine monohydrate, and KOH was monitored by ^{31}P NMR spectroscopy. The chloride complex **4** converted to approximately 31% of the aryl hydroxide complex **5** upon mixing. After 50 min at 35 °C, this reaction gave the aryl hydrazine product in 89% yield and the Pd(0) complex (CyPF-*t*Bu)Pd(PPh$_3$). A close examination of the reaction time course revealed a kinetic profile for the concentration of the aryl hydroxide complex that did not follow an exponential decay (blue dotted trace, Figure 5.4). The concentration of this species initially increased and then decreased; this behavior is consistent with pathway A. The fast conversion of the chloride complex to an aryl hydroxide complex and a subsequent reaction between the aryl hydroxide complex and hydrazine at a rate that is similar to that of the reaction between the chloride complex and potassium hydroxide would lead to an increase in the concentration of the aryl hydroxide complex at the outset of the reaction followed by a decay of the aryl hydroxide compound. Simulation of this scenario to the experimental data on the concentration of palladium complexes vs. time with the modelling program COPASI[131] gave an excellent fit (Figure 5.4), which is consistent with our observation of an arylpalladium(II) chloride and an arylpalladium(II) hydroxide complex as the catalyst resting state species (Scheme 5.2). An alternative pathway that cannot be ruled out is that paths A and B (Figure 5.2) occurred concurrently in this experiment, and simulation of this scenario by COPASI also gives a good fit

to the rate data. Thus, we conducted further experiments to determine the mechanistic scenario that leads to the formation of aryl hydrazine.

Competition Experiments Involving the Resting States of the Catalyst

To assess the reactivity of the catalyst resting states further and to determine the mechanism of the formation of aryl hydrazine, we conducted competition experiments involving the reaction of chloride complex **4** or aryl hydroxide complex **5** with hydrazine and aryl hydrazine. We compared the selectivity from these reactions to those of similar competition experiments between hydrazine and aryl hydrazine in the catalytic reaction. The catalytic reaction of 1-*t*Bu-4-chlorobenzene with one equivalent of hydrazine monohydrate and one equivalent of 4-methylphenyl hydrazine with 1,3,5-trimethoxybenzene as an internal standard formed a 5:1 ratio of 4-*t*Bu-phenyl hydrazine to the 1,1-diaryl hydrazine at 69% conversion of the chloroarene, as determined by ^{1}H NMR spectroscopy (Scheme 5.6). A similar competition experiment performed by Stradiotto demonstrated that hydrazine also reacts preferentially over phenyl hydrazine with a palladium catalyst ligated by MorDalPhos.[31b]

Scheme 5.6. Competition experiment between hydrazine and *p*-tolyl hydrazine under catalytic conditions.

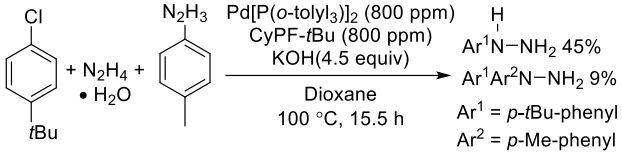

In contrast to this 5:1 ratio of products from the catalytic reaction of the two hydrazines together, the stoichiometric reaction of aryl hydroxide compound **5** with 2 equiv of hydrazine and *p*-tolyl hydrazine formed nearly equal amounts of the two coupled products showing that complex **5** reacts with hydrazine and aryl hydrazine with nearly identical rates (Scheme 5.7). This result does not match the high selectivity for monoarylation that we observe in the catalytic reaction (Table 5.1 and Scheme 5.6). This low selectivity implies that the primary pathway for the formation of aryl hydrazine likely occurs by a palladium complex other than aryl hydroxide complex **5**, even though **5** is capable of generating aryl hydrazine by reaction with hydrazine (Scheme 5.4).

Scheme 5.7. Competition experiment between hydrazine and *p*-tolyl hydrazine with aryl hydroxide complex **5**.

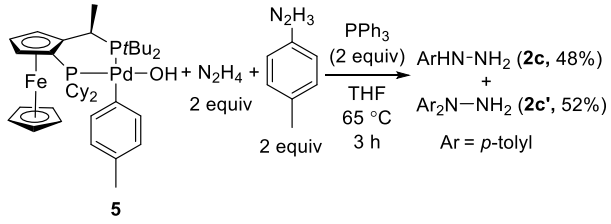

Table 5.2. Competition experiments between hydrazine and *p*-tolyl hydrazine with chloride complex **4**.

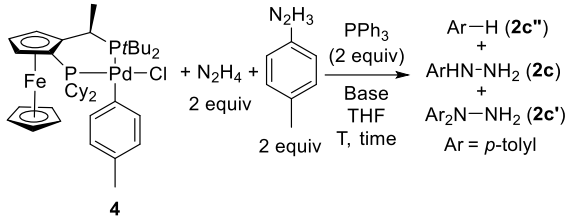

Entry	Base (equiv)	T (°C)	Time (min)	Yield (%)		
				2c	**2c'**	**2c"**
1	NaO*t*Bu (1.3)	25	10	93	4	3
2	LiHMDS (1.3)	25	10	87	6	8
3	KOH (10)	65	180	35	34	30

In contrast to the reaction of aryl hydroxide complex **5**, the reaction of chloride complex **4** with the same mixture of hydrazine and aryl hydrazine in the presence of NaO*t*Bu or LiHMDS occurred with high selectivity for the monoaryl hydrazine (Table 5.2, entries 1-2). The reactions with KOH in place of these bases, again, generated diaryl hydrazine and monoaryl hydrazine in approximately equal amounts and in nearly equal yield with toluene (Table 5.2, entry 3). Although chloride complex **4** could react with NaO*t*Bu to form an arylpalladium alkoxide complex,[128b] which could undergo reaction with hydrazine akin to aryl hydroxide complex **5**, this salt metathesis reaction to form an adduct between palladium and base is less likely to occur with LiHMDS, due to the steric bulk of this base and the ancillary ligands of chloride complex **4**, and the reaction with the silylamide base occurred with selectivity that is nearly identical to that from reaction with NaO*t*Bu. Thus, we propose that the formation of aryl hydrazine from chloride complex **4** with NaO*t*Bu or LiHMDS as base occurs by path B in Figure 5.2 and reactions by this pathway are highly selective for the monoarylation of hydrazine.

Because the selectivity of aryl hydroxide complex **5** for reaction with hydrazine over aryl hydrazine was lower than the reactions of chloride complex **4** through path A, we propose that monoaryl hydrazine is predominantly produced in the catalytic process by reaction of chloride complex **4** through Path A. If so, then the deprotonation of hydrazine coordinated to chloride complex **4** by hydroxide base (Figure 5.2, Path B) must be faster than the reaction of aryl hydroxide complex **5** with hydrazine (Figure 5.2, Path A), and the formation of the diaryl hydrazine products in the catalytic reaction would originate from the reaction between aryl hydrazine and an aryl hydroxide complex.

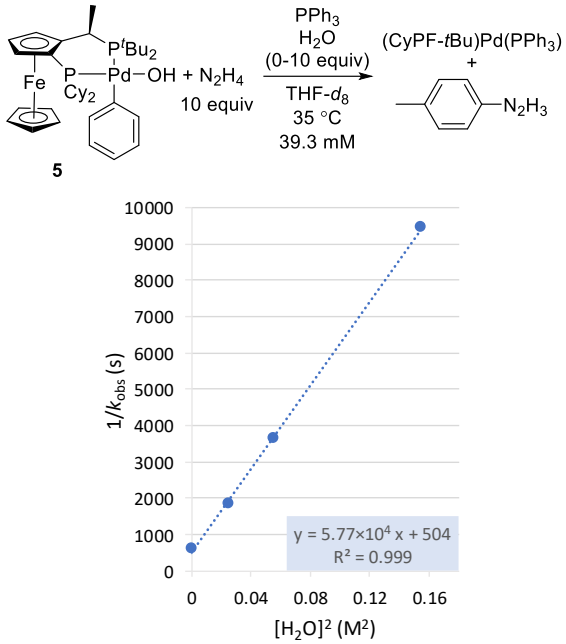

Figure 5.5. Dependence of the reciprocal of the observed rate constant $1/k_{obs}$ (s^{-1}) on $[H_2O]^2$ (0-0.155 M^2) with [**5**] = 0.0393 M in THF-d_6 at 35 °C.

To gauge whether the reaction of aryl hydroxide complex **5** and hydrazine is faster or slower than reaction of chloride complex **4**, we monitored the reaction of **5** with hydrazine. The rate of reaction of hydrazine monohydrate with aryl hydroxide complex **5** to form *p*-tolyl hydrazine was much slower than the reaction of anhydrous hydrazine. The reaction between aryl hydroxide complex **5** and hydrazine monohydrate occurred with an observed rate constant of 1.06×10^{-4} s^{-1}, while the same reaction with anhydrous hydrazine occurred with an observed rate constant of 1.65×10^{-3} s^{-1}, which is approximately 15 times faster than the reaction with hydrazine hydrate (Figure 5.5). A closer examination of the effect of water on the rate of the reaction between aryl hydroxide complex **5** and hydrazine indicated that this reaction was inverse second-order in the concentration of water (Figure 5.5). We propose that aryl hydroxide complex **5** forms a hydrogen bonding network containing multiple water molecules interacting with the hydroxide ligand, such as the one seen in its solid-state structure (Figure 5.3b), and reversibly dissociates two water molecules to reveal a bare palladium hydroxide complex that undergoes reaction with hydrazine. Arylpalladium(II) hydroxide complexes have been demonstrated by Goldberg to form strong hydrogen bonding networks with water, and these interactions are present even in solution.[132]

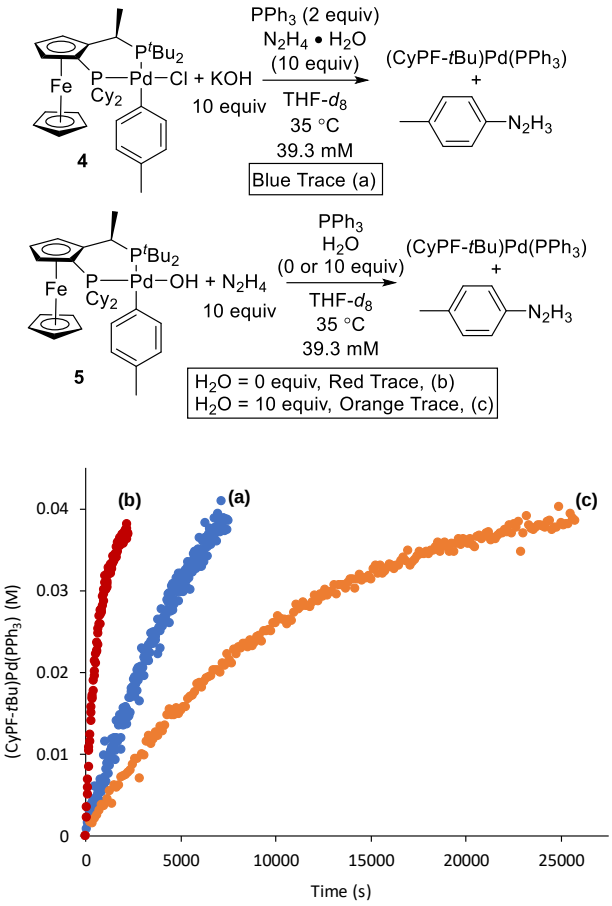

Figure 5.6. Comparison of rates of product formation for the reaction of arylpalladium(II) chloride complex **4** (39.3 mM) with KOH (10 equiv), hydrazine monohydrate (10 equiv), and PPh_3 (2 equiv) (a), the reaction of arylpalladium(II) hydroxide complex **5** (39.3 mM) with anhydrous hydrazine (10 equiv) and PPh_3 (2 equiv) (b), and the reaction of arylpalladium(II) hydroxide complex **5** (39.3 mM) with hydrazine monohydrate (10 equiv) and PPh_3 (2 equiv) (c) in 600 µL of THF-d_8 at 35 °C.

These data suggest that the inhibiting effect of water on the reaction between hydrazine and aryl hydroxide complex **5** causes the product distribution to result from reaction by Path B in Figure 5.2. To assess this hypothesis, we studied the relative rates of the stoichiometric reactions of the arylpalladium halide and hydroxo complexes with components of the catalytic system. The rates were determined by monitoring the formation of (CyPF-*t*Bu)Pd(PPh_3) from the reaction of aryl hydroxide complex **5** with anhydrous hydrazine or hydrazine monohydrate and the reaction of chloride complex **4** with KOH and hydrazine monohydrate. The reaction of aryl hydroxide complex **5** with hydrazine monohydrate (Figure 5.6, orange trace) occurred with a rate constant of 8.3(2) $\times 10^{-4}$ s^{-1} whereas the reaction of aryl hydroxide compound **5** with anhydrous hydrazine (Figure 5.6, red trace) occurred with a much larger rate constant of 1.6(1) $\times 10^{-3}$ s^{-1}. The reaction of chloride complex **4** with 10 equiv of hydrazine monohydrate and 10 equiv of KOH occurred with a rate constant of 2.9(1) $\times 10^{-4}$ s^{-1}, which lies between the rate constants of the two reactions of the hydroxo complex with anhydrous hydrazine and hydrazine hydrate (Figure 5.6a, blue trace) and shows that that the formation of aryl hydrazine by reaction of hydrazine and base with chloride

complex **5** is faster than the reaction of hydrazine and aryl hydroxide complex **4** when water is present. Because the coupling reactions with hydroxide base contain water, we assert that the formation of aryl hydrazine in the catalytic system occurs primarily by a pathway involving the deprotonation of hydrazine bound to an arylpalladium(II) halide complex (Figure 5.2, path B), rather than by the reaction of an arylpalladium(II) hydroxide complex and hydrazine (Figure 5.2, path A).

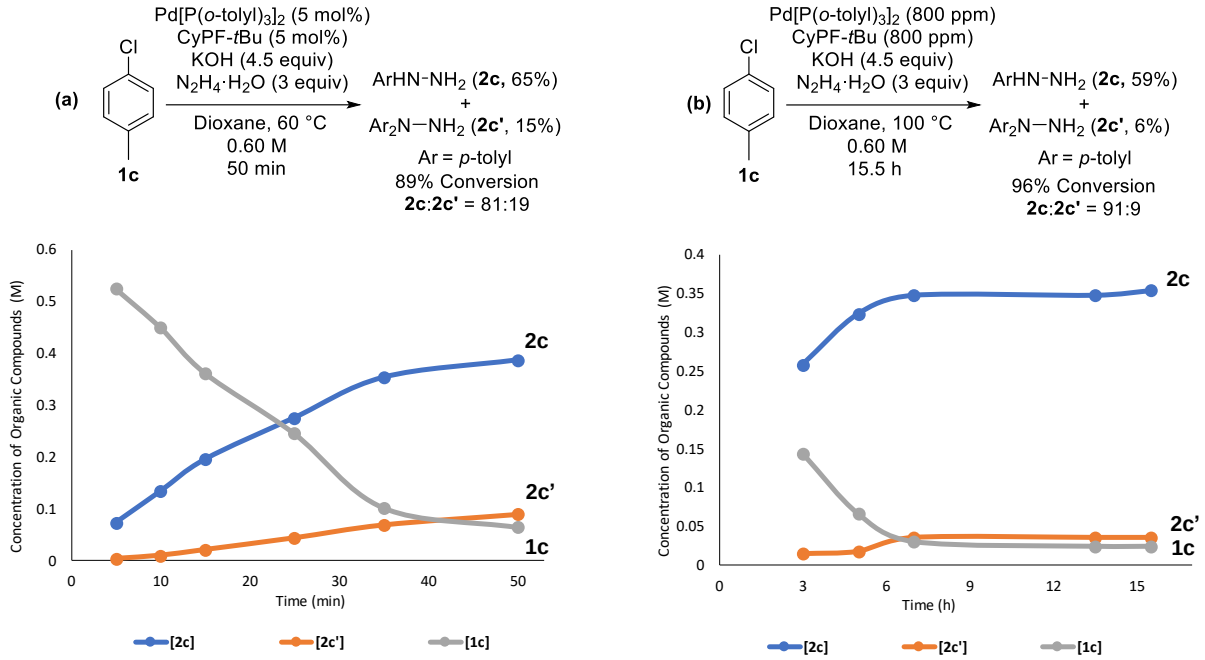

Figure 5.7. (a) Time course of the Pd-catalyzed C-N coupling reaction of *p*-chlorotoluene (**1c**) and hydrazine with 5 mol% of Pd catalyst at 60 °C for 50 min. (b) Time course of the Pd-catalyzed C-N coupling reaction of *p*-chlorotoluene (**1c**) and hydrazine with 800 ppm of Pd catalyst at 100 °C for 15.5 h.

The selectivity of the reaction for formation of monoarylation and diarylation products depended on the catalyst loading. The selectivity of the reaction of 4-chlorotoluene at 100 °C over 15.5 h with 800 ppm of catalyst was 91:9 at 96% conversion (Figure 5.7b). This value is higher than the ratio of 81:19 at 89% conversion with 5 mol % catalyst at 60 °C for 50 min (Figure 5.7a). While there are many variables concerning this reaction with a heterogeneous base at varying concentrations and temperatures, a potential explanation for this higher selectivity for the reaction at lower catalyst loading is due to the combination of the relative stability of the arylpalladium halide and hydroxo complexes and their selectivity presented above. Aryl hydroxide complex **6** is unstable at high temperatures (>80 °C). Thus, we propose that the aryl hydroxide complex undergoes decomposition at low catalyst loadings and contributes less to the formation of the aryl hydrazine than it does at lower temperatures, thereby reducing the generation of diarylated products by reaction by Path A (Figure 5.2). More quantitatively, the decomposition of aryl hydroxide complex **5** at 100 °C in a mixture of 1,4-dioxane and THF by ^{31}P NMR spectroscopy in the presence of 3.3 equiv of *p*-chlorotoluene to trap Pd(0) formed by the decomposition occurred with a rate constant of 1.8×10^{-4} s^{-1} (see Supporting Information), which corresponds to a half-life of about 1 h versus the approximately 8 h time of the overall reaction. Therefore, this

decomposition of aryl hydroxide complex **5** can remove aryl hydroxide intermediates from the catalytic cycle and generate the corresponding aryl chloride complex by the formation of Pd(0). Combined, these factors enhance the presence of the arylpalladium chloride complex and reaction of hydrazine by reaction by Path B (Figure 5.2), thereby increasing the selectivity for monoarylation versus diarylation.

Determination of the Rate-Limiting Step of Catalysis

Having established that the catalytic reaction occurs primarily through an aryl chloride complex like complex **4**, we conducted experiments to determine the rate-limiting step of the catalytic reaction. Based on our initial-rate data, the rate-limiting step of the catalytic reaction could be deprotonation of hydrazine to give an arylpalladium(II) hydrazido species or reductive elimination of aryl hydrazine after reversible deprotonation of hydrazine to form the arylpalladium hydrazido species. If deprotonation of hydrazine is rate limiting, then a primary KIE would be expected for reactions with hydrazine and deuterated hydrazine. If reductive elimination of aryl hydrazine is rate-limiting, then a secondary or equilibrium KIE would be observed. Under this scenario, the secondary KIE would arise from the deuterium on the α-nitrogen atom of the hydrazido group. Initial rates of the reaction of hydrazine-d_4 monodeuterate and potassium deuteroxide as base with **1b** as chloroarene versus those in parallel with protiated hydrazine monohydrate, and potassium hydroxide revealed a primary KIE of 3.7(7). This value is consistent with rate-limiting deprotonation of hydrazine (Scheme 5.8).

Scheme 5.8. KIE of the reaction of **1b** with hydrazine and KOH from reactions in separate vessels.

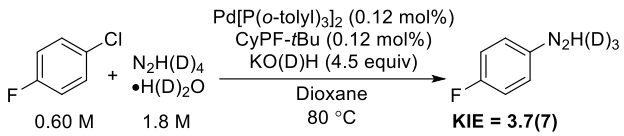

To assess our conclusions from our KIE measurement experiment further, we conducted DFT computations. More specifically, we sought to determine the free energies arylpalladium(II) hydrazido species containing unsubstituted and phenyl substituted hydrazido ligands and the barriers for reductive elimination of mono- or diaryl hydrazine from these compounds. We computed the structures and energies of phenylpalladium(II) α-phenyl hydrazido compound **INT-1α** and β-phenyl hydrazido compound **INT-1β** and their transition states for reductive elimination, **TS-1α** and **TS-1β** using a solvent continuum modelling 1,4-dioxane (Figure 5.8). The energies of these species were compared to those involving the unsubstituted hydrazido complex **INT-**1 and **TS-1**. The energies of the α and β phenyl substituted hydrazido compounds **INT-1α** and **INT-1β** are lower than that of the unsubstituted arylpalladium(II) hydrazido complex **INT-1** by 4.5 and 2.1 kcal/mol, respectively. The energy of the transition state for reductive elimination to generate 1,1-diphenyl hydrazine was the lowest with a barrier of 19.6 kcal/mol. For comparison, the energy of the transition state for the generation of phenyl hydrazine and 1,2-diphenyl hydrazine was computed to be 22.3 and 23.4 kcal/mol, respectively. All reactions to form di- or monophenyl hydrazine and (CyPF-*t*Bu)Pd (**INT-2**, **INT-2α**, **INT-2β**) are exothermic. From least to greatest, the reaction to form phenyl hydrazine is the least exothermic (−15.6 kcal/mol), followed by reaction to form 1,1-diphenyl hydrazine (−21.8 kcal/mol) and 1,2-diphenyl hydrazine (−30.8 kcal/mol).

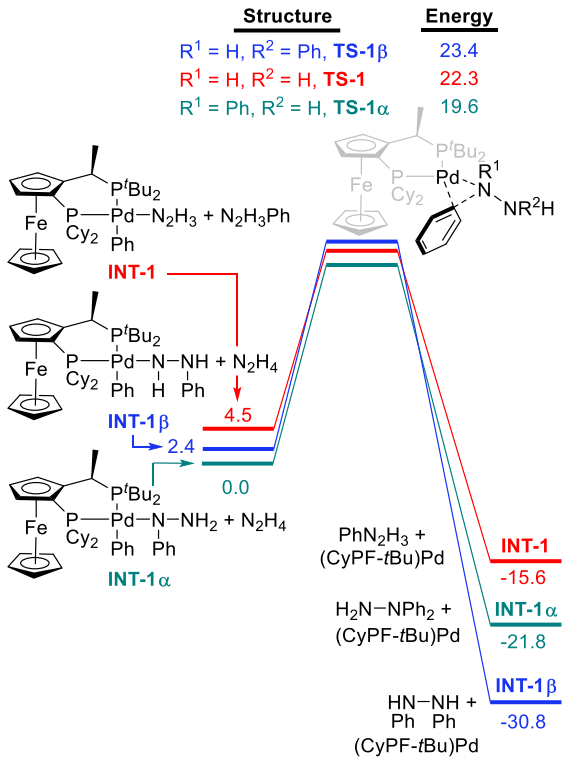

Figure 5.8. DFT calculated intermediates and transition states for unsubstituted and phenyl substituted hydrazido complexes in 1,4-dioxane. All values are Gibbs free energy in kcal/mol.

These computational data suggest that the formation of 1,1-diphenyl hydrazine is more kinetically and thermodynamically favorable than formation of monoaryl hydrazine when starting from their respective hydrazido complexes. In addition, the formation of 1,1-diphenyl hydrazine is expected to be favored if the hydrazido complexes are able to interconvert by reaction with hydrazine or phenyl hydrazine, due to the greater stability of the hydrazido complex containing an α-phenyl group on the hydrazine. By experiment, we observe predominant formation of monoaryl hydrazine in the catalytic reaction. Thus, these DFT calculations imply that the selectivity for formation of the monoaryl hydrazine product does not arise from the barriers for reductive elimination to form the C-N bond or from the relative stabilities of the arylpalladium hydrazido intermediates. Instead, the selectivity would arise from the relative barriers for formation of the hydrazido complexes. This conclusion is consistent with the observed primary kinetic isotope effect for reaction of hydrazine-d_4. This origin of selectivity for the monoarylation of hydrazine contrasts with that for the monoarylation of ammonia with the same palladium catalyst. Mechanistic studies on the coupling of aryl halides with ammonia revealed that the selectivity for monoarylation of ammonia results from both the faster generation and the greater stability of the arylpalladium amido complex that contains an unsubstituted amido ligand, relative to that of a complex containing an aryl substituted amido ligand.[24d]

Synthesis and Reactivity of an Arypalladium(II) Hydrazido Complex

Scheme 5.9. Synthesis of arylpalladium(II) hydrazido complex **8** and subsequent reductive elimination to obtain aryl hydrazine.

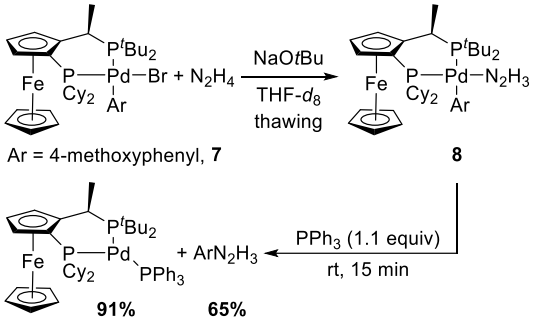

Our mechanistic proposal hinges on the intermediacy of an arylpalladium(II) hydrazido intermediate that undergoes reductive elimination to generate aryl hydrazine. Because these palladium complexes have not been synthesized and their reactivity determined directly, we sought to synthesize and characterize this hydrazido complex. Aryl palladium(II) hydrazido complex **8** was synthesized by the reaction of 4-methoxyphenylpalladium(II) bromide complex **7** and hydrazine in the presence of NaO*t*Bu in thawing THF (Scheme 5.9). At −30 °C, we observed a pair of doublets in the ^{31}P NMR spectrum at 59.1 ppm and 41.7 ppm with J = 42 Hz, corresponding to hydrazido complex **8**. A broad resonance at 2.48 ppm in the ^{1}H NMR spectrum with an integration of three protons corresponds to those of the hydrazido ligand. This assignment was based on a ^{1}H-^{15}N HSQC experiment, and this integration value is consistent with a -N_2H_3 hydrazido ligand. We were unable to determine the yield of hydrazido complex **8** accurately by NMR spectroscopy due to the limited solubility of **8** in THF-d_8 at −30 °C.

To characterize the hydrazido complex **8** further, the synthesis of **8** was repeated with ^{15}N-labelled hydrazine. NMR spectroscopic data were obtained at −60 °C to hinder decomposition of **8**. The chemical shifts of signals in the ^{1}H and ^{31}P NMR spectra obtained at this temperature did not differ significantly from those obtained at −30 °C. The broad singlet observed at 2.48 ppm in the ^{1}H NMR spectrum of the unlabeled compound was observed as two broad singlets (J = 64 Hz) in the spectrum of the ^{15}N labeled compound, which is consistent with $^{1}J(^{1}\text{H},^{15}\text{N})$ coupling,[133] and the ^{31}P NMR spectrum of the labeled compound consisted of a doublet at 58.8 ppm (J = 42 Hz) and a doublet of doublets at 12.9 ppm (J = 41, 20 Hz). The resonance at 58.8 ppm corresponds to the di-*t*butylphosphino moiety of CyPF-*t*Bu, and the absence of coupling to ^{15}N is consistent with the small *cis* $^{2}J(^{15}\text{N},^{31}\text{P})$ coupling in square planar metal complexes.[24d, 134] Thus, the coupling constant of 20 Hz in the resonance at 12.9 ppm corresponds to *trans* $^{2}J(^{15}\text{N},^{31}\text{P})$ coupling between the hydrazido ligand and the dicyclohexylphosphino group of CyPF-*t*Bu. At the same temperature, the ^{15}N NMR spectrum of **8**, which was obtained by an INEPT experiment, consisted of a single doublet at 77.2 ppm. The coupling constant observed in this resonance, J = 8.5 Hz, is similar to reported $^{1}J(^{15}\text{N},^{15}\text{N})$ coupling constants.[135] The *trans* $^{2}J(^{15}\text{N},^{31}\text{P})$ coupling of 20 Hz was not detected in the ^{15}N NMR spectrum, and this lack if coupling can be explained by a dynamic process by which a fast exchange of nitrogen atoms in the hydrazido ligand occurs (*vide infra*). These data indicate that all the protons and nitrogen atoms in the hydrazido ligand are equivalent.

Although it is unexpected that all protons and nitrogen atoms of the hydrazido ligand are observed as a single resonance in the ^{1}H and ^{15}N NMR spectra, we propose that hydrazido complex

8 undergoes an intramolecular exchange process that makes these hydrogen and nitrogen atoms equivalent. This proposal is based on a structurally related hydrazido complex synthesized by Schrock, WCp*Me_4(N_2H_3),[136] which contains an η^2-bound hydrazido ligand. The protons and the nitrogen atoms of the hydrazido ligand of WCp*Me_4(N_2H_3) undergo an exchange process and are equivalent at 0 °C and −10 °C, respectively. At these temperatures, $\Delta G^{\ddagger}$ for the exchange process was measured to be 12.7 kcal/mol for the N-H protons and 11.1 kcal/mol for the nitrogen atoms of the hydrazido moiety. At −80 °C, this exchange process for WCp*Me_4(N_2H_3) was slow on the NMR time scale and discrete resonances for the N-H protons and nitrogen atoms of WCp*Me_4(N_2H_3) were observed by NMR spectroscopy. On the basis of spin-saturation transfer experiments, Schrock proposed that this exchange process takes place by a rapid 1,2-shift of the hydrogen atoms on the hydrazido ligand along with a conversion in the binding mode of the hydrazido ligand from an η^2-binding mode to an η^1-mode and back to an η^2-mode. When palladium hydrazido complex **8** was cooled to −100 °C in THF-d_8, only one signal was observed by ^{15}N NMR spectroscopy, which indicates that the exchange process in palladium complex **8** occurs faster than the one in WCp*Me_4(N_2H_3). Because palladium complex **8** also contains equivalent protons and nitrogen atoms, we propose an exchange process, like that proposed by Schrock for WCp*Me_4(N_2H_3), occurs in palladium hydrazido complex **8**, wherein the hydrogen atoms of the hydrazido ligand undergo 1,2-shifts along with a conversion in binding mode of the hydrazido ligand from an η^1- to an η^2-binding mode by the formation of a transient five-coordinate palladium(II) complex.

Warming of the hydrazido complex **8** to room temperature generated palladium black and *p*-methoxyphenyl hydrazine within two minutes. This rapid reductive elimination at room temperature precluded isolation of the hydrazido complex. Generation of this complex in the presence of PPh_3 and warming to room temperature gave (CyPF-*t*Bu)Pd(PPh_3) in 91% yield, along with *p*-methoxyphenyl hydrazine in 65% yield (Scheme 5.9).

Scheme 5.10. Proposed catalytic cycle for the synthesis of aryl hydrazine.

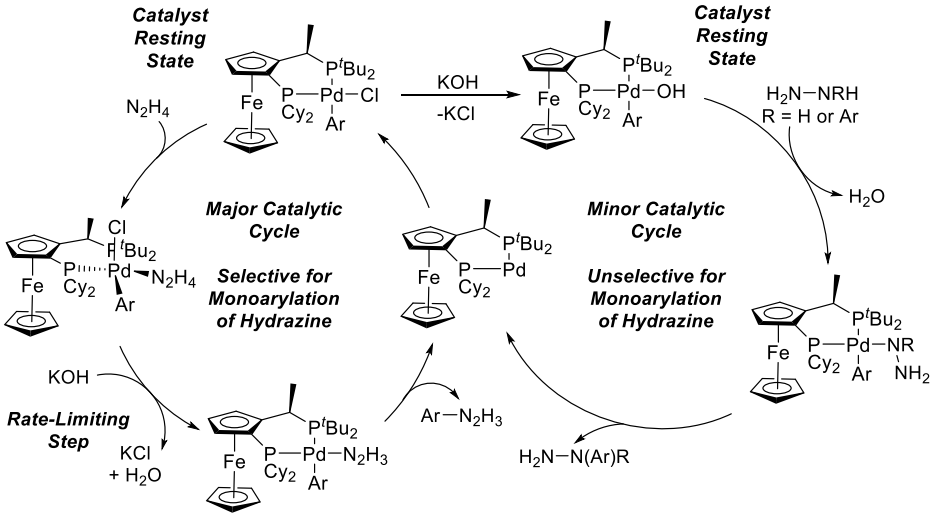

We conclude that the catalytic reaction proceeds by a rate-limiting reaction between hydrazine bound to an arylpalladium(II) halide complex and base to generate an arylpalladium(II) hydrazido complex, which undergoes facile reductive elimination to give aryl hydrazine (Scheme 5.10). Independent synthesis and stoichiometric reactions of the aryl palladium(II) hydroxide,

chloride, and hydrazido complexes demonstrate that the chloride and hydroxide complexes lead to the formation of aryl hydrazine by reaction with hydrazine and the hydrazido complex generates aryl hydrazine by reductive elimination. Kinetic data are consistent with this proposal. The catalytic reaction is first-order in concentration of palladium catalyst and hydrazine and zero-order in concentration of aryl halide. Our mechanistic experiments indicate that the reaction between a palladium aryl halide complex, base, and hydrazine selectively generates monoaryl hydrazine because reaction of the arylpalladium(II) chloride intermediate with hydrazine and base to form the parent hydrazido complex is faster than reaction with aryl hydrazine to form the corresponding 1- or 2-aryl hydrazido complex. The kinetic isotope effect indicates that formation of the hydrazido complex is irreversible and rate limiting, and this conclusion is consistent with our computational studies indicating that the relative thermodynamic stabilities of these hydrazido complexes and the barriers for the reductive elimination of mono- or diaryl hydrazine from these palladium species would lead to selectivity that is different form that observed. An arylpalladium(II) hydroxide and halide complexes were observed in the catalytic reaction; the aryl hydroxide complex forms by salt metathesis between the observed arylpalladium(II) complex and KOH. The aryl hydroxide complex is catalytically competent to be an intermediate, but it reacts with hydrazine hydrate more slowly than the corresponding arylpalladium(II) chloride complex reacts with hydrazine and base and is unselective for the monoarylation of hydrazine. Due to the high selectivity for the formation of monoaryl hydrazine product, the catalytic cycle involving the arylpalladium(II) hydroxide complex is slower than that involving the arylpalladium(II) chloride complex.

5.3. Conclusion

We have developed a C−N cross-coupling reaction between aryl- and heteroaryl chlorides and bromides with hydrazine to generate aryl hydrazines. This reaction occurs with low loadings of catalyst (100-1600 ppm) and occurs with an inexpensive hydroxide base. Under these conditions, several aryl hydrazine intermediates for agrochemicals were synthesized by this method. Mechanistic studies show that the reaction between hydrazine, base, and an arylpalladium(II) chloride complex to generate an arylpalladium(II) hydrazido complex is rate-limiting. Moreover, the origin of selectivity for the monoarylation of hydrazine was proposed to be due to a lower barrier for deprotonation of hydrazine in comparison to aryl hydrazine. The arylpalladium(II) hydroxide complex forms alongside the arylpalladium(II) halide complex, and reactions by the aryl hydroxide complex were unselective for the monoarylation of hydrazine. We have also synthesized the first example of an arylpalladium(II) hydrazido complex and demonstrated that it undergoes reductive elimination to generate aryl hydrazine. Future developments in this area will involve the design of improved systems that can catalyze C−N coupling reactions with classes of amines that contain N-heteroatom bonds.

5.4. Experimental

General Experimental Procedures

-CAUTION-

Hydrazine is highly toxic and should be handled with proper personal protection equipment (gloves, lab coat, and safety glasses) and handled in a well-ventilated fume hood or a hermetically sealed glovebox. When hydrazine was used in a glovebox, the glovebox was purged for at least 5 min prior to cycling any objects out of the glovebox antechambers, and at least 15 min to purge hydrazine from the atmosphere of the glovebox. Bear in mind that gloveboxes vary in volume and purge rates, and our procedures are not globally applicable. All hydrazine contaminated waste generated in a glovebox was kept in a sealed, secondary container in order to minimize exposure to hydrazine when waste was taken out of a glovebox. *Hydrazine smells like ammonia. The odor threshold is on the order of 1 ppm, which exceeds daily permissible exposure limits as set by various safety organizations.*

Hydrazine can also explode in the presence of elevated temperatures and oxygen, and this reaction is catalyzed by transition metals. *Oxygen must be excluded from reactions.* Moreover, hydrazine can explode in the presence of certain transition metals by forming explosive metal complexes or the metal catalyzes the decomposition of hydrazine into nitrogenous gases. Hydrazine contaminated glassware can be cleaned with a dilute, aqueous bleach solution to neutralize hydrazine, *but care must be taken as this leads to a vigorous, exothermic reaction that generates gases*. All other hydrazine contaminated waste was kept in a secondary container and submitted to waste management services as is.

In our hands, no explosions occurred during this study; however, many of the reactions in this work occur in closed systems and should be performed behind a blast shield.

All manipulations were conducted under a nitrogen atmosphere in a glovebox or on a Schlenk manifold unless otherwise stated. ^{1}H, ^{19}F, ^{13}C, ^{15}N, and ^{31}P NMR spectra were recorded on a Bruker 400, 500, 600, 700, or 900 MHz spectrometer. All ^{1}H chemical shifts are reported in parts per million relative to tetramethylsilane or residual protiated solvent as a reference, ^{13}C chemical shifts are reported in parts per million relative to the solvent as a reference, ^{31}P NMR chemical shifts are reported in parts per million relative to an 85% H_3PO_4 external standard, ^{19}F NMR chemical shifts are reported in parts per million relative to a $CFCl_3$ external standard, and all ^{15}N NMR chemical shifts are reported in parts per million relative to an NH_3 external standard. Elemental analyses were obtained at the Microanalytical Facility at the University of California, Berkeley. ESI-MS analyses were obtained at the Lawrence Berkeley National Laboratory Catalysis Facility on a Perkin Elmer ESI-MS instrument. X-ray crystal structures were obtained at the Small Molecule X-ray Crystallography Facility at the University of California, Berkeley. No-D NMR spectroscopic analyses were performed by the method outlined by Hoye.[137]

Pd(P(*o*-tolyl)$_3$)$_2$,[138] [(PPh$_3$)Pd(Ph)(μ-OH)]$_2$,[24b] (CyPF-*t*Bu)Pd(4-methylphenyl)(OH) (5),[128b] (CyPF-*t*Bu)Pd(4-methoxyphenyl)Br,[24d] and (CyPF-*t*Bu)Pd(4-methylphenyl)Cl (4)[128b] were synthesized by previously reported procedures. All glassware was dried in an oven at 130 ºC

for at least 12 hours. All liquid (hetero)aryl halides were purchased from commercial sources, and sparged briefly with nitrogen before use. All deuterated solvents were purchased from Cambridge Isotopes, freeze-pump-thawed thrice, and stored over molecular sieves for at least 12 hours before use. $^{15}N_2H_4 \cdot H_2SO_4$ (99 atom% ^{15}N) was purchased from ICON isotopes and was deprotonated with liquid ammonia by the method outlined by Schrock.[136] *p*-Tolyl hydrazine was prepared from the corresponding hydrochloride salt by the method outlined by Vincent.[139] Potassium hydroxide pellets were purchased from Fisher Scientific and was imported into a nitrogen glovebox and pulverized into a fine powder with a mortar and pestle. All other reagents were purchased from commercial sources and used as received. Anhydrous 1,4-dioxane was purchased from Sigma Aldrich and was sparged for 1 h with nitrogen prior to use. All other solvents were purchased from Sigma Aldrich, sparged with nitrogen for 45 min, and dried with a solvent purification system using a 1 m column containing activated alumina. (R)-1-[(S_P)-2-(Dicyclohexyl phosphino)ferrocenyl]ethyldi-tert-butyl phosphine (CyPF-*t*Bu, CAS: 158923-11-6) was purchased from Sigma Aldrich or Strem Chemicals.

Survey of Reaction Conditions

Catalyst Stock Solution

In an inert atmosphere glovebox, a 5 mL volumetric flask was charged with $Pd[P(o\text{-tolyl})_3]_2$ (34.4 mg, 0.0481 mmol) and CyPF-*t*Bu (26.7 mg, 0.0481 mmol). The flask was filled to the mark with 1,4-dioxane to obtain an orange suspension, and a Teflon-coated stir bar was added to the flask. The flask was capped, and the mixture was stirred for 45 min to obtain a homogenous, red-orange solution. The stock solution was frozen in a -35 ºC glovebox freezer when not in use.

General Experimental Procedure

In a representative experiment, an oven-dried 4 mL vial was charged with powdered KOH (122 mg, 2.17 mmol, 4.50 equiv), chlorobenzene (48.8 µL, 0.482 mmol, 1.00 equiv), 1,4-dioxane (800 µL), 40 µL of catalyst stock solution (800 ppm of catalyst), and a Teflon-coated stir bar in an inert atmosphere glovebox. Hydrazine monohydrate (70 µL, 1.4 mmol, 3.0 equiv) was added to the reaction. The 4 mL vial was capped with a Teflon-lined cap, and the reaction mixture was heated to 100 °C for 4 h. The reaction was then cooled to room temperature, and the yield of phenyl hydrazine was determined by No-D ^1H NMR spectroscopy of the crude reaction mixture.

*Synthesis of N-Aryl Pyrazoles and Aryl Hydrazine **2b***

Catalyst Stock Solution

The same catalyst stock solution was used as the one above.

General Experimental Procedure

In a representative experiment, an oven-dried 4 mL vial was charged with powdered KOH (122 mg, 2.17 mmol, 4.50 equiv), aryl halide (0.482 mmol, 1.00 equiv), 1,4-dioxane (800 µL), 40 µL of catalyst stock solution (800 ppm of catalyst), and a Teflon-coated stir bar in an inert atmosphere glovebox. Hydrazine monohydrate (70 µL, 1.4 mmol, 3.0 equiv) was added to the reaction. The 4 mL vial was then capped with a Teflon-lined cap, and the reaction mixture was heated to 100 °C for the indicated amount of time with stirring. The reaction mixture was cooled to room temperature, imported into a nitrogen glovebox, and acetylacetone (444 µL, 4.35 mmol, 9.00 equiv) was added to the reaction to obtain a white suspension. The reaction was re-capped

with a Teflon-lined cap and was heated to 100 °C for 6 h with stirring. Afterwards, the reaction mixture was loaded directly onto a silica chromatography column, and the product was isolated via automated column chromatography with a linear gradient of EtOAc/hexanes (0-35% EtOAc in hexanes or 0-75% EtOAc in hexanes for products in which the aryl halide starting material is heterocyclic or contains a heterocycle).

Reactions with Aryl and Heteroaryl Chlorides

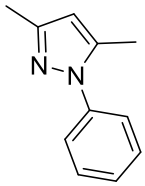

3a

3a was obtained as an off-white oil in 86% yield (71.4 mg) after a reaction time of 5 h. HRMS (ESI+) calcd for $C_{11}H_{11}N_2$ $[M+H]^+$: 173.1078. Found: 173.1074.

^{1}H NMR (400 MHz, DMSO-d_6) δ 7.52 – 7.40 (m, 4H), 7.38 – 7.18 (m, 1H), 6.04 (s, 1H), 2.29 – 2.16 (m, 3H), 2.14 (s, 3H).

^{13}C{^{1}H} NMR (226 MHz, Chloroform-*d*) δ 148.9, 139.9, 139.4, 129.0, 127.2, 124.7, 106.9, 13.5, 12.4.

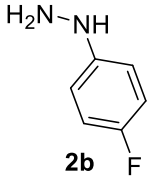

2b

2b was obtained in 79% yield after a reaction time of 25 h. The yield was determined by ^{19}F NMR spectroscopy with 4-fluorotoluene as an internal standard, which was added at the end of the reaction. Although the corresponding pyrazole can be made in low yield (ca. 40% yield) via reaction with acetylacetone, it forms alongside several byproducts that we were unable to separate from the desired pyrazole product by column chromatography.

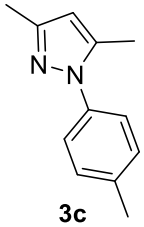

3c

3c was obtained as a colorless oil in 71% yield (63.4 mg) after a reaction time of 5 h. HRMS (ESI+) calcd for $C_{12}H_{14}N_2$ $[M+H]^+$: 187.1235. Found: 187.1238.

^{1}H NMR (600 MHz, DMSO-d_6) δ 7.33 (d, J = 8.4 Hz, 2H), 7.26 (d, J = 8.0 Hz, 2H), 6.02 (s, 1H), 2.34 (s, 3H), 2.23 (s, 3H), 2.14 (s, 3H).

^{13}C{^{1}H} NMR (226 MHz, Chloroform-*d*) δ 148.7, 139.3, 137.4, 137.1, 129.5, 124.7, 106.6, 21.1, 13.5, 12.3.

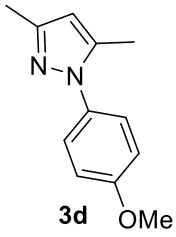

3d

3d was obtained as a yellow oil in 84% yield (71.4 mg) after a reaction time of 17 h. NaO*t*Bu (209 mg, 2.17 mmol, 4.50 equiv) was used instead of KOH in this reaction. HRMS (ESI+) calcd for $C_{12}H_{14}N_2O$ $[M+H]^+$: 203.1184. Found: 203.1183.

^{1}H NMR (600 MHz, Chloroform-*d*) δ 7.35 (d, J = 8.9 Hz, 2H), 6.98 (d, J = 8.9 Hz, 2H), 5.99 (s, 1H), 2.32 (s, 3H), 2.27 (d, J = 0.8 Hz, 3H).

^{13}C{^{1}H} NMR (226 MHz, Chloroform-*d*) δ 158.77, 148.5, 139.4, 133.1, 126.4, 114.1, 106.2, 55.5, 13.4, 12.1.

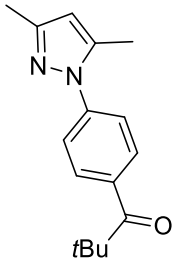

3e

A 4 mL vial was charged with Pd[P(*o*-tolyl$_3$)]$_2$ (3.4 mg, 4.8 µmol, 0.010 equiv), CyPF-*t*Bu (2.7 mg, 4.8 µmol, 0.010 equiv), dioxane (800 µL), and a Teflon-coated stir bar. The resulting orange suspension was stirred at room temperature for 20 min to obtain a homogenous orange solution. Aryl chloride **1e** (94.7 mg, 0.482 mmol, 1.00 equiv) was dispensed into the suspension along with NaO*t*Bu (208 mg, 2.17 mmol, 4.50 equiv) and hydrazine monohydrate (70 µL, 1.4 mmol, 3.0 equiv). The vial was capped with a Teflon-lined cap and was stirred at room temperature for 12 h. Then, acac (444 µL, 4.33 mmol, 9 equiv) was added to the reaction, which was heated to 100 °C for 2 h to obtain a grey suspension. The reaction was transferred into a separatory funnel containing 20 mL of brine and extracted with ether (3 x 20 mL). The combined organic fractions were dried with $MgSO_4$, filtered, and concentrated. The crude product was purified by column chromatography. **3e** was obtained as a colorless oil in 69% yield (76.2 mg). The yield of the corresponding hydrazine **2e** (76%) was determined by ^{1}H NMR spectroscopy with trimethoxybenzene as an internal standard. HRMS (ESI+) calcd for $C_{16}H_{20}N_2O$ $[M+H]^+$: 257.1654. Found: 257.1667.

^{1}H NMR (500 MHz, Chloroform-*d*) δ 7.83 (d, *J* = 8.6 Hz, 2H), 7.52 (d, *J* = 8.6 Hz, 2H), 6.05 (s, 1H), 2.38 (d, *J* = 0.7 Hz, 3H), 2.32 (s, 3H), 1.39 (s, 9H).

^{13}C{^{1}H} NMR (126 MHz, Chloroform-*d*) δ 208.0, 149.7, 141.9, 139.6, 136.6, 129.1, 123.6, 107.9, 44.2, 28.0, 13.5, 12.7.

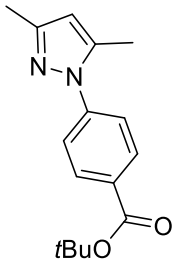

3f

3f was obtained as a colorless oil in 45% yield (59.3 mg) after a reaction time of 5 h. The yield of the corresponding hydrazine **2f** (81%) was determined by ^{1}H NMR spectroscopy with trimethoxybenzene as an internal standard. HRMS (ESI+) calcd for $C_{16}H_{20}N_2O_2$ $[M+H]^+$: 273.1603. Found: 273.1607.

^{1}H NMR (600 MHz, DMSO-d_6) δ 7.97 (d, *J* = 8.6 Hz, 2H), 7.63 (d, *J* = 8.7 Hz, 2H), 6.11 (s, 1H), 2.34 (s, 3H), 2.17 (s, 3H), 1.55 (s, 9H)

^{13}C{^{1}H} NMR (226 MHz, Chloroform-*d*) δ 165.1, 149.7, 143.2, 139.6, 130.3, 130.2, 123.5, 108.0, 81.3, 28.2, 13.5, 12.8.

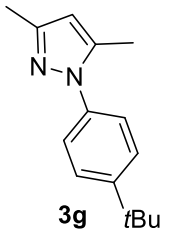

3g

3g was obtained as a colorless oil in 82% yield (88.3 mg) after a reaction time of 5 h. HRMS (ESI+) calcd for $C_{15}H_{20}N_2$ $[M+H]^+$: 229.1704. Found: 229.1695.

^{1}H NMR (600 MHz, Chloroform-*d*) δ 7.47 (d, *J* = 8.6 Hz, 2H), 7.36 (d, *J* = 8.6 Hz, 2H), 6.01 (s, 1H), 2.33 (s, 3H), 2.32 (s, 3H), 1.37 (s, 9H).

^{13}C{^{1}H} NMR (226 MHz, Chloroform-*d*) δ 150.3, 148.6, 139.3, 137.3, 125.8, 124.4, 106.5, 34.6, 31.3, 13.4, 12.3.

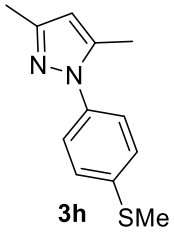

3h

3h was obtained as an off-white oil in 96% yield (101.4 mg) after a reaction time of 16 h. HRMS (ESI+) calcd for $C_{12}H_{14}N_2S$ $[M+H]^+$: 219.0956. Found: 219.0952.

^{1}H NMR (600 MHz, Chloroform-*d*) δ 7.38 (d, *J* = 8.4 Hz, 2H), 7.34 (d, *J* = 8.5 Hz, 2H), 6.01 (s, 1H), 2.54 (s, 3H), 2.32 (s, 3H), 2.31 (s, 3H).

^{13}C{^{1}H} NMR (226 MHz, Chloroform-*d*) δ 149.0, 139.4, 137.6, 137.1, 126.9, 125.1, 106.9, 16.0, 13.5, 12.3.

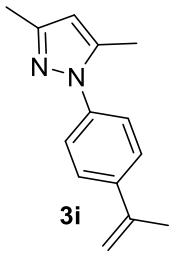

3i

3i was obtained as a yellow oil in 83% yield (84.6 mg) after a reaction time of 16 h. HRMS (ESI+) calcd for $C_{14}H_{16}N_2$ $[M+H]^+$: 213.1392. Found: 213.1393.

^{1}H NMR (400 MHz, Chloroform-*d*) δ 7.55 (d, *J* = 8.6 Hz, 2H), 7.40 (d, *J* = 8.5 Hz, 2H), 6.01 (s, 1H), 5.42 (s, 1H), 5.14 (s, 1H), 2.32 (s, 3H), 2.31 (s, 3H), 2.18 (d, *J* = 1.3 Hz, 3H).

^{13}C{^{1}H} NMR (226 MHz, Chloroform-*d*) δ 149.0, 142.4, 140.1, 139.4, 139.0, 126.0, 124.3, 112.9, 107.0, 21.7, 13.5, 12.4.

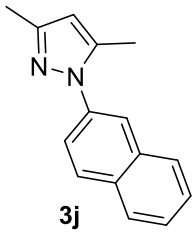

3j

3j was obtained as a yellow in 95% yield (101.8 mg) after a reaction time of 5 h. HRMS (ESI+) calcd for $C_{15}H_{14}N_2$ $[M+H]^+$: 223.1235. Found: 223.1231.

^{1}H NMR (300 MHz, DMSO-d_6) δ 8.12 – 7.96 (m, 4H), 7.72 (dd, *J* = 8.9, 2.1 Hz, 1H), 7.67 – 7.52 (m, 2H), 6.15 (s, 1H), 2.41 (s, 3H), 2.24 (s, 3H).

^{13}C{^{1}H} NMR (226 MHz, Chloroform-*d*) δ 149.2, 139.7, 137.4, 133.2, 132.1, 129.0, 128.0, 127.8, 126.7, 126.3, 123.3, 122.5, 107.1, 13.6, 12.6.

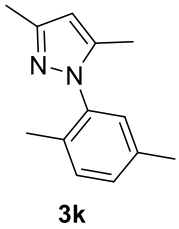

3k

3k was obtained as a colorless oil in 71% yield (68.2 mg) after a reaction time of 21 h. 1600 ppm of palladium catalyst was used in this reaction (80 µL of catalyst stock solution). HRMS (ESI+) calcd for $C_{13}H_{16}N_2$ $[M+H]^+$: 201.1392. Found: 201.1393.

^{1}H NMR (600 MHz, DMSO-d_6) δ 7.23 (d, *J* = 7.8 Hz, 1H), 7.18 (d, *J* = 7.5 Hz, 1H), 5.98 (s, 1H), 2.29 (s, 3H), 2.14 (s, 3H), 1.97 (s, 3H), 1.89 (s, 3H).

^{13}C{^{1}H} NMR (226 MHz, Chloroform-*d*) δ 148.4, 140.2, 138.5, 136.2, 132.8, 130.5, 129.6, 128.4, 104.8, 20.7, 16.7, 13.6, 11.3.

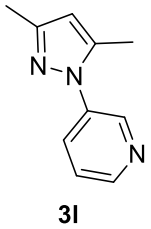

3l

3l was obtained as a yellow oil in 79% yield (65.5 mg) after a reaction time of 15.5 h. HRMS (ESI+) calcd for $C_{10}H_{11}N_3$ $[M+H]^+$: 174.1031. Found: 174.1036.

^{1}H NMR (600 MHz, Chloroform-*d*) δ 8.77 (d, *J* = 2.5 Hz, 1H), 8.62 (dd, *J* = 4.8, 1.5 Hz, 1H), 7.98 – 7.72 (m, 1H), 7.43 (dd, *J* = 8.2, 4.8 Hz, 1H), 6.07 (s, 1H), 2.37 (s, 3H), 2.33 (s, 3H).

^{13}C{^{1}H} NMR (226 MHz, Chloroform-*d*) δ 150.1, 148.1, 145.4, 139.7, 136.6, 131.8, 123.6, 107.8, 13.4, 12.3.

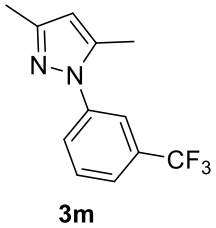

3m

3m was obtained as a colorless oil in 77% yield (88.9 mg) after a reaction time of 5 h. HRMS (ESI+) calcd for $C_{12}H_{11}F_3N_2$ $[M+H]^+$: 241.0952. Found: 241.0946.

^{1}H NMR (400 MHz, DMSO-*d*$_6$) δ 7.81 (d, *J* = 2.9 Hz, 2H), 7.75 – 7.62 (m, 2H), 6.10 (s, 1H), 2.32 (s, 3H), 2.16 (d, *J* = 1.1 Hz, 3H).

^{13}C{^{1}H} NMR (226 MHz, Chloroform-*d*) δ 149.8, 140.4, 139.5, 131.6 (q, *J* = 32.7 Hz), 129.6, 127.4, 123.6 (q, *J* = 271.2 Hz), 123.6 (q, *J* = 3.6 Hz), 121.4 (q, *J* = 3.7 Hz), 107.8, 13.4, 12.4.

^{19}F NMR (376 MHz, DMSO-*d*$_6$) δ -60.39.

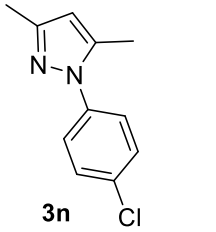

3n

3n was obtained as a yellow oil in 85% yield (85.0 mg) after a reaction time of 24 h. 100 ppm of catalyst was used in this reaction (5 µL of the catalyst stock solution). HRMS (ESI+) calcd for $C_{11}H_{11}ClN_2$ $[M+H]^+$: 207.0689. Found: 207.0679.

^{1}H NMR (300 MHz, Chloroform-*d*) δ 7.50 – 7.39 (m, 4H), 6.05 (s, 1H), 2.35 (s, 3H), 2.34 (s, 3H).

^{13}C{^{1}H} NMR (226 MHz, Chloroform-*d*) δ 149.3, 139.4, 138.4, 132.9, 129.1, 125.8, 107.3, 13.4, 12.4.

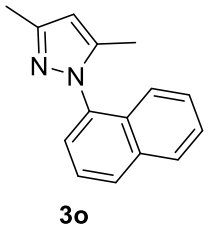

3o

3o was obtained as a colorless oil in 81% yield (86.2 mg) after a reaction time of 15.5 h. HRMS (ESI+) calcd for $C_{15}H_{14}N_2$ $[M+H]^+$: 223.1235. Found: 223.1234.

^{1}H NMR (600 MHz, Chloroform-*d*) δ 7.97 (d, *J* = 8.2 Hz, 1H), 7.94 (d, *J* = 8.1 Hz, 1H), 7.59 – 7.52 (m, 2H), 7.52 – 7.47 (m, 2H), 7.37 (d, *J* = 8.4 Hz, 1H), 6.10 (s, 1H), 2.39 (d, *J* = 1.5 Hz, 3H), 2.09 (s, 3H).

^{13}C{^{1}H} NMR (226 MHz, Chloroform-*d*) δ 148.9, 141.5, 136.2, 134.2, 130.9, 129.2, 128.0, 127.2, 126.5, 125.3, 125.1, 123.2, 105.3, 13.6, 11.4.

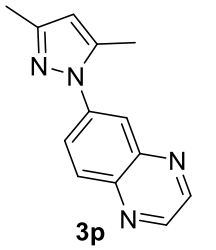

3p

3p was obtained as a yellow oil in 64% yield (68.6 mg) after a reaction time of 17.5 h. HRMS (ESI+) calcd for $C_{13}H_{12}N_4$ $[M+H]^+$: 225.1140. Found: 225.1143.

^{1}H NMR (600 MHz, Chloroform-*d*) δ 8.95 – 8.84 (m, 2H), 8.22 (d, *J* = 9.6 Hz, 1H), 8.15 – 8.07 (m, 2H), 6.12 (s, 1H), 2.51 (s, 3H), 2.37 (s, 3H).

^{13}C{^{1}H} NMR (226 MHz, Chloroform-*d*) δ 150.2, 145.7, 144.9, 143.0, 141.6, 141.0, 139.9, 130.5, 127.4, 122.0, 108.4, 13.5, 12.9.

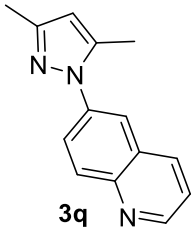

3q was obtained as a yellow oil in 97% yield (104.2 mg) after a reaction time of 15.5 h. HRMS (ESI+) calcd for $C_{14}H_{13}N_3$ $[M+H]^+$: 224.1188. Found: 224.1191.

^{1}H NMR (500 MHz, Chloroform-*d*) δ 8.94 (dd, *J* = 4.2, 1.7 Hz, 1H), 8.26 – 8.12 (m, 2H), 7.93 – 7.78 (m, 2H), 7.44 (dd, *J* = 8.3, 4.2 Hz, 1H), 6.06 (s, 1H), 2.39 (s, 3H), 2.34 (s, 3H).

^{13}C{^{1}H} NMR (101 MHz, Chloroform-*d*) δ 150.7, 149.6, 146.9, 139.7, 137.9, 136.1, 130.5, 128.2, 126.6, 122.0, 121.9, 107.7, 13.6, 12.7.

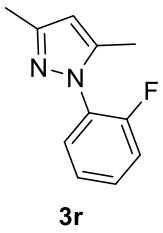

3r was obtained as a colorless oil in 75% yield (65.3 mg) after a reaction time of 15 h. 1600 ppm of palladium catalyst was used in this reaction (80 µL of catalyst stock solution). HRMS (ESI+) calcd for $C_{11}H_{11}FN_2$ $[M+H]^+$: 191.0985. Found: 191.0978.

^{1}H NMR (600 MHz, Chloroform-*d*) δ 7.44 (td, *J* = 7.7, 1.8 Hz, 1H), 7.37 (dddd, *J* = 8.3, 7.6, 4.9, 1.8 Hz, 1H), 7.27 – 7.15 (m, 2H), 5.99 (s, 1H), 2.29 (s, 3H), 2.17 (d, *J* = 1.0 Hz, 3H).

^{13}C{^{1}H} NMR (151 MHz, Chloroform-*d*) δ 156.8 (d, *J* = 251.1 Hz), 149.8, 141.3, 129.9 (d, *J* = 7.7 Hz), 129.2, 127.7 (d, *J* = 12.0 Hz). 124.6 (d, *J* = 3.8 Hz), 116.5 (d, *J* = 20.0 Hz), 106.1, 13.5, 11.1 (d, *J* = 4.3 Hz).

^{19}F NMR (565 MHz, Chloroform-*d*) δ -121.78.

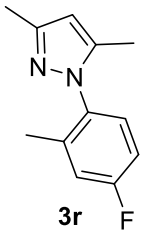

Reactions with Aryl and Heteroaryl Bromides

32 was obtained as a yellow oil in 79% yield (77.4 mg) after a reaction time of 18 h. HRMS (ESI+) calcd for $C_{12}H_{13}FN_2$ $[M+H]^+$: 205.1141. Found: 205.1141.

^{1}H NMR (600 MHz, Chloroform-*d*) δ 7.22 (dd, *J* = 8.6, 5.4 Hz, 1H), 7.03 (dd, *J* = 9.2, 2.9 Hz, 1H), 6.98 (td, *J* = 8.3, 2.9 Hz, 1H), 5.99 (s, 1H), 2.31 (s, 3H), 2.07 (s, 3H), 2.06 (s, 3H).

^{13}C{^{1}H} NMR (226 MHz, Chloroform-*d*) δ 162.4 (d, *J* = 247.9 Hz), 148.7, 140.4, 139.0 (d, *J* = 9.0 Hz), 134.8 (d, *J* = 2.8 Hz), 129.5 (d, *J* = 9.2 Hz), 117.3 (d, *J* = 22.6 Hz), 113.2 (d, *J* = 22.7 Hz), 105.1, 17.4, 13.5, 11.2.

^{19}F NMR (376 MHz, Chloroform-*d*) δ -112.07.

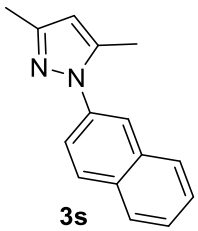

3t was obtained as a yellow in 96% yield (102.5 mg) after a reaction time of 18 h. HRMS (ESI+) calcd for $C_{15}H_{14}N_2$ $[M+H]^+$: 223.1235. Found: 223.1236.

^{1}H NMR (600 MHz, Chloroform-*d*) δ 7.95 (d, *J* = 8.7 Hz, 1H), 7.93 – 7.87 (m, 3H), 7.63 (dd, *J* = 8.7, 2.1 Hz, 1H), 7.58 – 7.52 (m, 2H), 6.08 (s, 1H), 2.40 (s, 3H), 2.37 (s, 3H).

^{13}C{^{1}H} NMR (226 MHz, Chloroform-*d*) δ 149.2, 139.7, 137.4, 133.2, 132.1, 129.0, 128.0, 127.7, 126.7, 126.3, 123.3, 122.5, 107.1, 13.6, 12.5.

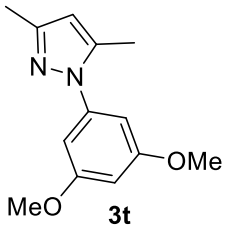

3t

3u was obtained as a colorless in 69% yield (77.6 mg) after a reaction time of 19 h. HRMS (ESI+) calcd for $C_{13}H_{16}N_2O_2$ $[M+H]^+$: 223.1290. Found: 223.1279.

^{1}H NMR (600 MHz, Chloroform-*d*) δ 6.58 (d, *J* = 2.3 Hz, 2H), 6.44 (t, *J* = 2.3 Hz, 1H), 5.98 (s, 1H), 3.82 (s, 6H), 2.32 (s, 3H), 2.29 (s, 3H).

^{13}C{^{1}H} NMR (226 MHz, Chloroform-*d*) δ 160.8, 148.9, 141.4, 139.5, 107.0, 103.1, 99.6, 55.5, 13.5, 12.5.

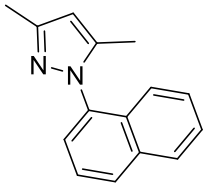

3u

3v was obtained as an off-white oil in 99% yield (106.3 mg) after a reaction time of 18 h. HRMS (ESI+) calcd for $C_{15}H_{14}N_2$ $[M+H]^+$: 223.1235. Found: 223.1236.

^{1}H NMR (600 MHz, Chloroform-*d*) δ 7.97 (d, *J* = 8.2 Hz, 1H), 7.94 (d, *J* = 8.0 Hz, 1H), 7.60 – 7.53 (m, 2H), 7.51 (dt, *J* = 7.2, 1.5 Hz, 2H), 7.40 – 7.35 (m, 1H), 6.11 (s, 1H), 2.39 (s, 3H), 2.09 (d, *J* = 0.8 Hz, 3H).

^{13}C{^{1}H} NMR (226 MHz, Chloroform-*d*) δ 148.9, 141.4, 136.2, 134.2, 130.9, 129.2, 128.0, 127.2, 126.5, 125.3, 125.1, 123.2, 105.3, 13.6, 11.4.

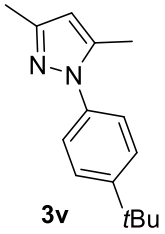

3v

3w was obtained as a colorless oil in 84% yield (92.3 mg) after a reaction time of 19 h. HRMS (ESI+) calcd for $C_{15}H_{20}N_2$ $[M+H]^+$: 229.1704. Found: 229.1701.

^{1}H NMR (600 MHz, Chloroform-*d*) δ 7.44 (d, *J* = 8.5 Hz, 2H), 7.33 (d, *J* = 8.6 Hz, 2H), 5.97 (s, 1H), 2.29 (s, 3H), 2.29 (s, 3H), 1.34 (d, 9H).

^{13}C{^{1}H} NMR (226 MHz, Chloroform-*d*) δ 150.3, 148.7, 139.3, 137.3, 125.8, 124.3, 106.5, 34.6, 31.3, 13.5, 12.3.

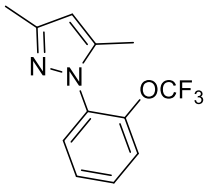

3w

3x was obtained as a colorless oil in 71% yield (87.1 mg) after a reaction time of 19 h. HRMS (ESI+) calcd for $C_{12}H_{11}F_3N_2O$ $[M+H]^+$: 257.0901. Found: 257.0898.

^{1}H NMR (600 MHz, Chloroform-*d*) δ 7.50 – 7.42 (m, 2H), 7.42 – 7.33 (m, 2H), 5.98 (s, 1H), 2.29 (s, 3H), 2.13 (s, 3H).

^{13}C{^{1}H} NMR (226 MHz, Chloroform-*d*) δ 149.7, 144.3, 141.2, 132.5, 129.8 (d, *J* = 9.1 Hz), 127.3, 121.4, 120.2 (q, *J* = 259.5 Hz), 105.9, 29.7, 13.5, 11.1.

^{19}F NMR (376 MHz, Chloroform-*d*) δ -56.98.

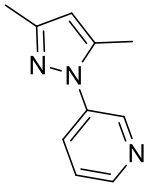

3x

3y was obtained as a yellow oil in 82% yield (68.8 mg) after a reaction time of 18 h. HRMS (ESI+) calcd for $C_{10}H_{11}N_3$ $[M+H]^+$: 174.1031. Found: 174.1028.

^{1}H NMR (600 MHz, Chloroform-*d*) δ 8.76 (d, *J* = 2.6 Hz, 1H), 8.61 (dd, *J* = 4.8, 1.6 Hz, 1H), 7.84 (ddd, *J* = 8.2, 2.6, 1.5 Hz, 1H), 7.43 (ddd, *J* = 8.1, 4.8, 0.8 Hz, 1H), 6.07 (s, 1H), 2.37 (s, 3H), 2.33 (s, 3H).

^{13}C{^{1}H} NMR (226 MHz, Chloroform-*d*) δ 150.1, 148.1, 145.4, 139.7, 136.6, 131.8, 123.6, 107.8, 13.4, 12.3.

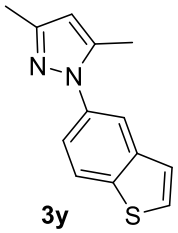

3y

3z was obtained as a yellow oil in 93% yield (102.3 mg) after a reaction time of 19 h. HRMS (ESI+) calcd for $C_{13}H_{12}N_2S$ $[M+H]^+$: 229.0799. Found: 229.0802.

^{1}H NMR (600 MHz, Chloroform-*d*) δ 7.95 – 7.91 (m, 1H), 7.85 (d, *J* = 8.4 Hz, 1H), 7.48 (d, *J* = 5.5 Hz, 1H), 7.44 (dd, *J* = 8.4, 1.9 Hz, 1H), 7.35 (dd, *J* = 5.4, 0.9 Hz, 1H), 6.02 (s, 1H), 2.33 (s, 3H), 2.32 (s, 3H).

^{13}C{^{1}H} NMR (151 MHz, Chloroform-*d*) δ 149.0, 140.0, 139.7, 138.5, 136.5, 127.5, 123.7, 123.5, 121.7, 118.7, 106.9, 13.5, 12.4.

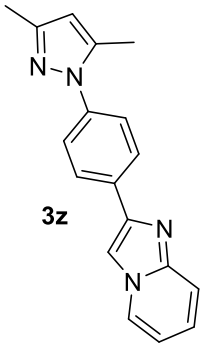

3z

3aa was obtained as a yellow solid in 90% yield (91.7 mg) after a reaction time of 19 h. HRMS (ESI+) calcd for $C_{18}H_{16}N_4$ $[M+H]^+$: 289.1453. Found: 289.1459.

^{1}H NMR (600 MHz, Chloroform-*d*) δ 8.07 (dd, *J* = 6.8, 1.2 Hz, 1H), 8.00 (d, *J* = 8.5 Hz, 2H), 7.83 (s, 1H), 7.59 (dd, *J* = 9.1, 1.0 Hz, 1H), 7.50 – 7.43 (m, 2H), 7.13 (ddd, *J* = 9.1, 6.7, 1.3 Hz, 1H), 6.73 (td, *J* = 6.7, 1.2 Hz, 1H), 5.98 (s, 1H), 2.31 (d, *J* = 0.8 Hz, 3H), 2.29 (s, 3H).

^{13}C{^{1}H} NMR (151 MHz, Chloroform-*d*) δ 149.0, 145.7, 144.8, 139.4, 139.4, 132.6, 126.5, 125.6, 124.8, 124.7, 117.5, 112.5, 108.3, 107.1, 13.5, 12.5.

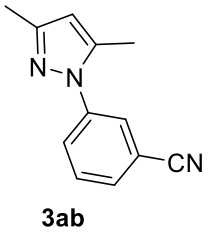

3ab

A 4 mL vial was charged with Pd[P(*o*-tolyl$_3$)]$_2$ (3.4 mg, 4.82 µmol, 0.01 equiv), CyPF-*t*Bu (2.7 mg, 4.82 µmol, 0.01 equiv), dioxane (800 µL), and a Teflon-coated stir bar. The resulting orange suspension was stirred at room temperature for 20 min to obtain a homogenous orange solution. Aryl chloride **1ab** (87.7 mg, 0.482 mmol, 1 equiv) was weighed into the suspension along with NaO*t*Bu (208 mg, 2.17 mmol, 4.5 equiv) and hydrazine monohydrate (70 µL, 1.4 mmol, 3.0 equiv). The vial was capped with a Teflon-lined cap, and the solution was stirred at room temperature for 3 h. Then, acac (444 µL, 4.33 mmol, 9 equiv) was added to the reaction, which was heated to 100 °C for 3 h over which time a grey suspension formed. The reaction was transferred into a separatory funnel containing 20 mL of brine and extracted with ether (3 x 20 mL). The combined organic fractions were dried with $MgSO_4$, filtered, and concentrated. The crude product was purified by column chromatography. **3ab** was obtained as a colorless solid in 58% yield (55.3 mg). The yield of the corresponding hydrazine, **2ab**, (75%) was determined by ^{1}H NMR spectroscopy with trimethoxybenzene as an internal standard. HRMS (ESI+) calcd for $C_{12}H_{12}N_3$ $[M+H]^+$: 198.1031. Found: 198.1039.

^{1}H NMR (600 MHz, Chloroform-*d*) δ 7.80 (t, *J* = 1.9 Hz, 1H), 7.75 (m, 1H), 7.64 (dt, *J* = 7.8, 1.4 Hz, 1H), 7.59 (t, *J* = 7.9 Hz, 1H), 6.07 (s, 1H), 2.38 (s, 3H), 2.32 (s, 3H).

^{13}C{^{1}H} NMR (126 MHz, Chloroform-*d*) δ 150.2, 140.7, 139.5, 130.3, 130.0, 128.3, 127.4, 118.0, 113.3, 108.3, 13.5, 12.6.

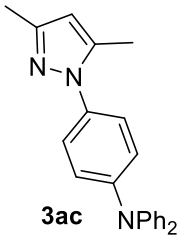

3ac was obtained as an orange oil in 73% yield (119.6 mg) after a reaction time of 16 h. 1200 ppm of [Pd] (60 µL of catalyst stock solution) and NaO*t*Bu (208 mg, 2.17 mmol, 4.5 equiv), instead of KOH, was used in this reaction. HRMS (ESI+) calcd for $C_{23}H_{22}N_3$ $[M+H]^+$: 340.1814. Found: 340.1812.

^{1}H NMR (500 MHz, Chloroform-*d*) δ 7.31 – 7.25 (m, 6H), 7.17 – 7.12 (m, 6H), 7.06 (tt, *J* = 7.3, 1.2 Hz, 2H), 6.00 (s, 1H), 2.33 (s, 3H), 2.31 (s, 3H).

^{13}C{^{1}H} NMR (126 MHz, Chloroform-*d*) δ 149.1, 148.0, 147.5, 139.8, 134.7, 129.8, 126.2, 124.9, 124.2, 123.6, 106.9, 14.0, 12.7.

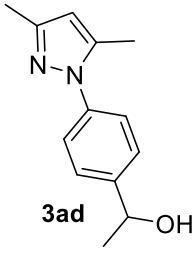

3ad was obtained as a colorless solid that was a 2:1 mixture of 3,5-dimethylpyrazole and **3ad**, respectively, in 88% yield (173.8 mg) after a reaction time of 14.5 h. A pure sample of **3ad** was obtained by preparative TLC of the mixture in 1:1 EtOAc/hexanes, and the top half of the band containing **3ad** was isolated. The process was repeated twice more and the top 1/3 and the top 1/5 of the band containing **3ad** was taken in the second and third iteration of this process, respectively, to obtain 1.7 mg **3ad** as a colorless oil. HRMS (ESI+) calcd for $C_{13}H_{17}N_2O$ $[M+H]^+$: 217.1341. Found: 217.1342.

^{1}H NMR (600 MHz, Chloroform-*d*) δ 7.47 (d, *J* = 8.5 Hz, 2H), 7.42 (d, *J* = 8.5 Hz, 2H), 6.01 (s, 1H), 4.98 (q, *J* = 6.5 Hz, 1H), 2.32 (m, 6H), 1.96 (br. s, 1H), 1.54 (d, *J* = 6.5 Hz, 3H).

^{13}C{^{1}H} NMR (151 MHz, Chloroform-*d*) δ 148.9, 145.0, 139.5, 139.0, 126.0, 124.8, 106.9, 69.9, 25.3, 13.5, 12.4.

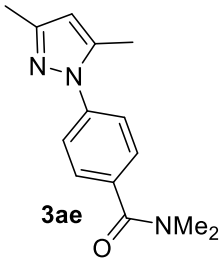

A 4 mL vial was charged with catalyst stock solution (120 µL, 0.0024 equiv), NaO*t*Bu (208 mg, 2.17 mmol, 4.5 equiv), dioxane (800 µL), aryl bromide **1ae** (111 mg, 0.482 mmol, 1 equiv), a Teflon-coated stir bar, and hydrazine monohydrate (70 µL, 1.4 mmol, 3.0 equiv). The vial was capped with a Teflon-lined cap and the mixture was stirred at room temperature for 24 h. Then, acac (444 µL, 4.33 mmol, 9 equiv) was added to the reaction, which was heated to 100 °C for 6 h over which time a grey suspension formed. The reaction was transferred into a separatory funnel containing 20 mL of brine and extracted with ether (3 x 20 mL). The combined organic fractions were dried with $MgSO_4$, filtered, and concentrated. The crude product was purified by column chromatography. **3ae** was obtained as a colorless solid in 56% yield (65.7 mg). The yield of the corresponding hydrazine, **2ae**, (80%) was determined by ^{1}H NMR spectroscopy with trimethoxybenzene as an internal standard. HRMS (ESI+) calcd for $C_{14}H_{18}N_3O$ $[M+H]^+$: 244.1450. Found: 244.1452.

^{1}H NMR (300 MHz, Chloroform-*d*) δ 7.67 – 7.49 (m, 4H), 6.10 (s, 1H), 3.21 (br. s, 3H), 3.09 (br. s, 3H), 2.41 (s, 3H), 2.38 (s, 3H).

^{13}C{^{1}H} NMR (126 MHz, Chloroform-*d*) δ 170.9, 149.5, 140.8, 139.6, 135.0, 128.0, 124.4, 107.5, 39.6, 35.4, 13.5, 12.5.

Synthesis of Palladium Complexes

*Synthesis of (CyPF-tBu)Pd(OH)Ph (**6**)*

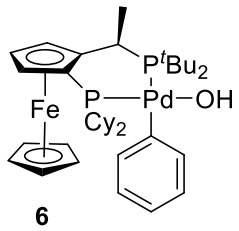

6

A 20 mL vial was charged with [Pd(PPh$_3$)(Ph)(μ-OH)]$_2$ (71.0 mg, 0.0767 mmol), CyPF-*t*Bu (89.3 mg, 0.161 mmol), a Teflon-coated stir bar, and 3 mL of THF. The orange solution was stirred rapidly at room temperature for 4 h, layered with pentane (17 mL), and stored at -35 °C for 14 h to obtain orange crystals. The mother liquor was removed, and the crystals were washed with pentane (3 x 2 mL) and dried under vacuum to obtain the title compound as an orange solid (53.0 mg, 46%). Single crystals of **6** were obtained by layering a concentrated solution of **6** in THF with pentane and cooling the biphasic mixture to -15° C. Anal. Calcd for $C_{38}H_{58}FeOP_2Pd$: C, 60.45; H, 7.74. Found: C, 60.44; H, 7.83.

^{1}H NMR (400 MHz, Benzene-d_6) δ 7.88 (br. s, 1H), 7.72 (br. s, 1H), 7.29 (br. s, 1H), 7.15 (s, 1H), 7.08 (t, *J* = 7.2 Hz, 1H), 4.55 (br. s, 1H), 4.16 (s, 1H), 4.08 (t, *J* = 2.6 Hz, 1H), 4.05 (s, 5H), 3.10 (t, *J* = 6.6 Hz, 1H), 2.24 (br. s, 3H), 2.06 (br. s, 1H), 1.87 (d, *J* = 12.6 Hz, 1H), 1.79 – 1.61 (m, 20H), 1.44 – 1.05 (m, 19H), 0.12 – 0.01 (m, 1H).

^{31}P{^{1}H} NMR (243 MHz, Benzene-d_6) δ 67.7 (br. s), 21.1 (br. s).

*Synthesis of (CyPF-tBu)Pd(4-methoxyphenyl)(N_2H_3) (**8**)*

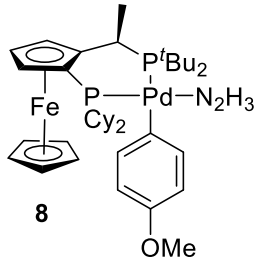

8

A J. Young NMR tube was charged with (CyPF-*t*Bu)Pd(4-methoxyphenyl)Br (15.0 mg, 0.0172 mmol, 1.00 equiv), NaO*t*Bu (1.7 mg, 0.017 mmol, 1.0 equiv), and 600 μL of THF-d_8. The resulting orange solution was frozen inside the coldwell of the glovebox, which was cooled with a liquid nitrogen bath. Then, 17.7 μL of a 1.0 M solution of N_2H_4 in THF-d_8 was added to the frozen solution, which was quickly exported from the glovebox into a Dewar flask filled with dry ice and acetone. The NMR tube was allowed to thaw inside the acetone bath and was taken briefly out of the bath (ca. 15 sec) and gently agitated by shaking the tube. This process was repeated until an orange suspension was obtained (ca. 4 times). The NMR tube was injected into an NMR spectrometer that was cooled to -30 °C.

^{1}H NMR (600 MHz, THF-d_8, 244 K) δ 7.73 (br. s, 1H), 7.17 (t, *J* = 7.7 Hz, 1H), 6.72 (d, *J* = 8.2 Hz, 1H), 6.52 (d, *J* = 7.1 Hz, 1H), 4.90 (s, 1H), 4.63 (s, 1H), 4.46 (s, 1H), 4.26 (s, 5H), 3.02 (br. s, 1H), 2.49 (br. s, 3H), 2.37 (br. s, 3H), 1.67 – 1.15 (m, 40H). The methoxy signal could not be assigned due to overlap with THF.

^{31}P{^{1}H} NMR (243 MHz, THF-d_8, 244 K) δ 59.1 (d, *J* = 41.9 Hz), 13.2 (d, *J* = 41.7 Hz).

*Synthesis of (CyPF-tBu)Pd(4-methoxyphenyl)($^{15}N_2H_3$) (**8-^{15}N**)*

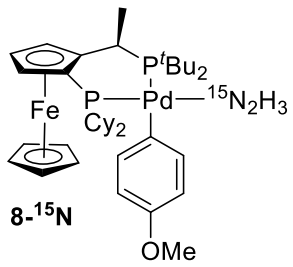

8-^{15}N

A J. Young NMR tube was charged with (CyPF-*t*Bu)Pd(4-methoxyphenyl)Br (20.0 mg, 0.0236 mmol, 1.00 equiv), NaO*t*Bu (4.1 mg, 0.043 mmol, 1.8 equiv), and 450 µL of THF-d_8. The resulting orange solution was frozen inside the coldwell of the glovebox, which was cooled with a liquid nitrogen bath. Then, 150 µL of a 0.182 M solution of $^{15}N_2H_4$ in THF-d_8 was added to the frozen solution, which was quickly exported from the glovebox into a Dewar flask filled with dry ice and acetone. The NMR tube was allowed to thaw inside the acetone bath and was taken briefly out of the bath (ca. 15 sec) and gently agitated by shaking the tube. This process was repeated until an orange suspension was obtained (ca. 4 times). The NMR tube was injected into an NMR spectrometer that was cooled to -60 °C.

^{1}H NMR (500 MHz, THF-d_8, 213 K) δ 7.72 (d, *J* = 6.5 Hz, 1H), 7.16 (s, 1H), 6.72 (d, *J* = 8.2 Hz, 1H), 6.51 (d, *J* = 8.5 Hz, 1H), 4.91 (s, 1H), 4.66 (s, 1H), 4.48 (s, 1H), 4.27 (s, 5H), 3.67 (s, 3H), 3.00 (s, 2H), 2.50 (d, *J* = 63.7 Hz, 3H), 2.37 (s, 3H), 1.69 – 1.26 (m, 40H).

^{31}P{^{1}H} NMR (202 MHz, THF-d_8, 213 K) δ 58.8 (d, *J* = 42.0 Hz), 12.9 (dd, *J* = 40.2, 17.4 Hz).

^{15}N{^{1}H} NMR (51 MHz, THF-d_8, 213 K) δ 77.1 (d, *J* = 8.5 Hz).

Synthesis of 1-(4-(tert-butyl)phenyl)-1-(p-tolyl)hydrazine

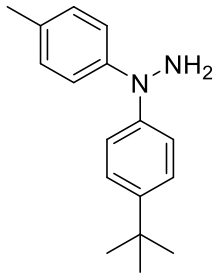

A 4 mL vial was charged with Pd[P(*o*-tolyl)$_3$]$_2$ (3.4 mg, 4.8 µmol, 0.010 equiv), CyPF-*t*Bu (2.7 mg, 4.8 µmol, 0.010 equiv), 800 µL of 1,4-dioxane, and a Teflon-coated stir bar. The orange suspension was stirred for 15 min at room temperature to obtain a homogenous, orange solution. To this solution was added 4-*tert*-butyl-chlorobenzene (76.0 µL, 0.482 mmol, 1.00 equiv), 4-methylphenyl hydrazine (58.8 mg, 0.482 mmol, 1.00 equiv), and KOH (122 mg, 2.18 mmol, 4.50 equiv). The reaction was heated to 80 °C for 4 h with stirring. The reaction was cooled to room temperature and the crude reaction mixture was loaded directly onto a silica column for isolation via automated column chromatography (0-30% linear ramp Et_2O in hexanes) to obtain the title compound as a light yellow solid in 69% yield (84.0 mg). This compound decomposed during our attempts to obtain its mass by ESI-MS. Thus, we synthesized its hydrazone analogue for further confirmation of its structure. See below.

^{1}H NMR (600 MHz, Benzene-d_6) δ 7.24 (d, *J* = 8.5 Hz, 1H), 7.18 – 7.15 (m, 2H), 7.11 (d, *J* = 8.2 Hz, 2H), 6.97 (d, *J* = 8.0 Hz, 2H), 3.41 (s, 2H), 2.14 (s, 3H), 1.26 (s, 9H).

^{13}C{^{1}H} NMR (151 MHz, Benzene-d_6) δ 147.5, 143.9, 130.6, 129.4, 125.6, 119.7, 119.1, 112.2, 33.8, 31.3, 20.4.

Synthesis of 1-(4-(tert-butyl)phenyl)-2-(propan-2-ylidene)-1-(p-tolyl)hydrazine

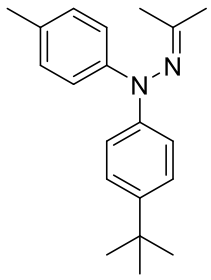

In air, a 20 mL vial was charged with 1-(4-(*tert*-butyl)phenyl)-1-(*p*-tolyl)hydrazine (78.6 mg, 0.309 mmol), 4 mL of acetone, a drop of glacial acetic acid, and a Teflon-coated stir bar. The reaction was capped with a Teflon-lined cap and heated to 65 °C for 18 h with stirring. The reaction mixture was cooled to room temperature, concentrated via rotary evaporation, and loaded directly onto a silica-gel column for isolation via automated column chromatography (0-20% linear ramp EtOAc in hexanes) to obtain the title compound as an orange oil in 90% yield (81.5 mg). HRMS (ESI+) calcd for $C_{20}H_{27}N_2$ $[M+H]^+$: 295.2174. Found: 295.2176.

^{1}H NMR (400 MHz, Chloroform-*d*) δ 7.31 (d, *J* = 8.8 Hz, 2H), 7.14 (d, *J* = 8.0 Hz, 2H), 6.99 (d, *J* = 8.5 Hz, 2H), 6.96 (d, *J* = 8.7 Hz, 2H), 2.36 (s, 3H), 2.17 (s, 3H), 1.86 (s, 3H), 1.34 (s, 9H). **^{13}C**{^{1}H} NMR (101 MHz, Chloroform-*d*) δ 169.4, 146.6, 146.1, 145.1, 132.4, 129.6, 125.7, 121.8, 120.0, 34.2, 31.5, 25.1, 20.8, 20.4.

Synthesis of Potassium Deuteroxide

A 20 mL vial was charged with 10 mL of anhydrous THF and ca. 750 mg of potassium metal. D_2O was added dropwise until the cessation of bubbling and the disappearance of potassium metal (ca. 1.2 mL). A crystal of benzophenone was added to determine if any unreacted potassium metal was present, and the absence of a color change indicated the complete consumption of potassium. The resulting white suspension was isolated on a fritted glass funnel and washed with THF (3 x 10 mL) and pentane (2 x 10 mL). The white powder was dried under dynamic vacuum at 150 °C for 20 h to remove residual organic solvents and D_2O to obtain a white solid (933 mg, ~85% yield). The KOH used in our KIE measurements was prepared in the same manner by substitution of D_2O with H_2O.

Control Experiment with 3,5-Dimethylpyrazole

A 4 mL vial was charged with chlorobenzene (48.8 µL, 0.482 mmol, 1.00 equiv), 3,5-dimethylpyrazole (139 mg, 1.44 mmol, 3.00 equiv), KOH (122 mg, 2.18 mmol, 4.50 equiv), 800 µL of 1,4-dioxane, a Teflon-coated stir bar, and 40 µL of catalyst stock solution. The reaction mixture was heated to 100 °C for 18.5 h with stirring. The reaction mixture was cooled to room temperature and the sample was analyzed by ^{1}H NMR spectroscopy and GC/MS analysis. 3,5-Dimethyl-1-phenylpyrazole was not detected by either of these analysis methods.

Mechanistic Experiments

Determination of the Resting State of the Catalyst

A 4 mL vial was charged with $Pd[P(o\text{-tolyl})_3]_2$ (17.2 mg, 0.0241 mmol, 0.05 equiv), CyPF-*t*Bu (13.4 mg, 0.0241 mmol, 0.05 equiv), 800 µL of 1,4-dioxane, and a Teflon-coated stir bar. The reaction was stirred for 15 min at room temperature to obtain a homogenous, orange solution. To this solution was added 4-chlorotoluene (57.0 µL, 0.482 mmol, 1.00 equiv), hydrazine monohydrate (70.2 µL, 1.44 mmol, 3.00 equiv), and KOH (122 mg, 1.44 mmol, 4.5 equiv). The reaction was capped with a Teflon-coated cap, exported from the glovebox, and heated to 50 °C with stirring for 50 min. The reaction mixture was cooled to room temperature and imported into the glovebox, and 1,3,5-trimethoxybenzene (27.0 mg, 0.161 mmol, 0.333 equiv) was added into the vial. The conversion and yield were determined by No-D ^{1}H NMR spectroscopy, and the resting state of the catalyst was determined by ^{31}P NMR spectroscopy of the reaction.

Initial Rate Measurements

Order in [Pd]

A 4 mL vial was charged with 500 µL of a 0.963 M solution of 4-fluorotoluene and 4-fluoro-chlorobenzene in 1,4-dioxane and a Teflon-coated stir bar. Then, a 9.62 mM solution of $Pd[P(o\text{-tolyl})_3]_2$ and CyPF-*t*Bu in 1,4-dioxane was added to this solution corresponding to the desired amount of catalyst (20-60 µL, 400-1200 ppm of [Pd]) and KOH (122 mg, 1.44 mmol, 4.5 equiv). 72 µL of hydrazine monohydrate was added to the solution, followed by an appropriate amount of 1,4-dioxane, such that the total volume of liquid inside the vial reached 800 µL. the vial containing the reaction was sealed with a Teflon-lined cap. This process was repeated three more times, such that a total of four vials were obtained with 400, 600, 800, and 1200 ppm of palladium catalyst. A 15 µL aliquot was removed from each reaction and was deposited into an NMR, tube followed by 550 µL of $CDCl_3$ for a t = 0 min time point. The reactions were heated to 80 °C with stirring for a set amount of time (see below). At the end of each time point, all vials were cooled to room temperature and imported into an inert atmosphere glovebox. A 15 µL aliquot of the reaction mixture was taken from each vial and was deposited into an NMR tube, followed by 550 µL of $CDCl_3$. The vials were re-capped and warmed back to 80 °C until the next time point, and this process was repeated until a total of six time points were obtained. The initial rate was measured by monitoring the decay of 4-fluoro-chlorobenzene over time via ^{19}F NMR spectroscopy.

Table S1. Initial rate dependence on palladium catalyst loading.

[Pd] (ppm)	Time Point Interval (min)	Initial Rate ($M/min \times 10^{-3}$)
400	25	0.428
600	20	0.602
800	20	0.915
1200	10	1.48

Order in [ArCl]

A 4 mL vial was charged with 40 µL a 9.62 mM solution of $Pd[P(o\text{-tolyl})_3]_2$ and CyPF-*t*Bu in 1,4-dioxane and a Teflon-coated stir bar. Then, an amount of a 3.21 M solution of 4-fluoro-chlorobenzene and 4-fluorotoluene in 1,4-dioxane corresponding to the desired amount of aryl chloride (150-600 µL, 0.482-1.93 mmol), followed by 72 µL of hydrazine monohydrate and KOH (122 mg, 1.44 mmol, 4.5 equiv) were added to the vial. An amount of 1,4-dioxane was added to the reaction, such that the total volume of liquid inside the reaction reached 800 µL. The vial containing the reaction was sealed with a Teflon-lined cap. This process was repeated three more times, such that a total of four vials were obtained with 0.482 mmol, 0.964 mmol, 1.45 mmol, and 1.93 mmol of aryl chloride. A 15 µL aliquot was taken from each reaction and was deposited into an NMR tube, followed by 550 µL of $CDCl_3$ for a t = 0 min time point. The reaction mixtures were heated to 80 °C with stirring for a set amount of time (see below). At the end of each time point, all vials were cooled to room temperature and imported into an inert atmosphere glovebox. A 15 µL aliquot of the reaction mixture was taken from each vial and was deposited into an NMR tube, followed by 550 µL of $CDCl_3$. The reactions were re-capped and warmed back to 80 °C until the next time point, and this process was repeated until a total of six time points were obtained. The initial rate was measured by monitoring the decay of 4-fluoro-chlorobenzene over time via ^{19}F NMR spectroscopy.

Table S2. Initial rate dependence on aryl chloride concentration.

[ArCl] (M)	Amount of ArCl (mmol)	Time Point Interval (min)	Initial Rate (M/min × 10^{-3})
0.603	0.482	15	0.851
1.21	0.964	15	0.846
1.81	1.45	15	0.825
2.41	1.93	15	0.866

Order in [N_2H_4]

A 4 mL vial was charged with 40 µL a 9.62 mM solution of Pd[P(*o*-tolyl)$_3$]$_2$ and CyPF-*t*Bu in 1,4-dioxane, 600 µL of a 0.803 M solution of 4-fluoro-chlorobenzene and 4-fluorotoluene in 1,4-dioxane, and a Teflon-coated stir bar. Then, an appropriate amount of hydrazine monohydrate was added to the reaction corresponding to the desired amount of hydrazine (46.7-117 µL, 0.963-2.41 mmol) and KOH (122 mg, 1.44 mmol, 4.5 equiv). An amount of 1,4-dioxane was added to the reaction, such that the total volume of liquid inside the reaction reached 800 µL. The vial containing the reaction was sealed with a Teflon-lined cap. This process was repeated three more times, such that a total of four vials were obtained with 0.963 mmol, 1.45 mmol, 1.93 mmol, and 3.41 mmol of hydrazine monohydrate. A 15 µL aliquot was taken from each vial and was deposited into an NMR tube followed by 550 µL of $CDCl_3$ for a t = 0 min time point. The reaction mixtures were heated to 80 °C with stirring for a set amount of time (see below). At the end of each time point, all vials were cooled to room temperature and imported into an inert atmosphere glovebox. A 15 µL aliquot of the reaction mixture was taken from each vial and was deposited into an NMR tube followed by 550 µL of $CDCl_3$. The vials were re-capped and warmed back to 80 °C until the next time point, and this process was repeated until a total of six time points were obtained. The initial rate was measured by monitoring the decay of 4-fluoro-chlorobenzene over time via ^{19}F NMR spectroscopy.

Table S3. Initial rate dependence on hydrazine monohydrate concentration.

[N_2H_4] (M)	Amount of N_2H_4 (mmol)	Time Point Interval (min)	Initial Rate (M/min × 10^{-3})
1.21	0.964	20	0.760
1.81	1.45	20	1.18
2.41	1.93	15	1.57
3.01	2.41	15	1.96

Time Course of the Pd-Catalyzed C-N Coupling Reaction of 4-Chlorotolune with Hydrazine.

A 5 mL volumetric flask was charged with CyPF-*t*Bu (83.8 mg, 0.151 mmol), Pd[P(*o*-tolyl)$_3$]$_2$ (107.5 mg, 0.150 mmol), and 1,3,5-trimethoxybenzene (168.8 mg, 1.004 mmol). The flask was filled to the mark with 1,4-dioxane and charged with a Teflon-coated stir bar. The resulting orange suspension was stirred rapidly at room temperature for 10 min to obtain a homogeneous, orange solution. Six 4 mL vials were charged with 800 µL of this solution along with 4-chlorotoluene (57 µL, 0.48 mmol), hydrazine monohydrate (70.1 µL, 1.44 mmol), and a Teflon-coated stir bar. The 4 mL vials were then capped with a Teflon-coated cap and placed onto an aluminum heating block warmed to 60 °C. A vial was taken off the heating block after 5 minutes, and the reaction mixture was filtered through a syringe filter into an NMR tube. The contents of the NMR tube were frozen in a cold bath containing dry ice and acetone until analysis by NO-D and ^{31}P NMR spectroscopy. This process was repeated for each vial at the time points below (Table

S4). The concentration of the chloroarene and hydrazine products were determined against trimethoxybenzene as an internal standard by No-D NMR spectroscopy. The concentrations of aryl hydroxide complex **5** and chloride complex **4** were determined by using the slight excess of CyPF-*t*Bu as an internal standard by ^{31}P NMR spectroscopy.

Table S4. Time course data on the arylation of hydrazine with 4-chlorotoluene.

Time (min)	[4-chlorotoluene] (M)	[*p*-tolyl hydrazine] (M)	[1,1-bis(p-tolyl hydrazine)] (mM)	[**4**] (mM)	[**5**] (mM)
5	0.52	0.073	3.2	14	11
10	0.45	0.13	10	9.6	14
15	0.36	0.20	21	8.4	12
25	0.25	0.28	44	6.6	12
35	0.10	0.35	69	8.7	9.5
50	0.064	0.39	90	0.77	1.7

KIE Measurements

A 4 ml vial was charged with 4-fluoro-chlorobenzene (51.3 µL, 0.482 mmol, 1.00 equiv), 4-fluorotoluene (53.0 µL, 0.482 mmol), finely ground powder of KOH or KOD (2.17 mmol, 4.50 equiv), 60 µL of catalyst stock solution (1200 ppm [Pd]), 570 µL of 1,4-dioxane, hydrazine monohydrate or hydrazine-d_4 monodeuterate (1.45 mmol, 3.00 equiv), and a Teflon-coated stir bar. A 20 µL aliquot was taken from each vial and was deposited into an NMR tube followed by 550 µL of $CDCl_3$ for a t = 0 min time point. The reaction mixtures were heated to 78 °C with stirring for a set amount of time (see below). At the end of each time point, all vials were cooled to room temperature and imported into an inert atmosphere glovebox. A 20 µL aliquot of the reaction mixture was taken from each vial and was deposited into an NMR tube followed by 550 µL of $CDCl_3$. The vials were re-capped and warmed back to 78 °C until the next time point, and this process was repeated until a total of six time points were obtained. The initial rate was measured by monitoring the decay of 4-fluoro-chlorobenzene over time via ^{19}F NMR spectroscopy.

*Decomposition of Aryl Hydroxide Complex **5***

A J. Young NMR tube was charged with hydroxide complex **5** (8.9 mg, 0.012 mmol, 1.0 equiv), 150 µL of THF, 350 µL of 1,4-dioxane, and 4-chlorotoluene (4.6 µL, 0.039 mmol, 3.3 equiv). The J. Young NMR tube was capped and shaken by hand until complex **5** was dissolved. The NMR tube was then injected into an NMR spectrometer held at 100 °C and a ^{31}P NMR spectrum was acquired every 92 seconds for 4 h.

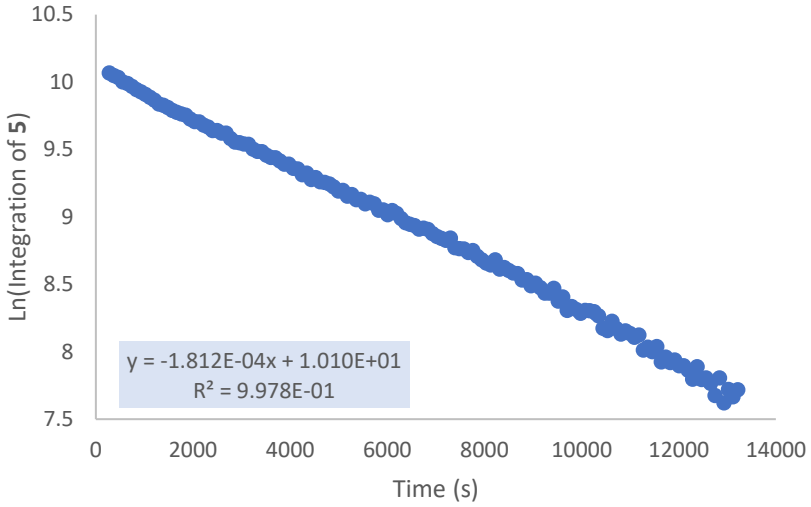

Figure S1. Natural log of the integration of **5** vs time.

Competition Experiments

Competition Experiment with Catalytic Conditions

A 4 ml vial was charged with 4-*tert*-butyl-chlorobenzene (80.6 µL, 0.482 mmol, 1.00 equiv), 4-methyl phenyl hydrazine (58.9 mg, 0.482 mmol, 1.00 equiv), KOH (122 mg, 2.17 mmol, 4.50 equiv), 40 µL of catalyst stock solution (800 ppm [Pd]), 800 µL of 1,4-dioxane, hydrazine monohydrate (23.4 µL, 0.482 mmol, 1.00 equiv), and a Teflon-coated stir bar. The vial was sealed with a Teflon-lined cap, exported from the glovebox, and heated to 100 °C for 15.5 h. The reaction vial was cooled to room temperature, imported into the glovebox, and was charged with 1,3,5-trimethoxybenzene (27.0 mg, 0.161 mmol, 0.333 equiv). The yield of the products was determined by No-D ^{1}H NMR spectroscopy against 1,3,5-trimethoxybenzene as an internal standard.

*Competition Experiment with Aryl Hydroxide Complex **5***

A 4 ml vial was charged with *p*-tolylhydrazine (5.8 mg, 0.047 mmol, 2.0 equiv), aryl hydroxide complex **5** (18.2 mg, 0.0237 mmol, 1.00 equiv), PPh_3 (12.4 mg, 0.0473 mmol, 2.00 equiv), hydrazine (47.2 µL, 1.0 M solution in THF, 0.0473 mmol, 2.00 equiv), a Teflon-coated stir bar, and 553 µL of THF. The vial was sealed with a Teflon-lined cap, exported from the glovebox, and heated to 65 °C for 3 h with stirring. The yield of the products was determined by No-D ^{1}H NMR spectroscopy against (CyPF-*t*Bu)Pd(PPh)$_3$.

*Competition Experiments with Aryl Chloride Complex **4***

In a representative experiment, a 4 ml vial was charged with *p*-tolylhydrazine (5.8 mg, 0.047 mmol, 2.0 equiv), aryl chloride complex **4** (18.6 mg, 0.0237 mmol, 1.00 equiv), PPh_3 (12.4 mg, 0.0473 mmol, 2.00 equiv), hydrazine (47.2 µL, 1.0 M solution in THF, 0.0473 mmol, 2.00 equiv), a Teflon-coated stir bar, and 553 µL of THF. Then, base was weighed into the vial (KOH (13.3 mg, 0.237 mmol, 10.0 equiv), LiHMDS (5.1 mg, 0.031 mmol, 1.3 equiv), or NaO*t*Bu (3.0 mg, 0.031 mmol, 1.3 equiv). The vial was sealed with a Teflon-lined cap, exported from the glovebox, and heated to 65 °C for 3 h with stirring. The yield of the products was determined by No-D ^{1}H NMR spectroscopy against (CyPF-*t*Bu)Pd(PPh)$_3$.

Stoichiometric Reactions with Palladium Complexes

*Reaction of Palladium Aryl Chloride Complex **4** with TBA(OH)*

A J. Young NMR tube was charged with palladium complex **4** (15.0 mg, 0.0190 mmol, 1.00 equiv), TBA(OH) · 30 H_2O (22.9 mg, 0.0286, 1.50 equiv), $PMes_3$ (7.4 mg, 0.019 mmol, 1.0 equiv), and 600 µL of THF-d_8. The reaction was shaken briefly, ca. 5 s, at which point a ^{31}P NMR spectrum was immediately obtained. This spectrum indicated quantitative conversion of complex **4** to hydroxo complex **5**.

*Reaction of Palladium Hydroxo Complex **5** With Hydrazine*

A J. Young NMR tube was charged with palladium complex **5** (20.0 mg, 0.0260 mmol, 1.00 equiv), hydrazine monohydrate (8.0 µL, 0.79 mmol, 6.0 equiv), PPh_3 (7.5 mg, 0.029 mmol, 1.1 equiv), 1,3,5-trimethoxybenzene (4.4 mg, 0.026 mmol, 1.00 equiv) and 600 µL of THF-d_8. The reaction was quickly exported from an inert atmosphere glovebox and heated to 65 °C for 45 min. The yield of 4-methylphenyl hydrazine was determined by ^1H NMR spectroscopy against trimethoxybenzene as an internal standard. A ^{31}P NMR spectrum was obtained, and the only observable signals corresponded to (CyPF-*t*Bu)Pd(PPh_3).

*Time Course of Reaction of Palladium Aryl Chloride Complex **4** with KOH and Hydrazine*

A screw cap NMR tube was charged with hydrazine monohydrate (11.5 µL, 0.236 mmol, 10.0 equiv) and KOH (13.3 mg, 0.236 mmol, 10.0 equiv). Palladium complex **4** (18.6 mg, 0.0236 mmol, 1.00 equiv), $PMes_3$ (18.4 mg, 0.0472 mmol, 2.00 equiv), and PPh_3 (12.4 mg, 0.0472 mmol, 2.00 equiv) were dissolved in 600 µL of THF-d_8. The solution was injected through the septum of the NMR tube, and the NMR tube was placed into an NMR spectrometer heated to 35 °C, a ^{31}P NMR spectrum was obtained every 30 s for 50 min. The concentration vs. time data were analyzed with COPASI (see details below).

*Time Course of Reaction of Palladium Hydroxo Complex **5** With Hydrazine*

A J. Young NMR tube was charged with palladium complex **5** (18.2 mg, 0.0236 mmol, 1.00 equiv), hydrazine monohydrate (11.5 µL, 0.236 mmol, 10.0 equiv) or anhydrous hydrazine (1.0 M in THF, 0.236 mL, 0.236 mmol, 10.0 equiv), $PMes_3$ (18.4 mg, 0.0472 mmol, 2.00 equiv), PPh_3 (12.4 mg, 0.0472 mmol, 2.00 equiv), and a corresponding amount of THF-d_8, such that the total volume of the reaction was 600 µL. The reaction was quickly exported from an inert atmosphere glovebox and placed into a dry ice/acetone cooling bath. The reaction was warmed to room temperature and placed into an NMR spectrometer held at 35 °C, and a ^{31}P NMR spectrum was obtained every 122 s for 7.2 h for the reaction with hydrazine monohydrate and every 23 s for 38 min for the reaction with anhydrous hydrazine. All reactions proceeded for at least 3.5 half-lives. k_{obs} was determined by the decay of starting material via a least-squares fit of concentration vs. time to the following equation, $[\text{Starting Material}] = Ae^{-k_{obs}t} + C$. The rate constant k was obtained by dividing k_{obs} by the concentration of hydrazine (0.393 M).

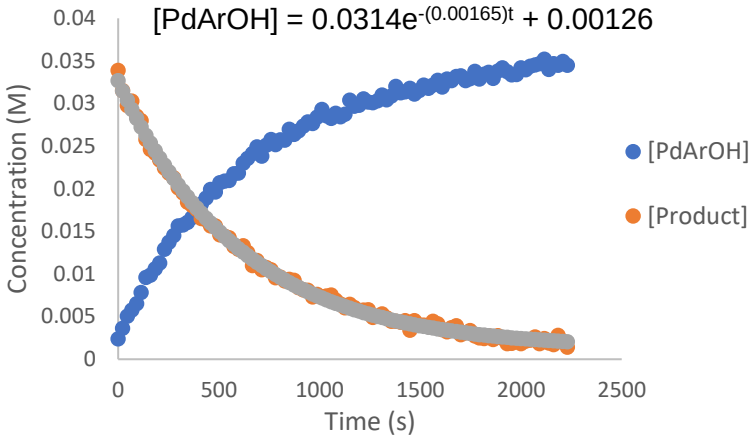

Figure S2. Representative fit of the reaction between hydroxo complex **5** with anhydrous hydrazine.

*Time Course of Reaction of Palladium Hydroxo Complex **4** With KOH in the Presence of Hydrazine Hydrate*

A J. Young NMR tube was charged with KOH (13.3 mg, 0.236 mmol, 10.0 equiv), and 600 µL of a THF-d_8 solution containing palladium complex **4** (18.6 mg, 0.0236 mmol, 1.00 equiv) and $PMes_3$ (18.4 mg, 0.0472 mmol, 2.00 equiv). Hydrazine monohydrate (11.5 µL, 0.236 mmol, 10.0 equiv) was added to the NMR tube. The NMR tube was capped, quickly exported from an inert atmosphere glovebox, and placed into a dry ice/acetone cooling bath for sample storage and transportation purposes. The NMR tube was taken out of the cooling bath and placed into an NMR spectrometer and a ^{31}P NMR spectrum was obtained for an initial time point. The sample was taken from the NMR spectrometer and placed into the dry ice/acetone bath for one minute. The NMR tube and the sample within it was taken out of the bath and allowed to equilibrate to room temperature over the course of 1.5 min. During this time, the NMR tube was gently shaken for ca. 15 s. Then, the NMR tube was placed into an NMR spectrometer and another ^{31}P NMR spectrum was obtained. The total time the NMR tube spent outside of the cooling bath was recorded. This process was repeated 8 more times to obtain the data in Figure S3.

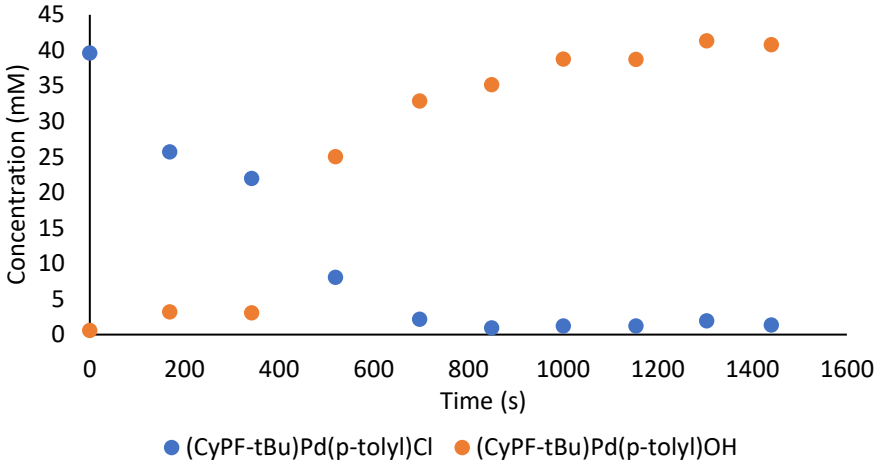

Figure S3. Concentration of arylpalladium(II) chloride complex (**4**) and arylpalladium(II) hydroxo complex (**5**) over time in the presence of KOH and hydrazine monohydrate in THF-d_8.

*Experiments to Determine Yield of Reactions with Palladium Hydrazido Complex **8***

*Experiment to Determine the Yield of Hydrazido Complex **8***

A J. Young tube was charged with (CyPF-*t*Bu)Pd(4-methoxyphenyl)Br (22.9 mg, 0.0270 mmol, 1.00 equiv), NaO*t*Bu (2.9 mg, 0.0297, 1.10 equiv), PPh_3 (14.1 mg, 0.0540 mmol, 2.00 equiv), $PMes_3$ (10.5 mg, 0.0270 mmol, 1.00 equiv), and 500 µL of THF-d_8. The reaction was frozen in the coldwell of the glovebox, which was cooled with a liquid nitrogen bath. Then, hydrazine (1.0 M in THF, 29.7 µL, 0.0297 mmol, 1.10 equiv) was added to the NMR tube, which was quickly exported from the glovebox into a dry ice/acetone cooling bath. The NMR tube was injected into an NMR spectrometer cooled to -50 °C, and a ^{31}P NMR spectrum was obtained. This spectrum indicated that the hydrazido complex **8** formed in 36% yield relative to the Pd(II) starting material . The NMR tube was ejected and warmed to ambient temperature for 3 min and was returned to the NMR spectrometer. A ^{31}P NMR spectrum was obtained, which indicated that (CyPF-*t*Bu)Pd(PPh_3) formed in 86% yield relative to the Pd(II) starting material.

Experiment to Determine the Yield of 4-Methoxyphenyl Hydrazine

A J. Young tube was charged with (CyPF-*t*Bu)Pd(4-methoxyphenyl)Br (14.4 mg, 0.0170 mmol, 1.00 equiv), NaO*t*Bu (1.8 mg, 0.019, 1.1 equiv), PPh_3 (6.7 mg, 0.026 mmol, 1.5 equiv), 1,3,5-trimethoxybenzene (2.9 mg, 0.017 mmol, 1.0 equiv), and 500 µL of THF-d_8. The reaction was shaken until a homogenous red-orange solution was obtained. Hydrazine (1.0 M in THF, 18.7 µL, 0.0187 mmol, 1.10 equiv) was added to the NMR tube, which was shaken for 30 s. The yield of 4-methoxyphenyl hydrazine was immediately determined by ^{1}H NMR spectroscopy.

COPASI Simulation Details

A .txt file of concentration vs. time data from the time course of reaction of palladium aryl chloride complex **4** with KOH and hydrazine was imported into COPASI 4.25 (build 207) and fitted to the mechanism below (Figure S2) with the evolutionary programming fitting method. 800 generations and a population size of 80 were used. The starting concentrations of (CyPF-*t*Bu)Pd(4-methylphenyl)Cl and (CyPF-*t*Bu)Pd(4-methylphenyl)OH were obtained from the t = 0 min measurement obtained from our concentration vs. time data. The starting concentration of [N_2H_4]

was set to 0.393 M. Because the concentration of KOH was difficult to measure in 1,4-dioxane, we used COPASI to determine the concentration of KOH during parameter estimation by making it a variable to be optimized. The fitting indicated that the concentration of KOH was 0.0346(8) M, which we believe to be due to hydrazine coordination to K^+, which may help solvate OH^- ions. If the concentration of KOH given by COPASI was overestimated, then k_1 in Figure S2 may be underestimated, and the actual value of k_1 is higher than what we obtain by COPASI. However, because we are simulating rate, which is governed by the product of k_1 and $[OH]^-$, and the concentration of $[OH]^-$ is likely constant throughout the reaction because it is in large excess (10 equiv), we believe this analysis is valid.

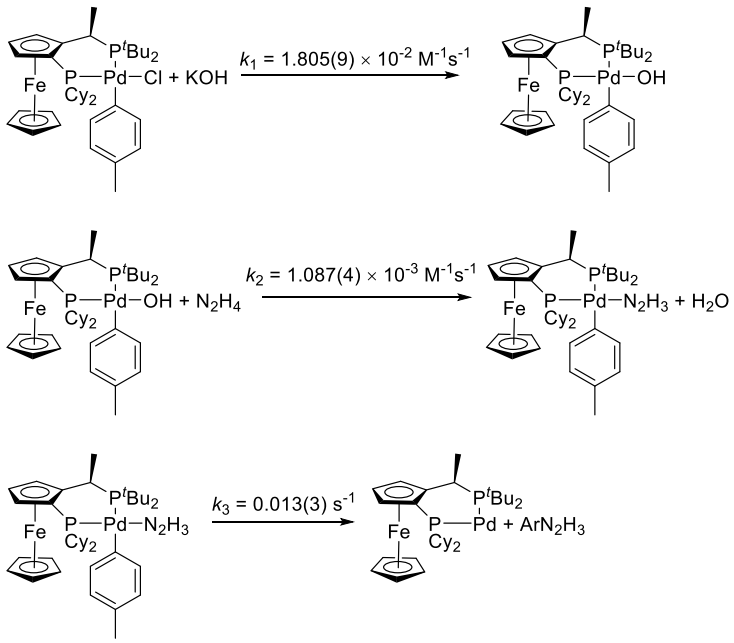

Figure S4. Mechanistic input for COPASI simulations and output for rate constants.

We recommend the following video tutorial by the McIndoe group on the usage of COPASI for simulating chemical kinetics: https://www.youtube.com/watch?v=Wo3FR1upfjY.

DFT Computational Details

All DFT calculations were performed using the B3LYP functional for geometry optimizations and for single point energy calculations, as implemented in Gaussian 09. The D3 version of Grimme's dispersion was added to the functional used during these calculations. The effective core potential and associated double ζ basis sets of LANL2DZ were utilized for palladium and iron atoms in geometry optimizations. The effective core potential and associated triple ζ basis sets of LANL2TZ were utilized for palladium and iron atoms in single point energy calculations. For iron and palladium atoms, an f polarization function was added to the basis set during single point energy calculations. The 6-31G** basis set was utilized for all other atoms during geometry optimizations, and the 6-311+G** basis set was utilized for all other atoms during single point energy calculations. Thermal corrections from the geometry optimizations were added to the energies found in single point energy calculations to find values for Gibbs free energy. All geometries were fully optimized and confirmed as minima or saddle points by analytical frequency calculations at the same level. The CPCM solvation model was used to account for solvation effects of 1,4-dioxane in single point energy calculations.

X-Ray Crystallographic Data

(*CyPF-tBu)Pd(Ph)OH* (**6**)

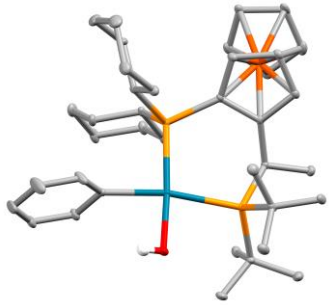

Figure S3. ORTEP drawing of **6** with selected hydrogens atoms omitted.

An orange block 0.33 x 0.28 x 0.22 mm in size was mounted on a Cryoloop with Paratone oil. Data were collected in a nitrogen gas stream at 100(2) K using omega scans. Crystal-to-detector distance was 50 mm and exposure time was 0.50 seconds per frame using a scan width of 0.5°. Data collection was 100% complete to 26.369° in θ. A total of 81918 reflections were collected covering the indices -12<=h<=12, -13<=k<=13, -14<=l<=14. 8862 reflections were founded to be symmetry independent, with an R_{int} of 0.0762. Indexing and unit cell refinement indicated a primitive, triclinic lattice. The space group was found to be P 1 (No. 1). The data were integrated using the CrysAlis^{Pro} 1.171.39.46e software program and scaled using the SCALE3 ABSPACK scaling algorithm. Solution by intrinsic phasing (SHELXT-2015) produced a heavy-atom phasing model consistent with the proposed structure. All non-hydrogen atoms were refined anisotropically by full-matrix least-squares (SHELXL-2014). All hydrogen atoms were placed using a riding model. Their positions were constrained relative to their parent atom using the appropriate HFIX command in SHELXL-2014.

Table 1. Crystal data and structure refinement for **6**.

Empirical formula	C46 H74 Fe O3 P2 Pd	
Formula weight	899.24	
Temperature	100(2) K	
Wavelength	0.71073 Å	
Crystal system	Triclinic	
Space group	P 1	
Unit cell dimensions	a = 10.23440(10) Å	a= 103.1520(10)°.
	b = 11.13410(10) Å	b= 102.2470(10)°.
	c = 11.75970(10) Å	g = 116.8760(10)°.
Volume	1084.70(2) $Å^3$	
Z	1	
Density (calculated)	1.377 Mg/m^3	
Absorption coefficient	0.861 mm^{-1}	
F(000)	476	
Crystal size	0.330 x 0.280 x 0.220 mm^3	
Theta range for data collection	2.917 to 26.369°.	
Index ranges	-12<=h<=12, -13<=k<=13, -14<=l<=14	
Reflections collected	81918	
Independent reflections	8862 [R(int) = 0.0762]	
Completeness to theta = 26.369°	99.9 %	
Absorption correction	Semi-empirical from equivalents	
Max. and min. transmission	1.00000 and 0.73970	
Refinement method	Full-matrix least-squares on F^2	
Data / restraints / parameters	8862 / 44 / 489	
Goodness-of-fit on F^2	1.022	
Final R indices [I>2sigma(I)]	R1 = 0.0299, wR2 = 0.0794	
R indices (all data)	R1 = 0.0300, wR2 = 0.0795	
Absolute structure parameter	-0.006(9)	
Extinction coefficient	n/a	
Largest diff. peak and hole	0.979 and -0.482 e.$Å^{-3}$	

Table 2. Atomic coordinates (x 10^4) and equivalent isotropic displacement parameters ($Å^2$x 10^3) for **6**. U(eq) is defined as one third of the trace of the orthogonalized U^{ij} tensor.

	x	y	z	U(eq)
C(1)	6994(5)	4668(5)	4576(4)	16(1)
C(2)	8605(5)	5688(5)	5098(4)	22(1)
C(3)	9502(6)	6134(6)	4376(5)	28(1)
C(4)	8808(7)	5561(8)	3087(6)	42(2)
C(5)	7210(8)	4516(10)	2543(6)	52(2)
C(6)	6333(6)	4104(7)	3277(5)	32(1)
C(7)	6687(5)	3099(5)	8527(4)	20(1)
C(8)	6104(6)	2125(6)	9275(5)	28(1)
C(9)	7756(5)	2738(5)	7982(5)	23(1)
C(10)	7709(5)	4703(5)	9403(4)	22(1)
C(11)	3399(5)	974(5)	6383(4)	18(1)
C(12)	4074(6)	24(5)	5999(5)	25(1)
C(13)	2335(6)	361(5)	7107(5)	24(1)
C(14)	2398(5)	911(5)	5176(5)	23(1)
C(15)	4340(5)	3971(4)	8131(4)	15(1)
C(16)	3957(6)	3713(5)	9287(4)	20(1)
C(17)	3021(5)	3938(5)	7237(4)	13(1)
C(18)	1442(5)	3260(4)	7184(4)	15(1)
C(19)	529(5)	3450(5)	6223(4)	17(1)
C(20)	1557(5)	4253(5)	5685(4)	17(1)
C(21)	3113(5)	4561(4)	6284(4)	14(1)
C(22)	2203(6)	7232(5)	7723(5)	21(1)
C(23)	1159(6)	6313(5)	8195(5)	26(1)
C(24)	2075(6)	6166(5)	9179(5)	26(1)
C(25)	3674(6)	6979(5)	9316(5)	25(1)
C(26)	3739(5)	7643(5)	8414(5)	22(1)
C(27)	2616(5)	3422(5)	3287(4)	20(1)
C(28)	2023(6)	3214(6)	1916(5)	30(1)
C(29)	1404(7)	4197(7)	1747(5)	37(1)
C(30)	2657(7)	5771(7)	2527(5)	33(1)
C(31)	3276(6)	6040(6)	3918(5)	24(1)
C(32)	3876(5)	5023(5)	4114(4)	17(1)
C(33)	6028(5)	7188(5)	6598(4)	16(1)
C(34)	7211(6)	7912(5)	5991(5)	21(1)
C(35)	8239(6)	9557(5)	6707(5)	26(1)
C(36)	9096(6)	9928(5)	8079(5)	27(1)
C(37)	7944(6)	9208(5)	8692(5)	25(1)
C(38)	6913(5)	7566(5)	7980(4)	18(1)
C(39)	7410(20)	8524(18)	12677(13)	169(8)
C(40)	7690(20)	9904(17)	13509(13)	133(6)
C(41)	7614(18)	10929(16)	12911(10)	110(4)
C(42)	7545(16)	10218(12)	11651(11)	107(5)
C(43)	1762(10)	8499(11)	11969(12)	92(3)
C(44)	970(30)	9080(30)	11220(20)	186(8)
C(45)	2010(30)	9780(20)	10565(17)	182(8)
C(46)	3630(30)	10098(16)	11229(12)	158(7)
Fe(1)	2331(1)	5416(1)	7539(1)	13(1)
O(1)	6718(5)	2506(4)	5390(4)	22(1)
O(2)	7325(14)	8792(14)	11478(10)	136(4)
O(3)	3436(13)	9394(12)	12143(10)	139(4)

P(1)	5056(1)	2921(1)	7243(1)	14(1)
P(2)	4764(1)	5213(1)	5738(1)	12(1)
Pd(1)	5921(1)	3889(1)	5746(1)	12(1)

Table 3. Bond lengths [Å] and angles [°] for **6**.

C(1)-C(6)	1.388(7)	C(2)-C(1)-Pd(1)	117.4(3)
C(1)-C(2)	1.395(7)	C(3)-C(2)-C(1)	122.7(5)
C(1)-Pd(1)	2.044(4)	C(4)-C(3)-C(2)	120.1(5)
C(2)-C(3)	1.385(7)	C(3)-C(4)-C(5)	118.3(5)
C(3)-C(4)	1.380(8)	C(6)-C(5)-C(4)	120.7(5)
C(4)-C(5)	1.391(10)	C(5)-C(6)-C(1)	122.3(5)
C(5)-C(6)	1.377(8)	C(9)-C(7)-C(10)	106.5(4)
C(7)-C(9)	1.533(6)	C(9)-C(7)-C(8)	107.7(4)
C(7)-C(10)	1.537(7)	C(10)-C(7)-C(8)	110.5(4)
C(7)-C(8)	1.542(6)	C(9)-C(7)-P(1)	110.7(3)
C(7)-P(1)	1.898(4)	C(10)-C(7)-P(1)	107.0(3)
C(11)-C(14)	1.531(7)	C(8)-C(7)-P(1)	114.3(3)
C(11)-C(13)	1.537(6)	C(14)-C(11)-C(13)	108.5(4)
C(11)-C(12)	1.541(6)	C(14)-C(11)-C(12)	107.3(4)
C(11)-P(1)	1.884(4)	C(13)-C(11)-C(12)	110.1(4)
C(15)-C(17)	1.505(6)	C(14)-C(11)-P(1)	106.5(3)
C(15)-C(16)	1.545(6)	C(13)-C(11)-P(1)	114.7(3)
C(15)-P(1)	1.881(4)	C(12)-C(11)-P(1)	109.4(3)
C(17)-C(18)	1.420(6)	C(17)-C(15)-C(16)	110.9(4)
C(17)-C(21)	1.444(6)	C(17)-C(15)-P(1)	110.1(3)
C(17)-Fe(1)	2.055(4)	C(16)-C(15)-P(1)	120.8(3)
C(18)-C(19)	1.426(6)	C(18)-C(17)-C(21)	108.0(4)
C(18)-Fe(1)	2.042(4)	C(18)-C(17)-C(15)	125.1(4)
C(19)-C(20)	1.413(6)	C(21)-C(17)-C(15)	127.0(4)
C(19)-Fe(1)	2.046(4)	C(18)-C(17)-Fe(1)	69.2(2)
C(20)-C(21)	1.440(6)	C(21)-C(17)-Fe(1)	70.0(2)
C(20)-Fe(1)	2.028(4)	C(15)-C(17)-Fe(1)	126.8(3)
C(21)-P(2)	1.832(4)	C(17)-C(18)-C(19)	109.2(4)
C(21)-Fe(1)	2.068(4)	C(17)-C(18)-Fe(1)	70.2(2)
C(22)-C(26)	1.407(7)	C(19)-C(18)-Fe(1)	69.7(2)
C(22)-C(23)	1.421(7)	C(20)-C(19)-C(18)	106.9(4)
C(22)-Fe(1)	2.050(4)	C(20)-C(19)-Fe(1)	69.0(2)

C(23)-C(24)	1.418(8)	C(18)-C(19)-Fe(1)	69.4(2)
C(23)-Fe(1)	2.039(5)	C(19)-C(20)-C(21)	109.9(4)
C(24)-C(25)	1.416(8)	C(19)-C(20)-Fe(1)	70.4(3)
C(24)-Fe(1)	2.041(5)	C(21)-C(20)-Fe(1)	70.9(2)
C(25)-C(26)	1.421(7)	C(20)-C(21)-C(17)	106.0(4)
C(25)-Fe(1)	2.061(5)	C(20)-C(21)-P(2)	127.4(3)
C(26)-Fe(1)	2.065(4)	C(17)-C(21)-P(2)	125.1(3)
C(27)-C(28)	1.519(6)	C(20)-C(21)-Fe(1)	67.9(2)
C(27)-C(32)	1.545(6)	C(17)-C(21)-Fe(1)	69.0(2)
C(28)-C(29)	1.521(8)	P(2)-C(21)-Fe(1)	138.0(2)
C(29)-C(30)	1.515(9)	C(26)-C(22)-C(23)	108.0(5)
C(30)-C(31)	1.527(7)	C(26)-C(22)-Fe(1)	70.6(3)
C(31)-C(32)	1.550(6)	C(23)-C(22)-Fe(1)	69.2(3)
C(32)-P(2)	1.850(5)	C(24)-C(23)-C(22)	107.5(4)
C(33)-C(38)	1.536(6)	C(24)-C(23)-Fe(1)	69.7(3)
C(33)-C(34)	1.540(6)	C(22)-C(23)-Fe(1)	70.1(3)
C(33)-P(2)	1.842(4)	C(25)-C(24)-C(23)	108.7(4)
C(34)-C(35)	1.532(6)	C(25)-C(24)-Fe(1)	70.6(3)
C(35)-C(36)	1.521(7)	C(23)-C(24)-Fe(1)	69.6(3)
C(36)-C(37)	1.524(6)	C(24)-C(25)-C(26)	107.1(5)
C(37)-C(38)	1.531(6)	C(24)-C(25)-Fe(1)	69.0(3)
C(39)-C(40)	1.485(11)	C(26)-C(25)-Fe(1)	70.0(3)
C(39)-O(2)	1.499(11)	C(22)-C(26)-C(25)	108.8(4)
C(40)-C(41)	1.492(10)	C(22)-C(26)-Fe(1)	69.5(3)
C(41)-C(42)	1.483(9)	C(25)-C(26)-Fe(1)	69.7(3)
C(42)-O(2)	1.457(10)	C(28)-C(27)-C(32)	111.7(4)
C(43)-O(3)	1.478(10)	C(27)-C(28)-C(29)	111.1(4)
C(43)-C(44)	1.509(11)	C(30)-C(29)-C(28)	110.8(4)
C(44)-C(45)	1.486(11)	C(29)-C(30)-C(31)	112.3(4)
C(45)-C(46)	1.513(11)	C(30)-C(31)-C(32)	110.5(4)
C(46)-O(3)	1.465(10)	C(27)-C(32)-C(31)	111.3(4)
O(1)-Pd(1)	2.049(4)	C(27)-C(32)-P(2)	110.9(3)
P(1)-Pd(1)	2.3882(11)	C(31)-C(32)-P(2)	118.2(3)

P(2)-Pd(1)	2.2708(12)	C(38)-C(33)-C(34)	109.6(4)
C(6)-C(1)-C(2)	115.9(4)	C(38)-C(33)-P(2)	111.6(3)
C(6)-C(1)-Pd(1)	125.7(4)	C(34)-C(33)-P(2)	111.7(3)
C(35)-C(34)-C(33)	111.1(4)	C(21)-P(2)-C(33)	107.16(19)
C(36)-C(35)-C(34)	111.3(4)	C(21)-P(2)-C(32)	104.4(2)
C(35)-C(36)-C(37)	111.0(4)	C(33)-P(2)-C(32)	104.0(2)
C(36)-C(37)-C(38)	111.3(4)	C(21)-P(2)-Pd(1)	112.65(14)
C(37)-C(38)-C(33)	111.3(4)	C(33)-P(2)-Pd(1)	117.59(15)
C(40)-C(39)-O(2)	100.1(12)	C(32)-P(2)-Pd(1)	109.96(15)
C(39)-C(40)-C(41)	116.9(12)	C(1)-Pd(1)-O(1)	82.90(17)
C(42)-C(41)-C(40)	99.8(11)	C(1)-Pd(1)-P(2)	91.90(13)
O(2)-C(42)-C(41)	111.6(11)	O(1)-Pd(1)-P(2)	168.91(12)
O(3)-C(43)-C(44)	103.8(13)	C(1)-Pd(1)-P(1)	169.61(12)
C(45)-C(44)-C(43)	106.6(15)	O(1)-Pd(1)-P(1)	88.71(13)
C(44)-C(45)-C(46)	108.0(15)	P(2)-Pd(1)-P(1)	97.39(4)
O(3)-C(46)-C(45)	104.6(14)	C(17)-Fe(1)-C(25)	110.1(2)
C(20)-Fe(1)-C(23)	120.0(2)	C(20)-Fe(1)-C(26)	126.5(2)
C(20)-Fe(1)-C(24)	154.9(2)	C(23)-Fe(1)-C(26)	67.76(19)
C(23)-Fe(1)-C(24)	40.7(2)	C(24)-Fe(1)-C(26)	67.50(19)
C(20)-Fe(1)-C(18)	68.14(18)	C(18)-Fe(1)-C(26)	160.9(2)
C(23)-Fe(1)-C(18)	118.08(19)	C(19)-Fe(1)-C(26)	158.25(19)
C(24)-Fe(1)-C(18)	104.33(19)	C(22)-Fe(1)-C(26)	40.0(2)
C(20)-Fe(1)-C(19)	40.59(17)	C(17)-Fe(1)-C(26)	127.94(19)
C(23)-Fe(1)-C(19)	102.1(2)	C(25)-Fe(1)-C(26)	40.3(2)
C(24)-Fe(1)-C(19)	118.1(2)	C(20)-Fe(1)-C(21)	41.15(17)
C(18)-Fe(1)-C(19)	40.81(18)	C(23)-Fe(1)-C(21)	158.8(2)
C(20)-Fe(1)-C(22)	108.12(19)	C(24)-Fe(1)-C(21)	160.5(2)
C(23)-Fe(1)-C(22)	40.65(19)	C(18)-Fe(1)-C(21)	68.63(16)
C(24)-Fe(1)-C(22)	68.0(2)	C(19)-Fe(1)-C(21)	69.18(16)
C(18)-Fe(1)-C(22)	154.95(19)	C(22)-Fe(1)-C(21)	125.92(18)
C(19)-Fe(1)-C(22)	120.05(19)	C(17)-Fe(1)-C(21)	41.01(17)
C(20)-Fe(1)-C(17)	68.69(18)	C(25)-Fe(1)-C(21)	127.03(19)
C(23)-Fe(1)-C(17)	155.49(19)	C(26)-Fe(1)-C(21)	113.04(17)

C(24)-Fe(1)-C(17)	122.1(2)	C(42)-O(2)-C(39)	110.6(11)
C(18)-Fe(1)-C(17)	40.57(17)	C(46)-O(3)-C(43)	111.6(13)
C(19)-Fe(1)-C(17)	68.90(18)	C(15)-P(1)-C(11)	109.25(19)
C(22)-Fe(1)-C(17)	163.34(18)	C(15)-P(1)-C(7)	103.2(2)
C(20)-Fe(1)-C(25)	163.4(2)	C(11)-P(1)-C(7)	111.5(2)
C(23)-Fe(1)-C(25)	68.3(2)	C(15)-P(1)-Pd(1)	110.81(13)
C(24)-Fe(1)-C(25)	40.4(2)	C(11)-P(1)-Pd(1)	108.47(15)
C(18)-Fe(1)-C(25)	122.5(2)	C(7)-P(1)-Pd(1)	113.55(14)
C(19)-Fe(1)-C(25)	155.73(19)		
C(22)-Fe(1)-C(25)	68.0(2)		

Table 4. Anisotropic displacement parameters ($Å^2 x\ 10^3$) for **6**. The anisotropic displacement factor exponent takes the form: $-2\pi^2[h^2 a^{*2} U^{11} + ... + 2 h k a^* b^* U^{12}]$

	U^{11}	U^{22}	U^{33}	U^{23}	U^{13}	U^{12}
C(1)	17(2)	21(2)	17(2)	9(2)	9(2)	14(2)
C(2)	18(2)	26(2)	21(2)	8(2)	10(2)	10(2)
C(3)	19(2)	31(3)	41(3)	18(2)	19(2)	13(2)
C(4)	38(3)	86(5)	39(3)	44(3)	32(3)	43(3)
C(5)	40(3)	106(6)	23(3)	26(3)	18(3)	44(4)
C(6)	20(2)	59(4)	18(2)	11(2)	9(2)	22(2)
C(7)	16(2)	27(2)	25(2)	16(2)	9(2)	14(2)
C(8)	26(2)	39(3)	35(3)	26(2)	15(2)	22(2)
C(9)	18(2)	28(2)	31(3)	13(2)	10(2)	16(2)
C(10)	19(2)	30(2)	21(2)	12(2)	9(2)	12(2)
C(11)	14(2)	14(2)	28(2)	8(2)	10(2)	7(2)
C(12)	21(2)	18(2)	38(3)	9(2)	13(2)	11(2)
C(13)	18(2)	18(2)	42(3)	18(2)	17(2)	10(2)
C(14)	18(2)	17(2)	27(2)	5(2)	5(2)	6(2)
C(15)	15(2)	16(2)	18(2)	9(2)	9(2)	9(2)
C(16)	23(2)	26(2)	20(2)	14(2)	12(2)	14(2)
C(17)	16(2)	10(2)	17(2)	6(2)	9(2)	7(2)
C(18)	14(2)	12(2)	19(2)	5(2)	8(2)	6(2)
C(19)	14(2)	16(2)	17(2)	3(2)	6(2)	8(2)
C(20)	15(2)	21(2)	15(2)	6(2)	5(2)	11(2)
C(21)	14(2)	13(2)	17(2)	7(2)	8(2)	8(2)
C(22)	22(2)	16(2)	33(2)	10(2)	17(2)	12(2)
C(23)	29(2)	20(2)	43(3)	14(2)	27(2)	17(2)
C(24)	37(3)	23(2)	24(2)	8(2)	20(2)	16(2)
C(25)	30(3)	21(2)	18(2)	1(2)	9(2)	13(2)
C(26)	19(2)	12(2)	30(2)	4(2)	11(2)	6(2)
C(27)	19(2)	26(2)	17(2)	9(2)	7(2)	12(2)
C(28)	27(2)	41(3)	18(2)	12(2)	8(2)	15(2)
C(29)	33(3)	55(4)	26(3)	22(3)	7(2)	25(3)
C(30)	37(3)	47(3)	35(3)	30(3)	16(2)	28(3)
C(31)	25(2)	30(2)	32(3)	22(2)	17(2)	21(2)
C(32)	17(2)	23(2)	18(2)	11(2)	10(2)	13(2)
C(33)	18(2)	14(2)	24(2)	10(2)	13(2)	10(2)

C(34)	23(2)	20(2)	27(2)	13(2)	16(2)	11(2)
C(35)	25(2)	16(2)	36(3)	12(2)	16(2)	7(2)
C(36)	21(2)	15(2)	36(3)	7(2)	16(2)	2(2)
C(37)	21(2)	19(2)	28(2)	7(2)	13(2)	5(2)
C(38)	18(2)	17(2)	21(2)	9(2)	12(2)	7(2)
C(39)	148(17)	145(13)	130(13)	23(10)	-19(11)	55(12)
C(40)	179(17)	148(12)	75(8)	41(7)	18(9)	101(12)
C(41)	117(10)	147(11)	66(6)	23(6)	43(7)	72(9)
C(42)	95(9)	77(7)	82(7)	-6(5)	45(6)	5(6)
C(43)	39(4)	76(6)	122(8)	-9(6)	4(5)	33(4)
C(44)	217(19)	210(20)	179(17)	49(15)	32(13)	176(17)
C(45)	350(20)	198(16)	111(11)	60(11)	85(13)	228(18)
C(46)	340(20)	139(12)	91(9)	51(8)	96(12)	182(15)
Fe(1)	14(1)	13(1)	17(1)	7(1)	9(1)	8(1)
O(1)	23(2)	29(2)	31(2)	17(2)	16(2)	19(2)
O(2)	137(9)	172(11)	114(8)	54(8)	36(7)	96(9)
O(3)	166(11)	137(9)	116(8)	32(7)	46(8)	89(9)
P(1)	12(1)	14(1)	19(1)	9(1)	9(1)	8(1)
P(2)	13(1)	13(1)	15(1)	7(1)	8(1)	8(1)
Pd(1)	11(1)	13(1)	15(1)	6(1)	7(1)	7(1)

Table 5. Hydrogen coordinates (x 10^4) and isotropic displacement parameters ($Å^2$x 10^3) for **6**.

	x	y	z	U(eq)
H(2)	9108	6093	5984	26
H(3)	10596	6834	4770	34
H(4)	9407	5874	2584	50
H(5)	6719	4082	1656	63
H(6)	5238	3409	2879	39
H(8A)	5295	2224	9529	42
H(8B)	6987	2418	10022	42
H(8C)	5659	1112	8749	42
H(9A)	7131	1748	7355	34
H(9B)	8576	2815	8655	34
H(9C)	8246	3421	7586	34
H(10A)	8035	5309	8910	34
H(10B)	8642	4863	10018	34
H(10C)	7102	4960	9841	34
H(12A)	4831	475	5613	38
H(12B)	3218	-939	5398	38
H(12C)	4602	-70	6744	38
H(13A)	2967	425	7897	35
H(13B)	1519	-655	6602	35
H(13C)	1842	923	7283	35
H(14A)	2024	1572	5385	35
H(14B)	1496	-80	4708	35
H(14C)	3034	1202	4661	35
H(15)	5229	5003	8468	18
H(16A)	3129	2698	9042	30
H(16B)	3596	4345	9624	30
H(16C)	4903	3931	9930	30
H(18)	1056	2761	7706	18
H(19)	-562	3102	5990	20
H(20)	1264	4547	5026	20
H(22)	1915	7518	7057	26
H(23)	50	5877	7904	31
H(24)	1682	5614	9666	31
H(25)	4540	7065	9901	30
H(26)	4667	8263	8298	26
H(27A)	3070	2813	3373	24
H(27B)	1722	3097	3581	24
H(28A)	1174	2190	1424	35
H(28B)	2890	3431	1593	35
H(29A)	1064	4068	852	44
H(29B)	478	3924	2002	44
H(30A)	2216	6383	2418	40
H(30B)	3542	6061	2221	40
H(31A)	2426	5867	4254	28
H(31B)	4144	7063	4381	28
H(32)	4742	5274	3775	20
H(33)	5338	7600	6569	20
H(34A)	7889	7500	5985	25
H(34B)	6634	7705	5112	25
H(35A)	9016	9988	6319	31

H(35B)	7571	9980	6646	31
H(36A)	9698	10992	8527	33
H(36B)	9851	9598	8144	33
H(37A)	7267	9621	8711	30
H(37B)	8534	9417	9567	30
H(38A)	6145	7137	8377	22
H(38B)	7579	7141	8032	22
H(39A)	6420	7677	12591	203
H(39B)	8297	8385	12976	203
H(40A)	8738	10416	14177	159
H(40B)	6903	9663	13920	159
H(41A)	6663	10977	12870	132
H(41B)	8561	11916	13350	132
H(42A)	6665	10117	11004	128
H(42B)	8532	10837	11540	128
H(43A)	1621	8613	12786	111
H(43B)	1337	7461	11505	111
H(44A)	-76	8281	10607	223
H(44B)	840	9792	11782	223
H(45A)	2059	10698	10584	218
H(45B)	1594	9135	9679	218
H(46A)	4008	9689	10629	190
H(46B)	4393	11156	11653	190
H(1)	6860(80)	2550(80)	4840(70)	30(20)

(*CyPF-tBu)Pd(p-tolyl)OH* (**5**)

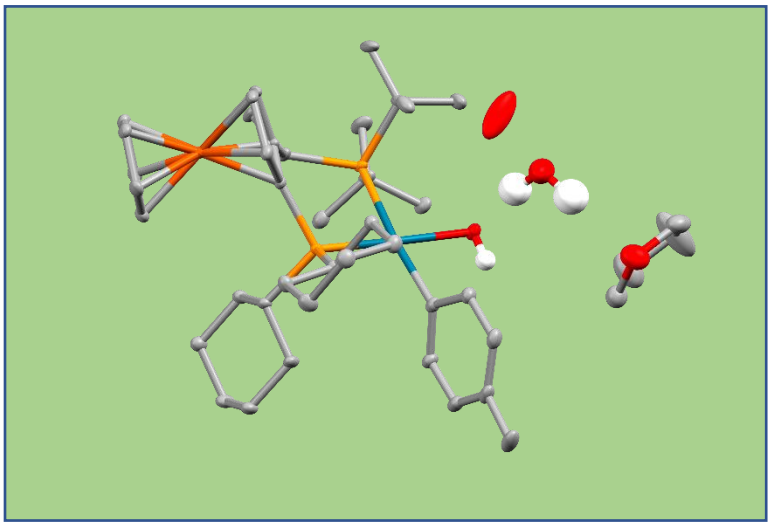

An orange block 0.51 x 0.35 x 0.23 mm in size was mounted on a Cryoloop with Paratone oil. Data were collected in a nitrogen gas stream at 100(2) K using omega scans. Crystal-to-detector distance was 30.23 mm and exposure time was 0.50 seconds per frame using a scan width of 0.5°. Data collection was 100% complete to 30.500° in θ. A total of 88552 reflections were collected covering the indices -14<=h<=14, -14<=k<=14, -15<=l<=15. 12325 reflections were found to be symmetry independent, with an R_{int} of 0.0704. Indexing and unit cell refinement indicated a primitive, triclinic lattice. The space group was found to be P 1 (No. 1). The data were integrated using the CrysAlis^{Pro} 1.171.40.63a software program and scaled using the SCALE3 ABSPACK scaling algorithm. Solution by intrinsic phasing (SHELXT-2015) produced a heavy-atom phasing model consistent with the proposed structure. All non-hydrogen atoms were refined anisotropically by full-matrix least-squares (SHELXL-2014). All hydrogen atoms were placed using a riding model. Their positions were constrained relative to their parent atom using the appropriate HFIX command in SHELXL-2014.

Table 1. Crystal data and structure refinement for JWang005_Hartwig.

Identification code	JWang005_Hartwig	
Empirical formula	C43 H70 Fe O3.25 P2 Pd	
Formula weight	863.18	
Temperature	100(2) K	
Wavelength	0.71073 Å	
Crystal system	Triclinic	
Space group	P 1	
Unit cell dimensions	a = 9.95510(10) Å	a= 95.3860(10)°.
	b = 10.38340(10) Å	b= 113.2540(10)°.
	c = 10.91290(10) Å	g = 92.2210(10)°.
Volume	1028.278(19) $Å^3$	
Z	1	
Density (calculated)	1.394 Mg/m^3	
Absorption coefficient	0.906 mm^{-1}	
F(000)	456	
Crystal size	0.510 x 0.350 x 0.230 mm^3	
Theta range for data collection	3.010 to 30.507°.	
Index ranges	-14<=h<=14, -14<=k<=14, -15<=l<=15	
Reflections collected	88552	
Independent reflections	12325 [R(int) = 0.0704]	
Completeness to theta = 30.500°	99.9 %	
Absorption correction	Semi-empirical from equivalents	
Max. and min. transmission	1.00000 and 0.75457	
Refinement method	Full-matrix least-squares on F^2	
Data / restraints / parameters	12325 / 5 / 480	
Goodness-of-fit on F^2	1.034	
Final R indices [I>2sigma(I)]	R1 = 0.0234, wR2 = 0.0581	
R indices (all data)	R1 = 0.0235, wR2 = 0.0581	
Absolute structure parameter	-0.010(6)	
Extinction coefficient	n/a	
Largest diff. peak and hole	0.452 and -0.450 $e.Å^{-3}$	

Table 2. Atomic coordinates (x 10^4) and equivalent isotropic displacement parameters ($Å^2$x 10^3) for jwang005_hartwig. U(eq) is defined as one third of the trace of the orthogonalized U^{ij} tensor.

	x	y	z	U(eq)
C(1)	6924(3)	6176(2)	5653(2)	14(1)
C(2)	8279(3)	5958(2)	6654(2)	17(1)
C(3)	9283(3)	6973(3)	7476(2)	20(1)
C(4)	8998(3)	8260(2)	7327(2)	19(1)
C(5)	10004(3)	9361(3)	8294(3)	28(1)
C(6)	7717(3)	8497(2)	6263(3)	20(1)
C(7)	6719(3)	7482(2)	5439(2)	17(1)
C(8)	2291(3)	4956(3)	1811(3)	23(1)
C(9)	2701(3)	3653(3)	1304(2)	18(1)
C(10)	1282(3)	2825(3)	407(2)	26(1)
C(11)	3591(3)	3961(3)	476(2)	23(1)
C(12)	4909(3)	1554(2)	2388(2)	16(1)
C(13)	4001(3)	638(3)	1097(3)	24(1)
C(14)	6275(3)	2130(2)	2239(2)	18(1)
C(15)	5467(3)	757(2)	3591(3)	18(1)
C(16)	2694(2)	2046(2)	3519(2)	14(1)
C(17)	1750(3)	791(3)	2749(2)	19(1)
C(18)	1806(3)	3011(2)	3901(2)	12(1)
C(19)	246(2)	3063(2)	3224(2)	15(1)
C(20)	-189(3)	4146(2)	3832(2)	16(1)
C(21)	1089(3)	4770(2)	4903(2)	14(1)
C(22)	2354(2)	4083(2)	4959(2)	12(1)
C(23)	973(3)	1140(2)	5934(2)	16(1)
C(24)	-531(3)	1348(2)	5222(2)	15(1)
C(25)	-834(3)	2496(2)	5864(2)	15(1)
C(26)	486(3)	2998(2)	6970(2)	16(1)
C(27)	1597(3)	2148(2)	7015(2)	16(1)
C(28)	4252(2)	6310(2)	6615(2)	13(1)
C(29)	3456(3)	7188(2)	5529(2)	14(1)
C(30)	3690(3)	8601(2)	6156(3)	18(1)
C(31)	3132(3)	8742(2)	7280(3)	19(1)
C(32)	3918(3)	7866(2)	8361(2)	20(1)
C(33)	3739(3)	6443(2)	7777(2)	16(1)
C(34)	5076(2)	3765(2)	7360(2)	11(1)
C(35)	6616(3)	4398(2)	8293(2)	16(1)
C(36)	7283(3)	3743(2)	9578(2)	17(1)
C(37)	7363(3)	2299(2)	9235(2)	18(1)
C(38)	5857(3)	1649(2)	8312(2)	16(1)
C(39)	5169(3)	2311(2)	7025(2)	14(1)
C(40)	9094(4)	7974(3)	3248(3)	31(1)
C(41)	9136(6)	7004(4)	2150(4)	53(1)
C(42)	8775(10)	7714(5)	999(5)	85(2)
C(43)	8040(4)	8877(3)	1253(3)	35(1)
Fe(1)	783(1)	2908(1)	5213(1)	10(1)
O(1)	6424(2)	5049(2)	3139(2)	17(1)
O(2)	8074(3)	8864(2)	2579(3)	40(1)
O(3)	5202(3)	7170(3)	1773(3)	52(1)
O(4)	2758(16)	8009(10)	1760(20)	81(6)
P(1)	3906(1)	2911(1)	2842(1)	12(1)
P(2)	4291(1)	4648(1)	5862(1)	10(1)
Pd(1)	5461(1)	4673(1)	4439(1)	10(1)

Table 3. Bond lengths [Å] and angles [°] for jwang005_hartwig.

C(1)-C(2)	1.404(3)
C(1)-C(7)	1.407(3)
C(1)-Pd(1)	2.055(2)
C(2)-C(3)	1.395(3)
C(2)-H(2)	0.9500
C(3)-C(4)	1.388(4)
C(3)-H(3)	0.9500
C(4)-C(6)	1.394(4)
C(4)-C(5)	1.508(4)
C(5)-H(5A)	0.9800
C(5)-H(5B)	0.9800
C(5)-H(5C)	0.9800
C(6)-C(7)	1.394(3)
C(6)-H(6)	0.9500
C(7)-H(7)	0.9500
C(8)-C(9)	1.544(4)
C(8)-H(8A)	0.9800
C(8)-H(8B)	0.9800
C(8)-H(8C)	0.9800
C(9)-C(10)	1.532(3)
C(9)-C(11)	1.539(3)
C(9)-P(1)	1.891(2)
C(10)-H(10A)	0.9800
C(10)-H(10B)	0.9800
C(10)-H(10C)	0.9800
C(11)-H(11A)	0.9800
C(11)-H(11B)	0.9800
C(11)-H(11C)	0.9800
C(12)-C(14)	1.537(3)
C(12)-C(15)	1.543(3)
C(12)-C(13)	1.543(3)
C(12)-P(1)	1.896(2)
C(13)-H(13A)	0.9800
C(13)-H(13B)	0.9800
C(13)-H(13C)	0.9800
C(14)-H(14A)	0.9800
C(14)-H(14B)	0.9800
C(14)-H(14C)	0.9800
C(15)-H(15A)	0.9800
C(15)-H(15B)	0.9800
C(15)-H(15C)	0.9800
C(16)-C(18)	1.497(3)
C(16)-C(17)	1.537(3)
C(16)-P(1)	1.885(2)
C(16)-H(16)	1.0000
C(17)-H(17A)	0.9800
C(17)-H(17B)	0.9800
C(17)-H(17C)	0.9800
C(18)-C(19)	1.438(3)
C(18)-C(22)	1.444(3)
C(18)-Fe(1)	2.067(2)
C(19)-C(20)	1.420(4)
C(19)-Fe(1)	2.044(2)
C(19)-H(19)	0.9500
C(20)-C(21)	1.423(3)
C(20)-Fe(1)	2.041(2)
C(20)-H(20)	0.9500
C(21)-C(22)	1.454(3)
C(21)-Fe(1)	2.025(2)
C(21)-H(21)	0.9500
C(22)-P(2)	1.826(2)
C(22)-Fe(1)	2.067(2)
C(23)-C(27)	1.419(3)
C(23)-C(24)	1.425(3)
C(23)-Fe(1)	2.051(2)
C(23)-H(23)	0.9500
C(24)-C(25)	1.428(3)
C(24)-Fe(1)	2.046(2)
C(24)-H(24)	0.9500
C(25)-C(26)	1.426(3)
C(25)-Fe(1)	2.046(2)
C(25)-H(25)	0.9500
C(26)-C(27)	1.430(4)
C(26)-Fe(1)	2.047(2)
C(26)-H(26)	0.9500
C(27)-Fe(1)	2.057(2)
C(27)-H(27)	0.9500
C(28)-C(33)	1.540(3)
C(28)-C(29)	1.543(3)
C(28)-P(2)	1.849(2)
C(28)-H(28)	1.0000
C(29)-C(30)	1.528(3)
C(29)-H(29A)	0.9900
C(29)-H(29B)	0.9900
C(30)-C(31)	1.531(4)
C(30)-H(30A)	0.9900
C(30)-H(30B)	0.9900
C(31)-C(32)	1.537(3)
C(31)-H(31A)	0.9900
C(31)-H(31B)	0.9900
C(32)-C(33)	1.528(3)
C(32)-H(32A)	0.9900
C(32)-H(32B)	0.9900
C(33)-H(33A)	0.9900
C(33)-H(33B)	0.9900
C(34)-C(39)	1.535(3)
C(34)-C(35)	1.543(3)
C(34)-P(2)	1.858(2)
C(34)-H(34)	1.0000
C(35)-C(36)	1.532(3)
C(35)-H(35A)	0.9900
C(35)-H(35B)	0.9900
C(36)-C(37)	1.524(3)
C(36)-H(36A)	0.9900
C(36)-H(36B)	0.9900
C(37)-C(38)	1.524(3)
C(37)-H(37A)	0.9900
C(37)-H(37B)	0.9900

C(38)-C(39)	1.540(3)
C(38)-H(38A)	0.9900
C(38)-H(38B)	0.9900
C(39)-H(39A)	0.9900
C(39)-H(39B)	0.9900
C(40)-O(2)	1.426(4)
C(40)-C(41)	1.506(5)
C(40)-H(40A)	0.9900
C(40)-H(40B)	0.9900
C(41)-C(42)	1.445(6)
C(41)-H(41A)	0.9900
C(41)-H(41B)	0.9900
C(42)-C(43)	1.495(6)
C(42)-H(42A)	0.9900
C(42)-H(42B)	0.9900
C(43)-O(2)	1.436(4)
C(43)-H(43A)	0.9900
C(43)-H(43B)	0.9900
O(1)-Pd(1)	2.0571(18)
O(1)-H(1)	0.80(4)
O(3)-H(3A)	0.963(14)
O(3)-H(3B)	0.962(14)
P(1)-Pd(1)	2.4156(6)
P(2)-Pd(1)	2.2808(6)

C(2)-C(1)-C(7)	115.2(2)
C(2)-C(1)-Pd(1)	121.91(17)
C(7)-C(1)-Pd(1)	122.45(18)
C(3)-C(2)-C(1)	122.3(2)
C(3)-C(2)-H(2)	118.9
C(1)-C(2)-H(2)	118.9
C(4)-C(3)-C(2)	121.3(2)
C(4)-C(3)-H(3)	119.3
C(2)-C(3)-H(3)	119.3
C(3)-C(4)-C(6)	117.3(2)
C(3)-C(4)-C(5)	121.7(3)
C(6)-C(4)-C(5)	121.0(2)
C(4)-C(5)-H(5A)	109.5
C(4)-C(5)-H(5B)	109.5
H(5A)-C(5)-H(5B)	109.5
C(4)-C(5)-H(5C)	109.5
H(5A)-C(5)-H(5C)	109.5
H(5B)-C(5)-H(5C)	109.5
C(7)-C(6)-C(4)	121.2(2)
C(7)-C(6)-H(6)	119.4
C(4)-C(6)-H(6)	119.4
C(6)-C(7)-C(1)	122.2(2)
C(6)-C(7)-H(7)	118.9
C(1)-C(7)-H(7)	118.9
C(9)-C(8)-H(8A)	109.5
C(9)-C(8)-H(8B)	109.5
H(8A)-C(8)-H(8B)	109.5
C(9)-C(8)-H(8C)	109.5
H(8A)-C(8)-H(8C)	109.5
H(8B)-C(8)-H(8C)	109.5
C(10)-C(9)-C(11)	109.81(19)
C(10)-C(9)-C(8)	108.5(2)
C(11)-C(9)-C(8)	107.4(2)
C(10)-C(9)-P(1)	114.74(19)
C(11)-C(9)-P(1)	109.34(16)
C(8)-C(9)-P(1)	106.83(15)
C(9)-C(10)-H(10A)	109.5
C(9)-C(10)-H(10B)	109.5
H(10A)-C(10)-H(10B)	109.5
C(9)-C(10)-H(10C)	109.5
H(10A)-C(10)-H(10C)	109.5
H(10B)-C(10)-H(10C)	109.5
C(9)-C(11)-H(11A)	109.5
C(9)-C(11)-H(11B)	109.5
H(11A)-C(11)-H(11B)	109.5
C(9)-C(11)-H(11C)	109.5
H(11A)-C(11)-H(11C)	109.5
H(11B)-C(11)-H(11C)	109.5
C(14)-C(12)-C(15)	106.59(19)
C(14)-C(12)-C(13)	108.05(19)
C(15)-C(12)-C(13)	109.3(2)
C(14)-C(12)-P(1)	109.73(16)
C(15)-C(12)-P(1)	107.07(15)
C(13)-C(12)-P(1)	115.73(18)
C(12)-C(13)-H(13A)	109.5
C(12)-C(13)-H(13B)	109.5
H(13A)-C(13)-H(13B)	109.5
C(12)-C(13)-H(13C)	109.5
H(13A)-C(13)-H(13C)	109.5
H(13B)-C(13)-H(13C)	109.5
C(12)-C(14)-H(14A)	109.5
C(12)-C(14)-H(14B)	109.5
H(14A)-C(14)-H(14B)	109.5
C(12)-C(14)-H(14C)	109.5
H(14A)-C(14)-H(14C)	109.5
H(14B)-C(14)-H(14C)	109.5
C(12)-C(15)-H(15A)	109.5
C(12)-C(15)-H(15B)	109.5
H(15A)-C(15)-H(15B)	109.5
C(12)-C(15)-H(15C)	109.5
H(15A)-C(15)-H(15C)	109.5
H(15B)-C(15)-H(15C)	109.5
C(18)-C(16)-C(17)	111.47(19)
C(18)-C(16)-P(1)	108.86(16)
C(17)-C(16)-P(1)	120.80(16)
C(18)-C(16)-H(16)	104.7
C(17)-C(16)-H(16)	104.7
P(1)-C(16)-H(16)	104.7
C(16)-C(17)-H(17A)	109.5
C(16)-C(17)-H(17B)	109.5
H(17A)-C(17)-H(17B)	109.5
C(16)-C(17)-H(17C)	109.5
H(17A)-C(17)-H(17C)	109.5
H(17B)-C(17)-H(17C)	109.5
C(19)-C(18)-C(22)	107.8(2)
C(19)-C(18)-C(16)	125.4(2)
C(22)-C(18)-C(16)	126.8(2)

C(19)-C(18)-Fe(1)	68.68(13)	Fe(1)-C(27)-H(27)	126.9
C(22)-C(18)-Fe(1)	69.55(13)	C(33)-C(28)-C(29)	111.90(18)
C(16)-C(18)-Fe(1)	129.37(17)	C(33)-C(28)-P(2)	117.24(15)
C(20)-C(19)-C(18)	109.1(2)	C(29)-C(28)-P(2)	111.48(15)
C(20)-C(19)-Fe(1)	69.55(13)	C(33)-C(28)-H(28)	105.0
C(18)-C(19)-Fe(1)	70.36(13)	C(29)-C(28)-H(28)	105.0
C(20)-C(19)-H(19)	125.5	P(2)-C(28)-H(28)	105.0
C(18)-C(19)-H(19)	125.5	C(30)-C(29)-C(28)	109.98(18)
Fe(1)-C(19)-H(19)	126.2	C(30)-C(29)-H(29A)	109.7
C(19)-C(20)-C(21)	107.6(2)	C(28)-C(29)-H(29A)	109.7
C(19)-C(20)-Fe(1)	69.77(13)	C(30)-C(29)-H(29B)	109.7
C(21)-C(20)-Fe(1)	68.93(13)	C(28)-C(29)-H(29B)	109.7
C(19)-C(20)-H(20)	126.2	H(29A)-C(29)-H(29B)	108.2
C(21)-C(20)-H(20)	126.2	C(29)-C(30)-C(31)	110.44(19)
Fe(1)-C(20)-H(20)	126.7	C(29)-C(30)-H(30A)	109.6
C(20)-C(21)-C(22)	109.1(2)	C(31)-C(30)-H(30A)	109.6
C(20)-C(21)-Fe(1)	70.12(14)	C(29)-C(30)-H(30B)	109.6
C(22)-C(21)-Fe(1)	70.71(12)	C(31)-C(30)-H(30B)	109.6
C(20)-C(21)-H(21)	125.4	H(30A)-C(30)-H(30B)	108.1
C(22)-C(21)-H(21)	125.4	C(30)-C(31)-C(32)	110.5(2)
Fe(1)-C(21)-H(21)	125.3	C(30)-C(31)-H(31A)	109.6
C(18)-C(22)-C(21)	106.4(2)	C(32)-C(31)-H(31A)	109.6
C(18)-C(22)-P(2)	124.37(17)	C(30)-C(31)-H(31B)	109.6
C(21)-C(22)-P(2)	127.62(17)	C(32)-C(31)-H(31B)	109.6
C(18)-C(22)-Fe(1)	69.56(12)	H(31A)-C(31)-H(31B)	108.1
C(21)-C(22)-Fe(1)	67.68(12)	C(33)-C(32)-C(31)	112.0(2)
P(2)-C(22)-Fe(1)	138.69(12)	C(33)-C(32)-H(32A)	109.2
C(27)-C(23)-C(24)	108.0(2)	C(31)-C(32)-H(32A)	109.2
C(27)-C(23)-Fe(1)	70.02(13)	C(33)-C(32)-H(32B)	109.2
C(24)-C(23)-Fe(1)	69.44(12)	C(31)-C(32)-H(32B)	109.2
C(27)-C(23)-H(23)	126.0	H(32A)-C(32)-H(32B)	107.9
C(24)-C(23)-H(23)	126.0	C(32)-C(33)-C(28)	110.00(18)
Fe(1)-C(23)-H(23)	126.1	C(32)-C(33)-H(33A)	109.7
C(23)-C(24)-C(25)	108.1(2)	C(28)-C(33)-H(33A)	109.7
C(23)-C(24)-Fe(1)	69.85(12)	C(32)-C(33)-H(33B)	109.7
C(25)-C(24)-Fe(1)	69.59(12)	C(28)-C(33)-H(33B)	109.7
C(23)-C(24)-H(24)	126.0	H(33A)-C(33)-H(33B)	108.2
C(25)-C(24)-H(24)	126.0	C(39)-C(34)-C(35)	109.33(18)
Fe(1)-C(24)-H(24)	126.2	C(39)-C(34)-P(2)	114.05(15)
C(26)-C(25)-C(24)	107.9(2)	C(35)-C(34)-P(2)	109.98(14)
C(26)-C(25)-Fe(1)	69.63(12)	C(39)-C(34)-H(34)	107.8
C(24)-C(25)-Fe(1)	69.55(12)	C(35)-C(34)-H(34)	107.8
C(26)-C(25)-H(25)	126.1	P(2)-C(34)-H(34)	107.8
C(24)-C(25)-H(25)	126.1	C(36)-C(35)-C(34)	112.01(18)
Fe(1)-C(25)-H(25)	126.3	C(36)-C(35)-H(35A)	109.2
C(25)-C(26)-C(27)	107.8(2)	C(34)-C(35)-H(35A)	109.2
C(25)-C(26)-Fe(1)	69.60(12)	C(36)-C(35)-H(35B)	109.2
C(27)-C(26)-Fe(1)	70.01(13)	C(34)-C(35)-H(35B)	109.2
C(25)-C(26)-H(26)	126.1	H(35A)-C(35)-H(35B)	107.9
C(27)-C(26)-H(26)	126.1	C(37)-C(36)-C(35)	110.45(19)
Fe(1)-C(26)-H(26)	125.9	C(37)-C(36)-H(36A)	109.6
C(23)-C(27)-C(26)	108.3(2)	C(35)-C(36)-H(36A)	109.6
C(23)-C(27)-Fe(1)	69.56(12)	C(37)-C(36)-H(36B)	109.6
C(26)-C(27)-Fe(1)	69.22(12)	C(35)-C(36)-H(36B)	109.6
C(23)-C(27)-H(27)	125.9	H(36A)-C(36)-H(36B)	108.1
C(26)-C(27)-H(27)	125.9	C(38)-C(37)-C(36)	110.90(19)

C(38)-C(37)-H(37A)	109.5
C(36)-C(37)-H(37A)	109.5
C(38)-C(37)-H(37B)	109.5
C(36)-C(37)-H(37B)	109.5
H(37A)-C(37)-H(37B)	108.0
C(37)-C(38)-C(39)	111.85(19)
C(37)-C(38)-H(38A)	109.2
C(39)-C(38)-H(38A)	109.2
C(37)-C(38)-H(38B)	109.2
C(39)-C(38)-H(38B)	109.2
H(38A)-C(38)-H(38B)	107.9
C(34)-C(39)-C(38)	111.17(18)
C(34)-C(39)-H(39A)	109.4
C(38)-C(39)-H(39A)	109.4
C(34)-C(39)-H(39B)	109.4
C(38)-C(39)-H(39B)	109.4
H(39A)-C(39)-H(39B)	108.0
O(2)-C(40)-C(41)	105.4(3)
O(2)-C(40)-H(40A)	110.7
C(41)-C(40)-H(40A)	110.7
O(2)-C(40)-H(40B)	110.7
C(41)-C(40)-H(40B)	110.7
H(40A)-C(40)-H(40B)	108.8
C(42)-C(41)-C(40)	104.6(3)
C(42)-C(41)-H(41A)	110.8
C(40)-C(41)-H(41A)	110.8
C(42)-C(41)-H(41B)	110.8
C(40)-C(41)-H(41B)	110.8
H(41A)-C(41)-H(41B)	108.9
C(41)-C(42)-C(43)	107.3(4)
C(41)-C(42)-H(42A)	110.2
C(43)-C(42)-H(42A)	110.2
C(41)-C(42)-H(42B)	110.2
C(43)-C(42)-H(42B)	110.2
H(42A)-C(42)-H(42B)	108.5
O(2)-C(43)-C(42)	106.4(3)
O(2)-C(43)-H(43A)	110.4
C(42)-C(43)-H(43A)	110.4
O(2)-C(43)-H(43B)	110.4
C(42)-C(43)-H(43B)	110.4
H(43A)-C(43)-H(43B)	108.6
C(21)-Fe(1)-C(20)	40.95(9)
C(21)-Fe(1)-C(19)	68.63(10)
C(20)-Fe(1)-C(19)	40.68(10)
C(21)-Fe(1)-C(24)	151.63(10)
C(20)-Fe(1)-C(24)	116.03(9)
C(19)-Fe(1)-C(24)	104.67(9)
C(21)-Fe(1)-C(25)	116.90(10)
C(20)-Fe(1)-C(25)	101.48(10)
C(19)-Fe(1)-C(25)	119.78(9)
C(24)-Fe(1)-C(25)	40.86(9)
C(21)-Fe(1)-C(26)	106.14(10)
C(20)-Fe(1)-C(26)	120.61(10)
C(19)-Fe(1)-C(26)	156.76(10)
C(24)-Fe(1)-C(26)	68.65(9)
C(25)-Fe(1)-C(26)	40.77(9)
C(21)-Fe(1)-C(23)	165.41(10)
C(20)-Fe(1)-C(23)	153.56(10)
C(19)-Fe(1)-C(23)	121.69(10)
C(24)-Fe(1)-C(23)	40.72(9)
C(25)-Fe(1)-C(23)	68.63(10)
C(26)-Fe(1)-C(23)	68.58(10)
C(21)-Fe(1)-C(27)	126.95(10)
C(20)-Fe(1)-C(27)	160.07(10)
C(19)-Fe(1)-C(27)	159.25(10)
C(24)-Fe(1)-C(27)	68.22(9)
C(25)-Fe(1)-C(27)	68.41(9)
C(26)-Fe(1)-C(27)	40.78(10)
C(23)-Fe(1)-C(27)	40.41(9)
C(21)-Fe(1)-C(22)	41.61(9)
C(20)-Fe(1)-C(22)	69.58(9)
C(19)-Fe(1)-C(22)	69.02(9)
C(24)-Fe(1)-C(22)	163.76(9)
C(25)-Fe(1)-C(22)	155.32(9)
C(26)-Fe(1)-C(22)	123.02(9)
C(23)-Fe(1)-C(22)	128.93(9)
C(27)-Fe(1)-C(22)	112.14(9)
C(21)-Fe(1)-C(18)	69.07(10)
C(20)-Fe(1)-C(18)	69.04(10)
C(19)-Fe(1)-C(18)	40.96(9)
C(24)-Fe(1)-C(18)	124.81(10)
C(25)-Fe(1)-C(18)	158.72(9)
C(26)-Fe(1)-C(18)	160.35(9)
C(23)-Fe(1)-C(18)	111.05(10)
C(27)-Fe(1)-C(18)	126.11(10)
C(22)-Fe(1)-C(18)	40.89(9)
Pd(1)-O(1)-H(1)	95(3)
C(40)-O(2)-C(43)	108.3(3)
H(3A)-O(3)-H(3B)	109(5)
C(16)-P(1)-C(9)	108.57(10)
C(16)-P(1)-C(12)	103.08(10)
C(9)-P(1)-C(12)	111.38(11)
C(16)-P(1)-Pd(1)	111.72(7)
C(9)-P(1)-Pd(1)	106.79(8)
C(12)-P(1)-Pd(1)	115.21(7)
C(22)-P(2)-C(28)	103.76(11)
C(22)-P(2)-C(34)	108.56(10)
C(28)-P(2)-C(34)	102.54(10)
C(22)-P(2)-Pd(1)	111.32(7)
C(28)-P(2)-Pd(1)	110.91(7)
C(34)-P(2)-Pd(1)	118.48(7)
C(1)-Pd(1)-O(1)	82.96(9)
C(1)-Pd(1)-P(2)	91.42(7)
O(1)-Pd(1)-P(2)	169.38(6)
C(1)-Pd(1)-P(1)	173.06(7)
O(1)-Pd(1)-P(1)	90.23(6)
P(2)-Pd(1)-P(1)	95.51(2)

Symmetry transformations used to generate equivalent atoms:

Table 4. Anisotropic displacement parameters ($Å^2 x\ 10^3$)for jwang005_hartwig. The anisotropic displacement factor exponent takes the form: $-2p^2[\ h^2 a^{*2} U^{11} + ... + 2\ h\ k\ a^*\ b^*\ U^{12}\ ]$

	U^{11}	U^{22}	U^{33}	U^{23}	U^{13}	U^{12}
C(1)	13(1)	13(1)	16(1)	-1(1)	7(1)	-1(1)
C(2)	14(1)	15(1)	19(1)	0(1)	5(1)	-2(1)
C(3)	15(1)	22(1)	19(1)	0(1)	5(1)	-5(1)
C(4)	21(1)	18(1)	20(1)	-4(1)	11(1)	-8(1)
C(5)	31(1)	27(1)	26(1)	-9(1)	15(1)	-16(1)
C(6)	23(1)	14(1)	26(1)	1(1)	14(1)	-2(1)
C(7)	16(1)	15(1)	20(1)	3(1)	7(1)	0(1)
C(8)	19(1)	35(1)	18(1)	12(1)	9(1)	11(1)
C(9)	11(1)	32(1)	10(1)	3(1)	3(1)	0(1)
C(10)	12(1)	50(2)	11(1)	2(1)	2(1)	-4(1)
C(11)	17(1)	40(2)	13(1)	6(1)	7(1)	1(1)
C(12)	14(1)	18(1)	15(1)	-5(1)	6(1)	-2(1)
C(13)	21(1)	28(1)	21(1)	-12(1)	10(1)	-6(1)
C(14)	13(1)	21(1)	20(1)	-2(1)	10(1)	0(1)
C(15)	17(1)	14(1)	25(1)	-2(1)	10(1)	0(1)
C(16)	12(1)	17(1)	12(1)	-3(1)	5(1)	-4(1)
C(17)	16(1)	21(1)	18(1)	-9(1)	8(1)	-8(1)
C(18)	10(1)	18(1)	8(1)	1(1)	3(1)	-2(1)
C(19)	10(1)	25(1)	10(1)	5(1)	2(1)	-2(1)
C(20)	10(1)	20(1)	16(1)	7(1)	3(1)	0(1)
C(21)	13(1)	13(1)	18(1)	5(1)	8(1)	2(1)
C(22)	11(1)	13(1)	12(1)	3(1)	5(1)	0(1)
C(23)	18(1)	15(1)	16(1)	4(1)	6(1)	2(1)
C(24)	16(1)	14(1)	16(1)	1(1)	7(1)	-3(1)
C(25)	12(1)	19(1)	16(1)	3(1)	7(1)	-1(1)
C(26)	19(1)	19(1)	10(1)	1(1)	7(1)	-1(1)
C(27)	16(1)	19(1)	12(1)	5(1)	5(1)	1(1)
C(28)	14(1)	10(1)	13(1)	0(1)	5(1)	1(1)
C(29)	14(1)	12(1)	15(1)	2(1)	6(1)	2(1)
C(30)	20(1)	12(1)	23(1)	2(1)	10(1)	2(1)
C(31)	23(1)	13(1)	23(1)	0(1)	10(1)	4(1)
C(32)	25(1)	16(1)	17(1)	-2(1)	8(1)	5(1)
C(33)	21(1)	14(1)	14(1)	1(1)	8(1)	2(1)
C(34)	10(1)	11(1)	10(1)	0(1)	2(1)	0(1)
C(35)	14(1)	15(1)	14(1)	1(1)	0(1)	-4(1)
C(36)	15(1)	17(1)	13(1)	2(1)	0(1)	-1(1)
C(37)	15(1)	18(1)	17(1)	3(1)	0(1)	3(1)
C(38)	17(1)	13(1)	16(1)	2(1)	4(1)	1(1)
C(39)	14(1)	13(1)	12(1)	1(1)	4(1)	1(1)
C(40)	32(2)	26(1)	35(2)	6(1)	13(1)	2(1)
C(41)	83(3)	43(2)	50(2)	13(2)	39(2)	32(2)
C(42)	174(7)	54(3)	46(2)	13(2)	61(3)	49(4)
C(43)	28(2)	32(2)	35(2)	6(1)	1(1)	0(1)
Fe(1)	9(1)	12(1)	9(1)	1(1)	4(1)	0(1)
O(1)	16(1)	19(1)	18(1)	-1(1)	9(1)	-3(1)
O(2)	46(1)	31(1)	40(1)	2(1)	14(1)	15(1)
O(3)	40(2)	51(2)	57(2)	24(1)	8(1)	-2(1)
O(4)	66(9)	14(4)	187(18)	5(7)	76(11)	8(5)
P(1)	9(1)	17(1)	9(1)	-2(1)	4(1)	-2(1)
P(2)	10(1)	10(1)	9(1)	1(1)	3(1)	0(1)

Pd(1)	8(1)	11(1)	10(1)	0(1)	3(1)	0(1)

Table 5. Hydrogen coordinates (x 10^4) and isotropic displacement parameters ($Å^2$x 10^3) for jwang005_hartwig.

	x	y	z	U(eq)
H(2)	8522	5090	6775	20
H(3)	10179	6779	8152	23
H(5A)	9638	9624	8984	43
H(5B)	10036	10099	7805	43
H(5C)	10993	9076	8721	43
H(6)	7521	9366	6096	24
H(7)	5872	7678	4707	20
H(8A)	1752	4797	2371	34
H(8B)	1674	5381	1041	34
H(8C)	3187	5519	2341	34
H(10A)	1524	1994	75	38
H(10B)	719	3284	-355	38
H(10C)	698	2668	928	38
H(11A)	4521	4450	1064	34
H(11B)	3029	4481	-231	34
H(11C)	3788	3150	67	34
H(13A)	3095	297	1148	36
H(13B)	4574	-83	1007	36
H(13C)	3757	1119	316	36
H(14A)	5973	2652	1486	26
H(14B)	6828	1425	2068	26
H(14C)	6896	2680	3068	26
H(15A)	6018	1340	4416	28
H(15B)	6108	120	3447	28
H(15C)	4629	304	3672	28
H(16)	3386	1784	4391	17
H(17A)	1136	942	1828	29
H(17B)	1122	528	3199	29
H(17C)	2389	102	2730	29
H(19)	-391	2468	2488	18
H(20)	-1158	4406	3571	19
H(21)	1112	5515	5488	17
H(23)	1471	447	5722	19
H(24)	-1213	816	4455	18
H(25)	-1753	2860	5600	18
H(26)	607	3760	7569	19
H(27)	2584	2243	7659	19
H(28)	5298	6676	7022	15
H(29A)	3842	7105	4819	17
H(29B)	2394	6911	5110	17
H(30A)	3159	9156	5458	21
H(30B)	4747	8893	6525	21
H(31A)	2062	8503	6901	23
H(31B)	3309	9658	7690	23
H(32A)	4976	8161	8794	23

H(32B)	3517	7947	9060	23
H(33A)	2696	6109	7444	19
H(33B)	4325	5921	8486	19
H(34)	4431	3853	7865	13
H(35A)	7270	4339	7806	19
H(35B)	6547	5328	8536	19
H(36A)	8281	4155	10134	20
H(36B)	6676	3861	10106	20
H(37A)	8052	2182	8790	22
H(37B)	7743	1881	10073	22
H(38A)	5201	1683	8797	19
H(38B)	5949	725	8064	19
H(39A)	5768	2195	6489	17
H(39B)	4172	1893	6476	17
H(40A)	8766	7537	3862	37
H(40B)	10077	8429	3775	37
H(41A)	10124	6687	2404	64
H(41B)	8410	6254	1959	64
H(42A)	8109	7162	174	101
H(42B)	9676	7986	880	101
H(43A)	8570	9682	1197	42
H(43B)	7015	8832	581	42
H(1)	7080(50)	5530(40)	3680(40)	26(9)
H(3A)	5510(60)	6420(40)	2230(50)	69(16)
H(3B)	6030(50)	7800(50)	2040(60)	78(18)

Table 6. Torsion angles [°] for jwang005_hartwig.

C(7)-C(1)-C(2)-C(3)	6.8(3)
Pd(1)-C(1)-C(2)-C(3)	179.57(18)
C(1)-C(2)-C(3)-C(4)	-1.2(4)
C(2)-C(3)-C(4)-C(6)	-4.4(4)
C(2)-C(3)-C(4)-C(5)	174.0(2)
C(3)-C(4)-C(6)-C(7)	4.1(4)
C(5)-C(4)-C(6)-C(7)	-174.2(2)
C(4)-C(6)-C(7)-C(1)	1.8(4)
C(2)-C(1)-C(7)-C(6)	-7.1(3)
Pd(1)-C(1)-C(7)-C(6)	-179.79(18)
C(17)-C(16)-C(18)-C(19)	-24.5(3)
P(1)-C(16)-C(18)-C(19)	111.2(2)
C(17)-C(16)-C(18)-C(22)	158.6(2)
P(1)-C(16)-C(18)-C(22)	-65.7(3)
C(17)-C(16)-C(18)-Fe(1)	65.8(3)
P(1)-C(16)-C(18)-Fe(1)	-158.49(14)
C(22)-C(18)-C(19)-C(20)	0.2(3)
C(16)-C(18)-C(19)-C(20)	-177.1(2)
Fe(1)-C(18)-C(19)-C(20)	58.96(15)
C(22)-C(18)-C(19)-Fe(1)	-58.71(15)
C(16)-C(18)-C(19)-Fe(1)	123.9(2)
C(18)-C(19)-C(20)-C(21)	-0.7(2)
Fe(1)-C(19)-C(20)-C(21)	58.73(14)
C(18)-C(19)-C(20)-Fe(1)	-59.45(16)
C(19)-C(20)-C(21)-C(22)	0.9(2)
Fe(1)-C(20)-C(21)-C(22)	60.18(14)
C(19)-C(20)-C(21)-Fe(1)	-59.26(15)
C(19)-C(18)-C(22)-C(21)	0.3(2)
C(16)-C(18)-C(22)-C(21)	177.6(2)
Fe(1)-C(18)-C(22)-C(21)	-57.85(14)
C(19)-C(18)-C(22)-P(2)	-166.08(15)
C(16)-C(18)-C(22)-P(2)	11.3(3)
Fe(1)-C(18)-C(22)-P(2)	135.75(17)
C(19)-C(18)-C(22)-Fe(1)	58.17(15)
C(16)-C(18)-C(22)-Fe(1)	-124.5(2)
C(20)-C(21)-C(22)-C(18)	-0.8(2)
Fe(1)-C(21)-C(22)-C(18)	59.05(15)
C(20)-C(21)-C(22)-P(2)	165.04(16)
Fe(1)-C(21)-C(22)-P(2)	-135.14(17)
C(20)-C(21)-C(22)-Fe(1)	-59.82(15)
C(27)-C(23)-C(24)-C(25)	0.3(2)
Fe(1)-C(23)-C(24)-C(25)	-59.30(15)
C(27)-C(23)-C(24)-Fe(1)	59.64(15)
C(23)-C(24)-C(25)-C(26)	0.2(2)
Fe(1)-C(24)-C(25)-C(26)	-59.29(15)
C(23)-C(24)-C(25)-Fe(1)	59.46(15)
C(24)-C(25)-C(26)-C(27)	-0.6(2)
Fe(1)-C(25)-C(26)-C(27)	-59.85(15)
C(24)-C(25)-C(26)-Fe(1)	59.23(15)
C(24)-C(23)-C(27)-C(26)	-0.7(2)
Fe(1)-C(23)-C(27)-C(26)	58.55(15)
C(24)-C(23)-C(27)-Fe(1)	-59.27(15)
C(25)-C(26)-C(27)-C(23)	0.8(2)
Fe(1)-C(26)-C(27)-C(23)	-58.76(15)

C(25)-C(26)-C(27)-Fe(1)	59.59(15)
C(33)-C(28)-C(29)-C(30)	57.0(2)
P(2)-C(28)-C(29)-C(30)	-169.55(15)
C(28)-C(29)-C(30)-C(31)	-58.0(2)
C(29)-C(30)-C(31)-C(32)	58.0(3)
C(30)-C(31)-C(32)-C(33)	-56.8(3)
C(31)-C(32)-C(33)-C(28)	54.7(3)
C(29)-C(28)-C(33)-C(32)	-54.9(3)
P(2)-C(28)-C(33)-C(32)	174.50(16)
C(39)-C(34)-C(35)-C(36)	-56.7(2)
P(2)-C(34)-C(35)-C(36)	177.32(16)
C(34)-C(35)-C(36)-C(37)	57.3(3)
C(35)-C(36)-C(37)-C(38)	-55.9(3)
C(36)-C(37)-C(38)-C(39)	55.8(3)
C(35)-C(34)-C(39)-C(38)	55.3(2)
P(2)-C(34)-C(39)-C(38)	178.90(15)
C(37)-C(38)-C(39)-C(34)	-56.0(3)
O(2)-C(40)-C(41)-C(42)	28.0(6)
C(40)-C(41)-C(42)-C(43)	-19.1(7)
C(41)-C(42)-C(43)-O(2)	3.5(6)
C(41)-C(40)-O(2)-C(43)	-26.5(4)
C(42)-C(43)-O(2)-C(40)	14.6(5)
C(18)-C(16)-P(1)-C(9)	-60.81(18)
C(17)-C(16)-P(1)-C(9)	70.0(2)
C(18)-C(16)-P(1)-C(12)	-179.03(15)
C(17)-C(16)-P(1)-C(12)	-48.2(2)
C(18)-C(16)-P(1)-Pd(1)	56.69(16)
C(17)-C(16)-P(1)-Pd(1)	-172.48(17)
C(10)-C(9)-P(1)-C(16)	-37.6(2)
C(11)-C(9)-P(1)-C(16)	-161.44(17)
C(8)-C(9)-P(1)-C(16)	82.67(18)
C(10)-C(9)-P(1)-C(12)	75.2(2)
C(11)-C(9)-P(1)-C(12)	-48.6(2)
C(8)-C(9)-P(1)-C(12)	-164.52(16)
C(10)-C(9)-P(1)-Pd(1)	-158.17(17)
C(11)-C(9)-P(1)-Pd(1)	77.96(18)
C(8)-C(9)-P(1)-Pd(1)	-37.94(17)
C(14)-C(12)-P(1)-C(16)	-162.27(16)
C(15)-C(12)-P(1)-C(16)	-46.96(17)
C(13)-C(12)-P(1)-C(16)	75.17(19)
C(14)-C(12)-P(1)-C(9)	81.50(18)
C(15)-C(12)-P(1)-C(9)	-163.19(15)
C(13)-C(12)-P(1)-C(9)	-41.1(2)
C(14)-C(12)-P(1)-Pd(1)	-40.31(18)
C(15)-C(12)-P(1)-Pd(1)	75.00(16)
C(13)-C(12)-P(1)-Pd(1)	-162.88(15)
C(18)-C(22)-P(2)-C(28)	161.00(19)
C(21)-C(22)-P(2)-C(28)	-2.4(2)
Fe(1)-C(22)-P(2)-C(28)	-101.10(19)
C(18)-C(22)-P(2)-C(34)	-90.5(2)
C(21)-C(22)-P(2)-C(34)	106.1(2)
Fe(1)-C(22)-P(2)-C(34)	7.4(2)
C(18)-C(22)-P(2)-Pd(1)	41.7(2)
C(21)-C(22)-P(2)-Pd(1)	-121.78(18)
Fe(1)-C(22)-P(2)-Pd(1)	139.56(16)
C(33)-C(28)-P(2)-C(22)	70.58(19)

C(29)-C(28)-P(2)-C(22)	-60.22(17)
C(33)-C(28)-P(2)-C(34)	-42.38(19)
C(29)-C(28)-P(2)-C(34)	-173.18(15)
C(33)-C(28)-P(2)-Pd(1)	-169.81(15)
C(29)-C(28)-P(2)-Pd(1)	59.39(16)
C(39)-C(34)-P(2)-C(22)	67.79(18)
C(35)-C(34)-P(2)-C(22)	-168.99(15)
C(39)-C(34)-P(2)-C(28)	177.15(16)
C(35)-C(34)-P(2)-C(28)	-59.62(17)
C(39)-C(34)-P(2)-Pd(1)	-60.40(17)
C(35)-C(34)-P(2)-Pd(1)	62.82(17)

5.5. References

1. (a) Johansson Seechurn, C. C. C.; Kitching, M. O.; Colacot, T. J.; Snieckus, V., Palladium-Catalyzed Cross-Coupling: A Historical Contextual Perspective to the 2010 Nobel Prize. *Angew. Chem. Int. Ed.* **2012,** *51*, 5062-5085; (b) Diccianni, J. B.; Diao, T., Mechanisms of Nickel-Catalyzed Cross-Coupling Reactions. *Trends in Chemistry* **2019,** *1*, 830-844.
2. Dorel, R.; Grugel, C. P.; Haydl, A. M., The Buchwald–Hartwig Amination After 25 Years. *Angew. Chem. Int. Ed.* **2019,** *58*, 17118-17129.
3. (a) Hartwig, J. F., Evolution of a Fourth Generation Catalyst for the Amination and Thioetherification of Aryl Halides. *Acc. Chem. Res.* **2008,** *41*, 1534-1544; (b) Yang, J.; Chen, T.; Han, L.-B., C–P Bond-Forming Reactions via C–O/P–H Cross-Coupling Catalyzed by Nickel. *J. Am. Chem. Soc.* **2015,** *137*, 1782-1785; (c) Wauters, I. D., W.; Stevens, C. V., Preparation of phosphines through C–P bond formation. *Beilstein J. Org. Chem.* **2014,** *10*, 1064-1096; (d) Sather, A. C.; Buchwald, S. L., The Evolution of Pd0/PdII-Catalyzed Aromatic Fluorination. *Acc. Chem. Res.* **2016,** *49*, 2146-2157.
4. Ruiz-Castillo, P.; Buchwald, S. L., Applications of Palladium-Catalyzed C–N Cross-Coupling Reactions. *Chem. Rev.* **2016,** *116*, 12564-12649.
5. Kosugi, M.; Kameyama, M.; Migita, T., Palladium-Catalyzed Aromatic Amination of Aryl Bromides with N,N-Di-Ethylamino-tributyltin. *Chem. Lett.* **1983,** *12*, 927-928.
6. Hartwig, J. F., Carbon−Heteroatom Bond-Forming Reductive Eliminations of Amines, Ethers, and Sulfides. *Acc. Chem. Res.* **1998,** *31*, 852-860.
7. Louie, J.; Hartwig, J. F., Palladium-catalyzed synthesis of arylamines from aryl halides. Mechanistic studies lead to coupling in the absence of tin reagents. *Tetrahedron Lett.* **1995,** *36*, 3609-3612.
8. Guram, A. S.; Rennels, R. A.; Buchwald, S. L., A Simple Catalytic Method for the Conversion of Aryl Bromides to Arylamines. *Angew. Chem. Int. Ed. Engl.* **1995,** *34*, 1348-1350.
9. (a) Driver, M. S.; Hartwig, J. F., A Second-Generation Catalyst for Aryl Halide Amination: Mixed Secondary Amines from Aryl Halides and Primary Amines Catalyzed by (DPPF)PdCl2. *J. Am. Chem. Soc.* **1996,** *118*, 7217-7218; (b) Wolfe, J. P.; Wagaw, S.; Buchwald, S. L., An Improved Catalyst System for Aromatic Carbon−Nitrogen Bond Formation: The Possible Involvement of Bis(Phosphine) Palladium Complexes as Key Intermediates. *J. Am. Chem. Soc.* **1996,** *118*, 7215-7216.
10. (a) Senn, H. M.; Ziegler, T., Oxidative Addition of Aryl Halides to Palladium(0) Complexes: A Density-Functional Study Including Solvation. *Organometallics* **2004,** *23*, 2980-2988; (b) Littke, A. F.; Fu, G. C., Palladium-Catalyzed Coupling Reactions of Aryl Chlorides. *Angew. Chem. Int. Ed.* **2002,** *41*, 4176-4211.

11. Beller, M.; Riermeier, T. H.; Reisinger, C.-P.; Herrmann, W. A., First palladium-catalyzed aminations of aryl chlorides. *Tetrahedron Lett.* **1997,** *38*, 2073-2074.
12. (a) Muci, A. R.; Buchwald, S. L., Practical Palladium Catalysts for C-N and C-O Bond Formation. In *Cross-Coupling Reactions: A Practical Guide*, Miyaura, N., Ed. Springer Berlin Heidelberg: Berlin, Heidelberg, 2002; pp 131-209; (b) Stambuli, J. P.; Kuwano, R.; Hartwig, J. F., Unparalleled Rates for the Activation of Aryl Chlorides and Bromides: Coupling with Amines and Boronic Acids in Minutes at Room Temperature. *Angew. Chem. Int. Ed.* **2002,** *41*, 4746-4748; (c) Kataoka, N.; Shelby, Q.; Stambuli, J. P.; Hartwig, J. F., Air Stable, Sterically Hindered Ferrocenyl Dialkylphosphines for Palladium-Catalyzed C−C, C−N, and C−O Bond-Forming Cross-Couplings. *J. Org. Chem.* **2002,** *67*, 5553-5566; (d) Marion, N.; Nolan, S. P., Well-Defined N-Heterocyclic Carbenes−Palladium(II) Precatalysts for Cross-Coupling Reactions. *Acc. Chem. Res.* **2008,** *41*, 1440-1449.
13. (a) Shen, Q.; Ogata, T.; Hartwig, J. F., Highly Reactive, General and Long-Lived Catalysts for Palladium-Catalyzed Amination of Heteroaryl and Aryl Chlorides, Bromides, and Iodides: Scope and Structure–Activity Relationships. *J. Am. Chem. Soc.* **2008,** *130*, 6586-6596; (b) Shen, Q.; Shekhar, S.; Stambuli, J. P.; Hartwig, J. F., Highly Reactive, General, and Long-Lived Catalysts for Coupling Heteroaryl and Aryl Chlorides with Primary Nitrogen Nucleophiles. *Angew. Chem. Int. Ed.* **2005,** *44*, 1371-1375.
14. Uehling, M. R.; King, R. P.; Krska, S. W.; Cernak, T.; Buchwald, S. L., Pharmaceutical diversification via palladium oxidative addition complexes. *Science* **2019,** *363*, 405-408.
15. Wolfe, J. P.; Buchwald, S. L., Nickel-Catalyzed Amination of Aryl Chlorides. *J. Am. Chem. Soc.* **1997,** *119*, 6054-6058.
16. Brenner, E.; Fort, Y., New efficient nickel(0) catalysed amination of aryl chlorides. *Tetrahedron Lett.* **1998,** *39*, 5359-5362.
17. Manolikakes, G.; Gavryushin, A.; Knochel, P., An Efficient Silane-Promoted Nickel-Catalyzed Amination of Aryl and Heteroaryl Chlorides. *J. Org. Chem.* **2008,** *73*, 1429-1434.
18. Ge, S.; Green, R. A.; Hartwig, J. F., Controlling First-Row Catalysts: Amination of Aryl and Heteroaryl Chlorides and Bromides with Primary Aliphatic Amines Catalyzed by a BINAP-Ligated Single-Component Ni(0) Complex. *J. Am. Chem. Soc.* **2014,** *136*, 1617-1627.
19. (a) Chen; Yang, L.-M., Ni(II)−(σ-Aryl) Complex: A Facile, Efficient Catalyst for Nickel-Catalyzed Carbon−Nitrogen Coupling Reactions. *J. Org. Chem.* **2007,** *72*, 6324-6327; (b) Omar-Amrani, R.; Thomas, A.; Brenner, E.; Schneider, R.; Fort, Y., Efficient Nickel-Mediated Intramolecular Amination of Aryl Chlorides. *Org. Lett.* **2003,** *5*, 2311-2314; (c) Desmarets, C.; Schneider, R.; Fort, Y., Nickel-catalysed synthesis of 3-chloroanilines and chloro aminopyridines via cross-coupling reactions of aryl and heteroaryl dichlorides with amines. *Tetrahedron Lett.* **2001,** *42*, 247-250; (d) Park, N. H.; Teverovskiy, G.; Buchwald, S. L., Development of an Air-Stable Nickel Precatalyst for the Amination of Aryl Chlorides, Sulfamates, Mesylates, and Triflates. *Org. Lett.* **2014,** *16*, 220-223.
20. (a) Green, R. A.; Hartwig, J. F., Nickel-Catalyzed Amination of Aryl Chlorides with Ammonia or Ammonium Salts. *Angew. Chem.* **2015,** *127*, 3839-3843; (b) Borzenko, A.; Rotta-Loria, N. L.; MacQueen, P. M.; Lavoie, C. M.; McDonald, R.; Stradiotto, M., Nickel-Catalyzed Monoarylation of Ammonia. *Angew. Chem. Int. Ed.* **2015,** *54*, 3773-3777.
21. (a) Tassone, J. P.; England, E. V.; MacQueen, P. M.; Ferguson, M. J.; Stradiotto, M., PhPAd-DalPhos: Ligand-Enabled, Nickel-Catalyzed Cross-Coupling of (Hetero)aryl

Electrophiles with Bulky Primary Alkylamines. *Angew. Chem. Int. Ed.* **2019,** *58*, 2485-2489; (b) Clark, J. S. K.; Ferguson, M. J.; McDonald, R.; Stradiotto, M., PAd2-DalPhos Enables the Nickel-Catalyzed C−N Cross-Coupling of Primary Heteroarylamines and (Hetero)aryl Chlorides. *Angew. Chem. Int. Ed.* **2019,** *58*, 6391-6395.

22. (a) Li, C.; Kawamata, Y.; Nakamura, H.; Vantourout, J. C.; Liu, Z.; Hou, Q.; Bao, D.; Starr, J. T.; Chen, J.; Yan, M.; Baran, P. S., Electrochemically Enabled, Nickel-Catalyzed Amination. *Angew. Chem. Int. Ed.* **2017,** *56*, 13088-13093; (b) Kawamata, Y.; Vantourout, J. C.; Hickey, D. P.; Bai, P.; Chen, L.; Hou, Q.; Qiao, W.; Barman, K.; Edwards, M. A.; Garrido-Castro, A. F.; deGruyter, J. N.; Nakamura, H.; Knouse, K.; Qin, C.; Clay, K. J.; Bao, D.; Li, C.; Starr, J. T.; Garcia-Irizarry, C.; Sach, N.; White, H. S.; Neurock, M.; Minteer, S. D.; Baran, P. S., Electrochemically Driven, Ni-Catalyzed Aryl Amination: Scope, Mechanism, and Applications. *J. Am. Chem. Soc.* **2019,** *141*, 6392-6402.
23. Lim, C.-H.; Kudisch, M.; Liu, B.; Miyake, G. M., C–N Cross-Coupling via Photoexcitation of Nickel–Amine Complexes. *J. Am. Chem. Soc.* **2018,** *140*, 7667-7673.
24. (a) Paul, F.; Patt, J.; Hartwig, J. F., Palladium-catalyzed formation of carbon-nitrogen bonds. Reaction intermediates and catalyst improvements in the hetero cross-coupling of aryl halides and tin amides. *J. Am. Chem. Soc.* **1994,** *116*, 5969-5970; (b) Driver, M. S.; Hartwig, J. F., Energetics and Mechanism of Alkylamine N−H Bond Cleavage by Palladium Hydroxides: N−H Activation by Unusual Acid−Base Chemistry. *Organometallics* **1997,** *16*, 5706-5715; (c) Shekhar, S.; Ryberg, P.; Hartwig, J. F.; Mathew, J. S.; Blackmond, D. G.; Strieter, E. R.; Buchwald, S. L., Reevaluation of the Mechanism of the Amination of Aryl Halides Catalyzed by BINAP-Ligated Palladium Complexes. *J. Am. Chem. Soc.* **2006,** *128*, 3584-3591; (d) Klinkenberg, J. L.; Hartwig, J. F., Slow Reductive Elimination from Arylpalladium Parent Amido Complexes. *J. Am. Chem. Soc.* **2010,** *132*, 11830-11833; (e) Brusoe, A. T.; Hartwig, J. F., Palladium-Catalyzed Arylation of Fluoroalkylamines. *J. Am. Chem. Soc.* **2015,** *137*, 8460-8468; (f) Arrechea, P. L.; Buchwald, S. L., Biaryl Phosphine Based Pd(II) Amido Complexes: The Effect of Ligand Structure on Reductive Elimination. *J. Am. Chem. Soc.* **2016,** *138*, 12486-12493.
25. Diccianni, J. B.; Katigbak, J.; Hu, C.; Diao, T., Mechanistic Characterization of (Xantphos)Ni(I)-Mediated Alkyl Bromide Activation: Oxidative Addition, Electron Transfer, or Halogen-Atom Abstraction. *J. Am. Chem. Soc.* **2019,** *141*, 1788-1796.
26. (a) Roy, A. H.; Hartwig, J. F., Reductive Elimination of Aryl Halides from Palladium(II). *J. Am. Chem. Soc.* **2001,** *123*, 1232-1233; (b) Portnoy, M.; Milstein, D., Mechanism of aryl chloride oxidative addition to chelated palladium(0) complexes. *Organometallics* **1993,** *12*, 1665-1673; (c) Amatore, C.; Pfluger, F., Mechanism of oxidative addition of palladium(0) with aromatic iodides in toluene, monitored at ultramicroelectrodes. *Organometallics* **1990,** *9*, 2276-2282; (d) Barrios-Landeros, F.; Hartwig, J. F., Distinct Mechanisms for the Oxidative Addition of Chloro-, Bromo-, and Iodoarenes to a Bisphosphine Palladium(0) Complex with Hindered Ligands. *J. Am. Chem. Soc.* **2005,** *127*, 6944-6945; (e) Barrios-Landeros, F.; Carrow, B. P.; Hartwig, J. F., Effect of Ligand Steric Properties and Halide Identity on the Mechanism for Oxidative Addition of Haloarenes to Trialkylphosphine Pd(0) Complexes. *J. Am. Chem. Soc.* **2009,** *131*, 8141-8154.
27. (a) Tsou, T. T.; Kochi, J. K., Mechanism of oxidative addition. Reaction of nickel(0) complexes with aromatic halides. *J. Am. Chem. Soc.* **1979,** *101*, 6319-6332; (b) Bajo, S.; Laidlaw, G.; Kennedy, A. R.; Sproules, S.; Nelson, D. J., Oxidative Addition of Aryl

Electrophiles to a Prototypical Nickel(0) Complex: Mechanism and Structure/Reactivity Relationships. *Organometallics* **2017,** *36*, 1662-1672.

28. Yamashita, M.; Hartwig, J. F., Synthesis, Structure, and Reductive Elimination Chemistry of Three-Coordinate Arylpalladium Amido Complexes. *J. Am. Chem. Soc.* **2004,** *126*, 5344-5345.
29. Wang, Y.; Shi, Y.-F.; Chen, Y.-B.; Wu, L.-M., Hydrazine reduction of metal ions to porous submicro-structures of Ag, Pd, Cu, Ni, and Bi. *J. Solid State Chem.* **2012,** *191*, 19-26.
30. Niemeier, J. K.; Kjell, D. P., Hydrazine and Aqueous Hydrazine Solutions: Evaluating Safety in Chemical Processes. *Org. Process Res. Dev.* **2013,** *17*, 1580-1590.
31. (a) DeAngelis, A.; Wang, D.-H.; Buchwald, S. L., Mild and Rapid Pd-Catalyzed Cross-Coupling with Hydrazine in Continuous Flow: Application to the Synthesis of Functionalized Heterocycles. *Angew. Chem. Int. Ed.* **2013,** *52*, 3434-3437; (b) Lundgren, R. J.; Stradiotto, M., Palladium-Catalyzed Cross-Coupling of Aryl Chlorides and Tosylates with Hydrazine. *Angew. Chem. Int. Ed.* **2010,** *49*, 8686-8690.
32. Schlummer, B.; Scholz, U., Palladium-Catalyzed C–N and C–O Coupling–A Practical Guide from an Industrial Vantage Point. *Adv. Synth. Catal.* **2004,** *346*, 1599-1626.
33. Katrizky, A. R.; Pozharskii, A. F., *Handbook of Heterocyclic Chemistry*. 2nd ed.; Pergamon: Oxford, 2000.
34. Karrouchi, K.; Radi, S.; Ramli, Y.; Taoufik, J.; Mabkhot, Y. N.; Al-aizari, F. A.; Ansar, M. h., Synthesis and Pharmacological Activities of Pyrazole Derivatives: A Review. *Molecules* **2018,** *23*, 134.
35. Potts, K. T., The Chemistry of 1,2,4-Triazoles. *Chem. Rev.* **1961,** *61*, 87-127.
36. Habeeb, A. G.; Praveen Rao, P. N.; Knaus, E. E., Design and Synthesis of Celecoxib and Rofecoxib Analogues as Selective Cyclooxygenase-2 (COX-2) Inhibitors: Replacement of Sulfonamide and Methylsulfonyl Pharmacophores by an Azido Bioisostere. *J. Med. Chem.* **2001,** *44*, 3039-3042.
37. Kotagiri, V. K.; Suthrapu, S.; Mukunda Reddy, J.; Prasad Rao, C.; Bollugoddu, V.; Bhattacharya, A.; Bandichhor, R., An Improved Synthesis of Rimonabant: Anti-Obesity Drug. *Org. Process Res. Dev.* **2007,** *11*, 910-912.
38. Hamprecht, G.; Witschel, M.; Hawkes, T. R.; Edmunds, A. J. F.; Morris, J. A.; van Almsick, A., Herbicides with Bleaching Properties. In *Modern Crop Protection Compounds*, Wiley-VCH Verlag & Co. KGaA: Weinheim, Germany, 2011; pp 197-276.
39. Theodoridis, G.; Liebl, R.; Zagar, C., Protoporphyrinogen IX Oxidase Inhibitors. In *Modern Crop Protection Compounds*, Wiley-VCH Verlag & Co. KGaA: Weinheim, Germany, 2011; pp 163-195.
40. Schirmann, J.-P.; Bourdauducq, P., Hydrazine. In *Ullmann's Encylopedia of Industrial Chemistry*, John Wiley and Sons: New York, 2001.
41. (a) Charier, S.; Ruel, O.; Baudin, J.-B.; Alcor, D.; Allemand, J.-F.; Meglio, A.; Jullien, L., An Efficient Fluorescent Probe for Ratiometric pH Measurements in Aqueous Solutions. *Angew. Chem.* **2004,** *116*, 4889-4892; (b) Sánchez, B.; Calderón, C.; Tapia, R. A.; Contreras, R.; Campodónico, P. R., Activation of Electrophile/Nucleophile Pair by a Nucleophilic and Electrophilic Solvation in a SNAr Reaction. *Front. Chem.* **2018,** *6*; (c) Wilsily, A.; Mennen, S. M.; Cosbie, A.; Milne, J. E., Synthesis of the Hydrazinyl Pyridine Intermediate: Phase-Appropriate Delivery. *Org. Process Res. Dev.* **2017,** *21*, 1286-1293; (d) Cho, H.-J.; Um, I.-H., The α-Effect in SNAr Reaction of 1-Fluoro-2,4-dinitrobenzene with Hydrazine: Ground-State Destabilization versus Transition-State Stabilization. *Bull.*

Korean Chem. Soc. **2014,** *35*, 2371-2374; (e) Cho, H.-J.; Kim, M.-Y.; Um, I.-H., The α-Effect in SNAr Reaction of Y-Substituted-Phenoxy-2,4-Dinitrobenzenes with Amines: Reaction Mechanism and Origin of the α-Effect. *Bull. Korean Chem. Soc.* **2014,** *35*, 2448-2452.

42. (a) Siva Kumar, K.; Mahesh Kumar, P.; Sreenivasa Rao, V.; Jafar, A. A.; Meda, C. L. T.; Kapavarapu, R.; Parsa, K. V. L.; Pal, M., A new cascade reaction: concurrent construction of six and five membered rings leading to novel fused quinazolinones. *Org. Biomol. Chem.* **2012,** *10*, 3098-3103; (b) Liu, X.; Barry, M.; Tsou, H.-R., Palladium-catalyzed arylation of N,N-dialkylhydrazines and the subsequent conversion to anilines. *Tetrahedron Lett.* **2007,** *48*, 8409-8412; (c) Cacchi, S.; Fabrizi, G.; Goggiamani, A.; Sgalla, S., Palladium-Catalyzed N-Arylation of N,N-Dialkylhydrazines with Aryl Chlorides. *Adv. Synth. Catal.* **2007,** *349*, 453-458; (d) Cacchi, S.; Fabrizi, G.; Goggiamani, A.; Licandro, E.; Maiorana, S.; Perdicchia, D., Synthesis of N,N-Dialkyl-N'-arylhydrazines via Palladium-Catalyzed N-Arylation by Using N,N-Dialkylhydrazines/2LiCl Adducts. *Org. Lett.* **2005,** *7*, 1497-1500.

43. (a) Barnard, C. F. J., Palladium-catalyzed carbonylation - A reaction come of age. *Organometallics* **2008,** *27*, 5402-5422; (b) Magano, J.; Dunetz, J. R., Large-Scale Applications of Transition Metal-Catalyzed Couplings for the Synthesis of Pharmaceuticals. *Chem. Rev.* **2011,** *111*, 2177-2250; (c) Brennführer, A.; Neumann, H.; Beller, M., Palladium-Catalyzed Carbonylation Reactions of Aryl Halides and Related Compounds. *Angew. Chem. Int. Ed.* **2009,** *48*, 4114-4133; (d) Quesnel, J. S.; Kayser, L. V.; Fabrikant, A.; Arndtsen, B. A., Acid Chloride Synthesis by the Palladium-Catalyzed Chlorocarbonylation of Aryl Bromides. *Chem. Eur. J.* **2015,** *21*, 9550-9555; (e) Quesnel, J. S.; Arndtsen, B. A., A Palladium-Catalyzed Carbonylation Approach to Acid Chloride Synthesis. *J. Am. Chem. Soc.* **2013,** *135*, 16841-16844.

44. Schoenberg, A.; Bartoletti, I.; Heck, R. F., Palladium-catalyzed carboalkoxylation of aryl, benzyl, and vinylic halides. *J. Org. Chem.* **1974,** *39*, 3318-3326.

45. (a) Sergeev, A.; Spannenberg, A.; Beller, M., Palladium-catalyzed formylation of aryl bromides: Elucidation of the catalytic cycle of an industrially applied coupling reaction. *J. Am. Chem. Soc.* **2008,** *130*, 15549-15563; (b) Ben-David, Y.; Portnoy, M.; Milstein, D., Chelate-assisted, palladium-catalyzed efficient carbonylation of aryl chlorides. *J. Am. Chem. Soc.* **1989,** *111*, 8742-8744.

46. (a) Jimenez-Rodriguez, C.; Eastham, G. R.; Cole-Hamilton, D. J., The methoxycarbonylation of aryl chlorides catalysed by palladium complexes of bis(di-tert-butylphosphinomethyl)benzene. *Dalton Trans.* **2005**, 1826-1830; (b) Lagerlund, O.; Larhed, M., Microwave-Promoted Aminocarbonylations of Aryl Chlorides Using $Mo(CO)_6$ as a Solid Carbon Monoxide Source. *J. Comb. Chem.* **2006,** *8*, 4-6; (c) Lundgren, R. J.; Peters, B. D.; Alsabeh, P. G.; Stradiotto, M., A P,N-Ligand for Palladium-Catalyzed Ammonia Arylation: Coupling of Deactivated Aryl Chlorides, Chemoselective Arylations, and Room Temperature Reactions. *Angewandte Chemie International Edition* **2010,** *49*, 4071-4074; (d) Martinelli, J. R.; Clark, T. P.; Watson, D. A.; Munday, R. H.; Buchwald, S. L., Palladium-catalyzed aminocarbonylation of aryl chlorides at atmospheric pressure: The dual role of sodium phenoxide. *Angew. Chem. Int. Ed.* **2007,** *46*, 8460-8463.

47. Wang, J. Y.; Strom, A. E.; Hartwig, J. F., Mechanistic Studies of Palladium-Catalyzed Aminocarbonylation of Aryl Chlorides with Carbon Monoxide and Ammonia. *J. Am. Chem. Soc.* **2018,** *140*, 7979-7993.

48. Miloserdov, F. M.; McMullin, C. L.; Belmonte, M. M.; Benet-Buchholz, J.; Bakhmutov, V. I.; Macgregor, S. A.; Grushin, V. V., The challenge of palladium-catalyzed aromatic azidocarbonylation: From mechanistic and catalyst deactivation studies to a highly efficient process. *Organometallics* **2014,** *33*, 736-752.
49. (a) Wu, X. F.; Neumann, H.; Beller, M., Selective palladium-catalyzed aminocarbonylation of aryl halides with CO and ammonia. *Chem. Eur. J.* **2010,** *16*, 9750-9753; (b) Alsabeh, P. G.; Stradiotto, M.; Neumann, H.; Beller, M., Aminocarbonylation of (Hetero)aryl bromides with ammonia and amines using a palladium/dalphos catalyst system. *Adv. Synth. Catal.* **2012,** *354*, 3065-3070; (c) Xu, T.; Alper, H., Palladium-catalyzed aminocarbonylation of aryl iodides using aqueous ammonia. *Tetrahedron Lett.* **2013,** *54*, 5496-5499.
50. (a) Schnyder, A.; Beller, M.; Mehltretter, G.; Nsenda, T.; Studer, M.; Indolese, A. F., Synthesis of primary aromatic amides by aminocarbonylation of aryl halides using formamide as an ammonia synthon. *J. Org. Chem.* **2001,** *66*, 4311-4315; (b) Wan, Y.; Alterman, M.; Larhed, M.; Hallberg, A., Formamide as a Combined Ammonia Synthon and Carbon Monoxide Source in Fast Palladium-Catalyzed Aminocarbonylations of Aryl Halides. *J. Comb. Chem.* **2003,** *5*, 82-84; (c) Wu, X.; Wannberg, J.; Larhed, M., Hydroxylamine as an ammonia equivalent in microwave-enhanced aminocarbonylations. *Tetrahedron* **2006,** *62*, 4665-4670.
51. Klinkenberg, J. L.; Hartwig, J. F., Catalytic Organometallic Reactions of Ammonia. *Angew. Chem. Int. Ed.* **2011,** *50*, 86-95.
52. Ozawa, F.; Soyama, H.; Yanagihara, H.; Aoyama, I.; Takino, H.; Izawa, K.; Yamamoto, T.; Yamamoto, A., Palladium-catalyzed double carbonylation of aryl halides to give α-keto amides. Mechanistic studies. *J. Am. Chem. Soc.* **1985,** *107*, 3235-3245.
53. (a) Wu, X.-F.; Neumann, H.; Spannenberg, A.; Schulz, T.; Jiao, H.; Beller, M., Development of a General Palladium-Catalyzed Carbonylative Heck Reaction of Aryl Halides. *J. Am. Chem. Soc.* **2010,** *132*, 14596-14602; (b) Wu, X.-F.; Neumann, H.; Beller, M., Palladium-Catalyzed Coupling Reactions: Carbonylative Heck Reactions To Give Chalcones. *Angew. Chem. Int. Ed.* **2010,** *49*, 5284-5288.
54. (a) Schoenberg, A.; Heck, R. F., Palladium-catalyzed formylation of aryl, heterocyclic, and vinylic halides. *J. Am. Chem. Soc.* **1974,** *96*, 7761-7764; (b) Klaus, S.; Neumann, H.; Zapf, A.; Strübing, D.; Hübner, S.; Almena, J.; Riermeier, T.; Groß, P.; Sarich, M.; Krahnert, W.-R.; Rossen, K.; Beller, M., A General and Efficient Method for the Formylation of Aryl and Heteroaryl Bromides. *Angew. Chem. Int. Ed.* **2006,** *45*, 154-158.
55. (a) Schoenberg, A.; Heck, R. F., Palladium-catalyzed amidation of aryl, heterocyclic, and vinylic halides. *J. Org. Chem.* **1974,** *39*, 3327-3331; (b) Martinelli, J. R.; Freckmann, D. M. M.; Buchwald, S. L., Convenient Method for the Preparation of Weinreb Amides via Pd-Catalyzed Aminocarbonylation of Aryl Bromides at Atmospheric Pressure. *Org. Lett.* **2006,** *8*, 4843-4846; (c) Wu, X.-F.; Neumann, H.; Beller, M., Selective Palladium-Catalyzed Aminocarbonylation of Aryl Halides with CO and Ammonia. *Chem. Eur. J.* **2010,** *16*, 9750-9753.
56. (a) Mägerlein, W.; Beller, M.; Indolese, A. F., Palladium-catalyzed carbonylation of aryl halides — a detailed investigation of the alkoxycarbonylation of 4-bromoacetophenone. *J. Mol. Catal. A: Chem.* **2000,** *156*, 213-221; (b) Munday, R. H.; Martinelli, J. R.; Buchwald, S. L., Palladium-Catalyzed Carbonylation of Aryl Tosylates and Mesylates. *J. Am. Chem. Soc.* **2008,** *130*, 2754-2755.

57. (a) Wu, X.-F.; Neumann, H.; Beller, M., Palladium-catalyzed carbonylative coupling reactions between Ar-X and carbon nucleophiles. *Chem. Soc. Rev.* **2011,** *40*, 4986-5009; (b) Miloserdov, F. M.; Grushin, V. V., Palladium-Catalyzed Aromatic Azidocarbonylation. *Angew. Chem. Int. Ed.* **2012,** *51*, 3668-3672.
58. Schmid, R., Homogeneous Catalysis with Metal Complexes in a Pharmaceuticals' and Vitamins' Company: Why, What for, and Where to Go? *Chimia* **1996,** *50*, 110-113.
59. Atkins, R. J.; Banks, A.; Bellingham, R. K.; Breen, G. F.; Carey, J. S.; Etridge, S. K.; Hayes, J. F.; Hussain, N.; Morgan, D. O.; Oxley, P.; Passey, S. C.; Walsgrove, T. C.; Wells, A. S., The Development of a Manufacturing Route for the GPIIb/IIIa Receptor Antagonist SB-214857-A. Part 2: Conversion of the Key Intermediate SB-235349 to SB-214857-A. *Org. Process Res. Dev.* **2003,** *7*, 663-675.
60. Torborg, C.; Beller, M., Recent Applications of Palladium-Catalyzed Coupling Reactions in the Pharmaceutical, Agrochemical, and Fine Chemical Industries. *Adv. Synth. Catal.* **2009,** *351*, 3027-3043.
61. (a) Quesnel, J. S.; Moncho, S.; Ylijoki, K. E.; Torres, G. M.; Brothers, E. N.; Bengali, A. A.; Arndtsen, B. A., Computational Study of the Palladium-Catalyzed Carbonylative Synthesis of Aromatic Acid Chlorides: The Synergistic Effect of PtBu3 and CO on Reductive Elimination. *Chem. Eur. J.* **2016,** *22*, 15107-15118; (b) Torres, G. M.; Quesnel, J. S.; Bijou, D.; Arndtsen, B. A., From Aryl Iodides to 1,3-Dipoles: Design and Mechanism of a Palladium Catalyzed Multicomponent Synthesis of Pyrroles. *J. Am. Chem. Soc.* **2016,** *138*, 7315-7324.
62. Garrou, P. E.; Heck, R. F., The mechanism of carbonylation of halo(bis ligand)organoplatinum(II), -palladium(II), and -nickel(II) complexes. *J. Am. Chem. Soc.* **1976,** *98*, 4115-4127.
63. Lin, Y.-S.; Yamamoto, A., Studies Relevant to Palladium-Catalyzed Carbonylation Processes. Mechanisms of Formation of Esters and Amides from Benzylpalladium and (Phenylacetyl)palladium Complexes on Reactions with Alcohols and Amines. *Organometallics* **1998,** *17*, 3466-3478.
64. Ben-David, Y.; Portnoy, M.; Milstein, D., Chelate-assisted, palladium-catalyzed efficient carbonylation of aryl chlorides. *J. Am. Chem. Soc.* **1989,** *111*, 8742-8744.
65. (a) Koji, K.; Michito, S.; Masanobu, H.; Yasuzo, U., Oxidative Additions of Alkyl Halides to Palladium(0) Carbonyl Complex. *Bull. Chem. Soc. Jpn.* **1973,** *46*, 2820-2822; (b) Stille, J. K.; Lau, K. S. Y., Oxidative addition of alkyl halides to zero-valent palladium complexes. Mechanisms. *J. Am. Chem. Soc.* **1976,** *98*, 5841-5849; (c) Lau, K. S. Y.; Wong, P. K.; Stille, J. K., Oxidative addition of benzyl halides to zero-valent palladium complexes. Inversion of configuration at carbon. *J. Am. Chem. Soc.* **1976,** *98*, 5832-5840; (d) Bloome, K. S.; McMahen, R. L.; Alexanian, E. J., Palladium-Catalyzed Heck-Type Reactions of Alkyl Iodides. *J. Am. Chem. Soc.* **2011,** *133*, 20146-20148; (e) Sargent, B. T.; Alexanian, E. J., Palladium-Catalyzed Alkoxycarbonylation of Unactivated Secondary Alkyl Bromides at Low Pressure. *J. Am. Chem. Soc.* **2016,** *138*, 7520-7523.
66. (a) Stromnova, T.; Moiseev, I., Palladium carbonyl complexes. *Russ. Chem. Rev.* **1998,** *67*, 485-514; (b) Crabtree, R. H.; Mingos, D. M. P., 8.04.1 Carbonyl Complexes. In *Comprehensive Organometallic Chemistry III, Volumes 1 - 13*, Elsevier: pp 197-210.
67. Grushin, V. V.; Alper, H., Transformations of Chloroarenes, Catalyzed by Transition-Metal Complexes. *Chem. Rev.* **1994,** *94*, 1047-1062.

68. (a) Huser, M.; Youinou, M.-T.; Osborn, J. A., Chlorocarbon Activation: Catalytic Carbonylation of Dichloromethane and Chlorobenzene. *Angew. Chem. Int. Ed. Engl.* **1989,** *28*, 1386-1388; (b) Mägerlein, W.; Indolese, A. F.; Beller, M., A More Efficient Catalyst for the Carbonylation of Chloroarenes. *Angew. Chem. Int. Ed.* **2001,** *40*, 2856-2859; (c) Wu, X.-F.; Neumann, H.; Beller, M., Development of a Second Generation Palladium Catalyst System for the Aminocarbonylation of Aryl Halides with CO and Ammonia. *Chem. Asian J.* **2010,** *5*, 2168-2172.

69. (a) Komiya, S.; Akai, Y.; Tanaka, K.; Yamamoto, T.; Yamamoto, A., Reductive elimination of aryl carboxylates from acyl(aryloxy)nickel(II) and -palladium(II) complexes. *Organometallics* **1985,** *4*, 1130-1136; (b) van Leeuwen, P. W. N. M.; Zuideveld, M. A.; Swennenhuis, B. H. G.; Freixa, Z.; Kamer, P. C. J.; Goubitz, K.; Fraanje, J.; Lutz, M.; Spek, A. L., Alcoholysis of Acylpalladium(II) Complexes Relevant to the Alternating Copolymerization of Ethene and Carbon Monoxide and the Alkoxycarbonylation of Alkenes: the Importance of Cis-Coordinating Phosphines. *J. Am. Chem. Soc.* **2003,** *125*, 5523-5539.

70. Ozawa, F.; Kawasaki, N.; Okamoto, H.; Yamamoto, T.; Yamamoto, A., Mechanisms of double and single carbonylation reactions of aryl iodides catalyzed by palladium complexes to give .alpha.-keto esters and esters. *Organometallics* **1987,** *6*, 1640-1651.

71. (a) Seligson, A. L.; Trogler, W. C., Cone angles for amine ligands. X-ray crystal structures and equilibrium measurements for ammonia, ethylamine, diethylamine, and triethylamine complexes with the [bis(dimethylphosphino)ethane]methylpalladium(II) cation. *J. Am. Chem. Soc.* **1991,** *113*, 2520-2527; (b) Nigst, T. A.; Antipova, A.; Mayr, H., Nucleophilic Reactivities of Hydrazines and Amines: The Futile Search for the α-Effect in Hydrazine Reactivities. *J. Org. Chem.* **2012,** *77*, 8142-8155.

72. (a) Trebbe, R.; Goddard, R.; Rufińska, A.; Seevogel, K.; Pörschke, K.-R., Preparation and Structural Characterization of the Palladium(0)−Carbonyl Complexes (R2PC2H4PR2)Pd(CO)2 and {(R2PC2H4PR2)Pd}2(μ-CO). *Organometallics* **1999,** *18*, 2466-2472; (b) Perez, P. J.; Calabrese, J. C.; Bunel, E. E., Synthesis, Characterization, and Reactivity of [((^{i}Pr)$_2$P(CH$_2$)$_3$P(^{i}Pr)$_2$)(PCy$_3$)PdH][OR]. *Organometallics* **2001,** *20*, 337-345.

73. Due to the poor solubility of 4 in neat DMSO, a 1:1 v/v mixture of DMSO and toluene was chosen as a solvent mixture capable of dissolving 4.

74. (a) Grevin, J.; Kalck, P.; Daran, J. C.; Vaissermann, J.; Bianchini, C., Synthesis of a novel palladium(0) carbonyl complex containing a tridentate phosphorus ligand. X-ray crystal structure of [Pd(CO)(CH3C(CH2PPh2)3)]. *Inorg. Chem.* **1993,** *32*, 4965-4967; (b) Bellabarba, R. M.; Tooze, R. P.; Slawin, A. M. Z., Synthesis, X-ray characterisation and reactions of a trigonal planar palladium(0) carbonyl complex, (tbpx)PdCO. *Chem. Commun.* **2003**, 1916-1917.

75. Bunel also observed the absence of 31P-13C coupling in (DIPP)Pd(13CO) (DIPP = 1,3-bis(diisopropylphosphino) propane) under 13CO, which was attributed to rapid exchange between bound and unbound 13CO. See ref. 28b.

76. At this temperature and pressure of CO, a resonance at the chemical shift of free CO was observed suggesting that exchange between bound and unbound CO was no longer present at the NMR time scale.

77. Even with 1000 Torr of 13CO at –40 °C, phosphorus-carbon coupling was still not detected.

78. We monitored this reaction by 19F NMR spectroscopy because the concentration of 4 could not be determined accurately by 31P NMR spectroscopy at low pressures of CO (<500 Torr) and elevated temperatures due to broad resonances.
79. The 12 kcal/mol barrier is given as the difference in energy between the transition state for oxidative addition and the computed energy of the experimentally determined resting state.
80. Singleton, D. A.; Thomas, A. A., High-Precision Simultaneous Determination of Multiple Small Kinetic Isotope Effects at Natural Abundance. *J. Am. Chem. Soc.* **1995,** *117*, 9357-9358.
81. It should be noted that the y-intercept of the fit of 1/kobs versus pressure of CO and the fit of 1/kobs versus 1/[ArCl] (Figure 4a) correspond to 1/k1 in the equation given for Path A in Figure 5. However, the values of this intercept were too close to zero to deduce an accurate value. This small value of the y-intercept reflects rapid exchange of unbound CO with the CO bound to dicarbonyl 4 and fits with the rapid exchange observed at room temperature by 13C NMR spectroscopy (vide supra).
82. Portnoy, M.; Milstein, D., Mechanism of aryl chloride oxidative addition to chelated palladium(0) complexes. *Organometallics* **1993,** *12*, 1665-1673.
83. (a) Fauvarque, J.-F.; Pflüger, F.; Troupel, M., Kinetics of oxidative addition of zerovalent palladium to aromatic iodides. *J. Organomet. Chem.* **1981,** *208*, 419-427; (b) Jutand, A.; Mosleh, A., Rate and Mechanism of Oxidative Addition of Aryl Triflates to Zerovalent Palladium Complexes. Evidence for the Formation of Cationic (.sigma.-Aryl)palladium Complexes. *Organometallics* **1995,** *14*, 1810-1817.
84. Hansch, C.; Leo, A.; Taft, R. W., A survey of Hammett substituent constants and resonance and field parameters. *Chem. Rev.* **1991,** *91*, 165-195.
85. Maes, B.; Verbeeck, S.; Verhelst, T.; Ekomié, A.; von Wolff, N.; Lefèvre, G.; Mitchell, E.; Jutand, A., Oxidative Addition of Haloheteroarenes to Palladium(0): Concerted versus SNAr-Type Mechanism. *Chem. Eur. J.* **2015,** *21*, 7858-7865.
86. (a) Meyer, A.; Penning, H.; Elsner, M., C and N isotope fractionation suggests similar mechanisms of microbial atrazine transformation despite involvement of different enzymes (AtzA and TrzN). *Environ. Sci. Technol.* **2009,** *43*, 8079-8085; (b) Grzybkowska, A.; Kaminski, R.; Dybala-Defratyka, A., Theoretical predictions of isotope effects versus their experimental values for an example of uncatalyzed hydrolysis of atrazine. *PCCP* **2014,** *16*, 15164.
87. Quesnel, J. S.; Kayser, L. V.; Fabrikant, A.; Arndtsen, B. A., Acid Chloride Synthesis by the Palladium-Catalyzed Chlorocarbonylation of Aryl Bromides. *Chem. Eur. J.* **2015,** *21*, 9550-9555.
88. Moser, W. R.; Wang, A. W.; Kildahl, N. K., Mechanistic studies of the palladium-catalyzed reaction of methanol with bromobenzene and carbon monoxide to produce methyl benzoate. 1. Stoichiometric study. *J. Am. Chem. Soc.* **1988,** *110*, 2816-2820.
89. The small increase in rate with increasing N(n-butyl)4PF6 suggests the reaction of 6a with ammonia depends slightly on the polarity of the solvent.
90. O'Toole, T. R.; Younathan, J. N.; Sullivan, B. P.; Meyer, T. J., 1,2-Difluorobenzene: a relatively inert and noncoordinating solvent for electrochemical studies on transition-metal complexes. *Inorg. Chem.* **1989,** *28*, 3923-3926.
91. Tsuji, J., Palladium-Catalyzed Decarbonylation of Acyl Halides and Aldehydes. In *Handbook of Organopalladium Chemistry for Organic Synthesis*, John Wiley & Sons, Inc.: 2002; pp 2643-2653.

92. (a) Surry, D. S.; Buchwald, S. L., Selective Palladium-Catalyzed Arylation of Ammonia: Synthesis of Anilines as Well as Symmetrical and Unsymmetrical Di- and Triarylamines. *J. Am. Chem. Soc.* **2007,** *129*, 10354-10355; (b) Vo, G. D.; Hartwig, J. F., Palladium-Catalyzed Coupling of Ammonia with Aryl Chlorides, Bromides, Iodides, and Sulfonates: A General Method for the Preparation of Primary Arylamines. *J. Am. Chem. Soc.* **2009,** *131*, 11049-11061; (c) Green, R. A.; Hartwig, J. F., Palladium-Catalyzed Amination of Aryl Chlorides and Bromides with Ammonium Salts. *Org. Lett.* **2014,** *16*, 4388-4391.

93. (a) Portnoy, M.; Frolow, F.; Milstein, D., Methanol reduces an organopalladium(II) complex to a palladium(I) hydride. Crystallographic characterization of a hydrido-bridged palladium complex. *Organometallics* **1991,** *10*, 3960-3962; (b) Portnoy, M.; Milstein, D., A binuclear palladium(I) hydride. Formation, reactions, and catalysis. *Organometallics* **1994,** *13*, 600-609; (c) Toth, I.; Elsevier, C. J., Formation of Dinuclear Palladium(I) Hydride [Pd2(.mu.-H)(.mu.-CO){(S,S)-BDPP}2]Cl by Methanolysis or Hydrolysis of Pd(COMe)(Cl){(S,S)-BDPP} {(S,S)-BDPP = (2S,4S)-2,4-Bis(diphenylphosphino)pentane}. *Organometallics* **1994,** *13*, 2118-2122; (d) Sperrle, M.; Gramlich, V.; Consiglio, G., Synthesis and Characterization of Cationic Palladium (6,6‘-Dimethoxybiphenyl-2,2‘-diyl)bis(diphenylphosphine) Complexes. *Organometallics* **1996,** *15*, 5196-5201; (e) Macchioni, A.; Romani, A.; Zuccaccia, C.; Guglielmetti, G.; Querci, C., Experimental Evidence for the Aggregation of [(Phen)2Pd2(μ-H)(μ-CO)]+ in Solution. *Organometallics* **2003,** *22*, 1526-1533.

94. Chan, S.; Lee, S.-M.; Lin, Z.; Wong, W.-T., Syntheses, structures and reactivities of [Os6Pd(CO)18(bipy)] and [{(bipy)Pd}20s3(CO)12]: Crystal and molecular structures of [{(bipy)Pd}2(μ-H)(μ-CO)][H3Os4(CO)12] and [(C4H9)4N]2[Pd2I6]. *J. Organomet. Chem.* **1996,** *510*, 219-231.

95. (a) Siedle, A. R.; Newmark, R. A.; Gleason, W. B., Protonation of phosphine complexes of zerovalent nickel, palladium, platinum, and ruthenium with fluorocarbon acids. *Inorg. Chem.* **1991,** *30*, 2005-2009; (b) Minghetti, G.; Bandini, A. L.; Banditelli, G.; Bonati, F.; Szostak, R.; Strouse, C. E.; Knobler, C. B.; Kaesz, H. D., Synthesis and characterization of cationic dinuclear hydridoplatinum complexes: crystal and molecular structure of [Pt2(.mu.-H,.mu.-CO)(dpe)2][BF4] (dpe = 1,2-bis(diphenylphosphino)ethane). *Inorg. Chem.* **1983,** *22*, 2332-2338.

96. Li, H.; Grasa, G. A.; Colacot, T. J., A Highly Efficient , Practical , and General Route for the Synthesis of (R3P)2 Pd(0): Structural Evidence on the Reduction Mechanism of Pd (II) to Pd (0). *Org. Lett.* **2010,** *12*, 3332-3335.

97. Banks, M. R.; Hudson, R. F., The Reaction of N-Alkylhydroxamic Acids with Sulphinyl Chlorides. *J. Chem. Soc. Perkin II* **1986**, 121-1.

98. Koide, Y.; Bott, S. G.; Barron, A. R., Alumoxanes as cocatalysts in the palladium-catalyzed copolymerization of carbon monoxide and ethylene: genesis of a structure-activity relationship. *Organometallics* **1996,** *15*, 2213-2226.

99. Sumino, S.; Fusano, A.; Fukuyama, T.; Ryu, I., Carbonylation Reactions of Alkyl Iodides through the Interplay of Carbon Radicals and Pd Catalysts. *Acc. Chem. Res.* **2014,** *47*, 1563-1574.

100. (a) Sargent, B. T.; Alexanian, E. J., Cobalt-Catalyzed Aminocarbonylation of Alkyl Tosylates: Stereospecific Synthesis of Amides. *Angew. Chem. Int. Ed.* **2019,** *58*, 9533-9536; (b) Sargent, B. T.; Alexanian, E. J., Cobalt-Catalyzed Carbonylative Cross-Coupling

of Alkyl Tosylates and Dienes: Stereospecific Synthesis of Dienones at Low Pressure. *J. Am. Chem. Soc.* **2017,** *139*, 12438-12440.

101. Choi, J.; Martín-Gago, P.; Fu, G. C., Stereoconvergent Arylations and Alkenylations of Unactivated Alkyl Electrophiles: Catalytic Enantioselective Synthesis of Secondary Sulfonamides and Sulfones. *J. Am. Chem. Soc.* **2014,** *136*, 12161-12165.
102. Luo, Y.-R., *Handbook of Bond Dissociation Energies in Organic Compounds*. CRC Press: 2003; p 380.
103. (a) Wei, C. S.; Davies, G. H. M.; Soltani, O.; Albrecht, J.; Gao, Q.; Pathirana, C.; Hsiao, Y.; Tummala, S.; Eastgate, M. D., The Impact of Palladium(II) Reduction Pathways on the Structure and Activity of Palladium(0) Catalysts. *Angew. Chem. Int. Ed.* **2013,** *52*, 5822-5826; (b) Grushin, V. V.; Alper, H., Alkali-induced disproportionation of palladium(II) tertiary phosphine complexes, $[L_2PdCl_2]$, to LO and palladium(90). Key intermediates in the biphasic carbonylation of ArX catalyzed by $[L_2PdCl_2]$. *Organometallics* **1993,** *12*, 1890-1901.
104. Hasanayn, F.; Nsouli, N. H.; Al-Ayoubi, A.; Goldman, A. S., Addition of Alkyl Radicals to Transition-Metal-Coordinated CO: Calculation of the Reaction of [Ru(CO)5] and Related Complexes and Relevance to Alkane Carbonylation. *J. Am. Chem. Soc.* **2008,** *130*, 511-521.
105. Barry, J. T.; Berg, D. J.; Tyler, D. R., Radical Cage Effects: The Prediction of Radical Cage Pair Recombination Efficiencies Using Microviscosity Across a Range of Solvent Types. *J. Am. Chem. Soc.* **2017,** *139*, 14399-14405.
106. Lee, E.; Hooker, J. M.; Ritter, T., Nickel-Mediated Oxidative Fluorination for PET with Aqueous [18F] Fluoride. *J. Am. Chem. Soc.* **2012,** *134*, 17456-17458.
107. Koo, K.; Hillhouse, G. L., Carbon-Nitrogen Bond Formation by Reductive Elimination from Nickel(II) Amido Alkyl Complexes. *Organometallics* **1995,** *14*, 4421-4423.
108. Mohadjer Beromi, M.; Banerjee, G.; Brudvig, G. W.; Charboneau, D. J.; Hazari, N.; Lant, H. M. C.; Mercado, B. Q., Modifications to the Aryl Group of dppf-Ligated Ni σ-Aryl Precatalysts: Impact on Speciation and Catalytic Activity in Suzuki–Miyaura Coupling Reactions. *Organometallics* **2018,** *37*, 3943-3955.
109. Truong, T.-T.; Coates, G. W.; Abruña, H. D., High power organic cathodes using thin films of electropolymerized benzidine polymers. *Chem. Commun.* **2015,** *51*, 14674-14677.
110. Kong, X.; Zhang, H.; Xiao, Y.; Cao, C.; Shi, Y.; Pang, G., Effective, transition metal free and selective C–F activation under mild conditions. *RSC Advances* **2015,** *5*, 7035-7048.
111. Bilke, J. L.; O'Brien, P., On the Two-Ligand Catalytic Asymmetric Deprotonation of N-Boc Pyrrolidine: Probing the Effect of the Stoichiometric Ligand. *J. Org. Chem.* **2008,** *73*, 6452-6454.
112. van Koten, G.; Noltes, J. G., Group IB organometallic chemistry: XIV. Intramolecular ring-closure reactions of novel arylcopper compounds RCuI2. Synthesis of 7,8-dihydrodibenzo[f,h][1,4]dioxecin and 7,8-dihydrodibenzo-6,9-dimethyl[f,h][1,4]diazecin. *J. Organomet. Chem.* **1976,** *104*, 127-138.
113. Robinson, B., The Fischer Indole Synthesis. *Chem. Rev.* **1963,** *63*, 373-401.
114. Gaikwad, D. D.; Chapolikar, A. D.; Devkate, C. G.; Warad, K. D.; Tayade, A. P.; Pawar, R. P.; Domb, A. J., Synthesis of indazole motifs and their medicinal importance: An overview. *European Journal of Medicinal Chemistry* **2015,** *90*, 707-731.

115. Baumann, M.; Baxendale, I. R.; Ley, S. V.; Nikbin, N., An overview of the key routes to the best selling 5-membered ring heterocyclic pharmaceuticals. *Beilstein J. Org. Chem.* **2011,** *7*, 442-495.
116. Earley, F.; Sauter, H.; Rheinheimer, J.; Rieck, H.; Coqueron, P.-Y.; Whittingham, W. G.; Walter, H., Fungicides Acting on Oxidative Phosphorylation. In *Modern Crop Protection Compounds*, Wiley-VCH Verlag & Co. KGaA: Weinheim, Germany, 2011; pp 559-691.
117. Babczinski, P.; Watanabe, Y.; Nakatani, M.; Yoshimura, T.; Hanai, R.; Tanetani, Y.; Shimizu, T., Herbicides Disturbing the Synthesis of Very Long-Chain Fatty Acids. In *Modern Crop Protection Compounds*, Wiley-VCH Verlag & Co. KGaA: Weinheim, Germany, 2011; pp 305-337.
118. (a) Zhu, M.-K.; Zhao, J.-F.; Loh, T.-P., Palladium-Catalyzed C–C Bond Formation of Arylhydrazines with Olefins via Carbon–Nitrogen Bond Cleavage. *Org. Lett.* **2011,** *13*, 6308-6311; (b) Kibriya, G.; Mondal, S.; Hajra, A., Visible-Light-Mediated Synthesis of Unsymmetrical Diaryl Sulfides via Oxidative Coupling of Arylhydrazine with Thiol. *Org. Lett.* **2018,** *20*, 7740-7743; (c) Hofmann, J.; Jasch, H.; Heinrich, M. R., Oxidative Radical Arylation of Anilines with Arylhydrazines and Dioxygen from Air. *J. Org. Chem.* **2014,** *79*, 2314-2320.
119. (a) For selected examples, refer to the following references; (b) Senthil Kumar, G.; Zeller, M.; Gonnade, R. G.; Rajendra Prasad, K. J., Highly regioselective C4-hydrazinylation of 2,4-dichloroquinolines: expedient synthesis of aminoquinoline substituted pyrrolidin-2,5-diones via hydrazinylquinolines. *Tetrahedron Lett.* **2014,** *55*, 4240-4244.
120. Crawford, S. M.; Lavery, C. B.; Stradiotto, M., BippyPhos: A Single Ligand With Unprecedented Scope in the Buchwald–Hartwig Amination of (Hetero)aryl Chlorides. *Chem. Eur. J.* **2013,** *19*, 16760-16771.
121. Carrasco, S.; Martín-Matute, B., Hydrazine-Free Facile Synthesis of Palladium-Tetrakis(Triphenylphosphine). *Eur. J. Inorg. Chem.* **2019,** *2019*, 1951-1955.
122. Hartwig, J. F., Carbon–heteroatom bond formation catalysed by organometallic complexes. *Nature* **2008,** *455*, 314-322.
123. (a) Fernández-Rodríguez, M. A.; Shen, Q.; Hartwig, J. F., Highly Efficient and Functional-Group-Tolerant Catalysts for the Palladium-Catalyzed Coupling of Aryl Chlorides with Thiols. *Chem. Eur. J.* **2006,** *12*, 7782-7796; (b) Fernández-Rodríguez, M. A.; Hartwig, J. F., A General, Efficient, and Functional-Group-Tolerant Catalyst System for the Palladium-Catalyzed Thioetherification of Aryl Bromides and Iodides. *J. Org. Chem.* **2009,** *74*, 1663-1672.
124. Shen, Q.; Hartwig, J. F., Palladium-Catalyzed Coupling of Ammonia and Lithium Amide with Aryl Halides. *J. Am. Chem. Soc.* **2006,** *128*, 10028-10029.
125. (a) Kuwano, R.; Utsunomiya, M.; Hartwig, J. F., Aqueous Hydroxide as a Base for Palladium-Catalyzed Amination of Aryl Chlorides and Bromides. *J. Org. Chem.* **2002,** *67*, 6479-6486; (b) Van Baelen, G.; Maes, B. U. W., Study of the microwave-assisted hydrolysis of nitriles and esters and the implementation of this system in rapid microwave-assisted Pd-catalyzed amination. *Tetrahedron* **2008,** *64*, 5604-5619; (c) Tardiff, B. J.; Stradiotto, M., Buchwald–Hartwig Amination of (Hetero)aryl Chlorides by Employing Mor-DalPhos under Aqueous and Solvent-Free Conditions. *Eur. J. Org. Chem.* **2012,** *2012*, 3972-3977.

126. Filali, E.; Lloyd-Jones, G. C.; Sale, D. A., Cleavage of tert-Butyl Benzoates with NaH in DMF: Comments on the Mechanism and a Simple and Safe Alternative Procedure. *Synlett* **2009,** *2009*, 205-208.
127. Hartwig, J. F., *Organotransition Metal Chemistry: From Bonding to Catalysis*. University Science Books: Sausalito, 2010.
128. (a) Xia, A.; Sharp, P. R., Platinum(II) Hydrazido Complexes. *Inorg. Chem.* **2001,** *40*, 4016-4021; (b) Alvaro, E.; Hartwig, J. F., Resting State and Elementary Steps of the Coupling of Aryl Halides with Thiols Catalyzed by Alkylbisphosphine Complexes of Palladium. *J. Am. Chem. Soc.* **2009,** *131*, 7858-7868.
129. (a) Johansson, R.; Öhrström, L.; Wendt, O. F., Hydrogen Bond Control of Dimensionality in Organometallic {2,6-Bis[(di-t-butylphosphino)methyl]phenyl}palladium(II) Compounds: Dimers, Chains, and a 3D-Net with an Apparent Channel Structure. *Crystal Growth & Design* **2007,** *7*, 1974-1979; (b) Cámpora, J.; Palma, P.; del Río, D.; Álvarez, E., CO Insertion Reactions into the M−OH Bonds of Monomeric Nickel and Palladium Hydroxides. Reversible Decarbonylation of a Hydroxycarbonyl Palladium Complex. *Organometallics* **2004,** *23*, 1652-1655.
130. Carrow, B. P.; Hartwig, J. F., Distinguishing Between Pathways for Transmetalation in Suzuki−Miyaura Reactions. *J. Am. Chem. Soc.* **2011,** *133*, 2116-2119.
131. Hoops, S.; Sahle, S.; Gauges, R.; Lee, C.; Pahle, J.; Simus, N.; Singhal, M.; Xu, L.; Mendes, P.; Kummer, U., COPASI—a COmplex PAthway SImulator. *Bioinformatics* **2006,** *22*, 3067-3074.
132. Fulmer, G. R.; Herndon, A. N.; Kaminsky, W.; Kemp, R. A.; Goldberg, K. I., Hydrogenolysis of Palladium(II) Hydroxide, Phenoxide, and Alkoxide Complexes. *J. Am. Chem. Soc.* **2011,** *133*, 17713-17726.
133. Hesse, M.; Meier, H.; Zeeh, B., *Spectroscopic Methods in Organic Chemistry*. 2nd ed.; Thieme Chemistry: New York, 2007; p 237.
134. Motschi, H.; Pregosin, P. S.; Venanzi, L. M., ^{15}N-NMR. and ^{31}P-NMR. Studies of palladium and platinum complexes. *Helv. Chim. Acta* **1979,** *62*, 667-677.
135. (a) Berkhoudt, T.; Jakobsen, H. J., Determination of the sign for a one-bond $^{15}N–^{15}N$ spin-spin coupling constant: The flip angle effect. *Journal of Magnetic Resonance (1969)* **1982,** *50*, 323-327; (b) Perera, S. A.; Gregušová, A.; Bartlett, R. J., First Calculations of $^{15}N–^{15}N$ *J* Values and New Calculations of Chemical Shifts for High Nitrogen Systems: A Comment on the Long Search for HN_5 and Its Pentazole Anion. *The Journal of Physical Chemistry A* **2009,** *113*, 3197-3201.
136. Schrock, R. R.; Liu, A. H.; O'Regan, M. B.; Finch, W. C.; Payack, J. F., Preparation and characterization of two unsubstituted hydrazido(1-) complexes, $W(\eta^5\text{-}C_5Me_5)Me_4(\eta^2\text{-}NHNH_2)$ and $[W(\eta^5\text{-}C_5Me_5)Me_3(\eta^2NHNH_2)]^+[SO_3CF_3]^-$. *Inorg. Chem.* **1988,** *27*, 3574-3583.
137. Hoye, T. R.; Eklov, B. M.; Ryba, T. D.; Voloshin, M.; Yao, L. J., No-D NMR (No-Deuterium Proton NMR) Spectroscopy: A Simple Yet Powerful Method for Analyzing Reaction and Reagent Solutions. *Org. Lett.* **2004,** *6*, 953-956.
138. Li, H.; Grasa, G. A.; Colacot, T. J., A Highly Efficient, Practical, and General Route for the Synthesis of $(R_3P)_2Pd(0)$: Structural Evidence on the Reduction Mechanism of Pd(II) to Pd(0). *Org. Lett.* **2010,** *12*, 3332-3335.

139. Tomakinian, T.; Guillot, R.; Kouklovsky, C.; Vincent, G., Synthesis of benzofuro[3,2-*b*]indoline amines via deamination-interrupted Fischer indolization and their unexpected reactivity towards nucleophiles. *Chem. Commun.* **2016,** *52*, 5443-5446.